

**SUCTION CHARACTERISTICS
AND
ELASTIC-PLASTIC MODELLING OF
UNSATURATED SAND-BENTONITE MIXTURE**

by

Gary Xiangmin Tang

A Thesis

Submitted to the Faculty of Graduate Studies
in Partial Fulfillment of the Requirements for the Degree of

Doctor of Philosophy

Department of Civil and Geological Engineering
University of Manitoba
Winnipeg, Manitoba

©September 1999



National Library
of Canada

Acquisitions and
Bibliographic Services

395 Wellington Street
Ottawa ON K1A 0N4
Canada

Bibliothèque nationale
du Canada

Acquisitions et
services bibliographiques

395, rue Wellington
Ottawa ON K1A 0N4
Canada

Your file *Votre référence*

Our file *Notre référence*

The author has granted a non-exclusive licence allowing the National Library of Canada to reproduce, loan, distribute or sell copies of this thesis in microform, paper or electronic formats.

The author retains ownership of the copyright in this thesis. Neither the thesis nor substantial extracts from it may be printed or otherwise reproduced without the author's permission.

L'auteur a accordé une licence non exclusive permettant à la Bibliothèque nationale du Canada de reproduire, prêter, distribuer ou vendre des copies de cette thèse sous la forme de microfiche/film, de reproduction sur papier ou sur format électronique.

L'auteur conserve la propriété du droit d'auteur qui protège cette thèse. Ni la thèse ni des extraits substantiels de celle-ci ne doivent être imprimés ou autrement reproduits sans son autorisation.

0-612-45012-0

Canada

**THE UNIVERSITY OF MANITOBA
FACULTY OF GRADUATE STUDIES

COPYRIGHT PERMISSION PAGE**

**Suction Characteristics and Elastic-Plastic Modelling of
Unsaturated Sand-Bentonite Mixture**

BY

Gary Xiangmin Tang

**A Thesis/Practicum submitted to the Faculty of Graduate Studies of The University
of Manitoba in partial fulfillment of the requirements of the degree
of
Doctor of Philosophy**

GARY XIANGMIN TANG©1999

Permission has been granted to the Library of The University of Manitoba to lend or sell copies of this thesis/practicum, to the National Library of Canada to microfilm this thesis and to lend or sell copies of the film, and to Dissertations Abstracts International to publish an abstract of this thesis/practicum.

The author reserves other publication rights, and neither this thesis/practicum nor extensive extracts from it may be printed or otherwise reproduced without the author's written permission.

ABSTRACT

This thesis examines two aspects of unsaturated sand-bentonite behavior. The first is the suction characteristics of sand-bentonite at different saturation, water content, ion concentration, and moisture change history. Suctions of sand-bentonite are significantly outside the range normally encountered in normal geotechnical testing. The high suctions necessitate their measurement by using filter paper, vapour equilibrium and psychrometer techniques. Results produce suction - water content relationships and soil-water characteristic curves using different procedures.

The second aspect is the strength properties and elastic-plastic stress-strain behavior of the compacted unsaturated sand-bentonite. Quick undrained triaxial tests were conducted on specimens at saturations ranging from 50% - 98% to examine how saturation, matric suction and osmotic suction influence strength. The specimens possessed initial suctions arising from unsaturation, some of them had even higher suctions that resulted from introduced chemical agents. Strength properties were also examined using a series of tensile tests. Specimens compacted to 85% saturation at dry density of 1.67 Mg/m^3 and water content of 19.4% were used for this series of tests. Some specimens were also dried to lower water contents, that is, to higher suctions. The pivotal component of the testing program in this thesis is an extensive series of stress-controlled triaxial tests that involved monitoring suction changes and measuring deformations during the tests. The specimens were compacted at dry density of 1.67 Mg/m^3 with initial water content of 19.40% (corresponding to 85% saturation) and their subsequent alteration through drying to suction of approximately 6 MPa by imposing controlled relative humidity. The specimens were sheared under several selected stress paths. The results have developed a database to examine elastic-plastic stress-strain behavior of unsaturated compacted sand-bentonite mixture.

The equipment and test methodologies for measuring or controlling suctions have been developed for the first time in the geotechnical laboratories at the University of Manitoba.

Data showed that suction changes under pressure correspond to changes in the mean stress component of the stress tensor and are independent of the shear stress component. In unsaturated buffer specimens, the changes in suction with mean stress are largely reversible. The stress-strain behavior and strengths are found to be significantly dependent of suctions.

A new elastic-plastic conceptual model has been developed for highly plastic clays. The new model stems from two stress variables - stress ratio and equivalent pressure which are proposed as alternatives of commonly used matric suction and net mean stress. Based on the developed model, new concepts of yield envelope and stress state boundary are defined in p - q - S space. The model provides interpretation to all aspects of the elastic-plastic behavior and failure mechanism of unsaturated sand-bentonite observed in the testing program. For the first time, experimental yielding data of unsaturated specimens and saturated specimens can be normalized to a unified yield envelope.

ACKNOWLEDGMENTS

I wish to thank, most sincerely, my supervisor, Dr. James Graham for his valuable advice, continuous encouragement and support. He gave of his time and wisdom graciously so that I could accomplish this program. In many ways, his influence as my mentor is profound and will help me in my future career way more than another five years.

Thanks are also extended to the fellow graduate students for their friendship and support during my program. In particular I would like to acknowledge Dr. A.W-L. Wan from AECL, and G. Ferris, B. Wiebe, J. Blatz, T. Kirkham, T. Crilly, K. Bannister, K. Gelmich, K. Yuen and N. Tanaka from the University of Manitoba. They were also willing to engage in discussions about the experimental techniques and mechanical behavior of sand-bentonite. I acknowledge with thanks N. Piamsalee providing valuable technical assistance by which suction could be sensed right into micropores of samples. N. Lindsay and I. Trestrail provided office assistance.

I am indebted to Dr. D.G. Fredlund from University of Saskatchewan, Dr. M.N. Gray from Atomic Energy of Canada Limited for their valuable suggestions and discussions.

Financial support was provided by a research contract with Atomic Energy of Canada Limited, Pinawa, the Natural Sciences and Engineering Research Council of Canada, and U of M Teaching Assistantships throughout this study. In addition, a fellowship was awarded by Petro-Canada Ltd. They were greatly appreciated.

Finally, and most importantly, I would like to express my sincere thanks and love to my parents Xianyu Tang and Zhuqin Huang, and in particular to my wife Yan Zhu Tang, for their continuous encouragement, tremendous support and sacrifices in my study.

TABLE OF CONTENTS

ABSTRACT.....	i-ii
ACKNOWLEDGMENTS.....	iii
TABLE OF CONTENTS.....	iv-viii
LIST OF SYMBOLS AND ABBREVIATIONS.....	ix-xii
LIST OF TABLES.....	xiii
LIST OF FIGURES.....	xiv-xvi
CHAPTER 1 INTRODUCTION	1
1.1 General	1
1.2 Hypotheses.....	3
1.3 Objectives and Proposed Methodology of Research	5
1.4 Organization of Thesis	8
CHAPTER 2 LITERATURE REVIEW	11
2.1 Introduction.....	11
2.2 Soil Structure	11
2.2.1 Clay Mineralogy	12
2.2.2 Soil Structure	13
2.2.3 Soil Water	15
2.3 Soil Suction.....	16
2.3.1 Suction and Water Potential.....	16
2.3.2 Soil-Water Characteristic Curve	22
2.4 Experimental Techniques for Measuring and Controlling Suctions.....	24
2.5 Unsaturated Soil Mechanics	27
2.5.1 Volume Change	29
2.5.2 Shear Strength.....	30
2.5.3 Tensile Strength	31
2.5.4 Conceptual Elastic-plastic Model for Unsaturated Soils	32
2.6 Justification for Research Program	40

CHAPTER 3 MATERIALS AND SPECIMEN PREPARATION	42
3.1 Introduction.....	42
3.2 Materials	43
3.2.1 Buffer Material.....	43
3.2.2 Bentonite and Silica Sand.....	43
3.3 Mixing and Compaction of Unsaturated Specimens	44
3.4 Specimens with Special Treatment.....	45
3.4.1 Specimens with Matric Suctions Elevated by Drying at Controlled Suctions.....	46
3.4.2 Specimens with Osmotic Suctions Elevated by Introducing Osmotic Solutions.....	47
3.5 Specimen Designation	47
 CHAPTER 4 TECHNIQUES TO MEASURE AND CONTROL SUCTIONS: DETERMINATION OF SOIL-WATER CHARACTERISTIC CURVES	 50
4.1 Introduction.....	50
4.2 Psychrometer Technique.....	51
4.2.1 Thermocouple Psychrometers.....	52
4.2.2 The Campbell Scientific CR-7 Measurement and Control System.....	53
4.2.3 Calibration of Psychrometers.....	53
4.2.4 Measurement of Suctions.....	56
4.3 Vapour Equilibrium Technique	56
4.3.1 Principle	56
4.3.2 Solutions	57
4.3.3 Experimental Program	57
4.4 Filter Papers	58
4.4.1 Methodology.....	59
4.4.2 Filter Paper Calibration.....	59
4.4.3 Suction Measurement by Filter Papers	60
4.5 Determination of Suction - Water Content Relationships and Soil- Water Characteristic Curves	60
4.5.1 Suction - Water Content Relationship for Specimens Formed at Different Water Contents.....	61
4.5.2 Measurement of Suctions on Specimens Formed at an Initial Water Content and Subsequently Dried	65
4.5.3 Discussion.....	67
4.6 Evaluation of Osmotic Suctions.....	69
4.6.1 Initial Osmotic Suction	69
4.6.2 Elevation of Total Suctions by Osmotic Agents.....	70
4.7 Drying and Wetting Behavior of Buffer on Exposure to Osmotic Solutions	71

4.7.1	Specimens	71
4.7.2	Experimental Procedures	72
4.7.3	Test Results	74
CHAPTER 5 EQUIPMENT FOR TRIAXIAL TESTS AND TENSILE TESTS		77
5.1	Introduction.....	77
5.2	High Pressure Triaxial Cell.....	78
5.3	Psychrometer Techniques to Monitor Suction Change during Triaxial Tests	80
5.3.1	Construction of a Triaxial Load Cap with a Psychrometer.....	81
5.3.2	Installation of a Psychrometer In a Specimen for Triaxial Testing.....	81
5.4	Non-contacting Displacement Measuring System.....	82
5.5	Peripheral Equipment.....	83
5.5.1	Load System.....	83
5.5.2	Data Acquisition System.....	84
5.6	Leonard Farnell and B-K Triaxial Cells	84
5.7	Testing Facilities for Tensile Tests	85
CHAPTER 6 TESTING PROGRAM AND TEST PROCEDURES.....		87
6.1	Introduction.....	87
6.2	Quick-undrained Triaxial Tests	89
6.2.1	Tests on Compacted Specimens at Different Saturations	89
6.2.2	Tests on Compacted Specimens with Elevated Osmotic Suctions.....	90
6.3	Stress Controlled Triaxial Tests with Measuring Suctions and Deformation	92
6.3.1	Specimen Preparation	93
6.3.2	Test Procedures.....	93
6.3.3	Specimen Installation and Initial Suctions.....	94
6.3.4	Application of Loading for Triaxial Tests	95
6.3.5	End of the Test.....	96
6.4	Tensile Tests	97
6.4.1	Specimen Preparation	97
6.4.2	Installation and Setup.....	97
6.4.3	Test Procedures.....	98
CHAPTER 7 RESULTS OF QUICK UNDRAINED TRIAXIAL TESTS AND TENSILE TESTS.....		100
7.1	Introduction.....	100
7.2	Effect of Water Content on Strength and Stiffness.....	102

7.2.1	Quality Control Tests.....	102
7.2.2	Quick Undrained Triaxial Tests.....	103
7.3	Effect of Osmotic Suction on Strength and Stiffness	105
7.3.1	Effects of Osmotic Suction on Strength.....	105
7.3.2	Effects of Osmotic Suction on Stiffness	107
7.3.3	Osmotic Suction as a Dominant State Variable.....	108
7.3.4	Suction Changes after Specimens Experienced Stressing	109
7.4	Summary and Discussion.....	109
7.4.1	Summary	109
7.4.2	Discussion.....	112
7.5	Results of Tensile Tests	115
7.5.1	Tensile Strength of Unsaturated Buffer	115
7.5.2	Discussion of the Testing Methodology	117
CHAPTER 8 RESULTS OF STRESS-CONTROLLED TRIAXIAL TESTS.....		122
8.1	Introduction.....	122
8.2	Initial Conditions of Specimens.....	124
8.3	Stress-strain Behavior under Selected Stress Paths	127
8.3.1	Stress Paths	127
8.3.2	Isotropic Compression	128
8.3.3	Shearing	134
8.4	Suction Change Under applied Stresses	144
8.4.1	Suction Equilibrium under Loading.....	145
8.4.2	Suction Response to Stresses and Suction Reversibility	146
8.5	Final Evaluation of the Specimens after Tests.....	149
8.6	Interpretation of Tests Results Using the Existing Conceptual Model for Unsaturated Soils	150
8.6.1	The Existing Critical State Model for Unsaturated Soils.....	152
8.6.2	Interpretation of Stress-strain Behavior and Strength Properties of Unsaturated Buffer Material.....	153
8.7	Summary	160
CHAPTER 9 A NEW ELASTIC-PLASTIC CONCEPTUAL MODEL FOR UNSATURATED SOILS		162
9.1	Introduction.....	162
9.2	A New Elastic-plastic Conceptual Model for Unsaturated Soils.....	163
9.2.1	Yield Curve in p-S Space for Isotropic Loadings.....	164
9.2.2	Yield Envelopes in p-q Space and in q-S Space	167
9.2.3	State Boundary Surface and Yield Envelopes	172
9.2.4	Hardening Law.....	175
9.2.5	Failure and Flow Rule.....	177

9.3	Interpretation of the Stress-strain Behavior of Unsaturated Buffer	178
9.3.1	Strain Hardening	179
9.3.2	Strain Softening	181
9.4	Development of an Elastic-plastic Model for Unsaturated Sand-bentonite.....	182
9.4.1	Yielding.....	182
9.4.2	State Boundary Surface and Yield Envelopes	186
9.4.3	Flow Rule.....	190
9.4.4	Hardening Law.....	192
9.4.5	Critical State and M-values.....	195
9.5	Discussion and Conclusion	199
CHAPTER 10 REVIEW, CONCLUSIONS AND SUGGESTIONS FOR		
	FURTHER WORK	201
10.1	Review and Summary	201
10.2	Conclusions.....	204
10.3	Recommendations for Future Research	208

REFERENCES

LIST OF SYMBOLS AND ABBREVIATIONS

Symbols

θ	- Contact angle between the air-water-interface and the soil particle
ε	- Strain - Electronic charge
ε_1	- Axial strain
ε_v	- Volume strain
ε_s	- Shear strain
η_s	- Stress ratio $\eta_s = S/p$
λ	- Slope of the critical state line in V-lnp' space
κ	- Slope of the unload reload line in V-lnp' space - also Boltzman constant
ν	- Slope of total suction <i>versus</i> mean stress - also Poisson ratio - also cation valence
ρ	- Bulk density
γ_d	- Dry unit weight
σ'	- Total stress
σ_i	- Total stresses in the principal directions (i = 1, 2, 3)
σ'_i	- Effective stresses in the principal directions (i = 1, 2, 3)
σ^*	- interparticle contact stress
σ_n	- Normal stress
τ	- Shear stress
τ_f	- Shear stress at failure

ϕ^b	- Angle of internal friction with respect to matric suction changes
ϕ'	- Effective angle of internal friction
χ	- Bishop's Chi parameter related to degree of saturation of a soil specimen
ψ	- Total potential
ψ_π	- Osmotic potential
ψ_p	- Pressure potential
ψ_g	- Gravitational potential
ψ_m	- Matric potential
c	- Concentration of salt
c'	- Effective cohesion
C_v, C_m, D_v, D_m	- Material parameters of volume change
D	- Dielectric constant
D_{10}	- Particle diameter at which 10% of the particle diameters are smaller
D_{85}	- Particle diameter at which 85% of the particle diameters are smaller
e	- Void ratio - also unit electronic charge
E	- Elastic modulus
E_{50}	- Compression modulus or stiffness
G_s	- Specific gravity
h	- negative pressure in the water
M	- Slope of the q, p_e failure envelope
M_p	- Slope of the q, p failure envelope
M_s	- Slope of the q, S failure envelope
M^b	- Slope of the q, S failure envelope
n	- Number of molecules per mole of salt
N	- Axial load
p	- Mean stress
$p - u_a$	- Net mean stress
p_c	- Cell pressure

	- also preconsolidation pressure
p_e	- Equivalent pressure
p_{ec}	- Preconsolidation equivalent pressure
q	- Deviator stress
q_{cs}	- Deviator stress at Critical State
q_f	- Deviator stress at failure
$R - A$	- Net repulsive subtract attractive forces between soil particles
r	- radius of curvature of meniscus
R	- Universal gas constant
S	- Total suction
	- also matric suction
S_o	- Osmotic suction
S_m	- Matric Suction
S_r	- Degree of saturation
T	- Absolute temperature in Kelvin
	- also temperature in Celsius
T_s	- Surface tension
T_{max}	- Maximum tensile force
u_a	- Pore air pressure
$u_a - u_w$	- Matric suction
u_v	- Partial pressure of pore water vapour
$u_v/u_{v,o}$	- Relative humidity in the void space at equilibrium
u_w	- Pore water pressure
$u_{v,o}$	- Saturation pressure of water vapour over a flat surface of pure water at the same temperature
V	- Specific volume
V_w	- Specific water volume
$v_{w,o}$	- Specific volume of water
w	- Gravimetric water content

- w_i - Initial water content
 w_v - Molecular mass of water vapour

Abbreviations

- AECL - Atomic Energy of Canada Limited
B-K - Brainerd-Kilman Triaxial Cell
CSL - Critical State Line
DDL - Diffuse Double Layer
DIWC - Different Initial Water Content
FEM - Finite Element Method
IWC - Initial Water Content
LSSV - Length of Stress Vector
LSY - Loading Suction Yield Line
LVDT - Linear Variable Differential Transformer
LY - Loading Yield Line
MIP - Mercury Intrusion Porosimetry
OCR - Overconsolidation ratio
PEG - Polyethylene glycol
PSD - Pore Size Distribution
QC - Quality Control Tests
RBM - Reference Buffer Material
SBS - State boundary surface
SWCC - Soil-water characteristic curve
SY - Suction Yield Line

LIST OF TABLES

- Table 2.1 Devices for measuring or controlling soil suction and its components (after Fredlund and Rahardjo 1993)
- Table 3.1 Test designation and test condition
- Table 4.1 Initial conditions of specimens for drying and wetting tests
- Table 7.1 Summary of quality control specimens
- Table 7.2 Summary of quick undrained triaxial tests (confining pressure = 200 kPa)
- Table 7.3 Summary of quick undrained triaxial tests on specimens with osmotic agents (confining pressure = 200 kPa)
- Table 7.4 Specimens and test results
- Table 8.1 Initial conditions of the 'as compacted' specimens
- Table 8.2 Initial conditions of the 'after drying' specimens
- Table 8.3 Yield and strength of the specimens at two suction levels
- Table 8.4 Comparison of water content change before and after triaxial tests
- Table 8.5 Stress at failure and M values
- Table 9.1 Normalization of yield stress
- Table 9.2 Parameters of stiffness
- Table 9.3 Stresses at failure and the related parameters

LIST OF FIGURES

- Figure 2.1 Clay structural units and mineral
Figure 2.2 Soil structure (after Wan 1996)
Figure 2.3 Critical State Cam Clay model
Figure 2.4 Yield curves under isotropic loading in p-S space
Figure 2.5 Schematic of volume change and yielding (Alonso *et al.* 1987)
Figure 2.6 A conceptual model for unsaturated soils
Figure 2.7 Compressibility for unsaturated soils (Delage and Graham 1995)
- Figure 4.1 A schematic psychrometer
Figure 4.2 The CR-7 System
Figure 4.3 Calibration lines for psychrometers
Figure 4.4 Variation of temperature and suction with time
Figure 4.5 Layout of specimens and osmotic solution in a desiccator
Figure 4.6 Comparison of calibrations of Whatman 42 filter papers
Figure 4.7 Layout of soil specimen with filter papers
Figure 4.8 Total suction *versus* water content measured by psychrometers
Figure 4.9 Suction *versus* water content measured by filter paper method
Figure 4.10 Suctions *versus* water content
Figure 4.11 Total suction - water content relationships determined using different procedures
Figure 4.12 Suction-water content relationship of sand-bentonite (Wan *et al.* 1995)
Figure 4.13 Specimen preparation effects on strength (Wiebe *et al.* 1998)
Figure 4.14 Osmotic suction *versus* water content
Figure 4.15 Elevation of osmotic suctions
Figure 4.16 Soil-water characteristic curve (w: 22.4%)
Figure 4.17 Volume change by drying
Figure 4.18 Water content *versus* volume
Figure 4.19 Volume change behavior under drying and wetting
- Figure 5.1 Triaxial cell and psychrometer installation
Figure 5.2 Schematic diagram of a load cap equipped with a psychrometer
Figure 5.3 Photographs of a load cap equipped with a psychrometer
Figure 5.4 Oblique view of the designed tensile mould
Figure 5.5 Side view of tensile mould and load frame
- Figure 7.1 Results from quality control tests ($S_r = 85\%, 98\%$)
Figure 7.2 Max. deviator stress *versus* saturation
Figure 7.3 Elastic modulus *versus* saturation
Figure 7.4 Effects of total suctions contributed from matric suction
Figure 7.5 Max. deviator stress *versus* saturation

- Figure 7.6 Max. deviator stress *versus* total suction
- Figure 7.7 Elastic modulus *versus* saturation
- Figure 7.8 Deviator stress *versus* axial strain
- Figure 7.9 Effects of matric suction and osmotic suction on strength
- Figure 7.10 Finite element mesh for square specimen
- Figure 7.11 Influence of Poisson ratio on stress distribution
- Figure 7.12 Failure of the specimen in tensile mould
- Figure 7.13 Typical failure surface of the specimen
- Figure 7.14 Tensile strength *versus* total suction
- Figure 7.15a Finite element mesh
- Figure 7.15b Stress distribution along failure plane
- Figure 7.16 Influence of Poisson ratio on stress distribution
- Figure 7.17 Finite element mesh for square specimen
- Figure 7.18 Stress distribution at two forms of mould
-
- Figure 8.1 Stress paths for isotropic loading in p-S space
- Figure 8.2 Selected stress paths for shearing at apparent OCR = 2 or 3
- Figure 8.3 Typical consolidation curves (T16533/T16540)
- Figure 8.4 Suction changes under isotropic compression
- Figure 8.5 Expansion of yield locus in p-S space
- Figure 8.6 Specific volume *versus* mean stress
- Figure 8.7 Volume change with mean stress and total suction
- Figure 8.8 Axial strain ϵ_1 and lateral strain ϵ_3 with time (T16533)
- Figure 8.9 Shear strain under isotropic compression (T16533)
- Figure 8.10 Stress paths at shearing for specimens at two start suction levels.
- Figure 8.11 Deviator stress *versus* shear strain
- Figure 8.12 Stress-strain behavior for specimens sheared at apparent OCR = 2 and 3
- Figure 8.13 Deviator stress *versus* shear strain
- Figure 8.14 Deviator stress *versus* shear strain
- Figure 8.15 Identification of yield stress using bi-linear model
- Figure 8.16 Volume strain and shear strain with time (T16541)
- Figure 8.17 Yield stress and shear strength in p-q space
- Figure 8.18 Deviator stress *versus* volume strain
- Figure 8.19 Suction change with time in triaxial testing (T16533)
- Figure 8.20 Equilibrium of suctions at mean stress increments (T16533)
- Figure 8.21 Suction changes during triaxial test (T16533)
- Figure 8.22 Suction changes at shearing with constant mean stress (T16541)
- Figure 8.23 Changes in suction in p-q-S space (T16534)
- Figure 8.24 Yield loci at isotropic loading in p-S space
- Figure 8.25 A conceptual model for unsaturated soils
- Figure 8.26 Yield loci at different suction levels
- Figure 8.27 Stress paths for specimens at one suction level
- Figure 8.28 Traditional model to show yield and failure along stress paths

- Figure 8.29 Evolvement of stress state surface due to strain hardening
- Figure 8.30 Evolvement of stress state surface due to strain softening
- Figure 8.31 Failures after strain hardening for unsaturated soils
- Figure 8.32 Failure of a specimen along a stress path with decreasing mean stress
- Figure 8.33 Conventional M values *versus* total suction
-
- Figure 9.1 Schematic of load-induced yielding and development of a hardening surface (Alonso *et al.* 1987)
- Figure 9.2 Schematic of suction-induced yielding and development of a hardening surface (Alonso *et al.* 1987)
- Figure 9.3 Yield curves under isotropic loading in p-S space
- Figure 9.4 Yield envelopes at isotropic loading in p-S space
- Figure 9.5 Yield envelopes for zero suction
- Figure 9.6 Yield envelopes in q-S space
- Figure 9.7 Yield envelopes in p-S space at stress ratio η ,
- Figure 9.8 State boundary surface of the proposed conceptual model for unsaturated soils
- Figure 9.9 Compressibility for unsaturated soils (Delage and Graham 1995)
- Figure 9.10 Volumetric hardening
- Figure 9.11 Elastic-plastic behavior along various stress paths
- Figure 9.12 State boundary surface and yield envelopes
- Figure 9.13 Strain hardening and evolvement of state boundary surface
- Figure 9.14 Stress-strain behavior at two stress paths
- Figure 9.15 Strain softening
- Figure 9.16 Expansion of yield locus in p-S space
- Figure 9.17 Yield loci and motion under isotropic compression in p-S space
- Figure 9.18 Yield stress and shear strength in p-q space
- Figure 9.19 Normalized yield data and yield envelope
- Figure 9.20 Strain increments for a given Δq (T16530)
- Figure 9.21 Mean stress *versus* volume strain at shearing (T16530)
- Figure 9.22 Suction change under isotropic compression
- Figure 9.23 Specific volume *versus* mean stress
- Figure 9.24 Volume change with mean stress and total suction
- Figure 9.25 Specific volume *versus* equivalent pressure
- Figure 9.26 M values *versus* stress ratio
- Figure 9.27 Conventional M values *versus* total suction

CHAPTER 1

INTRODUCTION

1.1 General

Canada has proposed to dispose of its nuclear fuel waste effectively and permanently in deep stable geological formations of the Canadian Shield at depths of 500 m - 1000 m (EIS 1994). To fill spaces between waste containers and the surrounding rock, compacted sand-clay mixtures will be used to limit water flows and radionuclide fluxes into and from the repositories. Atomic Energy of Canada Limited (AECL) has proposed to use a 1:1 mixture of compacted sand-bentonite known as 'buffer'. The material has low hydraulic conductivity, high sorption capacity, and a perceived ability to swell and, thereby, seal unfilled voids in the engineered rock mass (Gray 1992). The sand-bentonite buffer will support the container, transmit waste heat to the surrounding rock, form an advective barrier to ground water, and provide a diffusive barrier to movement of radionuclide following any breaking of the container.

At the time of emplacement, the fuel waste will still be generating heat. In close proximity to the hot containers, the buffer will experience drying, whereas the outer boundary of

buffer close to the rock will hydrate and expand (Graham *et al.* 1996). Under these conditions, the fundamental properties of buffer materials have to be well understood. Good conceptual and numerical models of material performance need to be available. The buffer will initially be unsaturated. As time proceeds, buffer may dry and become less saturated, or may adsorb water from surrounding rock and become saturated.

Mechanical and hydraulic properties of saturated buffer have been investigated extensively by researchers at the University of Manitoba in collaboration with Atomic Energy of Canada Limited (Graham *et al.* 1996, Lingnau and Graham 1994). However, the behavior of unsaturated buffer has received much less attention, exceptions being the theses by Wan (1996) and Wiebe (1996), and a small number of papers arising from their work. Much further research must be undertaken if the Canadian Nuclear Fuel Waste Management Program is to be successfully presented to the Canadian public.

Considerable attention has been paid to developing fundamentals of unsaturated soil mechanics (Fredlund 1995). In recent years, this effort has been mainly directed towards developing models that rationalize the constitutive behavior of unsaturated soils (Alonso *et al.* 1990, Wheeler and Sivakumar 1995, Delage and Graham 1995). Despite progress in developing the models which have been supported by some experimental evidence, the models are still conceptual at this stage and further improvement is needed. On the other hand, most experimental techniques are only applicable to unsaturated soils at low ranges of suction and therefore inherently unsuitable for studies of sand-bentonite buffer in

which the suctions are high. For instance, the widely used axis-translation technique is limited to suctions less than 1.5 MPa, the highest available high air entry value of porous disks (Fredlund and Rahardjo 1993). This greatly restricts usefulness for testing unsaturated buffer, where suctions of 2-10 MPa are common. Accordingly, validation of theoretical models based on evidence from available data is currently only credible for low plastic, natural or compacted soils. Existing technologies and concepts of the elastic-plastic models need to be improved to accommodate densely compacted highly plastic buffer.

This research program was designed to investigate the suction characteristics and elastic-plastic behavior of unsaturated sand-bentonite and further develop an elastic-plastic model to frame experimental results. It also aimed at achieving experimental innovation, intellectual interest, and engineering application. The results were specifically directed towards a better understanding of the buffer material for the Canadian Nuclear Fuel Waste Management Program. Ideas and understanding developed in the program can also be applied to highly plastic clays or clay mixtures that are commonly adopted as construction materials for compacted structures such as earth dams and embankments, or as engineered barriers or backfill materials in geoenvironmental engineering.

1.2 Hypotheses

As in all unsaturated soils, the stress-strain behavior and strength properties of unsaturated buffer depend strongly on suctions (Wan 1996, Wiebe 1996). Suctions in

plastic clays are generally understood to have matric and osmotic components. (These terms will be defined later.) Hypotheses examined in this thesis are as follows:

Hypothesis 1

Matric suction and osmotic suction are separate stress state variables, with disparate effects in controlling strength and compressibility. Total suction can be reliably used as a state variable in describing mechanical properties only when contributions from both components are clarified.

Hypothesis 2

Laboratory tests in which suctions are carefully measured or controlled can reveal major features of suction-dependent constitutive behavior and strength properties.

Hypothesis 3

Like saturated sand-bentonite, unsaturated sand-bentonite buffer exhibits stress-strain behavior that can be characterized as elastic-plastic. Well-developed theory for saturated soils can be extended into an elastic-plastic model with suction as an independent stress-state variable to embrace the effects of suctions. The generalized model can describe elastic-plastic features of both saturated and unsaturated behavior.

1.3 Objectives and Proposed Methodology of Research

The hypotheses will be examined experimentally using a range of laboratory tests. To do so, suction-related techniques and expertise used elsewhere needed to be established and improved for use at the University of Manitoba. Prior to the author beginning this project, no testing on unsaturated soils, and therefore no suction measurements had been performed in the geotechnical laboratories at the University of Manitoba. The project involved tests to examine various aspects of the mechanical properties of unsaturated buffer and development of a new elastic-plastic model to interpret and describe the properties. The objectives of the test program were as follows:

1. Establishment of techniques for measuring or controlling suctions

Experimental techniques and expertise needed to be developed for testing unsaturated soils and measuring their suctions. The program included: 1) examining the applicability of existing techniques used elsewhere for measuring or controlling suctions, 2) establishing measuring techniques that are suitable for the high suctions in unsaturated buffer, and 3) improving existing techniques of measuring suctions in the class of stress-strain tests known as triaxial tests.

2. Examination of the suction characteristics of unsaturated buffer

Once these techniques had been established, the suction characteristics of unsaturated buffer were examined. Both the initial suctions and suction changes during pressure

sequences are required if soil behavior is to be described realistically. Initial suctions in unsaturated buffer can be expected to depend on water content, soil structure and specimen preparation. The latter will be associated with factors such as dry density, saturation, and salt content in the pore water (Wan *et al.* 1990, Delage and Lefebvre 1984). Relationships between suctions and these various controlling factors can be expected to predetermine soil behavior. As an example, the relationship between soil suction and water content, namely the soil-water characteristic curve (SWCC), can be used to predict strength and hydraulic properties (Fredlund and Xing 1996). When loads are applied, suction changes may be induced under certain test conditions. Nevertheless, interpretation of soil behavior can only be understood using the independent stress variables suction, net mean stress and deviator stress (Wheeler and Sivakumar 1995).

3. Testing of elastic-plastic behavior of unsaturated buffer

In classic soil mechanics, modelling the elastic-plastic behavior of clayey soils involves determining features that include yielding, a volumetric hardening law, a flow rule and failure (Wood 1990). For unsaturated soils, additional challenges arise since suction is involved as a state variable. For instance, apart from the fact that all elastic-plastic features are affected by suctions, even if no external loading is applied, soils may yield when they dry and experience increasing suctions. Soils also gain increased tensile strength with increasing suctions. Consequently, elastic-plastic models for unsaturated soils should be developed on the basis of three stress variables

in p-q-S space (for example, Fredlund and Morgenstern 1977, Alonso *et al.* 1990, Delage and Graham 1995). Here p = net mean stress, q = deviator stress, and S = matric suction. Variables are defined in List of Symbols at the beginning of the thesis (pages ix to xii).

The concept of yielding is a central feature of any elastic-plastic models. That is, stress-strain behavior falls into two parts, one recoverable or 'elastic', and the second non-recoverable or 'plastic'. The elastic and plastic parts are separated by 'yielding'. All other considerations of the models stem from the yielding concept (Oswell 1991). In unsaturated soils, what is needed is to determine a State Boundary Surface in p-q-S space (Alonso *et al.* 1990). Usually this is achieved by determining a family of yield loci in p-q space at constant suctions (Alonso *et al.* 1990, Wheeler and Sivakumar 1993, Tang *et al.* 1998b). To identify yield stresses, three broad types of tests will be carried out: 1) triaxial tests in which stress paths are selected in p-q space and suction changes under loading are monitored, 2) drying and wetting tests using a range of controlled suctions, and 3) tensile tests on unsaturated specimens at different suction levels. Triaxial tests involve $\sigma_1 > \sigma_2 = \sigma_3$, with specimens contained in rubber sheaths to separate them from the cell fluid used to apply σ_2 and σ_3 . (Test techniques will be defined later.) Triaxial tests along selected stress paths with constant values of $\Delta p / \Delta q$ allow examination of stress-strain behavior. Yield and strain hardening or strain softening were observed depending on the stress path of the test. Drying and wetting tests examined volume changes produced by suction changes, and the possibility of

yielding induced by increasing suctions. Tensile tests were performed using a new test technique developed in this program.

4. Development of an elastic-plastic model for unsaturated highly plastic clay

Finally, an elastic-plastic model was developed to describe stress-strain behavior observed from the testing program. Parameters for the model were determined from the data. The model provides a realistic relationship between suction, volume change, mean stress and deviator stress for unsaturated buffer. The model with calibrated parameters of the buffer can be used for analysis of the coupled hydro-mechanical problem of the Canadian Nuclear Fuel Waste Management Program (Graham *et al.* 1996). In general, the model can be used to describe the elastic-plastic behavior of all highly plastic clays.

1.4 Organization of Thesis

This thesis is organized as follows. Chapter 2 reviews literature pertinent to this research project. Soil properties associated with suctions and experimental techniques are discussed. Recent advances in unsaturated soil mechanics are reviewed with emphasis being placed on the recently developed framework of elastic-plastic modelling of unsaturated soils. Chapter 3 introduces the sand-bentonite material used in this study and describes specimen preparation procedures. Chapter 4 begins with a description of the thermocouple psychrometers used for measuring suctions. Filter paper and vapour

equilibrium techniques are then briefly introduced. These techniques were used to evaluate suction - water content relationships or to determine soil-water characteristic curves.

Triaxial testing equipment is described in Chapter 5 and a new technique for incorporating psychrometers into triaxial tests is highlighted. A designed device for tensile tests on unsaturated buffer is also described. Chapter 6 describes the testing program and procedures. The tests were performed mostly to examine stress-strain behavior using stress-controlled triaxial compression procedures with suctions and strains being measured. In a subsidiary program, strength properties were examined by 'quick' undrained triaxial tests on specimens prepared at different saturations or with different contents of osmotic agents. Tensile strengths of specimens at different suction levels were also measured. Results of strength properties from quick undrained tests and tensile tests are presented in Chapter 7, and results of stress-strain behavior are described in Chapter 8. Chapter 8 also describes an interpretation of the test results using an existing conceptual model for unsaturated soils. The results led to apparent values of a series of soil properties that must be considered anomalous. It was concluded that the model is inadequate for these tests. Chapter 9 presents a new conceptual model and demonstrates the model provides a satisfactory, consistent interpretation for all aspects of elastic-plastic behavior of unsaturated sand-bentonite.

Chapter 10 summarizes the research program and outlines conclusions and suggestions for further research.

CHAPTER 2

LITERATURE REVIEW

2.1 Introduction

This chapter reviews the fundamentals of suction theory and advances in modelling of suction-influenced stress-strain behavior of unsaturated soils. It begins with a brief discussion of clay mineralogy, soil structure and soil water. It then describes suctions, suction components and suction-water content relationships. Since experiments are part of this research, it goes on to describe techniques for suction measurement and control used in laboratory testing, particularly used in triaxial tests. Finally, advances of unsaturated soil mechanics are discussed with emphasis being placed on elastic-plastic models which capture many aspects of unsaturated soil behavior. The chapter concludes with discussion of justification of this research program.

2.2 Soil Structure

The presence of only a small amount of clay minerals in soils can considerably influence their physical properties (Lambe and Whitman 1979). Evidence from experiments on

saturated sand-bentonite mixture indicates that although sand-bentonite material is made up of equal portions (by mass) of sand and bentonite, it is the bentonite that dominates the behavior (Graham *et al.* 1988), especially suction characteristics (Wan 1996). For this reason, this section reviews knowledge of clay and clay-water systems. Physical properties of sand and bentonite will be described in Chapter 3 - Materials and specimen preparation.

2.2.1 Clay Mineralogy

There are three major groups of clay minerals: kaolinite, illite and montmorillonite. They are colloidal size particles originating from the weathering of igneous or metamorphic rock (Grim 1953). The basic structural units of most clay minerals consist of a silica tetrahedron and an alumina octahedron (Figure 2.1a) (Mitchell 1976). (Figures are presented at the end of each chapter.) Silicon and aluminum in these units may be partially replaced by other elements with similar atomic size but different valency in the process known as 'isomorphous substitution'. The basic units combine to form sheet structures of silica tetrahedra and aluminum octahedra as represented symbolically in Figure 2.1b. Stacking of combinations of the basic sheet structures forms different clay minerals with various forms of bonding between the combined sheets. The bentonite used in this research program is primarily related to Na-montmorillonite (Dixon *et al.* 1996). A montmorillonite layer structure is composed of one sheet of aluminum octahedra between two sheets of silica tetrahedra as illustrated in Figure 2.1c.

There are substantial isomorphous substitutions in montmorillonite. As a result, the particles carry large amounts of negative surface charges. Bonding between these sheets results in part from van der Waals forces, and more significantly from the presence of exchangeable cations adsorbed between two adjacent silica tetrahedra. Like most clays, montmorillonite minerals are of 'plate-like' form having a high specific surface ($800\text{m}^2/\text{g}$) (Yong and Warkentin 1975). Because of their shape and high specific surface, mineral properties can be greatly influenced by electrical forces between neighboring clay particles (Lambe and Whitman 1979).

2.2.2 Soil Structure

Soil structure plays an important role in influencing the properties and behavior of compacted clays (Barden and Sides 1970, Mitchell 1976). Soil structure is the physical constitution of a soil as expressed by the size, shape, and arrangement of the solid particles and associated voids (Brewer 1964), and it is intimately related to inter-particles forces (Yong and Warkentin 1975). The development of soil structure in compacted clays is a phenomenon associated with material preparation and compaction. Early concepts of soil structure of compacted clays were based on individual particles (Lambe 1958). According to this concept, soils compacted to the dry side of the optimum water content tend to develop a flocculated, edge-to-face single particle arrangement. In

contrast, soils that are formed on the wet side of the optimum possess a dispersed structure in which clay particles are arranged in a more parallel face-to-face manner.

More recent studies have discovered that interactions between single isolated particles are seldom found in compacted clays according to observations using scanning electron microscopes (Barden 1971, Wan 1987). This is because clay particles tend to coalesce on initial wetting to form peds due to physico-chemical interactions within the clay-water system (see Figure 2.2). The peds behave essentially as individual particles, and so the behavior and properties of soils depend largely on interactions between the peds. To a large extent, the size and stiffness of the peds in a compacted clay soil depend on the moulding water content (Wan *et al.* 1990). At higher water contents, peds are larger and wetter, and tend to be easily distorted by compaction and shear forces. In contrast, peds formed at lower water contents are smaller and stiffer. The stiffness of these drier peds is attributable to suction within the fabric units (Barden and Sides 1970).

Yong and Warkentin (1975) identified three general classes of structure: a) macrostructure, b) microstructure, and c) ultra-microstructure. Macrostructure is made up of peds and aggregates which can be seen with the naked eye. The spaces between adjacent macrostructural units are known as macropores or inter-aggregate pores. Microstructure contains clusters which are discernible under an optical microscope, while ultra-microstructure includes both individual particles and domains which can only be seen under an electron microscope. These two classes are commonly termed

microstructure. Spaces between adjacent microstructural units are called micropores or intra-aggregate pores. The concept of macropores and micropores appears to be supported by evidence from mercury intrusion porosimetry tests. Pore size distribution (PSD) curves of clay specimens compacted dry of optimum exhibit a bimodal distribution (for example, Ahmed *et al.* 1974). This is also shown in the results from compacted sand bentonite and sand illite mixtures (Wan *et al.* 1995). It will be demonstrated that the bimodal distribution of macropores and micropores sand-bentonite provides an improved understanding of the suction characteristics featured in this study.

2.2.3 Soil Water

Water is a dipolar molecule (Grim 1953), where the resultant positive charge from the two hydrogen atoms does not coincide with the negative charge from the oxygen atom. As a result, water molecules can be attracted to negatively charged clay surfaces through hydrogen bonding (Dixon 1995).

In clay soils, water exists in three different forms (Cheung *et al.* 1987). The surface water is the first few molecular layers of water tightly attached to the clay particle surface and behaves in many ways like part of the clay surface when soil behaviour is considered. Further away from the mineral surface is adsorbed water. The surface water and adsorbed water are referred to jointly as structural water which is restricted from moving

through the soil (Mitchell 1976, Dixon 1995). The negative surface charges associated with the clay particles present an electrified interface. Since soil-water contains dissolved solutes with positive charges, the interaction between a negatively charged soil particle surface and the cations in the soil-water will generate a so-called diffuse double layer (DDL) (Yong, Mohamed and Warkentin 1992). The diffuse double layer theory provides a microscopic conceptual model to explain the influence of the clay-water system on plasticity, compaction, interparticle bonding, and water movement of clay soils (Yong and Warkentin 1975, Dixon 1995). The final form, free water, is unaffected by the electrical charges of nearby clay particles. It is free to move throughout the soil matrix provided that the pores are interconnected.

It will be shown later that suctions arise in structural water and free water from different mechanisms.

2.3 Soil Suction

2.3.1 Suction and Water Potential

The retention and movement of water, and deformation and strength properties in an unsaturated soil are related to the energy status of soil water (Brady 1974). In soil science, the energy status of the soil water is usually expressed in terms of potential. Total potential can be represented by the sum of matric potential ψ_m , gravitational

potential ψ_g , osmotic potential ψ_π , and pressure potential ψ_p (Yong and Warkentin 1975).

That is,

$$\psi = \psi_m + \psi_g + \psi_\pi + \psi_p \quad [2.1]$$

Particular care needs to be taken when using this expression to evaluate fluxes into and out of unsaturated soils. As used in geotechnical engineering, the terms suction and negative pore water pressure (for example in kPa) provide a more mechanistic picture of the state of soil water in relation to the strength, compressibility, stress-strain response and hydraulic conductivity of unsaturated soils. This usage reflects only two of the components that comprise total potential. The sum of the two components is called total suction.

$$S = S_m + S_\pi \quad [2.2]$$

where S is total suction, S_m and S_π are matric suction and osmotic suction respectively. They will be discussed in the following sections. (Suction, expressed as a positive value, is the negative of a potential which is itself negative.)

A more rigorous definition of total suction is given by the Kelvin equation (Aitchison 1965) from a thermodynamic context:

$$S = -\frac{RT}{v_{w0} w_v} \ln\left(\frac{u_v}{u_{v0}}\right) \quad [2.3]$$

where S = total suction, R = universal (molar) gas constant, T = absolute temperature, K , v_{w0} = specific volume of water, w_v = molecular mass of water vapour, u_v = partial pressure

of pore water vapour, u_{v_0} = saturation pressure of water vapour over a flat surface of pure water at the same temperature, and u_v/u_{v_0} = relative humidity in the void space at equilibrium. In this definition, total suction is related to temperature and relative humidity. Although mechanisms of suction are not explicit in this expression, total suction is related to relative humidity, which is measurable or controllable in laboratory testing. Suction measurements by thermocouple psychrometer techniques and the vapour equilibrium method are based on this definition.

2.3.1.1 Matric suction

Matric suction ($S_m = u_a - u_w$) is defined as the difference between the pore air pressure, u_a , and the pore water pressure, u_w . The pore water pressure 'results from that part of the boundary stresses that is transmitted to the water phase from pressures generated by capillary menisci and from water adsorption forces exerted by particles surfaces' (Mitchell 1976). Technically, the menisci result from the water potential and the pore size distribution. The verb 'generated' in Mitchell's statement may be misleading. There are two mechanisms that control matric suction properties in an unsaturated soil (Richards 1974). They are the capillary effect and adsorption of water on clay minerals. The contribution of each mechanism to matric suction as a whole depends on soil composition and soil structure.

For sands and other cohesionless materials, suctions are primarily attributed to capillary phenomena that can be expressed through differences between pore air pressure u_a and pore water pressure u_w . In these soils, the water is present as free water and pores with small radii act in a similar way to capillary tubes. The capillary model of matric suction can be used successfully to quantify the matric suctions. That is,

$$h = \frac{2T \cdot \cos\theta}{r} \quad [2.4]$$

where h is negative pressure in the water, T , is the surface tension of the air-water interface, and r is the radius of curvature of the meniscus. θ is contact angle.

Suctions are therefore related to the pore size distribution within the particle structure of granular soils. The pore size distribution is in turn affected by the packing of the soil particles and hence is directly related to the dry density of the soils (Fredlund and Xing 1994). Estimation of matric suction can be successfully made using a model based on capillarity.

In highly plastic clays, however, the particles are no longer inert, and pore water pressures are significantly affected in the structural water due to adsorption of water on clay mineral particles (Richards 1974, Yong and Warkentin 1975). This gives rise to a second component of matric suction in addition to capillary effects. Gens and Alonso (1992) indicate it is likely that microstructure (forming the aggregates) in active clays can be completely saturated, while the macrostructure is unsaturated. Air-water interfaces may not

exist inside the micropores at all, but may only be present at the edges of the aggregates where they combine to form macropores (Figure 2.2). Under these conditions the contribution of the capillary component is small, yet electro-chemical suctions are high. The capillary model no longer applies to these kinds of material. This is supported by the experimental observation that suctions in compacted clays are largely independent of dry densities. An explanation for the insensitivity of measured suction to density change has been provided by Croney *et al.* (1958). In general, the authors suggest that a compacted clay is composed of aggregates or peds of clay particles which may be saturated or unsaturated, and macroscopic intra-aggregate pores which are unsaturated. A change in soil density basically leads to a change in the magnitude and arrangement of the macroscopic voids. The presence of these macroscopic voids has little bearing on the suction of the soils as a whole which is controlled by the microstructure. The soil microstructures inside the aggregates are influenced by the moulding water content (Musa 1982, Wan 1996) and not by compaction unless considerable changes are made to compactive effort. The size and distribution of micropores is generally stated to be independent of changes in dry density. For normal ranges of compactive effort, it is primarily the initial forming water content which dictates the suction, and consequently the mechanical behaviour, of unsaturated clays. Even though there are two distinct mechanisms controlling matric suction (capillarity and electrochemistry), they cannot be separated experimentally.

In most unsaturated soils, osmotic suction changes only slowly; changes in the matric component are often larger due to drying-wetting, compression and heating-cooling. Matric

suction effects therefore tend to be more significant than osmotic suction effects (Wan 1996, Wiebe 1996). In this case, matric suction changes can be substituted for total suction changes, and vice versa (Fredlund and Rahardjo 1993).

2.3.1.2 Osmotic suction

Osmotic suction is closely related to the dissolved salt content in the pore water of soils, and is written in terms of pressure (Fredlund 1995). The osmotic suction can be approximated by the van't Hoff equation (Metten 1966):

$$S_x = nRTc \quad [2.5]$$

where: n = number of molecules per mole of salt; R = universal gas constant; T = absolute temperature; c = concentration of salt. Salts can exist in soil water in both saturated and unsaturated soils. For this reason osmotic suction can affect both saturated and unsaturated soil behaviour.

In expression [2.5], the concentration of salt - ' c ' can be changed by either changes in water content or the amount of dissolved salts, thereby producing changes in osmotic suction. With changing water content, evidence from suction vs. water content relationships indicates that osmotic suction does not change significantly (Fredlund and Rahardjo 1993). In support of this view, Wan *et al.* (1995) show that osmotic suctions vary only slowly with water content in highly plastic clays such as buffer. In contrast, osmotic suction can

be expected to change more significantly when the salt content of the pore water is altered.

Some researchers believe that, for soils with large quantities of clay minerals, the swelling pressure is related to osmotic suction (Pile 1980, Graham *et al.* 1988). The swelling pressure is associated with the electrostatic repulsive-minus-attractive stresses, R_A , between clay particles (Graham *et al.* 1992). According to the diffuse double layer theory, the presence of salt ions in pore water affects the thickness of the diffuse double layer, decreases the vapour pressure in the pore spaces, and gives rise to the development of osmotic suction (Barbour 1987, Barbour and Yang 1993).

Limited experimental evidence in the literature concerning the influence of osmotic suction on soil strength has provided confusing conclusions. Blight (1983) indicated that osmotic suction does not contribute significantly to shear strength. However, in contrast, Ho and Pufahl (1987) noted that strength increases with increase in osmotic suction. To date, the effects of changes in osmotic suction on the behaviour of compacted clays such as buffer are still relatively unknown. This topic will be examined in tests reported later.

2.3.2 Soil-Water Characteristic Curve

As described previously, soil suction depends on the water content and physical-chemical properties of soils such as composition, pore fluid chemistry, structure, and density. For

a given soil, suction increases inversely (but not linearly) with water content. The relationship between suction and water content is known as a Soil-Water Characteristic Curve (SWCC). Since SWCCs are intimately associated with the physical-chemical properties of soils, they can be used to estimate the strength and hydraulic conductivity (Fredlund *et al.* 1995).

The SWCCs are usually plotted in terms of matric suction or total suction *versus* water content. For granular soils, matric suction *versus* water content is commonly measured using a pressure plate apparatus (Fredlund and Rahardjo 1993). By controlling pore air pressure and pore water pressure separately, a soil specimen is allowed to dry gradually in successive increments of applied suction, thereby producing a continuous curve of suction *versus* water content. It should be noted that this is essentially a drying (or wetting) process in which water content changes in response to a range of controlled suction levels. The measurement procedures are most suitable for granular soils in which low suction and high permeability allow water move freely through the soil.

Although evaluation of SWCCs has become common practice in Soil Science where the interest is mainly on natural soils with low suctions, determination of SWCCs in geotechnical engineering has not yet been standardized, particularly for compacted clayey soils with high suctions. In highly plastic clays, most of the soil water is 'structured' and cannot yet be controlled easily. Pore water pressure (and hence matric suction) cannot be controlled, so the design of testing program becomes difficult. Instead, total suctions are

usually determined using psychrometer and filter paper, and vapour equilibrium techniques. These will be described later.

Using a combination of these techniques, Wan (1996) determined a total suction - water content relationship for a compacted sand-bentonite mixture. Different procedures were adopted. Psychrometers and filter papers were used to measure suctions of the specimens in cases where the specimens did not change water content during measurements. Different specimens at several water contents were used. In contrast, vapour equilibrium techniques measured suctions in specimens where water contents changed during measurements. In these tests, the same specimens were used at different suction levels. Using a combination of measuring techniques conveniently produces suction - water content relationship over a wide range of water content. However, SWCCs determined from dried specimens may differ from curves measured from separate specimens at different water contents. Work carried out in this study clarifies uncertainties regarding the influence of measurement methods on the results.

2.4 Experimental Techniques for Measuring and Controlling Suctions

Commonly used devices to determine suctions are listed in Table 2.1. They can be categorized as measurement and control methods. Most of the devices have been developed in the soil science discipline where suctions of soil samples need to be measured under

constant ambient conditions. As outlined in the preceding section, measuring suctions in dried soil samples produces the SWCCs. In geotechnical engineering, suction changes need to be monitored or controlled when a soil specimen is subject to other changes such as changes in loading, temperature, chemistry, etc. Modification of devices developed in soil science is therefore often necessary for geotechnical testing.

Table 2.1: Devices for measuring or controlling soil suction and its components
(after Fredlund and Rahardjo 1993)

Measurement Device	Suction Measured	Range (kPa)
Psychrometer	Total	100 - ~8000
Filter paper	Total and matric	(entire range)
Thermal conductivity sensors	Matric	0 - ~400+
Tensiometers	Negative pore water pressure	0 - 90
Pore fluid squeezer	Osmotic	(entire range)
Control Device	Suction Controlled	Range (kPa)
Pressure plate (axis-translation)	Matric	0 - 1500
Osmotic vapour technique	Matric	in development
Vapour equilibrium method	Total	(entire range)

For example, the pressure plate apparatus incorporating the axis-translation technique is commonly used to determine soil suctions by separately controlling pore air pressure u_a and pore water pressure u_w so that u_w and $(u_a - u_w)$ are both positive. This avoids cavitation problems when u_w drops below about -70 kPa relative to atmospheric pressure. Conventional test equipment such as oedometers and triaxial cells can be readily modified to accommodate such techniques by using ceramic porous disks which are similar to the porous plates in a pressure plate apparatus. Although this technique has been successfully used, it is usually limited to pressures less than about 1.5 MPa. As a result, it

is usually restricted to measuring the relatively low suctions in natural soils and granular materials (Ridley and Burland 1993). It appears not to be applicable to dense clay mixtures such as the AECL sand-bentonite material due to the limited suction range. An alternative approach is the osmotic technique in which suction is controlled by external osmosis (Kassif and Ben Shalom 1971, Delage *et al.* 1987). A soil sample is placed on a semi-permeable membrane which is permeable to water but not permeable to osmotic agents. A solution of polyethylene glycol (PEG) is circulated beneath the membrane. The large sized PEG molecules cannot go through the membrane, resulting in an osmotic suction applied to the sample. In its original form the osmotic technique is able to reach values of suction up to 1.5 MPa. Further development has extended the suction range to 10 MPa (Delage *et al.* 1995). With increasing suction, however, lower permeable membranes are required and equilibrium time is longer (about 40 days at a suction of 9 MPa).

So far, no means have been found that can be effectively used to control matric suction directly for unsaturated buffer in which suctions of 2 - 10 MPa are common. In other words, the influence of suction on the mechanical properties of unsaturated buffer cannot be examined using the traditional way of performing tests at various controlled suctions. However, the author realised that, it would be equally important if suction changes could simply be monitored under controlled stress conditions. To a large extent, examining the behavior of unsaturated soils means relating changes in suction to other geotechnical parameters.

Among the techniques used in laboratory tests to measure high suctions in unsaturated soils, the thermocouple psychrometer technique is the most promising due to its small size, quick response, accuracy and reliability (Fredlund and Rahardjo 1993, Wan 1996). The use of psychrometer techniques has not become common practice in geotechnical testing. For triaxial testing, the use of psychrometers requires the ability to obtain reliable measurements under conditions where loading and temperature may be changing independently. Two approaches have been developed for installing psychrometers in triaxial tests. One is done by inserting or burying a psychrometer in the center of a specimen (Wan *et al.* 1995). The second is done by inserting an open psychrometer inside a plastic load cap and then placing the cap in tight contact with the specimen (Edil and Motan 1984). Burying a psychrometer inside the specimen makes compaction more complicated and may lead to physical disturbance that affects the mechanical behaviour. Installing an open psychrometer in a load cap may readily lead to damage and contamination of the thermocouple because its shield is removed. The author decided that while psychrometers were promising, improvements in existing techniques were needed.

2.5 Unsaturated Soil Mechanics

The effective stress concept proposed by Terzaghi (Terzaghi 1936) is pivotal in soil mechanics:

$$\sigma' = \sigma - u_w \quad [2.6]$$

where σ' = effective stress, σ = total stress, u_w = pore water pressure.

This form of the effective stress concept only holds true for fully saturated granular silts, sands and gravels, or low plasticity clays. Terzaghi defined effective stress to be the component of the stress system that controls strength and compressibility of the material. For medium- to high-plastic clays where diffuse double layers significantly interfere with direct mineral-mineral interfaces, an (R-A) term that accounts for unit physico-chemical repulsive (R) and attractive (A) forces is incorporated into the equation (Graham *et al.* 1992).

$$\sigma' = \sigma^* + (R-A) = \sigma - u_w \quad [2.7]$$

where σ^* = interparticle contact stress (average unit force)

(R-A) = net unit repulsive and attractive force.

For unsaturated soils, a more complicated principle of effective stress is required to model the stress regime. The first attempt was made by Bishop (1959) who defined effective stress by combining net normal stress ($\sigma - u_a$) and matric suction ($u_a - u_w$) effect through a ' χ parameter':

$$\sigma' = (\sigma - u_a) + \chi (u_a - u_w) \quad [2.8]$$

The χ parameter is strongly non-linear with stress increases, and also intimately related to the degree of saturation of the soil. A soil property is therefore involved in the description of stress state. This led Jennings and Burland (1962) and Coleman (1962) to propose that

the two stress components in the expression for χ should be treated separately rather than be combined into a single-valued expression. As a result, the net normal stress and matric suction were seen as having separate influences in describing unsaturated behaviour (Matyas and Radhakrishna 1968). Later, matric suction proved to be a stress state variable (Fredlund and Morgenstern 1977). Subsequent studies allowed the basic theories of unsaturated soil mechanics to be examined in three primary areas of study: namely, seepage, shear strength and volume change (Fredlund 1979). Each of the areas has been examined extensively and numerous examples can be found in the literature. In a different, more integrated approach, elastic-plastic frameworks derived from critical state theory have been developed to provide better understanding of combined volume change and stress effects (Alonso *et al.* 1990). Following sections review major advances in this constitutive framework and in strength theory. Seepage and permeability studies have been excluded from the thesis. They are important and justify further work, but were not part of this project.

2.5.1 Volume Change

Volume change in saturated soils is equal to the change in the volume of water since soil particles are considered to be incompressible. In unsaturated soils, independent changes in water and air phases require two separate constitutive equations for complete volume-mass characterization. Because changes in volume of the air phase are not easily

determined, volume changes of the soil structure are commonly used instead. General expressions for the volume change in the soil structure and in the water phase of an unsaturated soil can be expressed in the following forms (Fredlund and Morgenstern 1976):

For soil structure,

$$\Delta e = C_r \Delta \log(\sigma - u_a) + C_m \Delta \log(u_a - u_w) \quad [2.9]$$

For water phase,

$$\Delta w = D_r \Delta \log(\sigma - u_a) + D_m \Delta \log(u_a - u_w) \quad [2.10]$$

where e is void ratio, w is water content, $(\sigma - u_a)$ is net mean stress, $(u_a - u_w)$ is matric suction, and C_r , C_m , D_r , D_m are material parameters determined experimentally.

These equations are written for the case of isotropic loading (Fredlund 1995). In other loading conditions, a full description of specimen deformation involves changes in volumetric strain, shear strain, and water content. These equations shown earlier do not reflect the changes in shear strain.

2.5.2 Shear Strength

In its simplest form, the shear strength of unsaturated soils has been formulated as a linear combination of the stress state variables and associated shear strength parameters (Fredlund *et al.* 1978).

$$\tau = c' + (\sigma - u_a) \tan\phi' + (u_a - u_w) \tan\phi^b \quad [2.11]$$

The representation of shear strength depends on net mean stress $\sigma - u_a$, matric suction $u_a - u_w$, effective cohesion c' , effective friction angle ϕ' , and the rate of increase in shear strength relative to matric suction $\tan\phi^b$, on the failure plane at failure. As the testing of unsaturated soils has been extended over a larger range of suctions and soil types, increasing evidence has shown that the shear strength relationship involving suction is nonlinear (Fredlund *et al.* 1987). That is, ϕ^b is not constant.

An alternative form of the linear shear strength equation for unsaturated soils makes use of the triaxial stress state variables $q = (\sigma_1 - \sigma_3)$, $(p - u_a) = (\sigma_1 + 2\sigma_3)/3 - u_a$ and $(u_a - u_w)$. At failure, the strength equation can now be written (Maatouk *et al.* 1995, Wiebe 1996):

$$Q_f = c_{pq} + M(p - u_a)_f + M^b (u_a - u_w)_f \quad [2.12]$$

where q_f = deviator stress on failure plane at failure; c_{pq} = intercept of the deviator stress and net mean stress failure envelope with the q-axis where the p stress and matric suction are separately zero; M = slope of the q, p failure envelope; and M^b = slope of the q, $(u_a - u_w)$ failure envelope.

2.5.3 Tensile Strength

Only a few tensile tests have been reported on saturated soils to examine cementation bonds of clays (Conlon 1966, Bishop and Garga 1969). Otherwise tensile strengths of soils are in most cases neglected. With increasing interest in the study of unsaturated

soils. there are a number of hypotheses on the importance of tensile strength of unsaturated soils (Alonso *et al.* 1990, Delage and Graham 1995). However, to date, no tensile tests on unsaturated soils have been reported and hypotheses remain unproved.

2.5.4 Conceptual Elastic-plastic Model for Unsaturated Soils

As described in the preceding section, volume change behavior and shear strength have been separately related to two stress state variables (Matyas and Radhakrishna 1968, Fredlund *et al.* 1978). Following the lead taken in saturated soil mechanics, more generalized constitutive models should be developed for unsaturated soils that link volume change and shear strength in an integrated way to describe stress-strain behavior. The first tentative steps were made by Alonso *et al.* (1987) towards the development of a framework for unsaturated soils based on critical state theory. In this section, elastic-plastic critical state modelling for saturated soils is briefly reviewed first. This is followed by a description of how this model can be extended to unsaturated soils.

2.5.4.1 Elastic-plastic critical state model for saturated soils

The best known of the elastic-plastic models, Cam Clay, is associated with Critical State soil mechanics. This approach links volume changes and stress changes to account for features of soil behavior that cannot be accommodated easily in traditional non-linear soil mechanics (Roscoe *et al.* 1958, Roscoe and Burland 1968). A three dimensional State Boundary Surface in the p' - q - V space can be defined as shown in Figure 2.3a, inside

which the behavior of the soil is elastic, and on which the behavior is plastic. In general, an elastic-plastic model has five elements: elasticity, yield, flow rule, a hardening law, and a strength law. Yielding often involves non-recoverable (plastic) compression and so the models are often known as volumetric hardening plasticity models. The commonly used model called Modified Cam Clay assumes that the soil is saturated, its elasticity is isotropic, its yield functions are elliptical, the flow rule is associated, the hardening law is logarithmic, and the strength law is the Mohr-Coulomb rule. That is, the yield locus for a given consolidation pressure is elliptical in p - q space (Figure 2.3b), the plastic hardening law is straight (with slope in V - $\ln p'$ space) (Figure 2.3c), and plastic strain increment vectors are normal to the elliptical yield locus.

2.5.4.2 State variables

It is now generally accepted that total stress σ , pore air pressure u_a and pore water pressure u_w must be combined in two independent stress state variables in order to describe the mechanical behavior of unsaturated soils (Fredlund and Morgenstern 1977). The two stress state variables normally selected are net mean stress ($\sigma - u_a$), and matric suction, ($u_a - u_w$). The volume change behavior (Matyas and Radhakrishna 1968, Fredlund and Morgenstern 1977), permeability and shear strength (Fredlund *et al.* 1978) of unsaturated soils have been successfully related to these two stress state variables. In this approach, soil states are defined in terms of stress. Soil responses including changes

in water content and specific volume (void ratio) are determined from changes in net mean stress and matric suction.

More formally, soil state is described on the basis of a State Boundary Surface (SBS). For a saturated soil, as shown earlier in Figure 2.3, the state boundary surface is defined in p' - q - V space. That is, the response of the soil depends on its mean effective stress p' , the deviator stress q that has been imposed, and the physical arrangement of its soil particles (measured by specific volume V). Alonso *et al.* (1990) extended the critical state framework for unsaturated soils to include the effect of four state variables: net mean stress p , deviator stress q , suction S , and specific volume V . In further development of this model, Wheeler and Sivakumar (1993) argued that a second volumetric parameter (in addition to specific volume V), such as water content w , specific water volume V_w , or degree of saturation S_r , is also required to fully define the volumetric state of an unsaturated soil. This means that an unsaturated critical state model is likely to involve five state variables: net mean stress σ_u , deviator stress q , suction S and specific volume V ($V=1+e$) and water content w . Changes in volume involve changes in the volumetric strain (calculated directly from the changes of the state variable V). Changes in shear strain are, calculated from an elastic shear modulus G , a suitable flow rule, and the change of water content w . In addition, they show that specific water volume V_w (the volume of water plus solids in a volume of soil containing a unit volume of solids), defined by $V_w = 1 + S_r e = 1 + w G_s$ is preferable as the parameter describing the amount of water within a soil element. The use of specific volume V and specific water

volume V_w provides a full description of the volumetric state of an unsaturated soil. However, care must be taken for highly plastic clays. It is gravimetric water content rather than volumetric water content that dominates soil behavior.

In these models, matric suction is usually used as the state variable for suction (Fredlund and Rahardjo 1993). In the case where the salt content of soils is altered by chemical contamination, the effect of the resulting changes in osmotic suction on the soil behavior may be significant. In this case, it is necessary to consider osmotic suction as part of the stress state system (Fredlund and Rahardjo 1993). Matric suction and osmotic suction are separate stress state variables. However, for highly plastic clays such as sand-bentonite buffer, matric suction and osmotic suction are difficult to measure separately. Usually, total suction is the measurable variable though presses have at times been used (for example at AECL) to squeeze out pore fluid and measure osmotic suction. This raises the fundamental question of whether total suction (the sum of matric and osmotic components) can be considered a state variable (Bailey 1965, Chattopadhyay 1972). It will be shown later in this thesis that the roles played by osmotic suction and matric suction in controlling strength and stiffness are not quantitatively equivalent. While matric and osmotic suctions combine algebraically to form total suction, their effects are different and distinct. It is unlikely that total suction can be used as a single stress state variable.

2.5.4.3 Extended elastic-plastic model for unsaturated soils

Extensions of the Cam-Clay model (Figure 2.3) have been developed in attempts to rationalize the constitutive behavior of unsaturated soils (Alonso *et al.* 1990, Wheeler and Sivakumar 1995, Delage and Graham 1995).

Figure 2.4 shows a suction, mean stress plane for isotropic ($q = 0$) loading. In this plane lie two separate yield curves. To the right lies a yield curve called the 'loading yield' line, LY, corresponding to the outer limit of states of stress and suction higher than have been previously experienced through pressure increase or suction decrease accompanying wetting (Delage and Graham 1995). This line was called the 'loading collapse' line LC by Alonso *et al.* (1987). A second line called the 'suction yield' line, SY (called the 'suction increase' line SI by Alonso *et al.* 1987), represents the line of past highest suction. In this model, it lies parallel to the mean stress axis. On the basis of the understanding of soil microstructure outlined in Section 2.2, Delage and Graham (1995) went one stage further and envisaged a single yield envelope shown as the LSY line in Figure 2.4. This line provides a common yield envelope for loading, suction increase, and suction decrease that depends on the initial microstructure of the clay. It should be noted that this yield line does not lie on a plane of constant volume. Within the boundaries of the LY and SY lines, soil is expected to behave elastically.

When soil states attempt to move beyond the LY and SY envelope, plastic strain hardening occurs, and the region of elastic behavior becomes larger. Figure 2.4 shows an initially unsaturated specimen within the elastic region at A. The specimen experiences loading at constant suction if it follows stress path ABCD. The behavior is elastic from A to B. The specimen yields at B. This is followed by plastic compression (with some recoverable component) and volumetric hardening to C, and elastic unloading to D. The volume change behavior is illustrated in Figure 2.5a. During plastic compression the yield line LY1 is dragged to the new position of LY2. The unload-reload coefficient κ , is assumed to be the same for loading and unloading. The specimen at D has experienced the plastic volume change AD as a result of the load-unload cycle.

If the specimen follows stress path AB'C'D' in Figure 2.4, yielding through increases in suction at constant mean pressure p will be observed. An increase in suction from point A to C' causes elastic deformation through AB' and plastic yielding to C'. Yielding through the SY curve results in movement of both yield lines (the SY and LY lines) to enlarge the elastic region. The yield lines are moved from SY1 to SY2 and from LY1 to LY2 respectively. (A better alternative is to think of moving LSY1 to LSY2). Some experimental evidence of this coupling is provided by Josa *et al.* (1987). At this time however, it is uncertain if yielding at constant suction will also cause a coupling of the yielding lines in p - S space. Further work is required on this important topic. In Figure 2.5b re-wetting to D', produces a net decrease in volume, AD', and the unload-reload line in V - $\ln S$ space has a constant slope analogous to what is observed in V - $\ln p'$ space in Figure 2.5a.

Figure 2.6 shows a graphical, three-dimensional representation for the elasto-plastic framework in the p - q - S space. For states that lie inside the state boundary surface the soil behavior is assumed to be elastic, with movement across a state boundary surface corresponding to volumetric hardening and expansion of a yield surface in stress space. In the surface shown in the figure there are three separate yield curves (Alonso *et al.* 1990, Wheeler and Sivakumar 1993). The yield curve HFBI (line LY in p - S space in Figure 2.4), corresponds to the outer limit of elastic behavior for states of stress and suction lower than that have been previously experienced through pressure increase or suction decrease through wetting. The second line IJK (line SY in p - S space in Figure 2.4), represents the line of past highest suction. It lies parallel to the mean stress axis. As illustrated in Figure 2.4, a coupled line HBMJK in Figure 2.6 is suggested (Delage and Graham 1995) as a load suction yield line for outer limit of elastic behavior.

For soil initially at a stress state A inside the current position of the yield surface, yield can also be produced by an increase of p (isotropic loading path ABC), an increase of q (shearing path ADE), a reduction of S (wetting path AFG) or an increase of S (drying path AJL), or by changing p , q and S simultaneously in any suitable fashion. The plastic volume change is taken as the hardening parameter, so that the plastic volumetric compression that occurs on section FG of the wetting path is identical to that which occurs on section BC of the isotropic loading path or section DE of the shearing path if all three paths produce the same plastic volumetric compression and subsequent expansion of the yield surface. Increases in suction also result in increasing tensile strength. The line OK in the figure

represents yield under tensile loading. Little or no information was available in the literature for the tensile yield or strength. Note the framework reduces to a conventional Cam-clay type model when the material becomes saturated ($S = 0$).

The stress state surface can be viewed as a family of elliptical yield envelopes in constant suction planes. In this model with three separate yield lines, all yield envelopes have the same shape with the size of yield envelopes increasing with suction. For example in Figure 2.6, yield envelopes OHWO, NBDN and KIPK increase in size with increasing suction. In this sense, however, introduction of a coupled load suction yield line gives rise to uncertainties. As seen in Figure 2.6, the yield envelope KJTK associated with load suction yield curve HBMJK is smaller in size than yield envelope NBDN. That is, higher suction produces smaller yield envelope at transition from load yield line to suction yield line. The uncertainties will be clarified later in Chapter 9 which presents a new elastic-plastic conceptual model for unsaturated soils.

Strength properties can be defined based on the similarities in shape of yield envelopes at any constant suctions. Like in saturated soils, all critical state lines are parallel with a constant slope of M (and hence a constant friction angle). As such, the effect of suction is represented by an increase in cohesion, maintaining the slope M of the CSL for saturated conditions (Alonso *et al.* 1990). CSLs of unsaturated specimens are therefore usually assumed to be parallel. Wheeler and Sivakumar (1993) reported that the slope $M(S)$ for specimens of a compacted silt at different suction levels is almost independent

of suction, and the intercept $t(S)$ varies with suction in a non-linear fashion. Equation [2.12] therefore reduces to:

$$q = t(S) + M_0 p \quad [2.13]$$

where q is shear stress at critical state, M_0 is the slope of critical state line of saturated specimens, $t(S)$ is yield curve under tensile, and p is mean stress.

In a similar way, yield and hardening can be examined in the p - S - V space. Figure 2.7 (Delage and Graham 1995) illustrates loading paths with pressure or suction changes that start from states such as Q inside a LSY locus. They will initially behave elasticity and experience only elastic recoverable volume strains. Specimens yield when they reach the boundary surface. Further changes in pressure or suction then involve combinations of elastic and volumetric hardening and are accompanied by enlargement of the region of elastic behavior.

At this stage in their development, this kind of model must still be considered conceptual. Limited experimental data is available. Details of the parameters involved and the influence of suctions need to be determined through experiments and analysis.

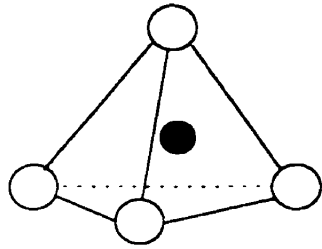
2.6 Justification for Research Program

As reviewed in the previous sections, plastic clay soils have complex suction characteristics. The physical-chemical interactions within clay particles - water system

add to difficulties in geotechnical laboratory testing in terms of suction measurement and control. For these reasons, experimental evidence is limited for unsaturated plastic clays. The engineered sand-bentonite mixture used in this research program behaves in many ways like a clay. The current understanding of mechanical behavior of unsaturated highly plastic clays, and unsaturated soils in general, is not sufficient to model and predict stress-strain behavior of unsaturated sand-bentonite under the conditions of changes in pressure, temperature, and pore fluid chemistry that will be encountered in a nuclear fuel waste disposal project.

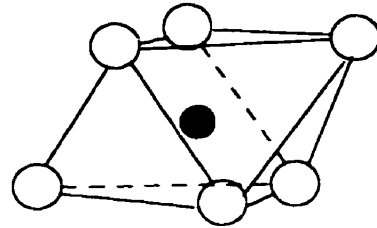
Experimentally, existing testing techniques and equipment used in soil science and conventional geotechnical tests cannot be directly used to examine elastic-plastic behavior of unsaturated sand-bentonite. Theoretically, the progress in development of conceptual elastic-plastic models for unsaturated soils provides concepts to rationalize some aspects of unsaturated soil behavior. Fulfillment of the project objectives stated in Chapter 1 will provide experimental evidence to develop a more realistic model of unsaturated sand-bentonite material. The new constitutive model which will be validated qualitatively and calibrated quantitatively for the first time in this project can be used in AECL's numerical analysis of hygro-thermal-mechanical modelling of performance of sand-bentonite buffer material in the Canadian Nuclear Fuel Waste Management Program.

Silicon tetrahedron



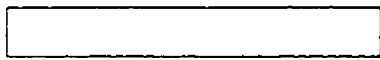
○ oxygen
● silicon

Alumina octahedron

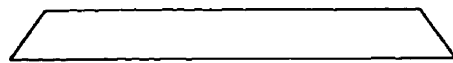


○ hydroxyl
● aluminum

a)

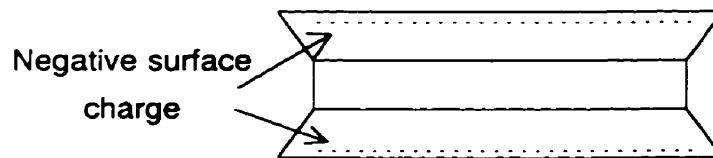


Silica sheet



Alumina sheet

b)



Montmorillonite particle

c)

Figure 2.1 Clay structural units and mineral

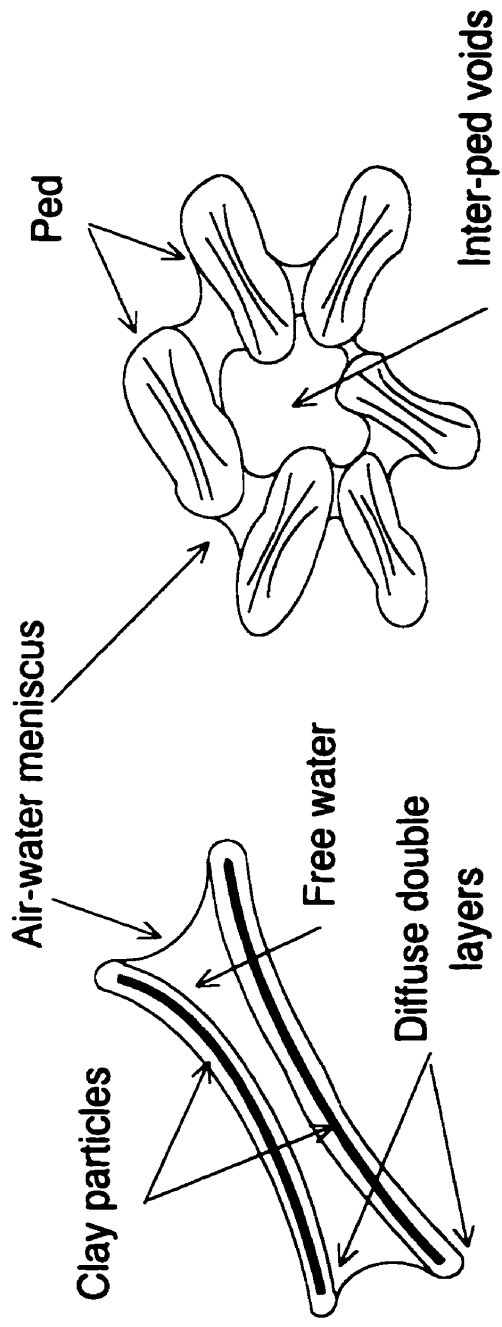


Figure 2.2 Soil structure (after Wan 1996)

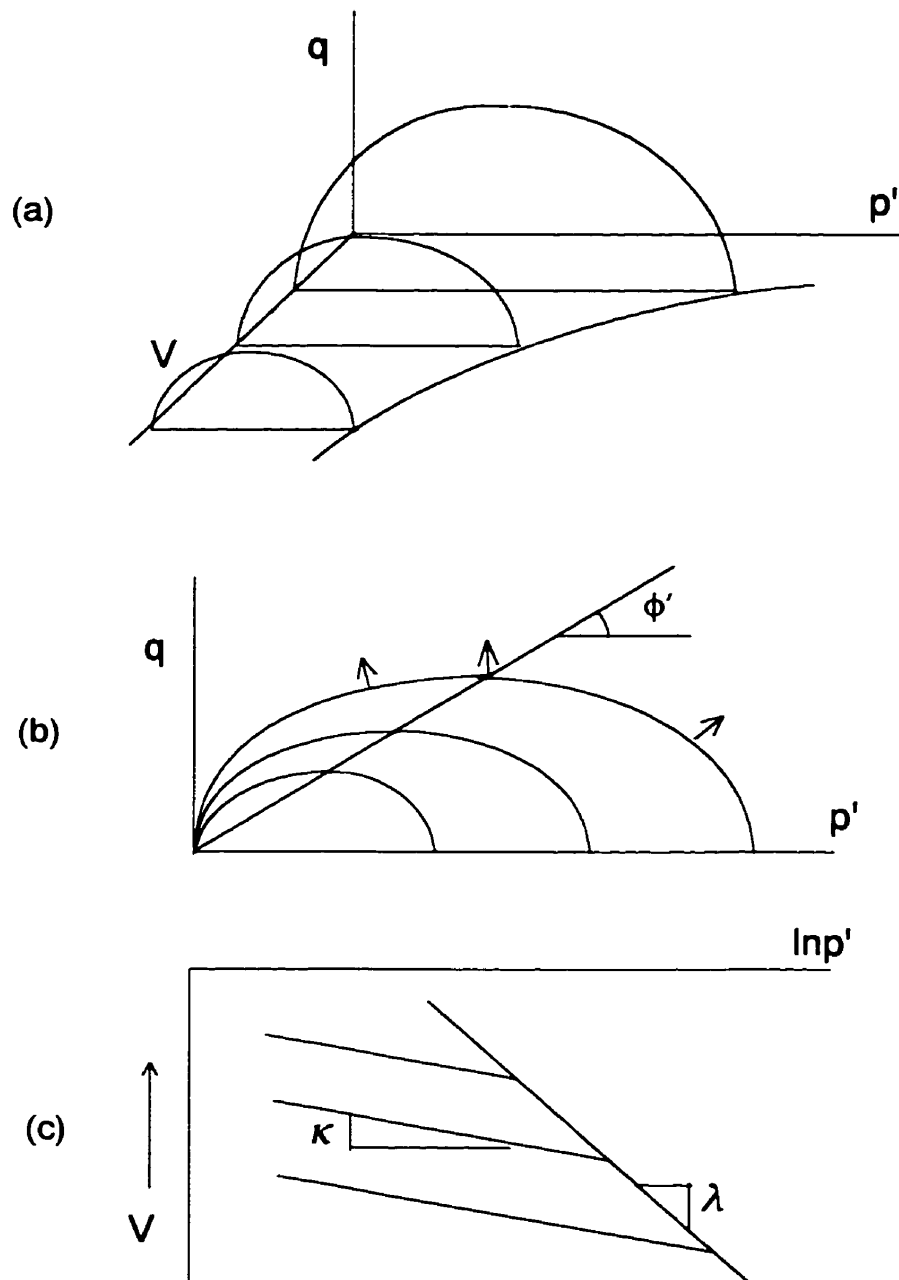


Figure 2.3 Critical State Cam Clay model

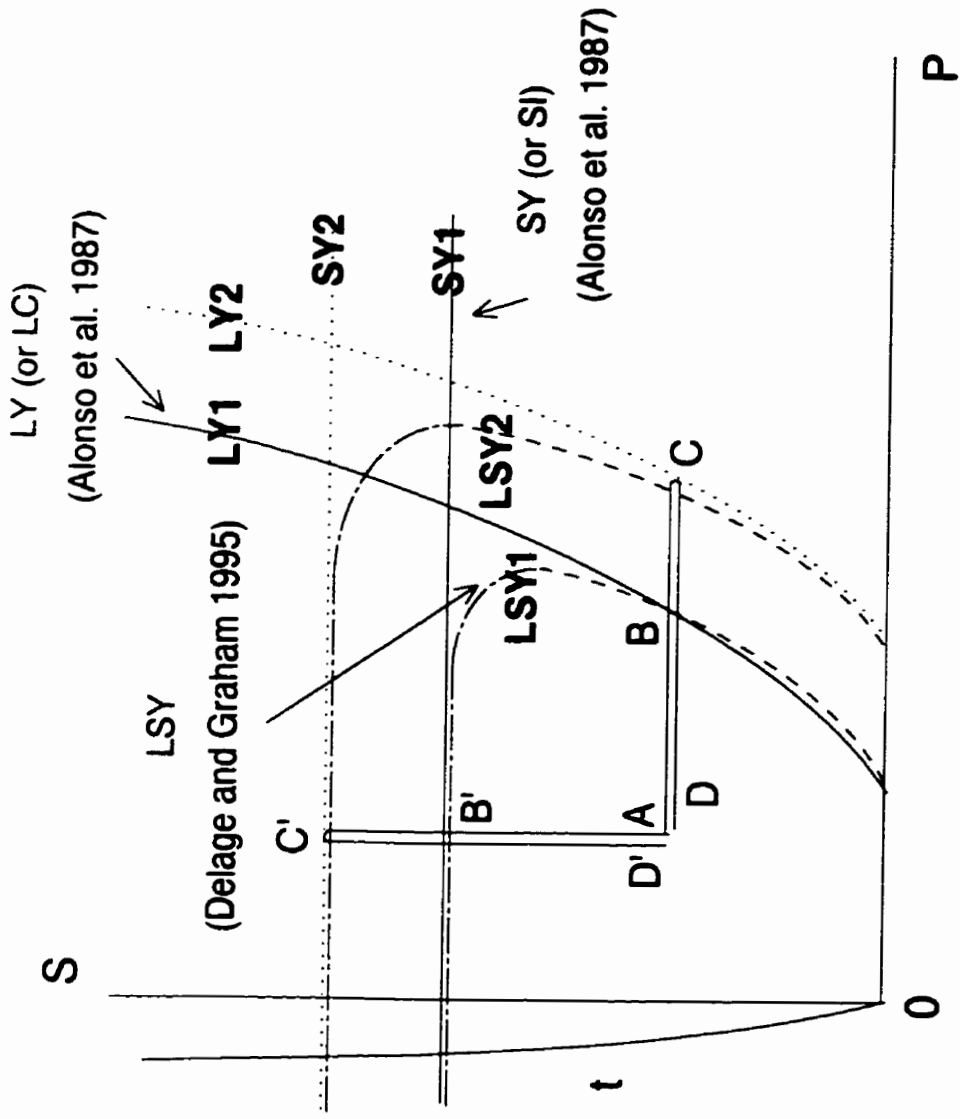
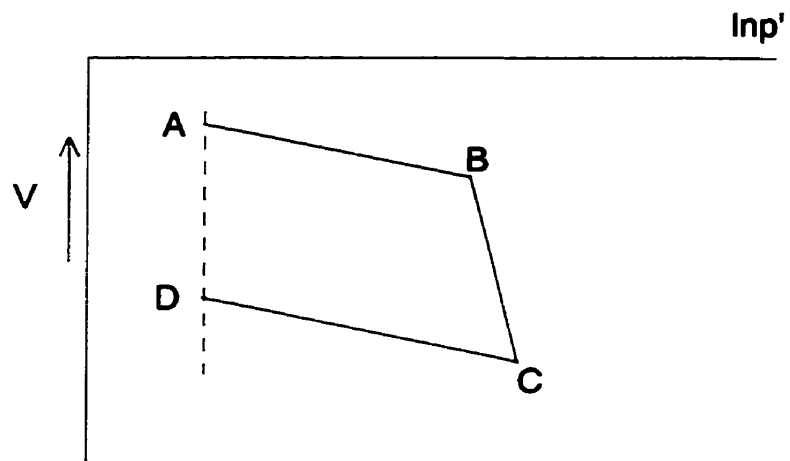
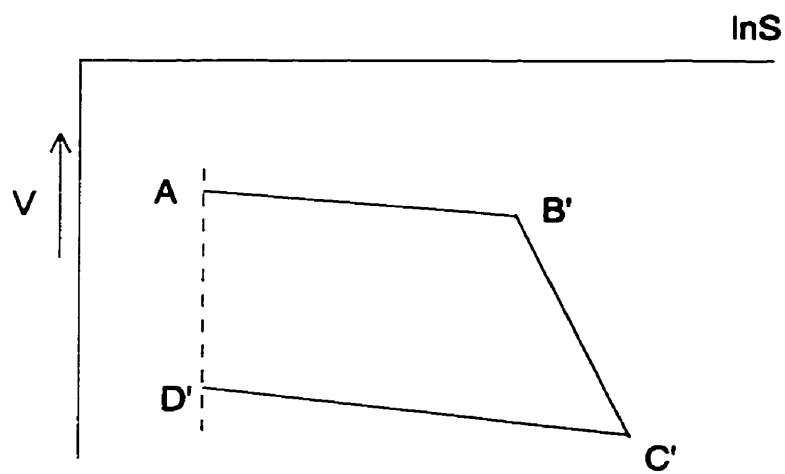


Figure 2.4 Yield curves under isotropic loading in p-S space



(a)



(b)

Figure 2.5 Schematic of volume change and yielding (Alonso et al. 1987)

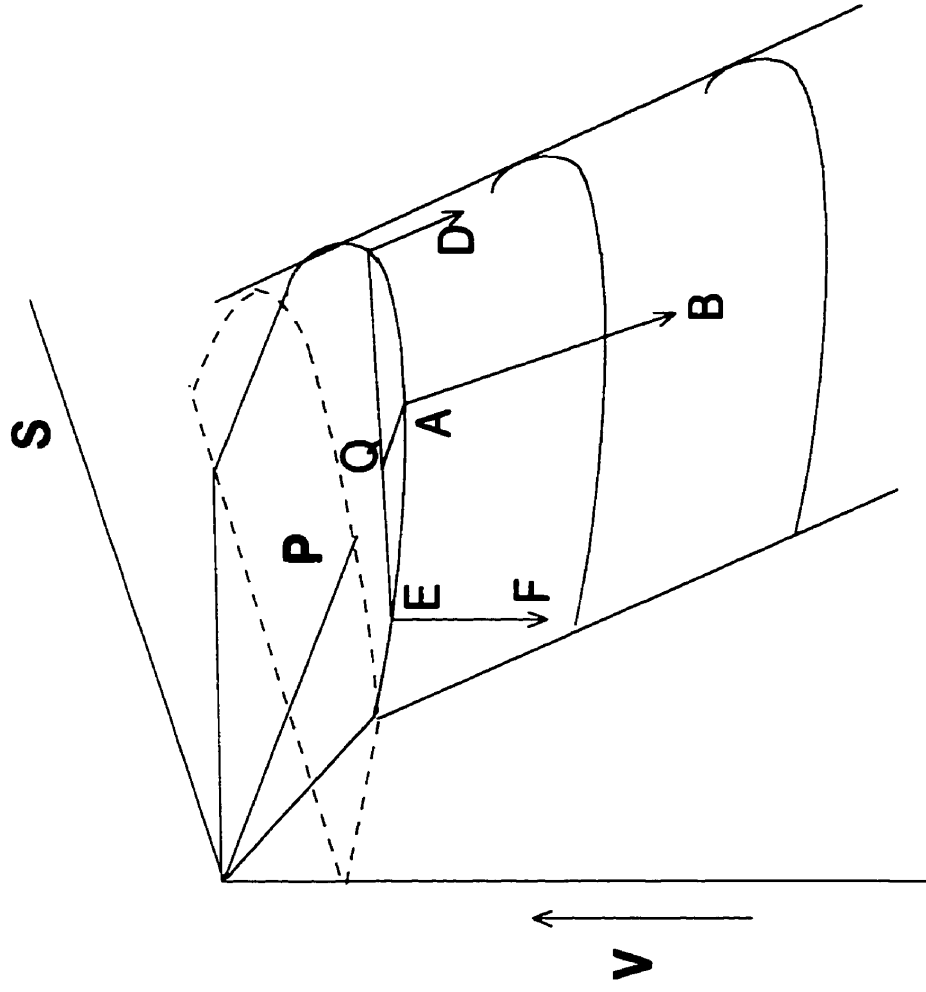


Figure 2.7 Compressibility for unsaturated soils
(Delage and Graham 1995)

CHAPTER 3

MATERIALS AND SPECIMEN PREPARATION

3.1 Introduction

This chapter begins with a review of the basic properties of the buffer material and its components. The specimen preparation techniques are then discussed. The unsaturated specimens formed by using these techniques had initial suctions that depended on selected water contents and saturations. Finally, the chapter introduces the special treatment of specimens in which suctions were elevated by drying or introducing osmotic agents. These specially treated specimens allowed examinations of the effects contributed by the matric component or osmotic component of the total suction.

Since this project has been one of a series performed at the University of Manitoba using the same material, only a limited description will be given of material properties and sample preparation. More details can be found in Wiebe (1996). Where new techniques and procedures have been developed, more complete details will be given.

3.2 Materials

3.2.1 Buffer Material

The reference buffer material (RBM) defined by the Canadian Nuclear Fuel Waste Management Program consists of a 50:50 mixture by dry mass of well-graded silica sand and sodium-based bentonite (Dixon and Gray 1985). It forms an engineered barrier between containers of used fuel waste and the host rock. The sand-bentonite mixture has been proposed for use because bentonite has low hydraulic conductivity, high sorption capacity, and a perceived ability to swell and, thereby, seal unfilled voids in the engineered rock mass (Gray 1992). Sand as a filler significantly increases the achievable compacted density, decreases the drying shrinkage, and increases the thermal conductivity of the buffer (Dixon and Gray 1985). In use, the material will be compacted to a dry density near 1.67 Mg/m^3 with a water content of about 19.4%, giving a degree of saturation of about 85%. This corresponds to 95% ASTM Modified Maximum Dry Density.

3.2.2 Bentonite and Silica Sand

The sodium-rich bentonite clay was supplied by Avonlea Minerals Industries, Saskatchewan. It is a whitish-gray powdered clay obtained by controlled drying and grinding processes on the natural soil (Quigley 1984). It has a liquid limit $w_L = 230\%$ - 250%, and plasticity index $I_p = 200$ (Dixon and Gray 1985). The sand is a crushed,

medium, sub-angular, well-graded, silica sand, with 80% of particles within the size range of 0.1 mm to 1.0 mm. Detailed specification of the sand has been given by Gray *et al.* (1984). The grain size distribution of the sand can be summarized by $D_{10} = 0.2$ mm, $D_{85} = 1.3$ mm, Curvature Coefficient = 0.91.

3.3 Mixing and Compaction of Unsaturated Specimens

Mixture The mixture was formed by combining equal dry weights of silica sand and sodium bentonite with the distilled de-aired water required to achieve the desired water content. After mixing, the mixture was sealed in two plastic bags and allowed to cure in a cool room for a period of three days before being compacted (Graham *et al.* 1995).

Compaction The specimens used in this study were compacted statically to achieve selected saturations varying from 30% to 98%. Static compaction involves compression by hydraulic jack in a cylindrical mould until the required density and saturation. The mould has an inside diameter of 50.8 mm and enough height to compact a 100 mm long specimen. The same compaction procedures were used as those described by Yarechewski (1993).

Specimens Specimens were cylindrical in shape with diameter 50.8 mm controlled by the mould. Specimen heights varied with the type of test. For triaxial tests, specimens had

height 100 mm. For suction measurements, shorter specimens were used, generally 40 mm or 20 mm. The dimensions of specimens will be listed later when particular tests are being described. Specimens were compacted to saturation at levels of 30%, 50%, 75%, 85%, and 98%. Most of the specimens had a dry density of 1.67 Mg/m^3 , the dry density of the Reference Buffer Material. The corresponding water contents varied from about 5% to 22%. Some specimens were also formed with other densities to further examine the effects of dry density on suction.

3.4 Specimens with Special Treatment

When prepared by the procedures described in the previous section, specimens with various saturations and water contents produce different initial suctions related to the lack of saturation and to dissolved salts in the pore water. The initial suctions can be related to changes of strength and volume change properties of the buffer material by conducting triaxial tests. However suctions produced by forming specimens at selected water contents do not necessarily represent suctions under more realistic situations where applied loading of pressure, temperature or pore fluid changes may affect both the matric and osmotic components of soil suctions. To examine this effect in buffer, therefore, additional soil specimens were prepared using the procedures outlined in the following sections.

3.4.1 Specimens with Matric Suctions Elevated by Drying at Controlled Suctions

Compacted specimens have different initial suctions depending on their water content at the time of initial hydration (Wan *et al.* 1995, Tang *et al.* 1997c, Tang *et al.* 1999). For each of these specimens, suction will change when drying or wetting changes water content. Drying or wetting will produce changes concentrated in the matric component of suction if it is assumed that osmotic suction remains largely unchanged with changing water content (Fredlund and Rahardjo 1993). Using the vapour equilibrium technique, two series of specimens with initial conditions of $w = 19.4\%$, $\gamma_d = 1.67 \text{ Mg/m}^3$ and $S_r = 85\%$ were dried to elevate their matric suctions (and hence their total suctions). Series 1 was used for stress-controlled triaxial tests. Drying was done by placing each of specimens in a dish inside a desiccator containing NaCl solution with a known suction of 6.5 MPa. Specimens were then allowed to reach equilibrium with the vapor pressure of the solution at a constant temperature of $25.7 \pm 0.05^\circ\text{C}$. After equilibrium was reached in about 30 days, specimens were carefully removed from the desiccator and wrapped in plastic sheet to allow redistribution of moisture content inside the specimens. A total of 6 specimens were examined. Three of them were used for stress-controlled triaxial tests, and the other 3 specimens for quality control assessment. Triaxial testing with suction measurement on this series of specimens will be discussed in Section 6.3. Similar procedures were used to prepare the second series of specimens which were used for tensile tests. Six specimens were dried to suctions of 6.5 MPa or 10.0 MPa. Tensile strengths of the specimens will be presented in Section 7.5.

3.4.2 Specimens with Osmotic Suctions Elevated by Introducing Osmotic Solutions

Osmotic suction is related to the concentration of dissolved salts in the pore water of soils (Fredlund 1995). Introducing concentrated solutions into soil specimens elevates their osmotic suctions (and hence total suctions) and changes their stress-strain behavior. Sodium chloride solutions instead of distilled water were mixed with sand and bentonite to make a series of specimens with elevated-osmotic-suctions. Otherwise, the procedures for mixing and compaction were the same as described earlier. After mixing, specimens were again cured for three days to allow moisture equalization. This was followed by static compaction as before. Specimens were formed at a dry density of 1.67 Mg/m^3 and saturation of 65%, 85% and 98% using sodium chloride solutions of 0.1 M, 0.5 M, and 1.0 M as the pore fluid. The 50 mm diameter cylindrical specimens had 40 mm length for suction measurements or 100 mm length for triaxial tests. Six specimens were made for suction measurement and five specimens for quick undrained triaxial tests. Results are described in Sections 4.6.2 and 6.2.2 respectively.

3.5 Specimen Designation

As is customary at the geotechnical laboratories of the University of Manitoba, each test is designated by a number such as T16101 where the first portion T16 indicates the test series performed by the author (researcher number 16), while the middle number 1

represents the test type in the program and the last portion 01 refers to serial number of test in this type. The types of test in this program are listed as follows.

Table 3.1: Test designation and test condition

Test designation	Test condition
T161**	quick undrained triaxial tests at a confining pressure of 0.2 MPa or 3.0 MPa.
T162**	tests for determining suctions <i>versus</i> water contents using filter papers and psychrometers.
T163**	tests to examine SWCC, shrinkage behavior at controlled suctions using vapour equilibrium technique.
T165**	triaxial tests with suction-monitoring by thermocouple psychrometers at strain-controlled tests and stress-controlled tests.
T166**	tests on specimens with additional osmotic agents.
T167**	tensile tests.

Test type of number 4 which was designated for tests performed by using a double wall cell is excluded from the table. As pointed out earlier in the introduction, this is the first doctoral project on unsaturated soil mechanics at the University of Manitoba. One of the objectives was to examine the applicability of existing techniques developed elsewhere, and to develop new techniques for testing densely compacted highly plastic clay. Investigations were made on a wide range of techniques and apparatus including psychrometers, filter papers, vapour equilibrium technique, pressure plate apparatus, high pressure triaxial cells, B-K cell, designed tensile mould, GDS system, double wall triaxial cell, non-contacting displacement transducers, Hall effect transducers, and lateral transducers designed and built at the University of Manitoba. Among all the examined techniques or facilities, those which were not successfully used are excluded from this

thesis. For the same reason, if a testing apparatus worked but measuring devices did not work, the tests were also excluded.

CHAPTER 4

**TECHNIQUES TO MEASURE AND CONTROL SUCTIONS:
DETERMINATION OF SOIL-WATER CHARACTERISTIC CURVES**

4.1 Introduction

Because this was the first doctoral project on unsaturated soil mechanics at the University of Manitoba, one of its most important initial objectives was to establish experimental techniques and expertise for measuring or controlling suctions. This would permit exploration of suction characteristics of unsaturated buffer materials. Presentation of this work will be in two parts. First, this chapter describes suction measuring techniques including the thermocouple psychrometer, vapour equilibrium, and the filter paper method which can be used for soils with high suctions (Fredlund and Rahardjo 1993, Wan 1995). Particular attention will be paid in this chapter to the psychrometer method since it is less commonly known, but has been used extensively in this research program. Some other common techniques such as the pressure plate apparatus and high air entry porous disks are not included. They were examined early in the program but proved not

to be applicable for highly plastic sand-bentonite (Graham *et al.* 1994) due to their limited suction range (Fredlund and Rahardjo 1993).

The second principal component of this chapter presents results and discussions from tests on buffer specimens using these techniques. Measurement of suctions in sand-bentonite specimens formed at different water contents led to establishment of a suction - water content relationship. Differences between this suction - water content relationship and the classic soil-water characteristic curve were clarified by another series of tests which measured the suctions of specimens prepared at the same initial water content and were then subsequently dried. Results of this work were reported by Tang *et al.* (1997c). The results, primarily presented in terms of total suction, will be better understood after initial osmotic suctions and their variations with water contents and introduced osmotic agents are discussed in the following section. Finally, drying and wetting behavior of buffer on exposure to osmotic solutions is described.

4.2 Psychrometer Technique

Among techniques used in laboratory tests of measuring high suctions in unsaturated soils, the thermocouple psychrometer technique is the most promising due to the small size, quick response, accuracy and reliability of the instruments (Fredlund and Rahardjo 1993, Wan 1996, Tang *et al.* 1997b).

4.2.1 Thermocouple Psychrometers

Principle A typical psychrometer is basically a thermocouple loop consisting of a sensing junction and a reference junction protected by a shield (Figure 4.1). It makes use of cooling produced by the Peltier effect to condense a small amount of moisture inside the shield on the sensing junction. The moisture comes from the vapour equilibrium established between the surrounding soil and the shielded space in the psychrometer sensor. As the condensed water begins to evaporate, a potential difference is set up between the sensing junction and the reference junction. This creates an induced electric current in the thermocouple loop due to the Seebeck effect. The magnitude of the current depends primarily on the rate of evaporation of the condensed water, and this in turn depends on the suction and the temperature in the soil (Brown 1970).

Psychrometer Two types of Wescor psychrometers are commercially available. They are the same in operating principle but differ in their construction and the shields which protect thermocouples. Most of the psychrometers used in this study were Wescor PST-55 stainless steel shield psychrometers. Porous ceramic psychrometers which were used by previous researchers (Edil and Motan 1984, Wan 1996) were used as well for comparison purposes.

4.2.2 The Campbell Scientific CR-7 Measurement and Control System

The psychrometers were controlled and operated by a Campbell Scientific CR-7 measurement and control system (the CR-7, see Figure 4.2). In principle, it controls and supplies cooling current to psychrometers, then logs and stores psychrometer outputs after cooling. The major advantage of the CR-7 is that it tracks and records the output history of psychrometers during the course of measurements, thus providing a continuous output profile. Temperatures in the specimens are also monitored continuously by the CR-7. Use of the CR-7 produces more accurate and reliable results than those from earlier manual instruments such as the HR-33T (Tang 1996).

4.2.3 Calibration of Psychrometers

A psychrometer needs to be calibrated carefully before measurements can be converted to suctions. Calibrating a psychrometer involves determining the relationship between the output of the psychrometer and the suction it is sensing. The principles and procedures of psychrometer calibration have been well documented in the open literature (Meyn and White 1972, Fredlund and Rahardjo 1993). However, calibration results may vary with the system which operates psychrometers. This section describes calibration of psychrometers operated by the CR-7 system at the University of Manitoba.

Calibration methodology Psychrometers were calibrated against known suctions produced by osmotic solutions. The psychrometer was either immersed into or suspended over the solution in a sealed bottle. Most commonly, calibration is done using immersion (*Instruction Manual of Wescor P55 Series Psychrometers*, Wescor Inc., Logan, Utah, USA, 1994). Comparison of the results from two methods shows the same output results of a psychrometer but different equilibrium times were required, with the suspension method taking longer. Data were reported by Graham *et al.* (1996). The authors have shown for the first time that suspension is equally effective, and probably less damaging to the psychrometer. To allow vapour pressure inside the psychrometer tip reach equilibrium, temperature fluctuations were minimized as much as possible. All calibrations were performed in a temperature controlled room at temperature of $25.7 \pm 0.05^\circ\text{C}$. The CR-7 controlled and supplied cooling voltages to the psychrometer, then logged and stored psychrometer outputs. The CR-7 provided a psychrometer with an excitation voltage of 20 mV and cooling time of 15 seconds.

Suction range and solutions for calibration For a particular usage, psychrometers must be calibrated in the suction range where measurements were required. In this testing program, psychrometers were expected to measure suctions from about 1.5 MPa to about 8 MPa. This range of suctions can be produced by solutions of sodium chloride or potassium chloride (Lang 1967). Sodium chloride solutions with concentrations of 0.5 M, 1.0 M and 1.5 M were selected to establish three suction levels of 2.3 MPa, 4.6 MPa, and 7.1 MPa respectively (Lang 1967).

Suction - psychrometer output relationship Figure 4.3 shows the results of calibrating 3 psychrometers using the CR-7 system for relationships between microvolt output and known suctions. The best-fit equation for each calibration exhibits good linearity, though each calibration line has an intercept value which is not negligible. Typically, a calibration factor equal to the slope of the output - suction line is used for converting readings into suctions. For data measured in this program, however, a calibration factor defined only by a slope cannot fully represent the calibration results. This feature of psychrometer calibration has not been mentioned in the literature. Calibration data of psychrometers operated by the CR-7 should be presented using a 2-parameter linear equation (slope plus intercept). The conventional single value calibration factor leads to less precise suction values.

Temperature fluctuation and correction Output readings of psychrometers at temperatures other than 25°C were corrected to 25°C by the following relationship (Brown 1970).

$$\text{Corrected reading} = \frac{\text{reading}}{0.325 + 0.027 \times T}$$

where T is temperature in degrees Celsius. This correction equation was applied to all calibrations and measurements throughout this research program. Figure 4.4 shows the results from a psychrometer used for measuring suctions in a soil specimen in which the temperature varied from about 21.5°C to about 23°C. The output from the psychrometer

(in μV) varied with temperature change. After applying this correction equation, the corrected output and the interpreted suctions (in MPa) were almost constant.

4.2.4 Measurement of Suctions

Psychrometers were used to measure suctions in two broad ranges of applications: (1) measuring suctions in compacted soil specimens and (2) tracking suctions during triaxial tests. This chapter only describes how to use psychrometers to measure suctions in sand-bentonite specimens. Results are presented in Section 4.5. Use of psychrometers in triaxial tests requires careful arrangement for incorporating psychrometers effectively into an instrumented triaxial cell. This will be described later in Section 5.3 of Chapter 5.

4.3 Vapour Equilibrium Technique

4.3.1 Principle

The vapour equilibrium technique allows control of the total suction in a soil by exposing specimens to an atmosphere in which the relative humidity or vapour pressure is controlled by an osmotic agent. Figure 4.5 shows schematically the layout of specimens and osmotic solution in a desiccator. A concentrated solution provides the constant suction/water potential environment. The water phase of the specimens will gradually come to thermal and vapour pressure equilibrium with the water vapour in the

surrounding atmosphere. When equilibrium is reached, the soil suction equals the osmotic suction of the solution. This can be determined from published data knowing the concentration of the osmotic agent and the temperature. Water contents of the specimens can either decrease (that is, in a drying phase) or increase (in a wetting phase) depending on whether the initial suctions of the specimens are higher or lower than that of the solution.

4.3.2 Solutions

Commonly used osmotic agents for the vapour equilibrium technique include sodium chloride NaCl, potassium chloride KCl and sulphuric acid H₂SO₄. In this study, desired suctions lower than 10 MPa were produced using sodium chloride or potassium chloride. Osmotic suctions for NaCl and KCl solutions at different molalities and temperatures are given by Lang (1967) and Campbell and Gardner (1971). Higher suctions were generated by sulphuric acid solutions, which are relatively insensitive to temperature changes (Young 1967).

4.3.3 Experimental Program

In this research program, the vapour equilibrium technique was used in the following tests:

Drying or wetting buffer specimens Buffer specimens were dried or wetted at different suction levels. Measurements of water content and volume change will be discussed later in Section 4.7.

Elevating suctions of specimens used for further triaxial tests and tensile tests Compacted specimens had their initial suctions increased to higher desired suctions by using the vapour equilibrium drying technique. The specimens were then used for triaxial tests and tensile tests. Testing programs will be described in Section 6.3 and Section 6.4 respectively.

4.4 Filter Papers

The filter paper method is time consuming and highly user-dependent. It has therefore not gained general acceptance in geotechnical engineering (Fredlund and Rahardjo 1993, Sibley *et al.* 1990). However, it appears capable of measuring a wide range of soil suctions. It offers a supplementary way of measuring high suctions in addition to the psychrometer method described earlier. The technique was used to measure total suctions and matric suctions in unsaturated buffer. Similar measurements were also taken by Wan (1995) at AECL's Whiteshell Laboratories. The measurements described here were designed to develop this technique at the University of Manitoba laboratories and to confirm Wan's results.

4.4.1 Methodology

The filter paper method is based on the observation that a filter paper will come to water mass equilibrium (with respect to moisture flow) with a soil having a specific suction. Equilibrium can be reached by either liquid or vapor moisture exchange between the soil and the filter paper (Fredlund and Rahardjo 1993). When a dry filter paper is placed in direct contact with a soil specimen, water flows from the soil to the paper until equilibrium is achieved. When a dry filter paper is suspended above the surface of a soil specimen (that is, without direct contact with the soil), vapor flow of water will occur from the soil to the filter paper until mass equilibrium is again achieved. Having established equilibrium conditions, the water content of the filter paper is measured. The water content of the filter paper corresponds to a suction value. This allows total or matric suctions to be evaluated from a predetermined calibration curve. Direct contact measures total suction; proximity measures matric suction (Fredlund and Rahardjo 1993).

4.4.2 Filter Paper Calibration

Calibration of Whatman 42 filter papers was conducted by exposing filter papers to concentrated solutions in sealed desiccators. In this study, sulphuric acid solutions and sodium chloride solutions were used to produce suction ranging from 2 MPa to 100 MPa at 8 levels. Four pieces of filter papers were used for each suction level. Equilibrium took seven days. Once equilibrated, water contents of the filter papers were determined

by taking filter papers out of the desiccator. An analytical balance with capacity of 50g and readability of 0.0001g was used to weigh the filter papers. The average water content of four filter papers was then related to the known suction of the solution. Detailed procedures were described by Graham *et al.* (1996).

Figure 4.6 compares the results with calibration line for Whatman 42 filter papers obtained by Fawcett and Collis-George (1967). It shows two lines that are almost parallel, suggesting that calibration depends on the operating procedures, and should be made over a particular range of suction if accurate evaluation is required. The results may also depend to some extent on manufacturing differences in the filter papers used by the different researchers (Sibley *et al* 1990).

4.4.3 Suction Measurement by Filter Papers

Measurements of total suction and matric suction were performed on unsaturated compacted specimens. The resulting water content - suction relationships are presented in the following section.

4.5 Determination of Suction - Water Content Relationships and Soil-Water Characteristic Curves

The soil-water characteristic curve can be used to produce approximate estimates of the stress-strain behavior of unsaturated soils (Fredlund 1995). This section first summarizes

results of suctions measured in specimens formed at different water contents. This is followed by SWCCs obtained from two sand-bentonite mixtures formed at two different water contents. It should again be noted that suction - water content relationships are different from SWCCs (Tang *et al.* 1997c).

4.5.1 Suction - Water Content Relationship for Specimens Formed at Different Water Contents

Using psychrometer and filter paper techniques, suctions were measured on sand-bentonite specimens formed at different water contents and saturations. Due to limitations of the measurable range, water contents of specimens measured using psychrometers ranged from about 15% to 50%. The filter paper method was used to make supplementary measurement on specimens having water contents from 5% to 17%.

4.5.1.1 Measurement by psychrometers

Specimens Sand-bentonite mixtures under four water content levels of 14.82%, 17.13%, 19.42% and 22.70% were used to produce both compacted unsaturated specimens and loose uncompacted samples. The compacted specimens were made by static compaction to degrees of saturation of 65%, 75%, 85%, and 98%. They all had same dry density of 1.67 Mg/m^3 and measured 40 mm long and 50 mm diameter. Compacted specimens were produced as described in Section 3.3. The same mixture and water content levels were also used to form loose, uncompacted specimens (at dry densities of about 1.4 Mg/m^3).

As soon as a compacted specimen had been made, a small hole was drilled in the center of the top of the specimen to accommodate a psychrometer tip. The specimen was then placed in a container for suction measurement. The loose samples were made by simply placing about 30 g of the mixture in a Lucite container. Since compacted specimens and loose samples came from the same mixture, they had the same microstructures resulting from their common hydrating water content (Wan *et al.* 1995). However macrostructures were obviously different due to their different densities and saturations. Testing these two kinds of specimens allowed comparison of how suction is affected by dry density. An additional series of tests was carried out on fully saturated specimens with water contents more than 22.70%. Their dry densities were therefore less than 1.67 Mg/m³. The specimens in this series had nominal water contents of 25%, 30%, and 50%. Dry densities varied with water contents to satisfy the relation: $eS_r = wG_s$ or $\gamma_d = G_s \gamma_w / (1 + wG_s)$ for $S_r = 100\%$.

Measurement After they had been formed, a calibrated psychrometer was inserted into the compacted specimen or loose sample. The container housing the specimen or sample was carefully sealed and placed in a temperature controlled room to allow water vapour pressure and thermal equilibrium. Thermocouple psychrometers with stainless steel shields (Wescor PST-55) or ceramic porous shields (Wescor PCT-55) were used along with the CR-7 measurement and control system.

4.5.1.2 Measurement by filter papers

Specimens Only compacted specimens were used for suction measurement by filter papers. All specimens measured 40 mm long and 50 mm diameter and had a dry density of 1.67 Mg/m³. Saturations ranged from 30% to 85%.

Measurement As described previously, filter papers were placed either in direct physical contact with the specimen in a plastic container, or in close proximity but not in contact (Figure 4.7). Three Whatman 42 filter papers with 50 mm diameter were used for each soil specimen. Following Wan *et al.* (1995), at least 40 days were used to establish suction equilibrium. Once equilibrium was achieved, the water contents of the filter papers were determined by weighing and converted to suctions using the calibration procedures mentioned earlier.

4.5.1.3 Results

Figure 4.8 shows total suctions measured by psychrometer in specimens formed at different water contents. The figure contains results from both compacted specimens and loose, mixed samples, and therefore, results come from widely different dry densities and saturations. As reported by Wan *et al.* (1995), the data indicate that total suctions in buffer specimens are independent of dry density provided the specimens have been formed with the same initial water content. Delage and Graham (1995) explain this observation in terms of the relationship between microstructures and macrostructures in

the clay. Microstructures, which control suctions, are formed at the time water is added to the mixture.

Figure 4.9 shows results measured using the filter paper method at water contents overlapping, but generally below the range shown in Figure 4.8. As expected, the figure shows that total suctions are consistently higher than matric suctions at the same water content.

Figure 4.10 combines the psychrometer and filter paper data over an extended range of water contents from 7% to 50%. There is good agreement between the two methods at water contents between about 15% and 17%, and hence the correlation between the two techniques seems reasonable (see also Wan *et al.* 1995).

Figure 4.10 also shows osmotic suctions inferred from filter paper and psychrometer data. As mentioned previously, in unsaturated specimens (below about 22.7% water content for dry density 1.67 Mg/m^3), the osmotic suction is the difference between total and matric suctions measured by filter paper. Above 22.7%, the specimens were saturated and matric suctions were zero. Total suctions measured by psychrometers can therefore be taken as osmotic suctions. In the unsaturated range, total suctions increase rapidly with decreasing water content, while the estimated osmotic suctions increase much more slowly. For the water content range in Figure 4.10, the osmotic suction is about 1-2.5 MPa. At low saturations, or to be more precise, at low average water contents, increases

in total suction arise mainly from changes in matric suction in the aggregates. This is the component of suction that is now commonly used to describe changes in strength and compressibility with suction (Fredlund and Rahardjo 1993, Wiebe *et al.* 1998). Changes in osmotic suction are generally less significant and contribute mainly to strength and compressibility through the net stress component (Graham *et al.* 1992).

4.5.2 Measurement of Suctions on Specimens Formed at an Initial Water Content and Subsequently Dried

This series of tests measured suctions on specimens at consecutive stages after they were formed and subsequently dried to different water contents. From the conclusion stated in the preceding section that total suctions are independent of dry density when specimens are formed with the same water content, a specimen's suction is representative of all densities made from this mixture. Since drying loose uncompacted mixtures was much easier and faster than drying compacted specimens, they were used instead of compacted specimens for this series of tests. Drying was done in a stepwise manner so that suction and water content could be measured at each step.

4.5.2.1 Samples and measuring procedures

Two mixtures with initial water contents of 19.3% and 22.4% were tested. For each mixture, after 3 days for equilibrating the initial water distribution, a portion of about 30 g of the mixture was sampled and its suction measured. Measurements were conducted

using the method described in Section 4.5.1. Another portion of the mixture was taken for water content evaluation. This finished one step of the measurements relating suction to water content. The remainder of the mixture was then air dried to decrease its water content by about 2%. After reaching the target water content, the mixture was again bagged and sealed for 3 days to equalize water content and suction, which were then measured. This process of drying, sampling, and measuring the suction and water content was continued until the suction was beyond the measuring limit of the psychrometers about 8 MPa. Plotting results of suctions and corresponding water contents at all stages produces the soil-water characteristic curve for each mixture.

4.5.2.2 Soil-Water Characteristic Curves

Figure 4.11 shows SWCCs for specimens with initial water contents (IWC) at the time of hydration of 19.3% (IWC19.3) and 22.4% (IWC22.4). The figure also includes data from Figure 4.8 for specimens with different initial water contents (DIWC). Considerable differences can be seen between the results for the three test conditions, particularly as water contents decrease below 18%. Results in Figure 4.11 are limited by the range of suctions that can be measured by psychrometer. However, the tendency is clear - larger differences in suction, and therefore in strength and compressibility, can be expected with low water contents.

4.5.3 Discussion

Compared with granular soils, clay soils have high suction and low permeability. Their soil-water characteristic curves are more difficult to obtain and several test techniques may have to be used to determine suctions over a sufficiently wide range of water contents. Figure 4.12 shows water content - suction measurements reported by Wan *et al.* (1995) for sand-bentonite buffer. Data in the figure were obtained by a combination of the filter paper method, the vapour equilibrium technique, and thermocouple psychrometers. The figure suggests a discontinuity in the data at water content of about 10%. This is not due to a transition in the way soil particles and water were interacting. Rather, it can be attributed to two different preparation procedures that were used for the different measuring techniques. Specimens used for the vapour equilibrium method were all formed at same initial water content of 18% then dried to lower water contents in desiccators. Specimens used for filter paper and psychrometer measurements were formed at the water content at which suction was to be measured. These are essentially the same two procedures that were used in this study, one purpose of which was to help understand the results in Figure 4.12. Reference to Figure 4.11 implies that discontinuity suggested by Figure 4.12 in fact represents sections of different SWCCs for buffer specimens prepared in different ways having, as a result, different microstructures.

The test results indicate that water content - suction relationships for buffer depend on the way the test specimens are prepared. Specimens with the same initial hydrating water

content but then dried to different water contents and densities have SWCCs that are different from the water content - suction relationship measured in specimens formed at constant dry density but different initial water contents and saturations. Following earlier discussion, the differences can be explained using the idea that microstructures are controlled by the initial water content during specimen preparation (Wan *et al.* 1995, Tang *et al.* 1997c). These microstructures dominate the suction that the soils can experience at given average densities, water contents, saturations, and stress levels.

Suction is now widely understood to be an independent state variable (Fredlund 1995) and so it has a major influence on soil properties (Tang *et al.* 1999). This understanding provides an explanation for the results in Figure 4.13 which is taken from strength tests described by Wiebe *et al.* (1998). The figure shows that specimens with the same water content can have different strengths depending on how they were prepared. Specimens formed at the same initial dry density but different initial water contents have consistently lower strength than those in which the same water content was reached by drying from a higher water content at the time of hydration. Predicting stress-strain behavior, for example strength and compressibility, from SWCCs in the way proposed by Fredlund (1995) must therefore be based on tests that reflect the water content history of the specimen and the accompanying microstructure.

4.6 Evaluation of Osmotic Suctions

4.6.1 Initial Osmotic Suction

Initial osmotic suctions from filter paper and psychrometer data were discussed in connection with Figure 4.10. In unsaturated specimens (below about 22.7% water content), the osmotic suction is approximately 2.5 MPa over the testing range from 7% to 17% water content, decreasing to about 1 MPa at 50% water content.

The van't Hoff equation (Mitchell 1976) has been used to provide approximate estimates of osmotic suctions. The calculations are based on the clay composition and pore fluid ion concentrations and details have been reported by Graham *et al.* (1996). Calculated values are plotted in Figure 4.14 and compared with osmotic suctions inferred from the total and matric suctions. Figure 4.14 suggests that good agreement has been obtained between measured and calculated results. However, it should be noted that the van't Hoff equation was originally derived for chemical solutions. It has also been applied with some success for osmotic suctions in suspensions and loose clays containing free water with free ions. Experience of its use with dense materials like compacted buffer is limited.

4.6.2 Elevation of Total Suctions by Osmotic Agents

Specimen As mentioned earlier in Section 3.4.2, osmotic solutions were used to mix sand and bentonite to increase the dissolved salt contents of the pore water and the osmotic suctions of the mixtures. Pore fluids of sodium chloride solutions with concentrations of 0.1 M, 0.5 M, and 1.0 M NaCl were used in these experiments. The mixtures were compacted into unsaturated specimens at saturation of 65%, 85%, and 98%. All specimens had a dry density of 1.67 Mg/m^3 and measured 40 mm high \times 50 mm diameter.

Measurement Total suctions were measured by psychrometers using the approach described in Sections 4.5.

Results Since osmotic suctions are controlled mainly by exchangeable cations in the mineral particles, they do not change greatly with water content when only deionized water is used. However, exchangeable cations available in the dry bentonite meant that the pore fluid became an electrolyte (Dixon *et al.* 1996). Osmotic suctions do change when salt solutions are introduced to the pore fluid. This produces corresponding changes in total suctions (Figure 4.15). Increases in total suction introduced by NaCl solutions are not simply additive. Measured total suctions are greater than the sum of the suction in a specimen made with deionized water and the osmotic suction of the solution itself. For example, 1 M NaCl solution has an osmotic suction of 4.6 MPa. However, its

use as pore fluid raises total suction in a saturated specimen by 5.9 MPa from 2.2 to 8.1 MPa (Figure 4.15). At the particulate level, increasing the pore fluid concentration, increases potentials near the particle surface, but decreases the thickness of the diffuse double layers (Mitchell 1976, Yong and Warkentin 1975).

4.7 Drying and Wetting Behavior of Buffer on Exposure to Osmotic Solutions

Two series of drying/wetting tests were carried out using the vapour equilibrium technique. The first series was designed to examine SWCC and shrinkage behavior. It involved drying specimens using different suction levels. In the second series, specimens underwent both drying and wetting. All tests were conducted in a temperature-controlled room at 25.7°C.

4.7.1 Specimens

Specimens were prepared at two saturation levels of 85% and 98% with a dry density of 1.67 Mg/m³. To facilitate comparison, most specimens were made with the same dimensions as used for suction measurement or for triaxial tests. That is, specimens were 50 mm diameter and 40 mm or 100 mm long, respectively. Two specimens with 20 mm height were also prepared. Detailed initial conditions of specimens used in these tests are listed in Table 4.1.

Table 4.1: Initial conditions of specimens for drying and wetting tests

Test	Number of specimens	Specimen size (in mm)	Dry density (Mg/m ³)	Water Content (%)	Specific Volume	Saturation (%)	Total Suction (MPa)
T16301	3	20.4 × 50.9	1.62	22.58	1.66	92.08	2.3
T16302	4	20.0 × 50.8	1.67	22.50	1.62	97.82	2.3
T16303	1	100.8 × 50.8	1.66	22.66	1.64	96.39	2.3
T16304	3	40.4 × 50.9	1.67	22.82	1.64	96.27	2.2
T16305	4	40.5 × 50.9	1.65	19.46	1.64	81.87	3.5
T16306	4	40.3 × 50.8	1.68	22.38	1.64	95.16	2.3

4.7.2 Experimental Procedures

A total of six tests were carried out. Drying tests included T16301 - T16304. The two tests with drying and wetting were T16305 and T16306.

Drying tests Drying tests were performed using both single-stage and multi-stage procedures. For a single-stage test, a specimen was dried using only one selected suction level in the desiccator and the test was terminated when equilibrium was achieved. Tests T16301 and T16302 were designed to examine shrinkage behavior of buffer. A suction of 125 MPa was assumed to be high enough to dry specimens to their shrinkage limit. Each test used 3 or 4 identical specimens for consistent assessment. A multi-stage test could be performed by drying a same specimen to equilibrium at successively higher suction levels. Only one specimen (T16303) was prepared in this way. It was dried sequentially using suction levels of 3.5 MPa, 10.0 MPa, and 48.9 MPa.

Drying and wetting tests T16305 was intended to determine the possibility of yielding induced by increasing the total suction up to 10 MPa. Four identical specimens at initial saturation of 85% were dried separately in desiccators with suctions of 3.5 MPa, 5 MPa, 7 MPa, and 10 MPa. After equilibrium, they were all re-wetted back to 3.5 MPa. T16306 was used to examine hysteresis in the SWCC. Suction levels were 5 MPa, 7 MPa, 10 MPa, and 48.9 MPa.

Changes in the specimens during drying and wetting were determined by measuring weights and dimensions periodically. Each stage involved the following procedures. After a specimen had been weighed and measured, it was placed on a plate over a solution in a desiccator as illustrated earlier in Figure 4.5. The desiccator was then sealed by lightly greasing the lid and sliding it into place. During the course of moving towards equilibrium, the specimen was periodically taken from the desiccator and weight, diameter and height were quickly measured. It was then returned to the desiccator for further equalization. Equilibrium was regarded as being reached when the measured water content remained largely unchanged ($\leq 0.04\%$) for 3 days. The test was then terminated. The specimen was then finally measured for its dimensions and weight. The water content of the specimen was evaluated again from the weight after final oven-drying.

4.7.3 Test Results

In a drying or wetting process, three variables were involved, namely specific volume, water content, and suction. Presentation of relationships among these variables allows development of the soil-water characteristic curve and shrinkage characteristics, and examination of the possibility of yielding (changes in the pressure-volume relationship) induced by increasing suction.

Soil-Water Characteristic Curve Figure 4.16 shows the soil-water characteristic curve for 3 specimens (T16301, T16303, T16306) with initial water content of about 22.4% and saturation of 95% determined. Drying data from the single stage test T16306 (referred to in the figure as T306D) and multistage drying test T16303 (shortened to T303) agree very well, suggesting reliability of the measurements. As expected, hysteresis is observed from the test data for the wetting period of T16306 (T306W). The suction - water content relationship established from compacted specimens formed at different water contents is again included in this figure and compared with the SWCC. At a given water content, a specimen experiencing drying has higher suction than that of a compacted specimen at this water content. This verifies the conclusion drawn earlier from tests by using psychrometers.

Specific volume - water content relationship During drying, both the specific volume and the water content decrease with time, with a decreasing rate that depends on the suction

being imposed on the specimens. Figure 4.17 shows that during equalization, specific volumes and corresponding water contents of specimens exposed to different suctions fall on the same curve. This indicates that specific volume is uniquely related to water content and that the relationship is independent of controlled suctions. Comparing data from Dixon at AECL and Wiebe at U of M (personal discussion 1996) the results of drying tests conducted in the different laboratories appear to be in reasonable agreement. Different initial conditions and different testing procedures provide same relationship between specific volume and water content.

Shrinkage behavior of buffer The shrinkage characteristic of buffer has also been examined by plotting the data in the form of percent volume change versus water content (Figure 4.18). The volume strain of these specimens was about 12% compression. During drying, the total volume of the specimens continuously decreased until the shrinkage limit at about 13% water content. Moisture continues to decrease until equilibrium is reached between the suction of the specimens and suction of osmotic solutions. For this reason, the limit of moisture decrease depends on the predetermined suction of osmotic solutions.

Possibility of yielding by increasing suction Figure 4.19 shows the results from drying and wetting tests, indicating that suction and specific volume relationships appear to be linear with perhaps some hysteresis. None of the specimens show a separation of

recoverable and plastic deformations. Suction changes do not appear to produce yielding for this material in the range of suctions that have been used.

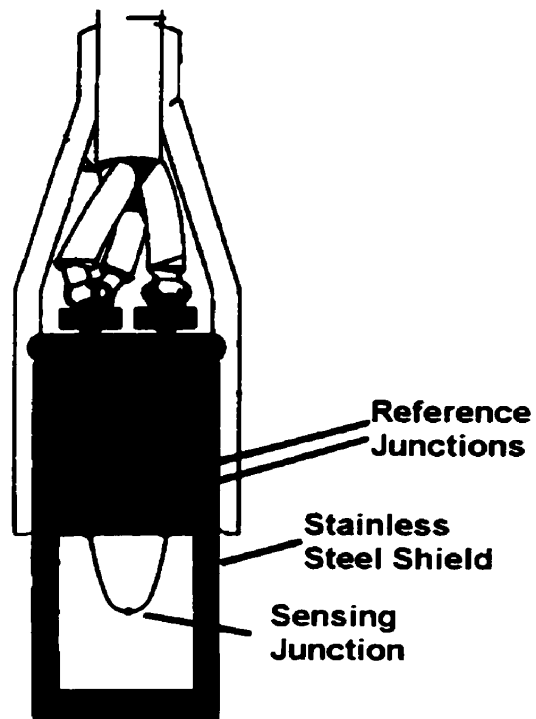


Figure 4.1 A schematic psychrometer

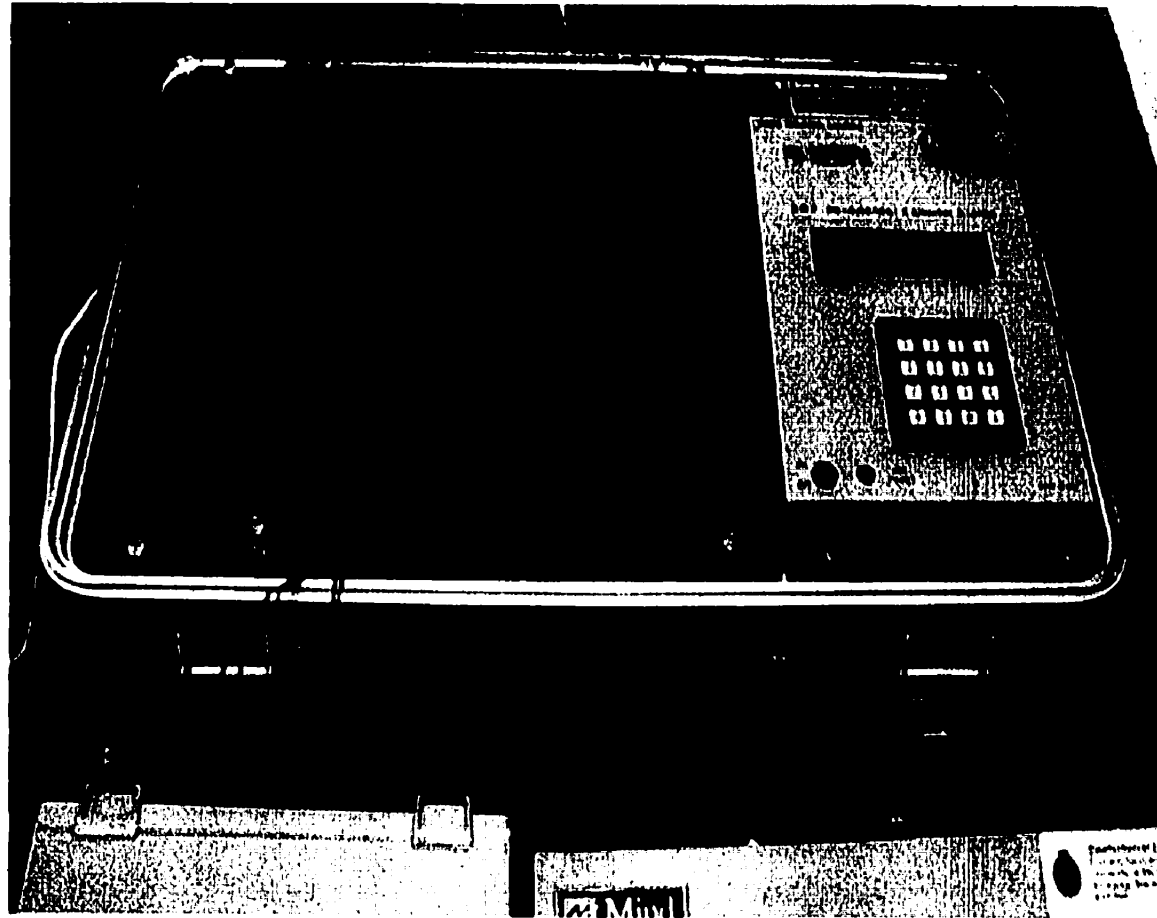


Figure 4.2 The CR-7 System

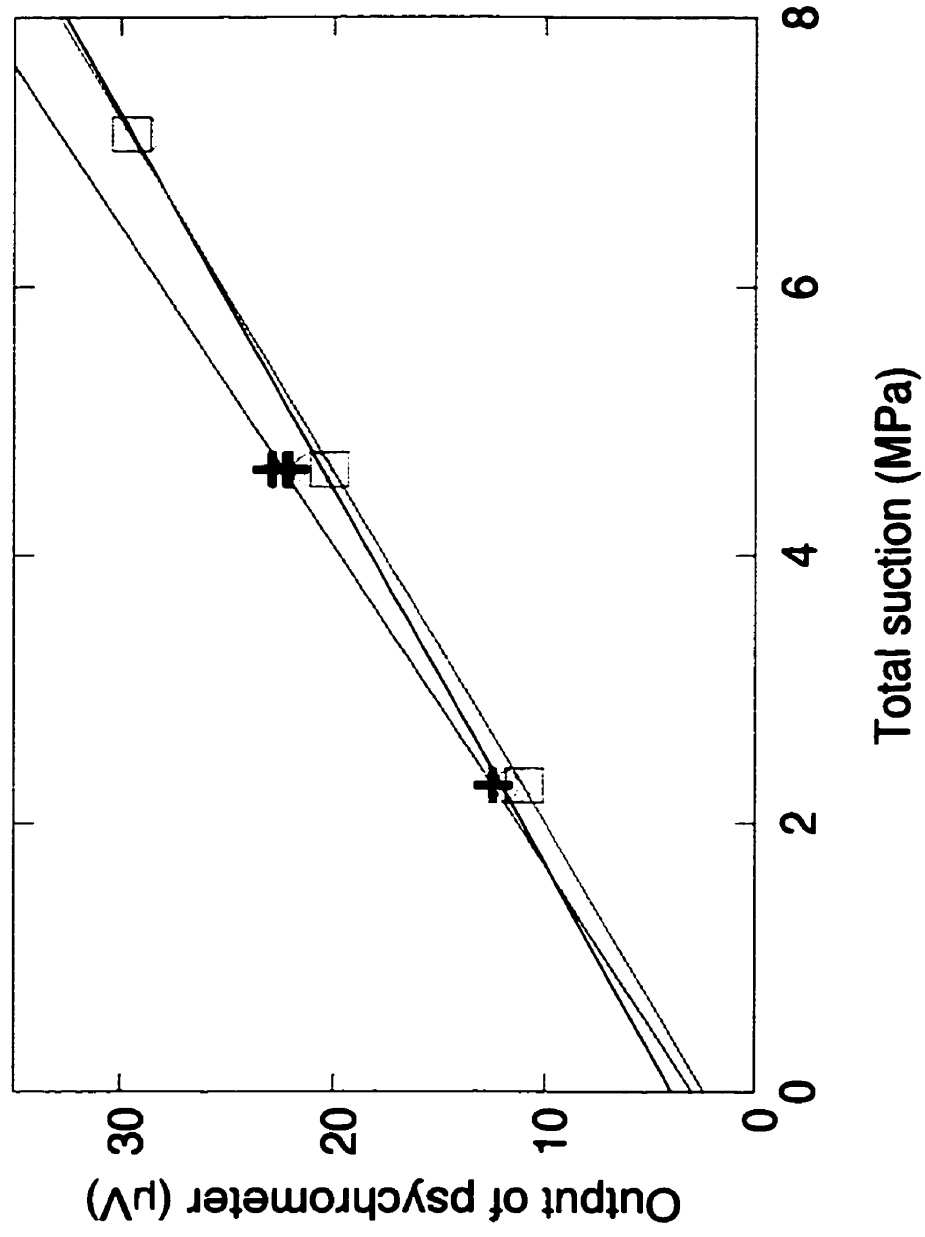


Figure 4.3 Calibration lines for psychrometers

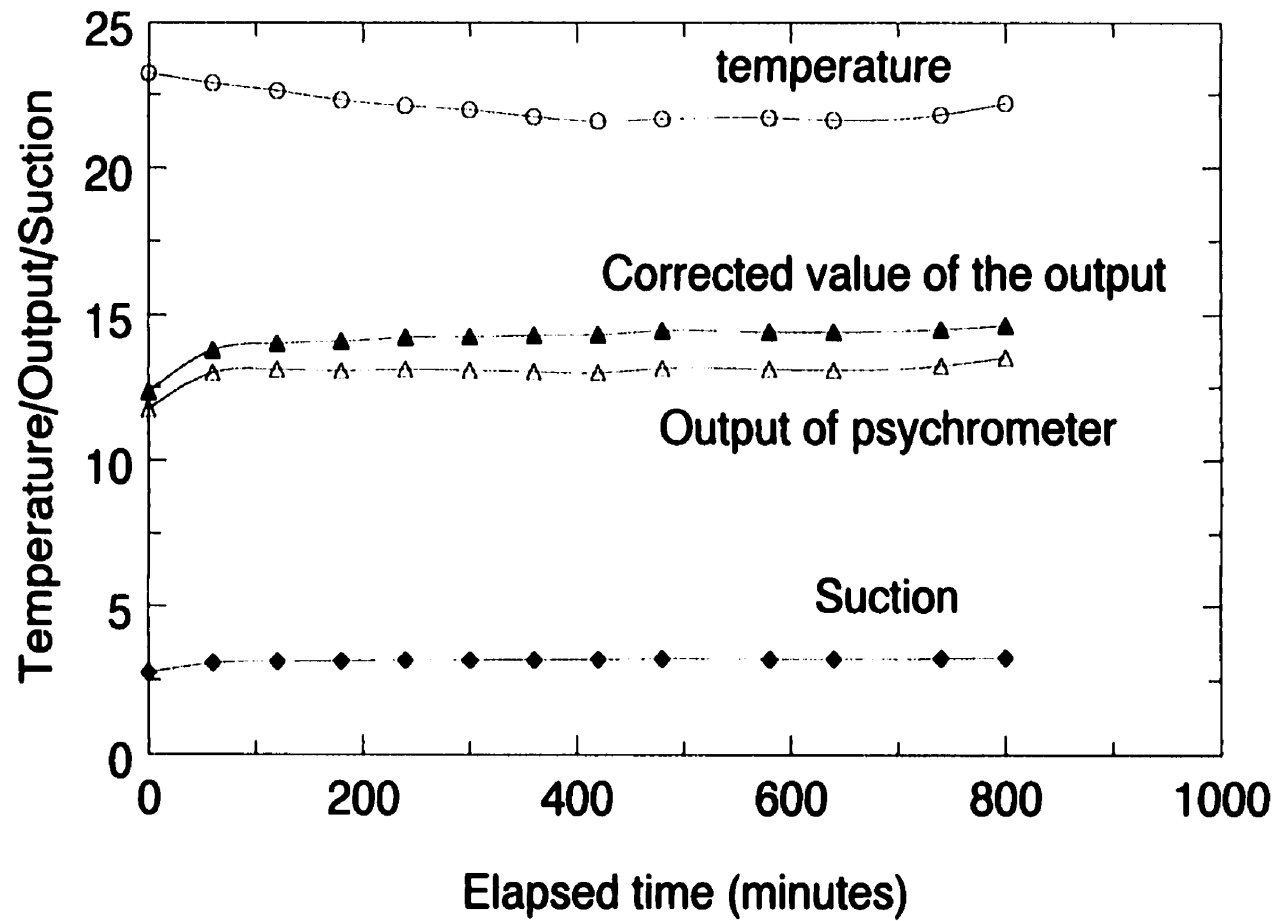


Figure 4.4 Variation of temperature and suction with time

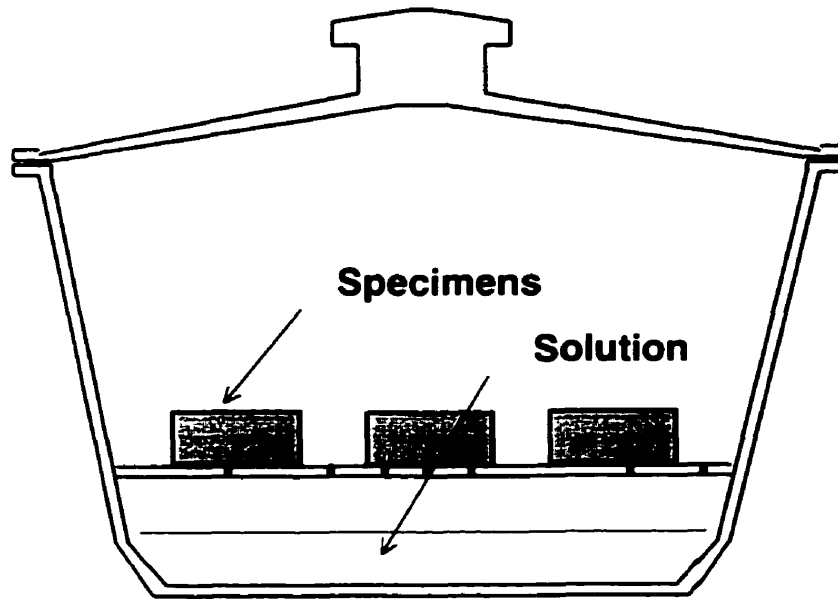


Figure 4.5 Layout of specimens and osmotic solution in a desiccator

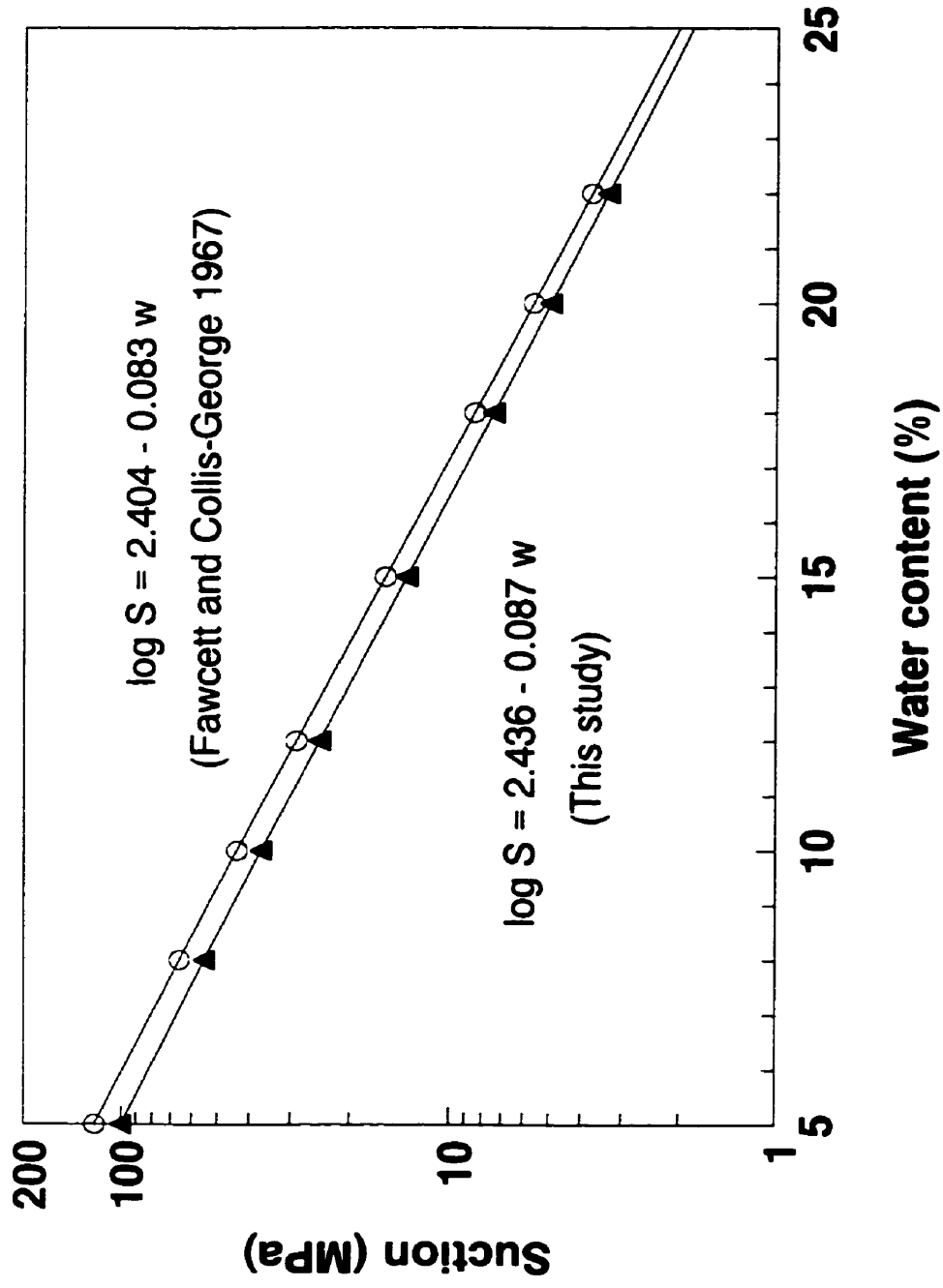


Figure 4.6 Comparison of calibrations of Whatman 42 filter papers

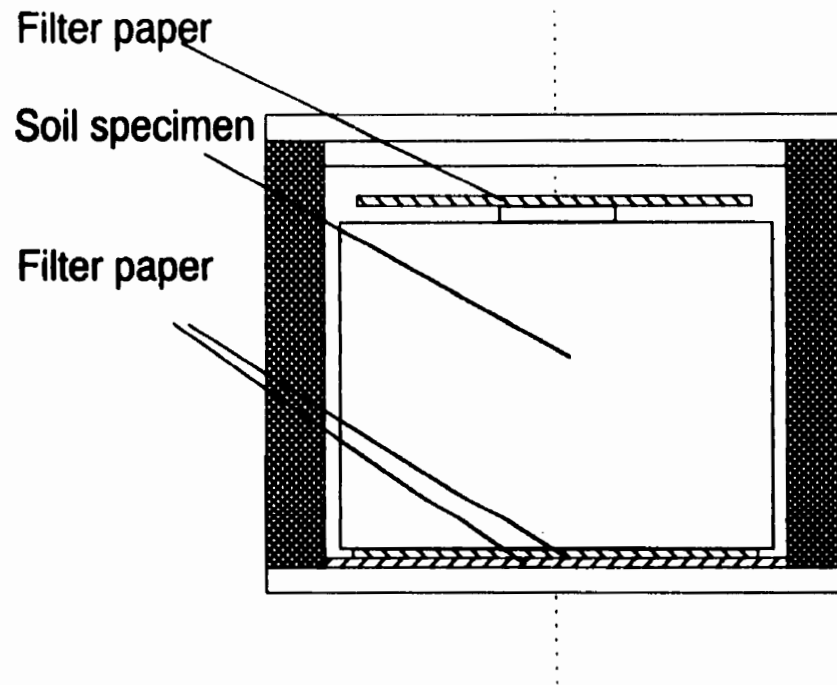


Figure 4.7 Layout of soil specimen with filter papers

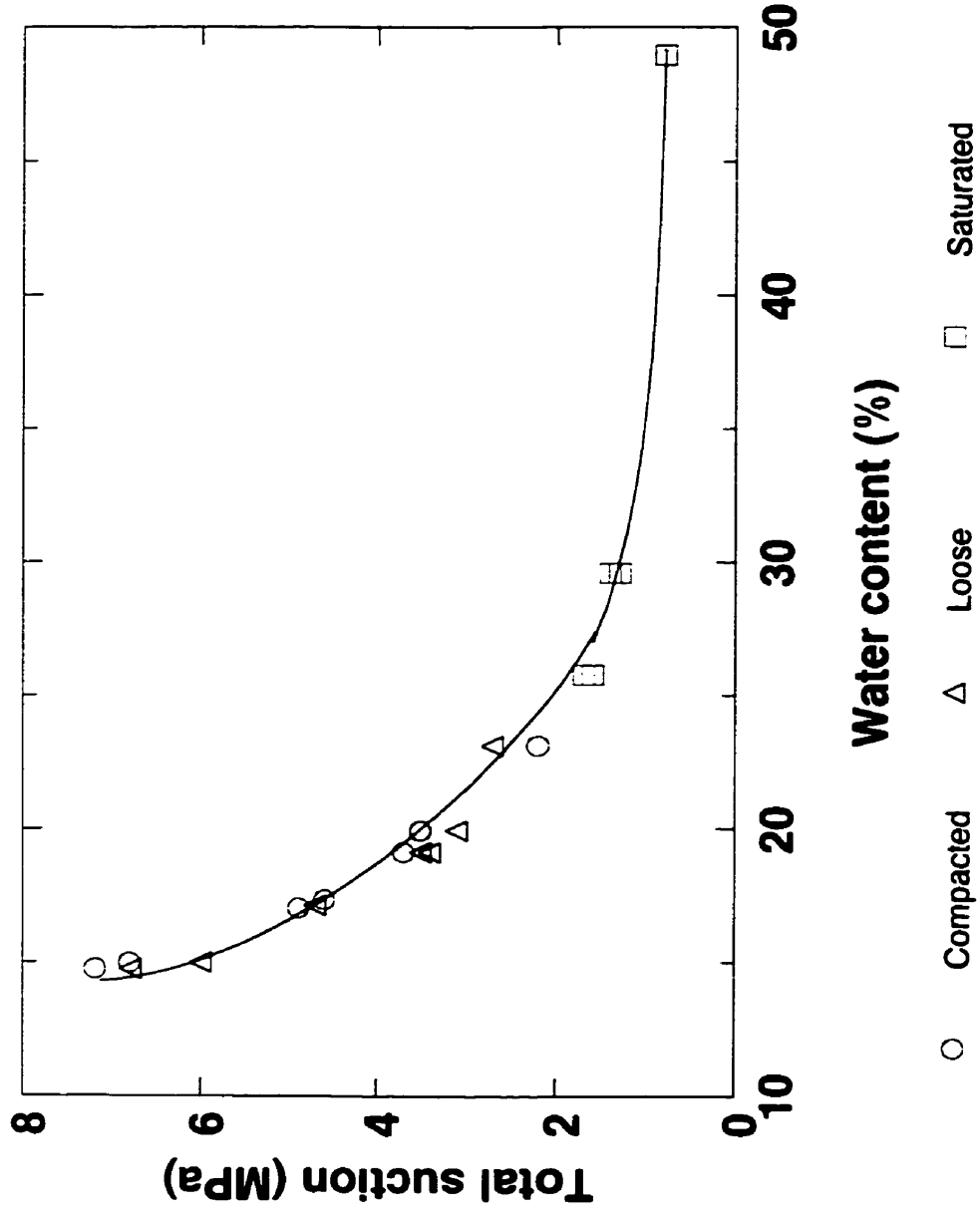
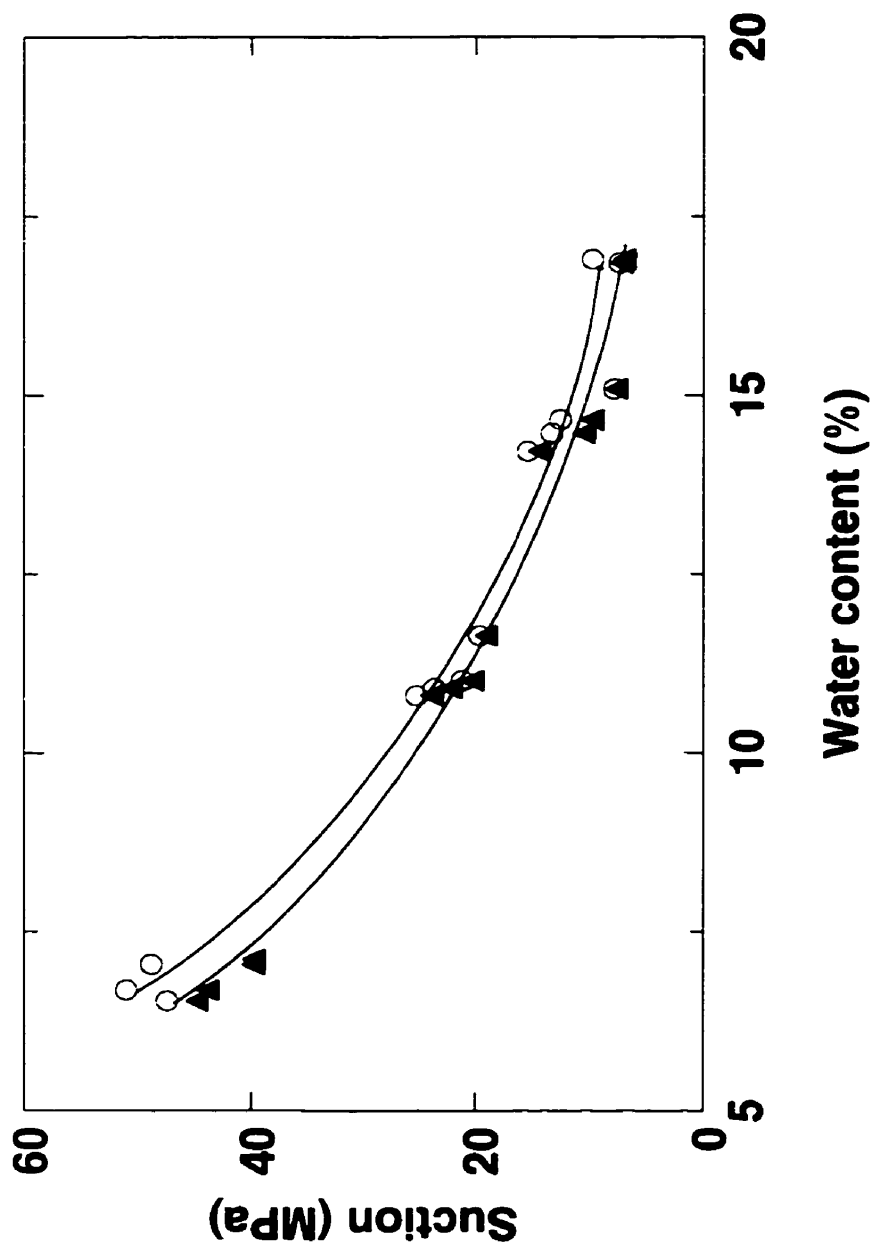


Figure 4.8 Total suction vs water content measured by psychrometers



○ Total Suction ▲ Matric Suction

Figure 4.9 Suction vs water content measured by filter paper method

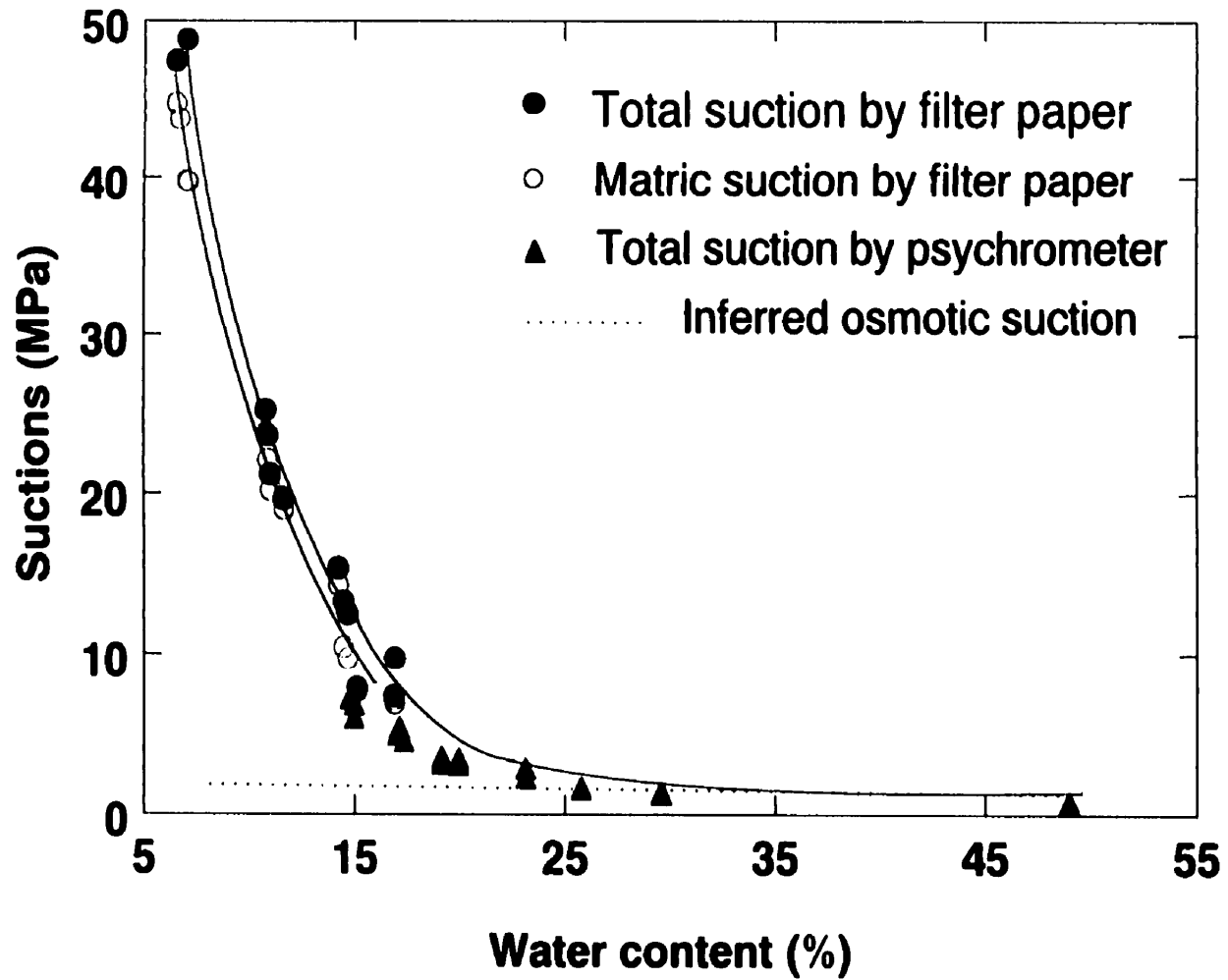


Figure 4.10 Suctions versus water content

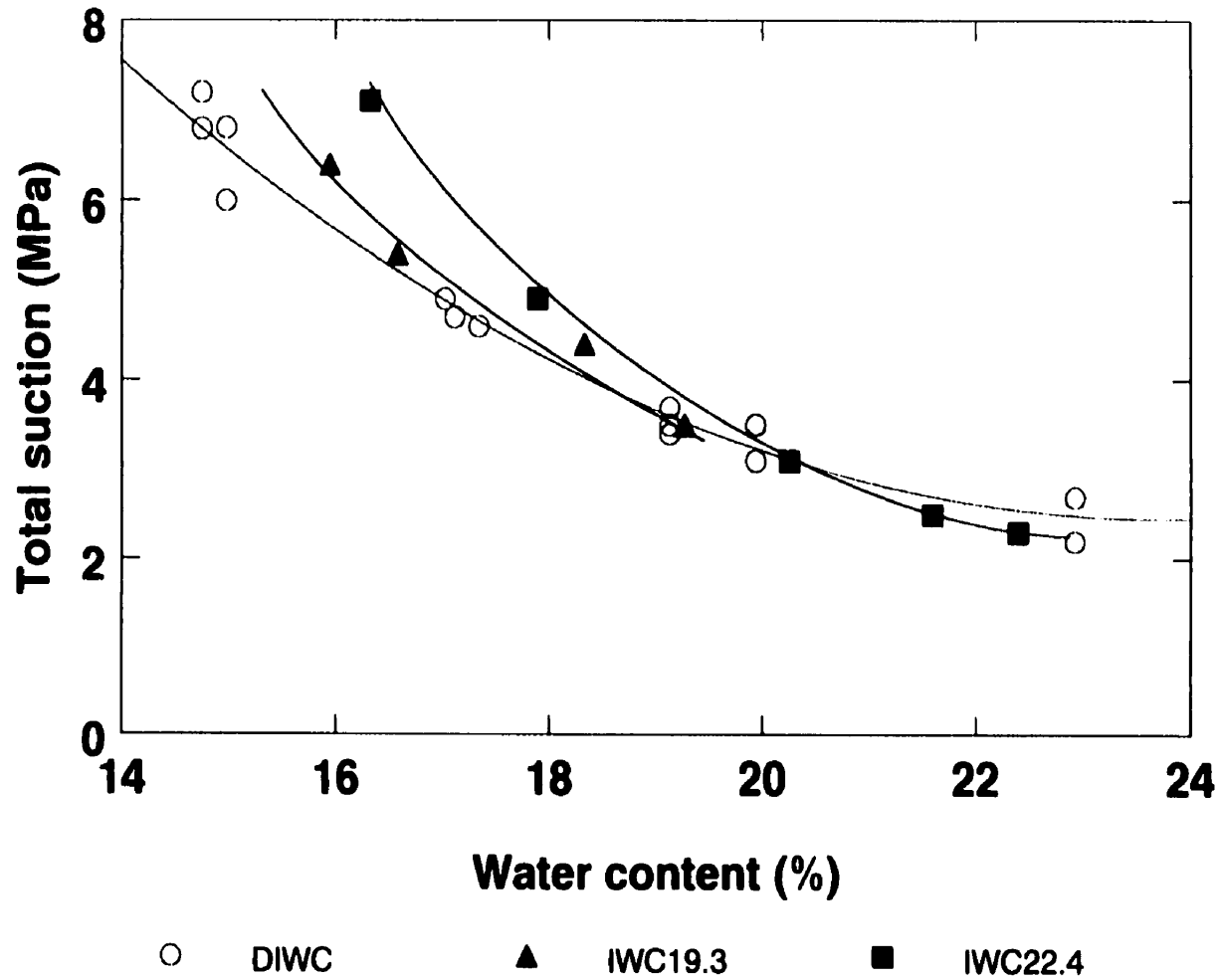


Figure 4.11 Total suction - water content relationships determined using different procedures

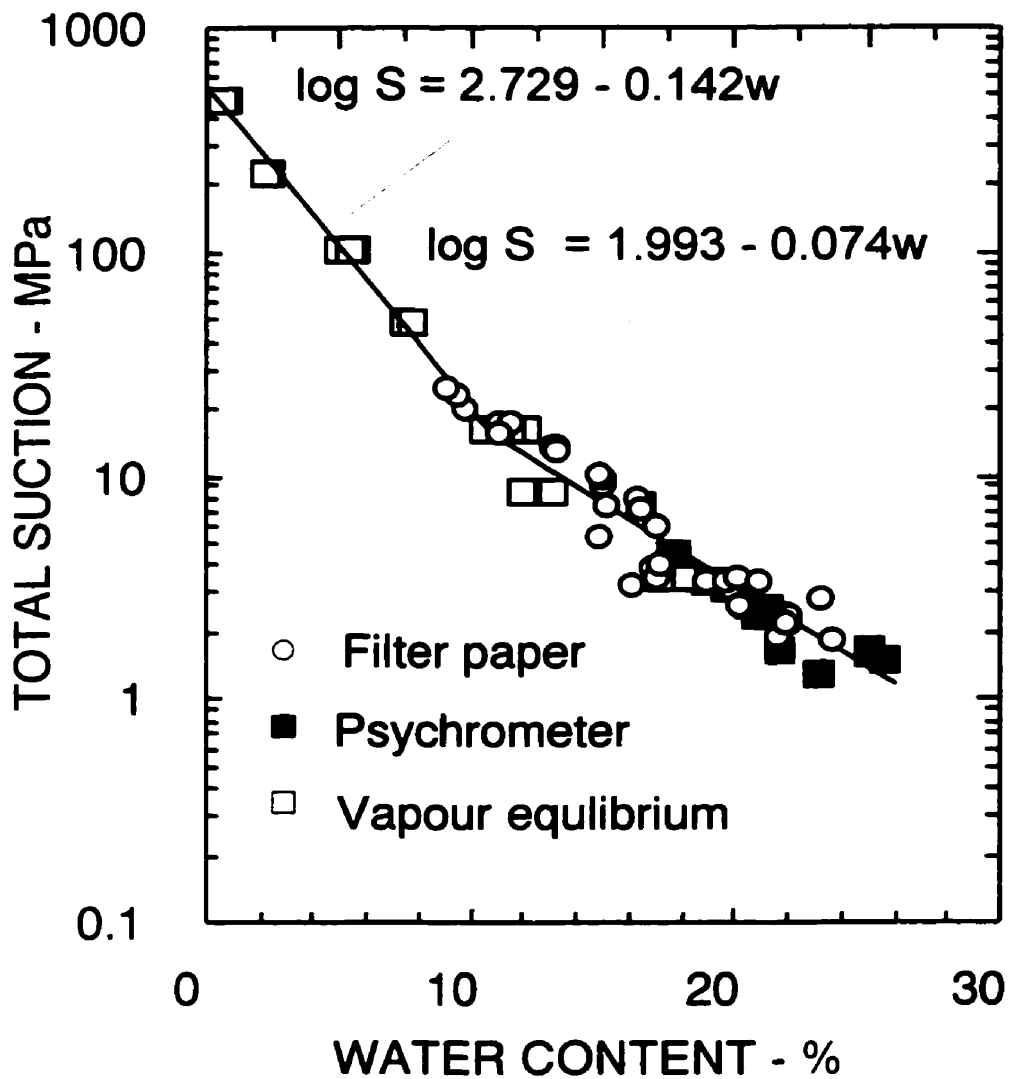


Figure 4.12. Suction-water content relationship of sand-bentonite (Wan *et al.* 1995)

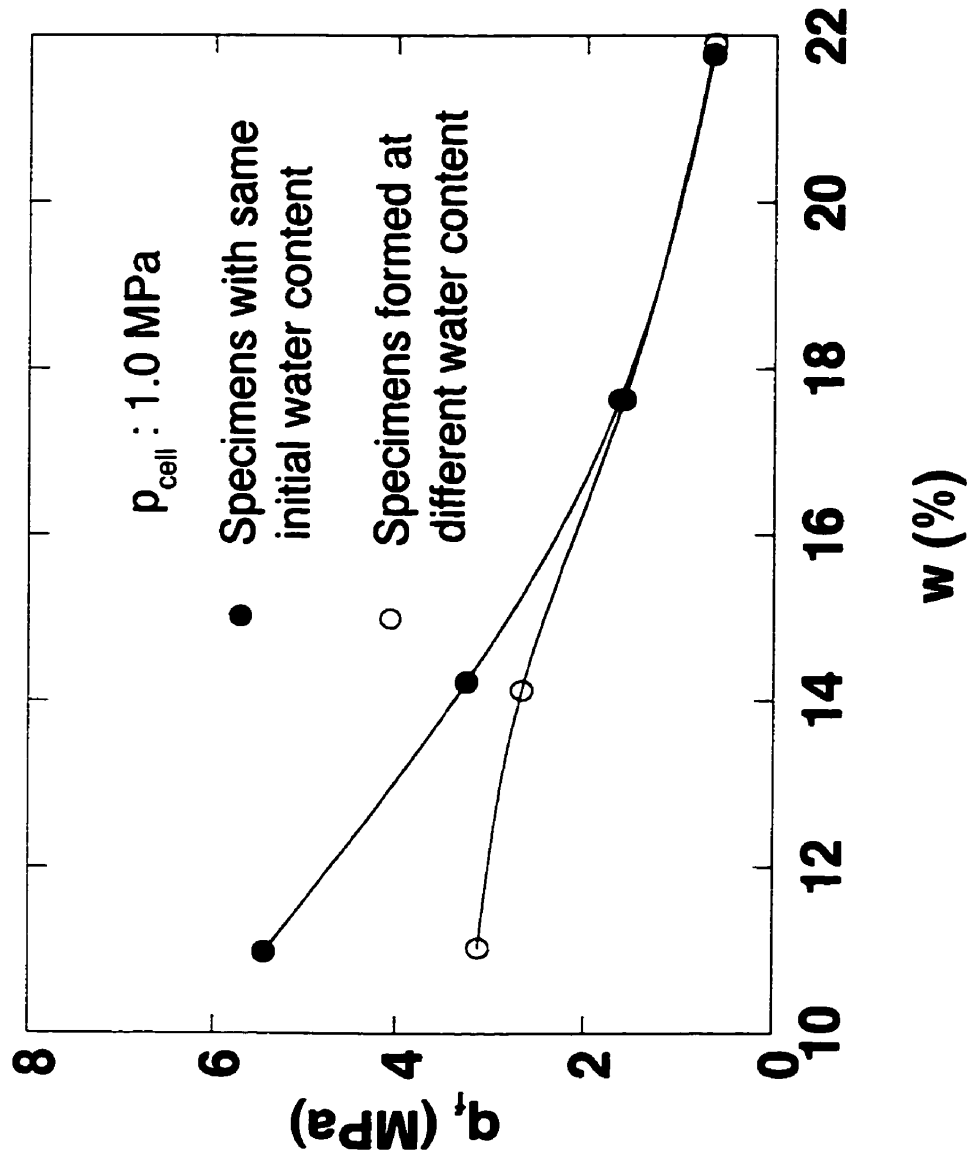


Figure 4.13 Specimen preparation effects
on strength (Wiebe et al. 1998)

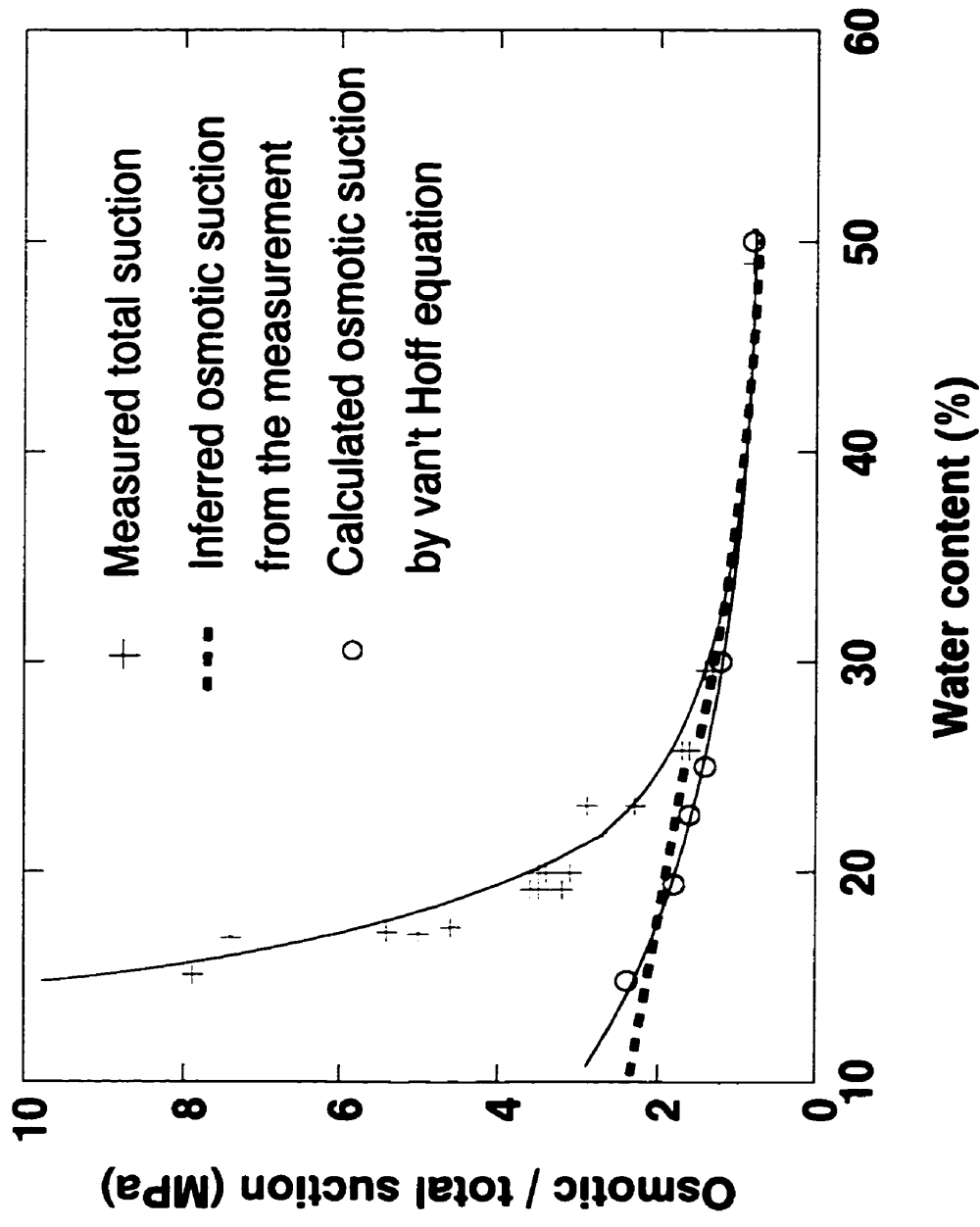


Figure 4.14 Osmotic suction versus water content

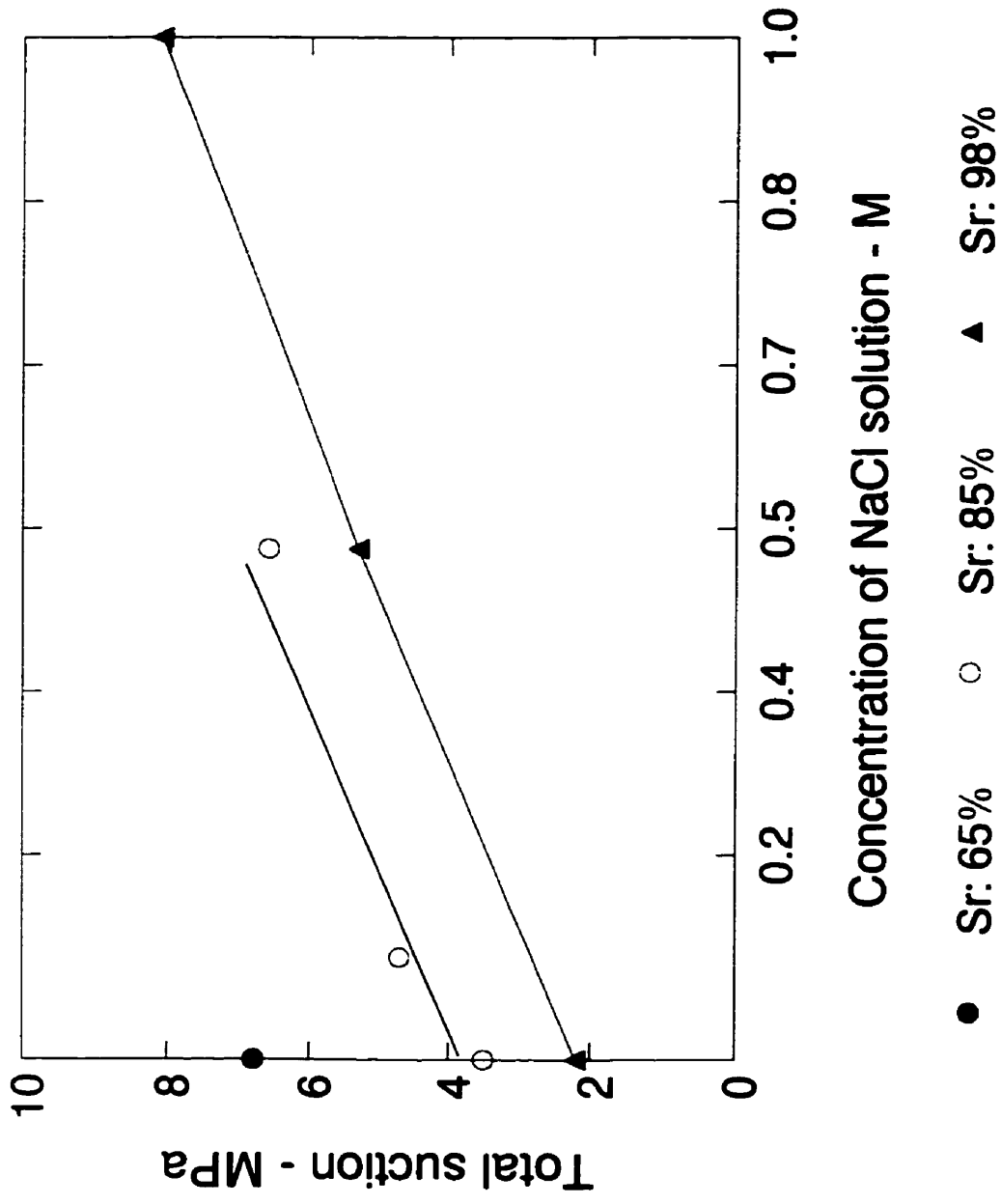


Figure 4.15 Elevation of osmotic suctions

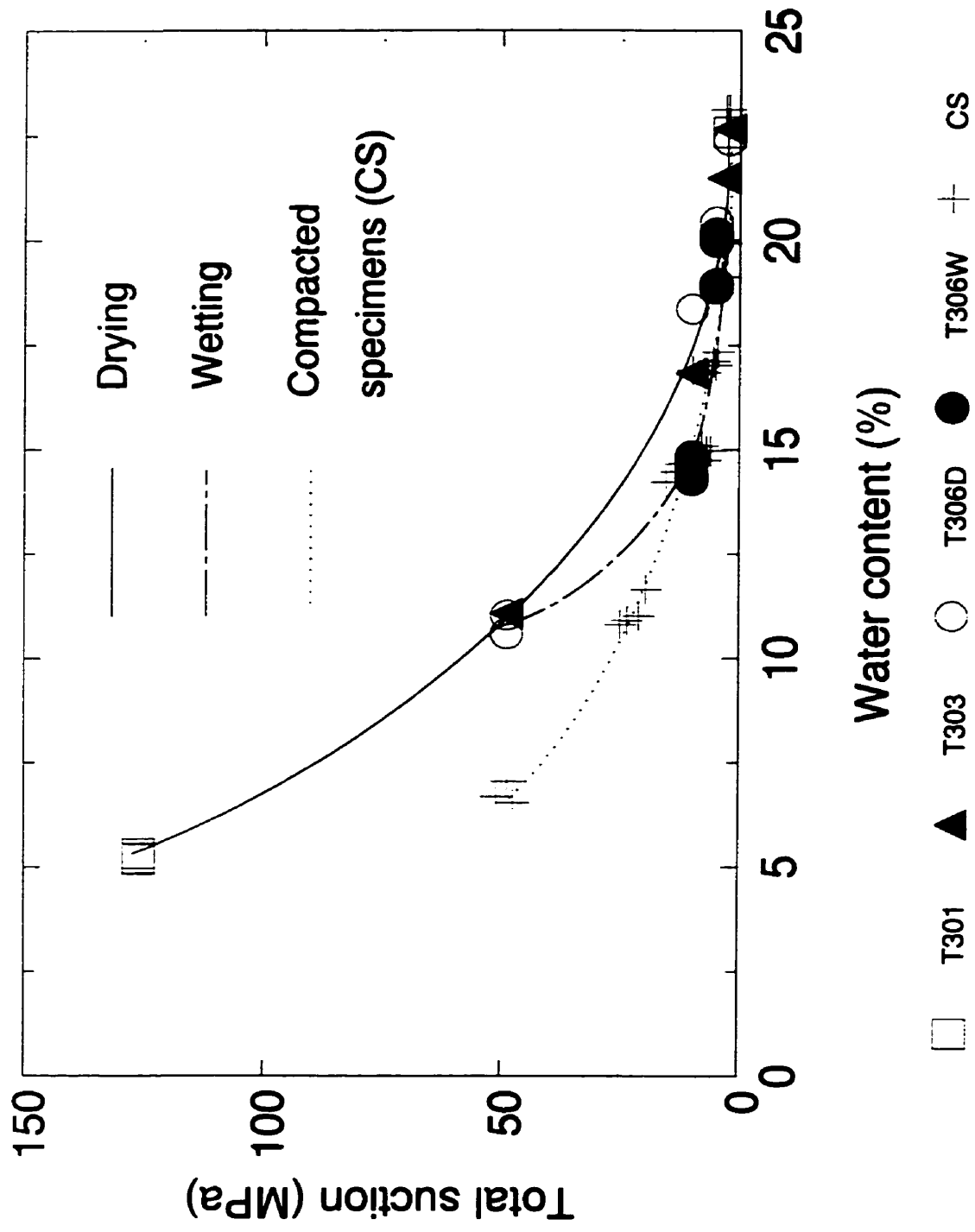


Figure 4.16 Soil Water Characteristic Curve (w: 22.4%)

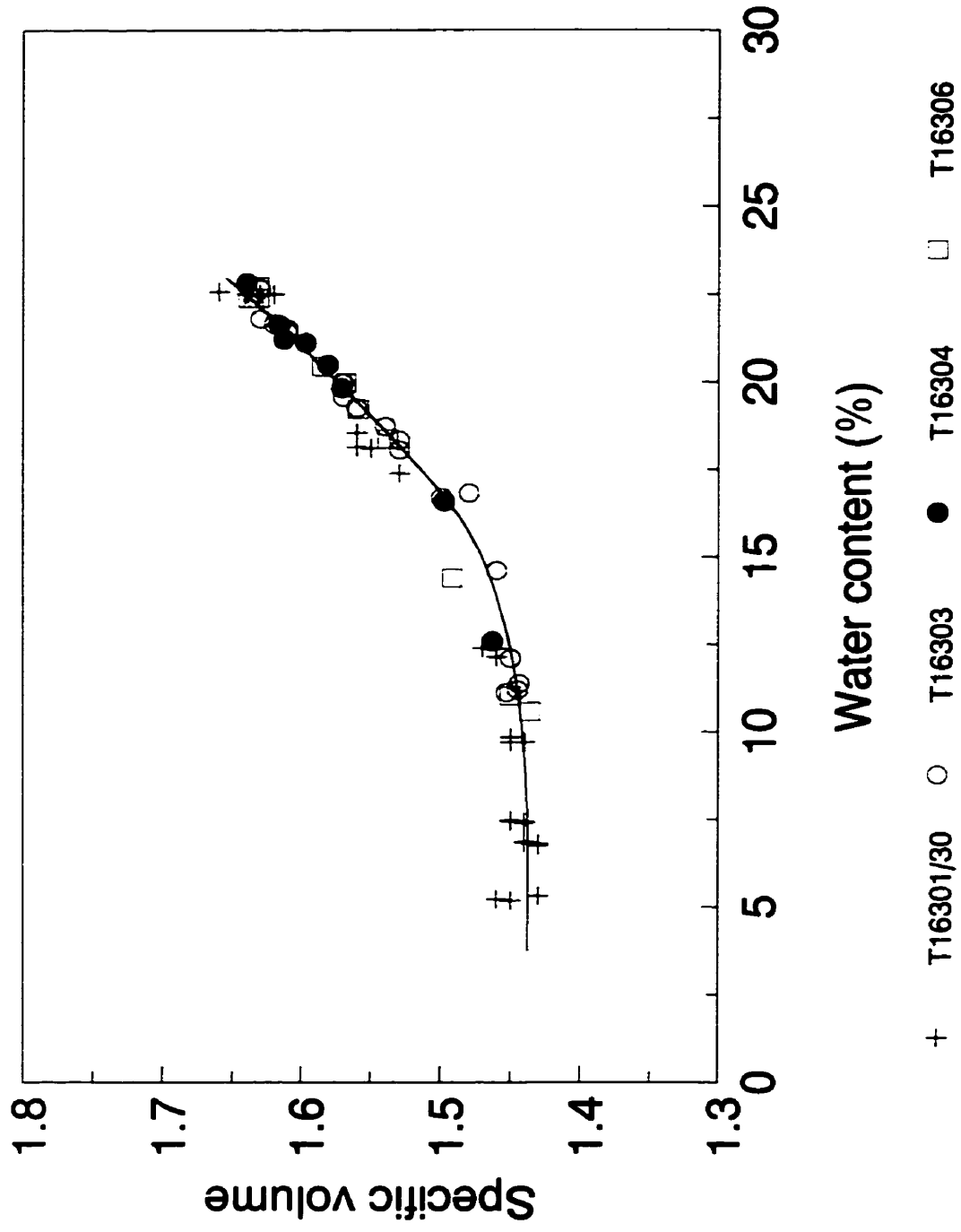


Figure 4.17 Volume change by drying

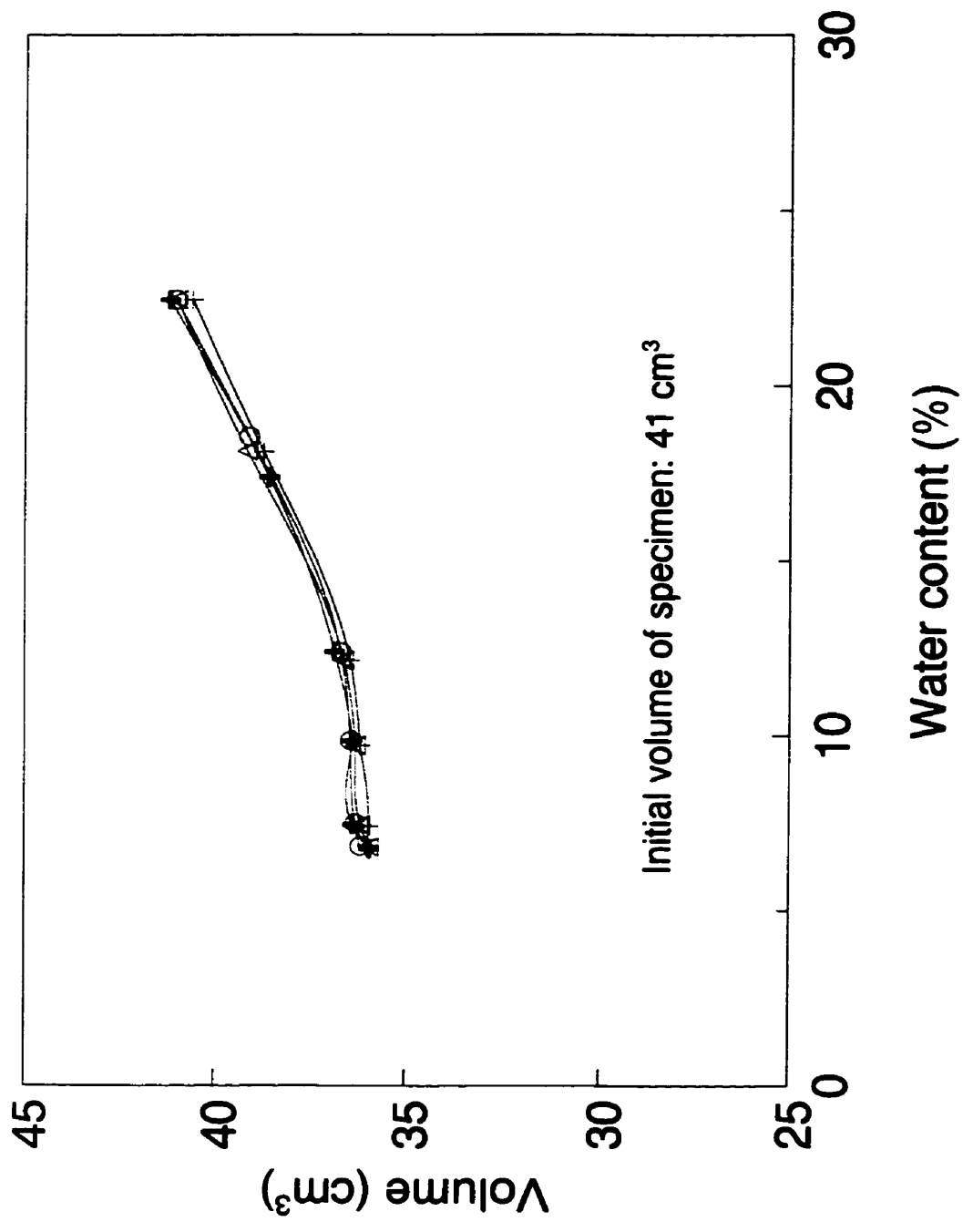


Figure 4.18 Water content versus volume

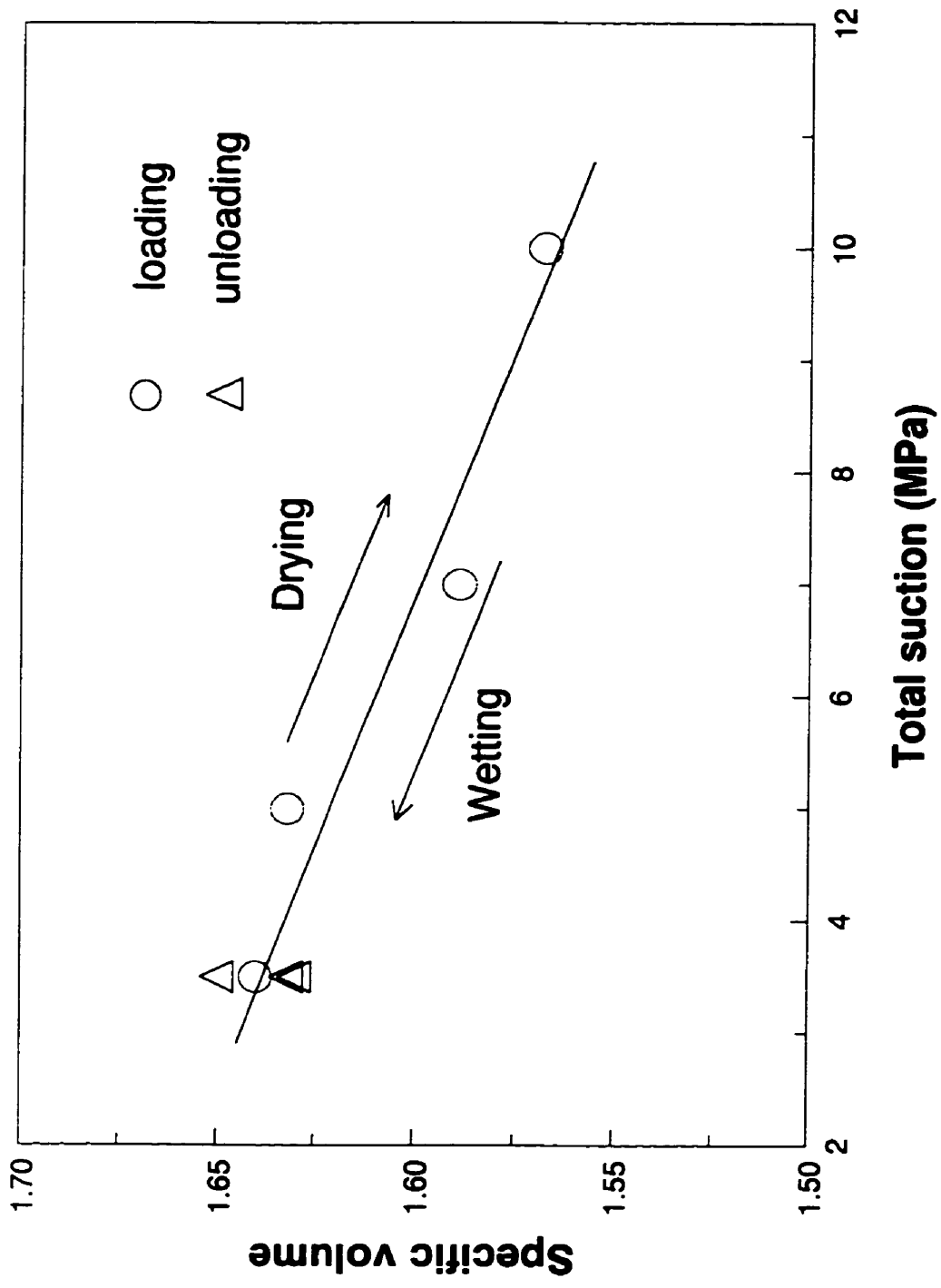


Figure 4.19 Volume change behavior under drying and wetting

CHAPTER 5

EQUIPMENT FOR TRIAXIAL TESTS AND TENSILE TESTS

5.1 Introduction

This chapter describes the triaxial cells and measuring equipment used for the triaxial compression tests and test facilities for tensile tests in this program. Stress-controlled and strain-controlled tests were both undertaken. Details of the planning of the test program will be given in Chapter 6. The triaxial tests were mostly performed in procedures that were stress path controlled with displacements and suctions being measured. The test facilities involved a 'high pressure triaxial cell', thermocouple psychrometer and non-contacting displacement transducers. Description of these facilities constitutes the major part of this chapter. The high pressure triaxial cell is introduced and the assembly of a specimen, psychrometer and non-contacting transducers is described. Psychrometers used to measure suctions on soil specimens have already been introduced in Chapter 4. The particular feature described in this chapter is a unique technique to incorporate psychrometers into triaxial testing. The non-contacting system for measuring

displacement is then described. It was chosen for use following an unsuccessful attempt to develop a home-made device based on LVDT's for measuring lateral displacement.

Strain-controlled tests were performed in the early stage of this program by using two simpler triaxial cells, namely a Leonard Farnell cell and a Brainerd-Kilman (B-K) cell. This part of the program included quick undrained triaxial tests and consolidated-undrained triaxial tests. However, suction changes and lateral strains could not be measured using these cells. The cells were used and described by previous students Oswell (1991) and Wiebe (1996). They are only introduced briefly in this chapter.

Existing experimental methods in geomechanics cannot be used to perform tensile tests on unsaturated soils (Tang and Graham 1998). This chapter also presents a new methodology and a designed rigid tensile mould for tensile tests on unsaturated soil samples. A series of tensile tests have been carried out and testing procedures will be introduced later in Chapter 6.

5.2 High Pressure Triaxial Cell

The high pressure triaxial cell designed by Lingnau (1993) was used for stress-controlled testing. A schematic of the triaxial cell is shown in Figure 5.1. It is constructed of nickel-plated mild steel with a stainless steel piston, top cap, and pedestal. The cell

consists of two thick circular plates at top and bottom, connected by four rods. To enclose the cell, a steel sleeve slips around the outside of the upper plate and is seated in a groove in the plate that forms the cell base. A thinner plate is bolted to the top plate with four large nuts to restrain the sleeve. The cell can withstand pressure up to 10 MPa and operates at temperatures up to 100°C. Tests in this research program were performed at room temperature and pressures up to 3 MPa.

The use of tie-rods inside the sleeve allows inspection of the specimen alignment and mounting of all instrumentation during the building-in process. The specimen is first mounted on the pedestal and the top cap placed on top of the specimen with a psychrometer intruding about 7 mm into the specimen (Tang *et al.* 1997b). The sealing membrane is then attached. Two aluminum foil targets are attached at the mid-height of the specimen using a rubber band. Two non-contacting transducers for measuring lateral displacements are mounted on tie-rods and one non-contacting transducer is installed for measuring vertical displacement. The piston and load cell are lowered until they are almost in contact with the load cap. The cell sleeve is then positioned and the cell fluid added. This procedure ensures that all the instrumentation components are properly aligned prior to testing. Silicon oil is used as the cell fluid for all tests. Its thermal stability and low electrical conductivity allow the load cell and lateral displacement transducers to be used inside the cell.

5.3 Psychrometer Techniques to Monitor Suction Change during Triaxial Tests

The principle and use of psychrometers were introduced in the preceding chapter. To apply this technique to a specimen in triaxial testing, special arrangements are required to prevent the psychrometer from interfering with the other instruments used for measuring axial load, confining pressure, and displacement. That is, to enable measurement of suctions in the stress fields of triaxial tests, psychrometers must be carefully selected, installed, and sealed. Two approaches have so far been used by other researchers (Edil *et al.* 1981, Wan 1996). One approach (Edil *et al.* 1981) is to install inside the top loading cap a thermocouple from a psychrometer which has had its shield removed. This may lead to damage and contamination of the thermocouple because it is no longer protected by a shield. Initial attempts by the author to duplicate this procedure led to breaking the sensing junctions of two thermocouples, and contaminating the junctions of two other instruments. The other major concern is that long test times may be required for equilibrium of partial vapour pressure between the thermocouple chamber inside the load cap and that in the pore voids of the specimen. The other approach (Wan 1996) embeds a psychrometer in the center of a specimen during compaction. This makes compaction more complicated and may lead to specimen disturbance that affects the mechanical behaviour. Improvements in techniques for using psychrometers in triaxial tests have to be developed to take account of the requirements of the experiments, economy, and reliability. This section presents a new technique which provides a promising means to incorporate suction measurement into triaxial testing.

5.3.1 Construction of a Triaxial Load Cap with a Psychrometer

Figure 5.2 illustrates the schematic layout of a psychrometer embedded in a load cap with only the tip protruding from the bottom of the load cap. Photographs of a stainless steel screen shield psychrometer with a 50 mm diameter load cap are shown in Figure 5.3. Stainless steel screen shield psychrometers (Wescor PST-55) were chosen for use because of their quick response, small tip size, and the robustness of their shields compared with porous ceramic psychrometers. This construction allows the major part of the psychrometer to be firmly held in the load cap with only a minimum portion (that is, the psychrometer sensing tip) inserting into the specimen.

5.3.2 Installation of a Psychrometer In a Specimen for Triaxial Testing

Figure 5.1 also shows the assembly of a compacted specimen in a triaxial cell where the load cap contains a psychrometer. The cap is placed on the specimen with the psychrometer tip being inserted into a small hole in the top of the specimen. The tip of a PST-55 psychrometer measures 5.0 mm diameter and 7.0 mm length and a triaxial test specimen measures 50 mm diameter and 100 mm. That is, only 0.07% of the specimen volume is occupied by the psychrometer. In this way, the psychrometer brings limited disturbance to the specimen (Tang *et al.* 1997b). The small hole is drilled as soon as compaction of the specimen is complete. The psychrometer senses the relative humidity in the air phase near the specimen while minimizing the size of the hole. The

specimen is then installed in a latex rubber membrane which is sealed to the load cap and triaxial pedestal using O-rings. This arrangement keeps the vapor pressure in measuring instrument equal to that in the small pores of the specimen.

Questions may be raised regarding the representativeness of suctions measured by psychrometers at the top part of the specimen. Figure 5.1 shows a cylindrical specimen which experiences external vertical stress σ_1 and lateral stress σ_3 . Due to friction of the load cap, some additional radial shear stresses may be expected at the top and bottom surfaces of the specimen. These end effects, along with influence of the small hole, mean that the stress field of the very top part of the specimen is different to some extent from the stress field at the center of the specimen. Nevertheless, as suction is a scalar variable, suction at any point in the specimen is equal after it reaches equilibrium in a specimen under certain external stress. This is similar to pore water pressure in saturated specimens, where pore water pressure is equal everywhere after equalization. This justifies the use of psychrometers to measure suctions at any location of specimens.

5.4 Non-contacting Displacement Measuring System

The non-contacting displacement measuring system - KDM-8200 consists of 3 transducers (or sensors) and an electronic measuring system, manufactured by the Kaman Sciences Corporation at Colorado Springs, Colorado. The measuring system is based on

the eddy-current loss principle between conductive surfaces of metal targets and the electronic transducers (Fredlund and Rahardjo 1993). As a conductive surface moves closer to a transducer, more eddy currents are generated and the losses within the bridge circuit of the oscillator demodulator become greater. These impedance variations are converted to a DC voltage output. The output is linearly proportional to the distance between the sensor and the conductive target. Data are collected and stored by a data acquisition system as introduced later in Section 5.5.2.

As shown in Figure 5.1, two transducers are arranged laterally to measure changes in the specimen diameter while the third is installed vertically to monitor changes in specimen height. The lateral transducers, Kaman type 6UEP, are clamped to tie-rods of the cell and have a measuring range of 6 mm. The vertical transducer, Kaman type 15U2, is installed on a post and has a measuring range of 15 mm. Its steel target is mounted on the steel load cap. The separate measurement of lateral and vertical deformations provides data for examining both compressibility and shearing deformations.

5.5 Peripheral Equipment

5.5.1 Load System

Axial load is applied to the specimen through a 25 cm diameter stainless steel piston using a system of hangers, levers, and weights. Schematic details of the system were

The *Leonard Farnell* triaxial cell was used for undrained triaxial compression tests in a *Wykeham-Farrance* 10 kN multi-speed load frame. The tests were conducted at ambient temperatures using low cell pressures of 0.2 MPa and water as cell fluid. A dial gauge was used to measure axial deformations by reading the movement of the loading ram relative to the cell cover. Loads were measured externally by a load cell, and displayed digitally. Strain rates were controlled at 0.762%/min. Specimens were compacted at different water contents (and hence saturations) to a dry density of 1.67 Mg/m³. Details of the procedures used for these tests will be given later in Section 6.2.

Testing at higher cell pressures used a B-K triaxial cell which can operate with cell pressures up to 3.5 MPa. Axial loads were applied by a 12.7 mm diameter ram mounted in a linear bearing to maintain alignment and reduce friction. An external load cell and LVDT at the top of the cell measured axial loads and displacements automatically. Silicon oil was used as cell fluid. This cell was used for consolidated-undrained triaxial tests to examine the effects of specimen preparation. Drainage of the air phase was allowed when specimens compressed at a cell pressure of 3.0 MPa before undrained shearing. Details of this test program are described in Section 6.2.2.

5.7 Testing Facilities for Tensile Tests

Testing facilities for tensile tests consist of a load frame and a specially designed tensile mould. The load frame is a conventional motor-driven mechanical jack which can apply

compressive or tensile force to soil specimens at constant displacement rate. The mould comprises two separate half cylindrical forms to hold specimens (Figure 5.4). The forms are welded to short lengths of channel which connect to the platen and cross-head of the load frame. Each form has 25 mm radius so that the specimen is held firmly using a film of adhesive. The depth of the form is 22 mm. After the specimen has been glued into the two forms, the gap between the edges of the forms is 6-8 mm. This ensures the specimen fails at a free surface close to its axis. The length of the form is 103 mm, long enough to hold traditional triaxial specimens. The stress distribution in the specimen and alternative forms of the mould was analyzed using finite element method. Results will be presented later in Section 7.3.3.

Figure 5.5 shows the setup of the tensile mould and load frame.

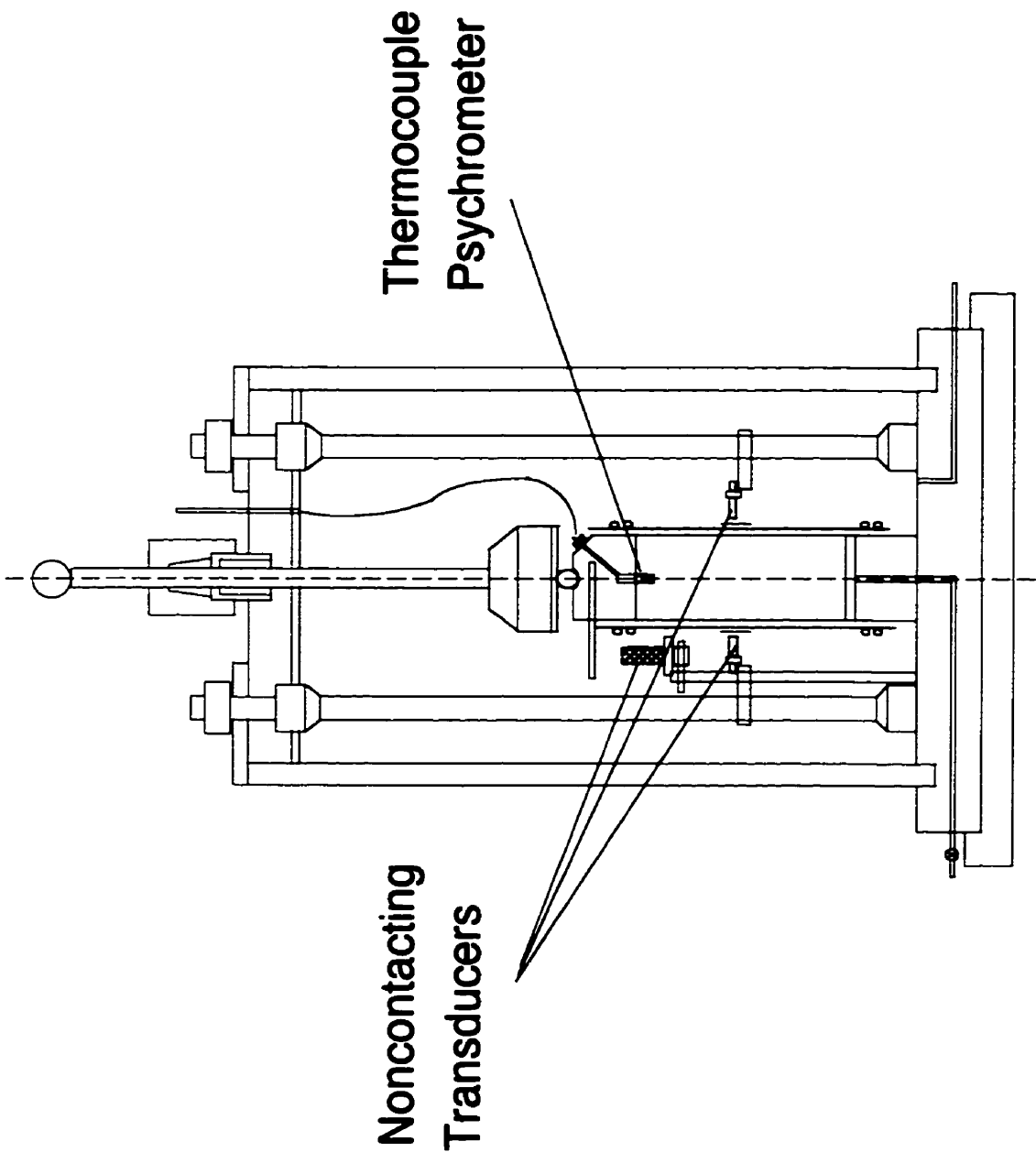


Figure 5.1. Triaxial cell and psychrometer installation

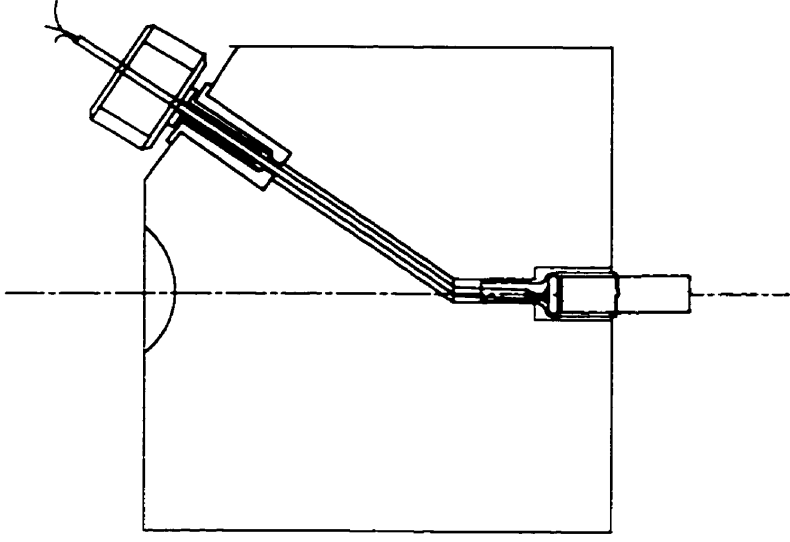


Figure 5.2 Schematic diagram of a load cap equipped with a psychrometer

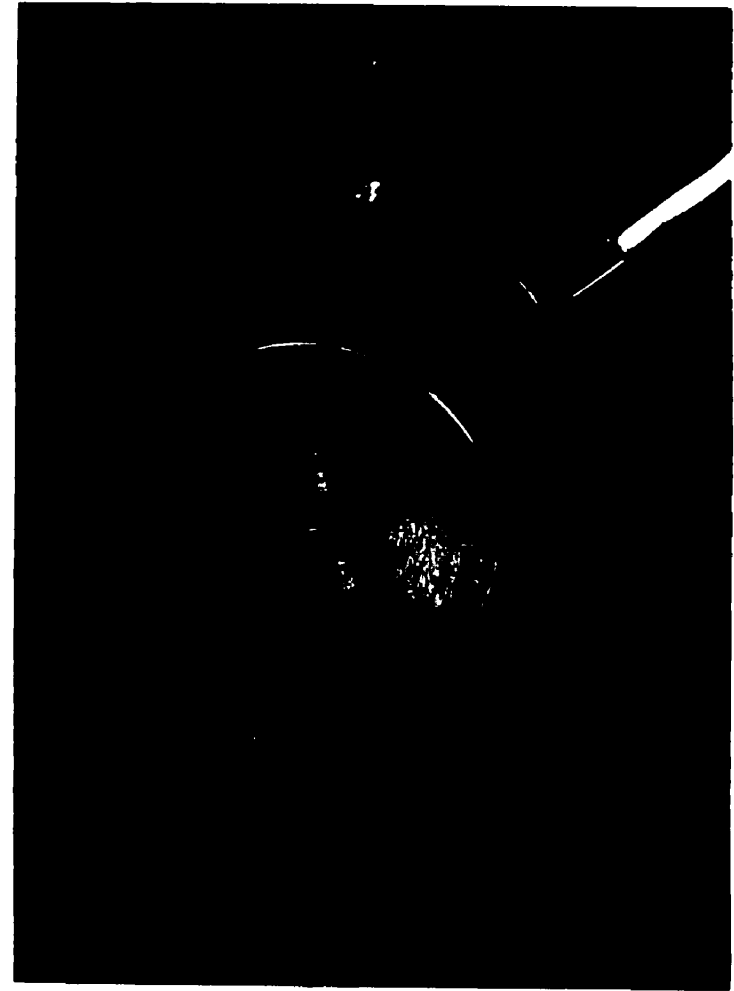
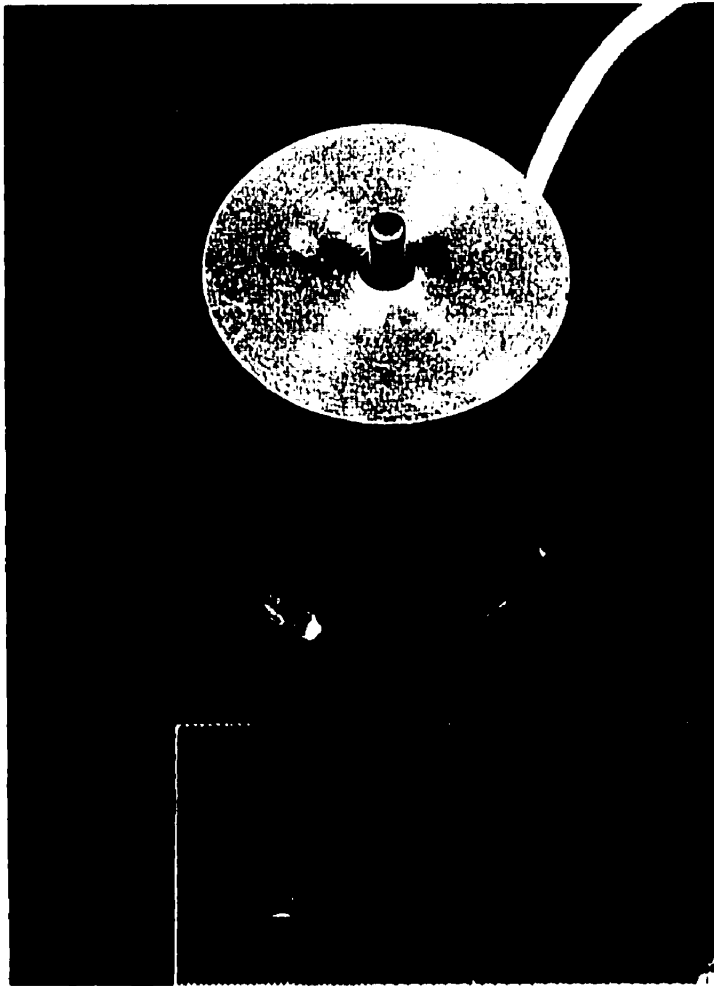


Figure 5.3 Photographs of a load cap equipped with a psychrometer

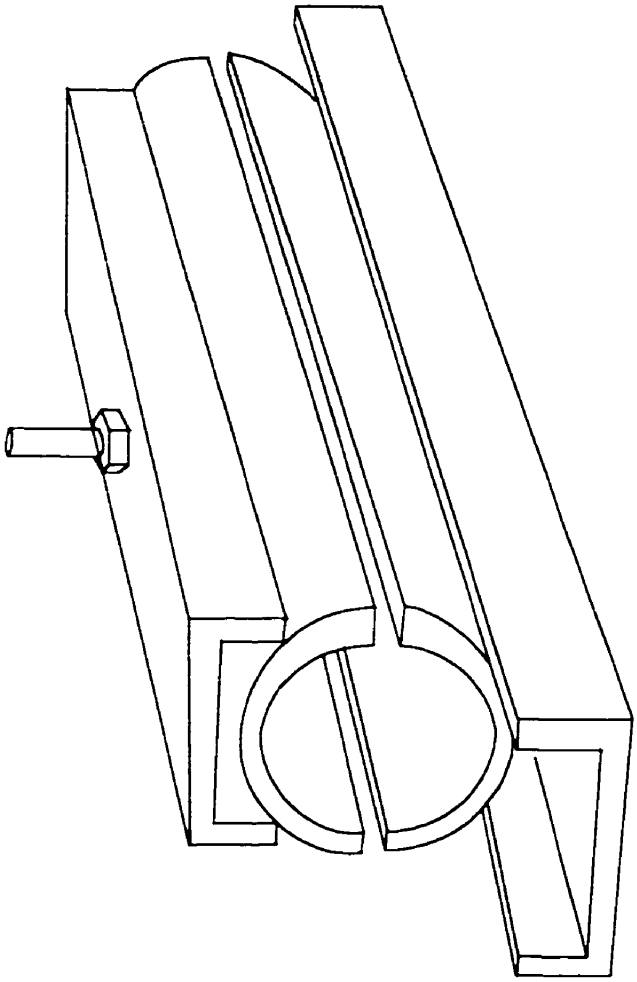


Figure 5.4 Oblique view of the designed tensile mould

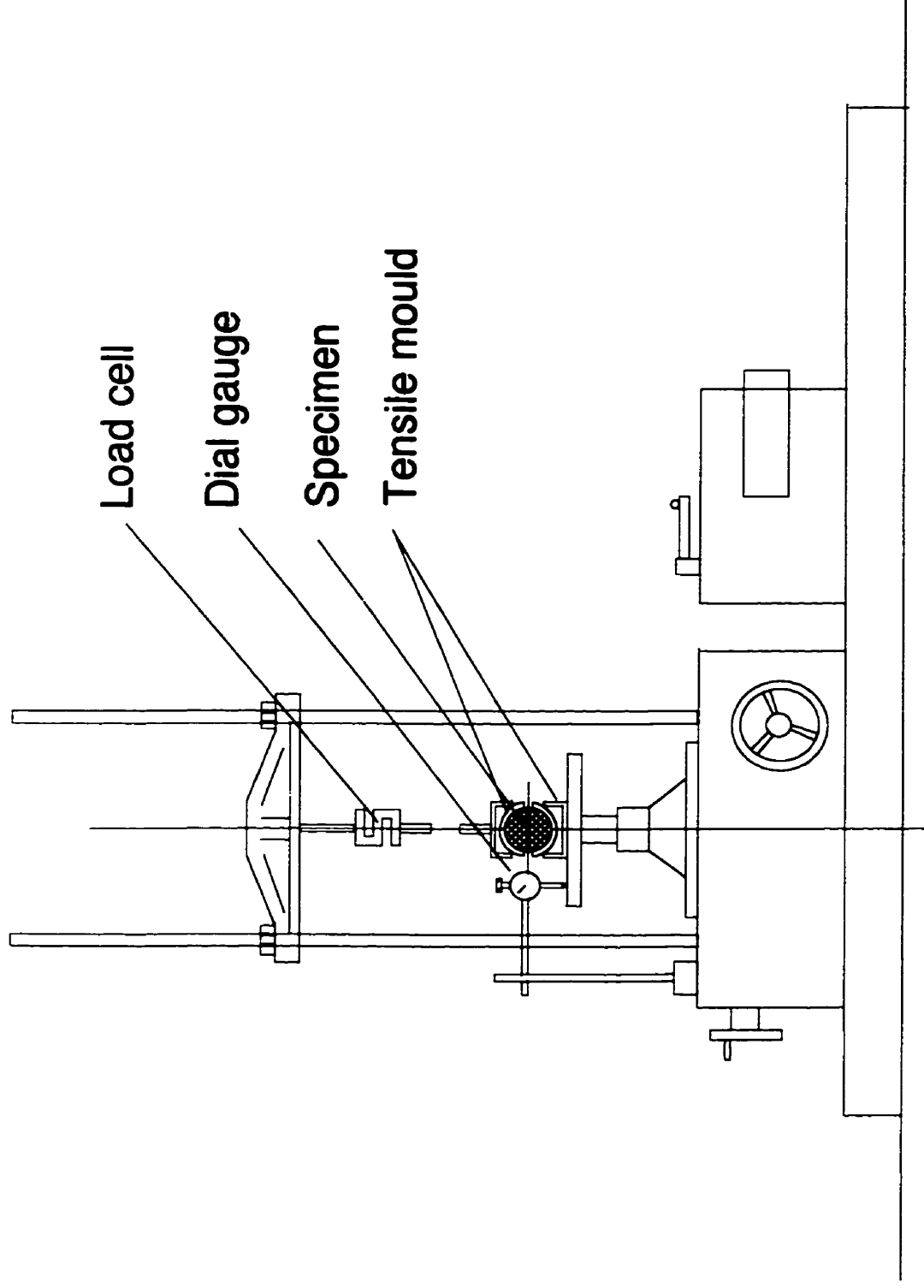


Figure 5.5 Side view of tensile mould and load frame

CHAPTER 6

TESTING PROGRAM AND TEST PROCEDURES

6.1 Introduction

Triaxial tests and tensile tests in this program examined how stress-strain behavior and strength properties of unsaturated buffer material depended on suction. Two broad types of unsaturated specimens were tested. The first type of soil specimen was prepared at different saturations and water contents but at the same dry density. The second type of soil specimen was formed at a constant value of saturation, water content and dry density. Some of these specimens were tested immediately after being compacted, while the remainders were dried for more than one month before triaxial testing.

Quick-undrained triaxial compression tests were carried out on the first type of specimen which were prepared with saturations ranging from 50% to 98% as described earlier in Chapter 3. Identical specimens were also made to evaluate initial suctions using psychrometers. The resulting data from the separate series of triaxial tests and suction measurement tests provide a preliminary understanding of how saturations and initial

suctions affect strength and compressibility. The different initial saturations produced different total suctions in such a way that only the matric suction components changed, while osmotic suctions were almost constant. That is, although total suctions were measured, the tests only examined the effects of matric suction. The effects of osmotic suctions on strength were examined in a separate series of specimens whose suctions were elevated by osmotic agents. Section 6.2 outlines the program of quick undrained triaxial testing. Similar, though not identical tests of this type were reported by Wiebe (1996).

The second type of specimen was tested using a more sophisticated triaxial system which could control stress paths and measure suctions and deformations. Loading was applied incrementally along selected stress paths. During triaxial tests, suction changes were monitored by psychrometer and deformations measured by non-contacting displacement sensors. Results allow examination of major features of elastic-plastic behavior of unsaturated buffer. The tests are therefore pivotal of this doctoral project. Details of the tests are given in Section 6.3.

Section 6.4 describes procedures developed for tensile tests on unsaturated buffer specimens. The second type of specimens was used for tensile tests. To the author's knowledge, this is first time tensile tests have been conducted on unsaturated soils. Traditional tensile test methods such as direct tensile pulling tests and the Brazilian test used for other materials cannot be used for testing soils. Soils cannot be easily formed

into the required bar-shape for direct tensile pulling tests without producing weak interfaces or material disturbance. The Brazilian test does not work well because ductility of most soils makes specimens deform into elliptical cylinders before fracture.

6.2 Quick-undrained Triaxial Tests

6.2.1 Tests on Compacted Specimens at Different Saturations

This series of tests examine the influence of saturation on strength and compressibility of the unsaturated buffer.

Specimens As described in Chapter 3, specimens with diameter 50 mm and height 100 mm were formed by static compaction to a dry density of 1.67 Mg/m^3 , and saturations of 65%, 75%, 85%, and 98%. For each saturation level, four specimens were used to check quality control of the techniques used for forming specimens, and four additional specimens were prepared for shear testing. At the time the tests were performed, no techniques were available for measuring suction during triaxial testing. All that could be done was to evaluate initial suctions of the specimens by forming identical specimens and measuring their suctions using the psychrometer techniques. Measuring procedures for suction measurement were described in Chapter 4.

Testing procedures All tests were done according to ASTM D2850-87 at room temperatures and at low confining pressure of 200 kPa using a Leonard-Farnell triaxial cell. The specimen was separated from the cell fluid (water) by a rubber latex membrane. Four O-rings were used to seal the membrane to the top end cap and the bottom pedestal. The triaxial cell was then closed by lowering the cell top over the pedestal base and the cell filled with water. Cell pressure was adjusted using air pressure applied to an external water reservoir. Before shearing, a small amount of deviator stress was applied to the specimen to ensure good contact. Loading was then applied at an axial strain rate of 0.76%/min. Vertical axial loads were measured using an external load cell. Vertical displacements were measured using a dial gauge mounted on the cell cap. Readings were made at every 0.1% vertical strain until peak failure or constant load was achieved. Assuming the volume of the specimen remained unchanged during shear, the area at mid-height of the specimen was derived from the measured vertical displacement, and therefore deviator stress was determined. After completion of the test, the specimen was removed from the cell and its water content and final dimensions were measured. A total of 21 tests were carried out.

6.2.2 Tests on Compacted Specimens with Elevated Osmotic Suctions

To examine the effects of osmotic suctions, total suctions were elevated by introducing osmotic solutions into specimens. A set of saturated and unsaturated specimens was prepared using solutions with different concentrations to produce different osmotic

suctions. The influence of these added osmotic agents was assessed in terms of the effect of this elevated total suction on strength and stiffness of the specimens by carrying out triaxial compression tests.

Specimens The sand and bentonite components of the specimens were mixed with required amounts of sodium chloride solutions at three concentrations of 0.1 M, 0.5 M, and 1.0 M. At each concentration level, 3 specimens were compacted to saturations of 65%, 85%, and 98%. Specimens measured 50 mm diameter \times 100 mm high and had a dry density of 1.67 Mg/m³. A total of 9 tests were performed. Total suctions of these specimens were also measured in separate tests. The relationship between total suctions and concentrations of the solution are described in Chapter 4.

Testing procedures Quick undrained triaxial tests on these suction-elevated specimens followed the same procedures as those described in the previous section.

Alternative testing procedures For comparison purposes, alternative triaxial procedures were adopted to examine the effect of specimen formation. A B-K triaxial cell was used for these tests. Tests were performed on two mixtures at water content of 19.42% (corresponding to 85% saturation of specimens at dry density of 1.67 Mg/m³). One was prepared with deionized water and the other was with 1.0 M NaCl solution. The mixtures were loosely compacted into specimens to a dry density of about 1.4 Mg/m³. They were then compressed in triaxial cells at 3 MPa for 12 hours with open drainage for the air

phase, and finally sheared to failure with the same confining pressure of 3 MPa. These alternative approaches provide an understanding of the relationship between compactive effort, elevated osmotic suctions, and strength. Interpretation of the results from conventional quick undrained triaxial test procedures and these alternative procedures will be discussed in Chapter 7.

6.3 Stress Controlled Triaxial Tests with Measuring Suctions and Deformation

As mentioned in Chapter 2 - Literature Review, investigating elastic-plastic behavior of unsaturated buffer involves five state variables namely mean stress p , deviator stress q , suction S , water content w and specific volume V . Given that w in a particular specimen is controlled by the compaction conditions and p and q are controlled by the test system, we must measure S and V at a series of intervals during each test. The hypotheses presented earlier suggested that major elastic-plastic behavior will be observed along selected stress paths. Data from such tests will allow development of an elastic-plastic model. This section describes two series of tests starting from two initial suction levels. Each series was performed at a number of stress paths with measurements of both suction and deformation.

6.3.1 Specimen Preparation

All specimens were compacted statically to achieve an initial water content of 19.4%, saturation of 85%, and dry density of 1.67 Mg/m^3 . The specimens had a diameter of 50 mm and a height of 100 mm. Initial suctions were about 4.0 MPa (Tang *et al.* 1997a). The specimens were used for two series of tests: 1) triaxial tests along generalized stress paths starting from the initial suction condition, and 2) tests in which specimens were dried (with corresponding suction increases) before subsequent triaxial testing. Drying was done by placing specimens in sealed desiccators with a controlled vapour pressure to elevate their suctions to about 6 MPa. Both sets of specimens had similar soil microstructures because the water content at initial hydration was constant (Wan *et al.* 1995, Tang *et al.* 1997c). However, the higher suctions in the dried specimens were expected to produce higher stiffness, larger regions of elastic behavior, and possibly more dilatation during shear.

6.3.2 Test Procedures

The tests were performed using incremental loading along controlled stress paths in p-q space. Two series of tests followed similar schedules starting from two different initial suction levels corresponding to 'as compacted' and 'after drying' respectively. Loading was applied in three phases (1) isotropic compression with pressures up to 3 MPa, (2) unloading to 1.5 MPa or 1.0 MPa to achieve an overconsolidation ratio of 2 or 3, (3)

shearing along selected stress paths with constant $\Delta p/\Delta q$. No drainage was permitted in either the air or water phases so all tests can be characterized as ‘constant mass tests’. The tests were conducted at room temperatures from 23°C to 26°C. Suction changes were monitored by psychrometer, with readings being corrected to 25°C. While pore air pressure u_a and pore water pressure u_w have not been measured separately, their difference $u_a - u_w$ (that is, matric suction) was evaluated using the psychrometers. (Psychrometers measure *total* suction equal to the sum of matric and osmotic suction. Osmotic suction remained constant in the tests.) Results can therefore be plotted in p-q-S space.

6.3.3 Specimen Installation and Initial Suctions

The specimen was encased in one latex rubber membrane which kept the water content constant. Before installing the top load cap, a small opening was drilled in the top of the specimen for the psychrometer which monitored suction changes. When the initial set-up was complete, the specimen was left for at least 2 hours to allow suction to equilibrate and the initial suction to be measured. As mentioned earlier, the first series of specimens which were tested immediately after compaction had initial total suctions of about 4 MPa. The second series which were dried before triaxial testing had initial suctions of about 6 MPa.

6.3.4 Application of Loading for Triaxial Tests

Isotropic compression Once the psychrometer had reached steady-state corresponding to the initial suction, isotropic loading was applied by increasing the confining pressure in the cell. To identify when yielding occurred during isotropic compression, the confining pressure was successively increased to 0.25 MPa, 0.50 MPa, 0.75 MPa, 1.00 MPa, 1.50 MPa, 2.25 MPa, 3.00 MPa. Each pressure was held constant until deformation and suction readings reached equilibrium, here taken as change in volume strain $\Delta\varepsilon_v < 0.0075\%$ /hour and change in suction $\Delta S < 0.0025$ MPa /hour. The duration of each increment depended on the pressure level but was typically less than 24 hours. Further small straining is considered to be creep straining at essentially constant suction.

Unloading After equilibrium had been reached at 3.0 MPa confining pressure, the specimens were unloaded to 1.50 MPa or 1.00 MPa to achieve an overconsolidation ratio $OCR = 2$ or 3 respectively. Because this response was considered to be elastic, only two or three pressure levels were used - 2.25 MPa, 1.50 MPa and 1.00 MPa.

Shearing Axial loads were applied using dead weights. Stresses were controlled incrementally so that stress paths of $\Delta p/\Delta q = 1, 1/3, 0,$ or $-1/3$ were followed. Stress increments were again held constant until deformations and suctions remained constant. Typically the increment durations were 24 hours in the early stages of the test, and 48 hours or longer towards the end of the test. Since the area of the cross-section of the

specimen changed with time, axial loads were adjusted periodically to keep constant axial stresses. The required axial loads were calculated from the expression: $P_{axial} = (\sigma_1 - \sigma_3) \times A = (1/4) \times \pi \times (\sigma_1 - \sigma_3) \times d^2 = (1/4) \times \pi \times (\sigma_1 - \sigma_3) \times (d_0 + \Delta d)^2$, where P_{axial} is axial load, σ_1 , σ_3 are axial stress and confining pressure respectively, A is area of the cross-section, d , d_0 , Δd are resulting diameter, initial diameter, diameter change respectively. At each increment, σ_1 and σ_3 depended on the chosen test conditions. d_0 was constant, and Δd was tracked by the non-contacting displacement transducers.

6.3.5 End of the Test

Once the test had been finished, the specimen was removed from the triaxial cell. It was divided along its axis into five sections, and these were then cored with a steel tube. The inside or outside portion of each section were used to measure the final water contents. These water contents were compared with the water contents which were measured before the specimen was installed.

Details of the initial conditions, initial suctions, and final conditions of the specimens as well as the results obtained from the tests will be presented in Chapter 8.

6.4 Tensile Tests

6.4.1 Specimen Preparation

Specimens for tensile testing were statically compacted to achieve an initial water content of 19.4%, saturation of 85%, and dry density of 1.67 Mg/m^3 . The specimens had 50 mm diameter and 100 mm length, the same dimensions as specimens used for triaxial compression testing. Specimens were prepared with three suction levels: 1) 4 MPa incorporated through the compaction process (Tang *et al.* 1998a), 2) 6.5 MPa produced by drying in a desiccator with controlled vapour pressure, and 3) 10 MPa after further drying. The specimens experiencing drying were cured for seven days to allow moisture be re-distributed after being removed from desiccators. A total of eight specimens were tested. The higher suctions in the dried specimens were expected to produce higher tensile strengths.

6.4.2 Installation and Setup

After a specimen was compacted and cured, it was immediately placed horizontally on the lower form of the mould which had already been coated with a thin film of adhesive. 'Sikadur 31, Hi-Mod Gel', a high-modulus, high-strength, structural, epoxy paste adhesive, was chosen because its paste was readily manageable. Its workable time of about 30 minutes allowed adjustment of alignment of the specimen and mould. The top form of the mould was then coated with adhesive and placed gently on the specimen. The

form was pressed slightly to get rid of excess adhesive. A hand level was used to ensure the top form was properly positioned in both longitudinal and transverse directions. To keep the water content constant, the outer surface of the specimen was waxed at the two exposed ends and the gap at each side of the forms. The assembled mould containing the specimen was then left for 18 hours to allow the adhesive to harden.

The mould holding the specimen was then transferred to the test frame. The mould was clamped to the platen of the testing machine and connected through a load cell to the top crosshead. Special care was taken to ensure good alignment. A simple dial gauge was mounted to measure vertical deflection. Once the set-up was complete, the test was ready to start.

6.4.3 Test Procedures

Tests were conducted at a constant rate of vertical displacement on the test frame. That is, the machine platen moved downwards to apply a tensile force on the specimen. As brittle rupture was expected, the loading speed was quite slow (0.0305 mm/min) to ensure readings of loads and deflections could be taken. Readings were usually taken at 0.05 mm intervals until halfway to failure load, and at 0.01 mm intervals thereafter. Tensile displacement and loads were continued until failure occurred. After completing the test, the mould was removed from the machine, and weighed immediately. The weight of the

mould containing the broken specimen was used for computing tensile force at failure as discussed later in Section 7.5.1.

CHAPTER 7
RESULTS OF QUICK UNDRAINED
TRIAXIAL TESTS AND TENSILE TESTS

7.1 Introduction

This chapter presents data on the strength properties of unsaturated buffer obtained from two series of quick undrained triaxial compression tests and one series of tensile tests. The first series of quick undrained triaxial tests examined how variation of water contents or matric suctions affects strength. The specimens used in this series were compacted to selected saturation levels but the same dry density. Water contents therefore varied with saturation levels. As described earlier in Chapter 4, suctions of unsaturated buffer depend on the water contents at the time of first hydration but are independent of dry densities or saturations. Therefore, the specimens in the first series had different matric suctions depending on the selected water contents and the corresponding saturation levels.

The second series of quick undrained triaxial tests was carried out to examine how osmotic suctions influence strength properties. For these tests, unsaturated specimens

were prepared using concentrated sodium chloride solutions as pore fluids instead of distilled water to produce additional osmotic suctions. The specimens had degrees of saturation from 50% to 98%, water contents from about 11% to 23%, and initial total suctions of about 2 MPa to 8 MPa. (The higher total suctions were achieved in specimens at low saturation (high matric suction) with high concentrations of pore fluids).

Most triaxial tests were performed at confining pressures of 0.2 MPa and at ambient temperatures. Drainage leads from the specimens were kept closed throughout the application of cell pressure and shearing. Compression took place in the air phase so the tests should be considered 'constant mass' tests rather than 'constant volume' tests. Results from two series of tests can be compared in terms of initial total suctions. A different procedure as described in Section 6.2.2 was adopted to test two specimens where the air phase was allowed to drain during the consolidation phase of the test at a cell pressure of 3 MPa. Drainage was closed during the subsequent shear phase.

Tensile tests were conducted on a series of unsaturated specimens at three suction levels up to 10.0 MPa. Typical cylindrical triaxial specimens were pulled to break on the mid-planes at a constant displacement rate. Pull load and displacement were measured. Simple test procedures were described earlier in Section 6.4.3. Results obtained from this series of tests relate tensile strength to suction.

7.2 Effect of Water Content on Strength and Stiffness

7.2.1 Quality Control Tests

All the specimens were compacted to specified degrees of saturation with constant dry densities. This meant that water contents had to be controlled. In order to gain confidence in the specimen preparation procedures, a quality control program was initiated. Quality control tests split the specimens into five disks and examined systematic variations. This allowed corrective measures to be taken if necessary.

A total of 14 specimens were used for quality control tests at saturations of 50%, 65%, 75%, 85% and 98%. Results are summarized in Table 7.1. It can be seen that good quality control was obtained in unsaturated specimens. Generally, the dry densities along the length of the specimens were within $\pm 0.025 \text{ Mg/m}^3$ of the target values. Similar results were obtained for the degree of saturation - $\pm 2\%$ along the specimen length, and $\pm 2\%$ from target values. Figure 7.1 provides the results of specimens at saturation of 85% and 98% showing measured values of dry density and saturation at five locations along the length of the specimens. The results have been also compared with those obtained from similar tests undertaken by fellow students Yuen (1995) and Wiebe (1997). Good agreement and consistency indicate the acceptable quality control is considered (Wiebe 1997).

Table 7.1: Summary of quality control specimens

Target saturation (%)	Number of specimens	Dry density (Mg/m ³)	Water content (%)	Degree of saturation (%)
98	2	1.655± 0.001	22.57±0.01	96.49±0.08
85	2	1.652±0.007	19.58±0.26	83.27±0.21
75	2	1.650±0.001	17.43±0.05	73.91±0.39
65	4	1.654±0.002	14.84±0.08	63.36±0.02
50	4	1.647±0.004	11.54±0.07	48.75±0.30

7.2.2 Quick Undrained Triaxial Tests

A total of 21 tests were performed on specimens at saturation levels of 98%, 85%, 75%, 65% and 50%. Initial conditions of specimens and results from quick undrained triaxial tests are summarized in Table 7.2. Data of initial conditions of the specimens shown in the table once again indicate good quality control was achieved in dry density, water content, and saturation. Average data are plotted in Figures 7.2 and 7.3 showing strength and stiffness *versus* saturation. (The confining pressure in these tests was 0.2 MPa). As expected, the undrained strength (expressed by maximum deviator stress) increases quite sharply from 634 kPa to 1716 kPa as the degree of saturation decreases from 98% to 50%. The stiffnesses in Figure 7.3 are secant moduli between the beginning of shear and 50% of peak deviator stress. These relationships indicate that unsaturation is a significant factor influencing the mechanical behavior of unsaturated buffer (Graham *et al.* 1995). More generally, strength and stiffness of unsaturated buffer increase with decreasing saturation. Results of the more extensive series of tests performed by Wiebe were reported by Wiebe *et al.* (1998).

At the time this series of tests was performed, techniques for measuring suctions in triaxial cells had not yet been established by the author in the geotechnical laboratories at the University of Manitoba. Initial suctions could only be established from SWCCs determined separately at a later date. As a result, the data obtained can only be interpreted in terms of saturations generated by compaction, not compression or shearing. The results of the SWCCs were presented earlier in Chapter 4. Initial total suctions measured on otherwise identical specimens but unsheared can therefore be related to strength properties examined in this series of tests. Data in Figure 7.2 are replotted into Figure 7.4 in terms of strength *versus* total suctions, showing that increases in total suctions produce higher strengths.

While total suctions were measured, the chosen variations of water contents and saturations only changed matric suctions, with the osmotic suctions remaining largely unchanged (Wan 1996, Tang *et al.* 1998a). In general, Figure 7.4 shows that strengths of unsaturated buffer increase significantly with increasing matric suctions.

Table 7.2: Summary of quick undrained triaxial tests (confining pressure = 200 kPa)

Target saturation (%)	Number of specimens	Dry density (Mg/m ³)	Water content (%)	Degree of saturation (%)	Maximum strength q _r kPa
98	3	1.668± 0.003	22.23±0.03	97.45±0.29	634±25
85	3	1.662±0.005	19.34±0.08	84.00±0.33	986±17
75	3	1.658±0.004	17.13±0.08	73.97±0.19	1293±13
65	6	1.658±0.003	14.78±0.10	63.83±0.28	1568±28
50	6	1.661±0.007	11.53±0.08	49.46±0.40	1716±62

7.3 Effect of Osmotic Suction on Strength and Stiffness

Earlier, Chapter 4 examined the osmotic suction properties of unsaturated buffer material. Results were presented in the form of soil-water characteristic curves. Conclusions drawn from the resulting data were: 1) compared with matric suctions, osmotic suctions decrease slowly with increasing water content, 2) osmotic suctions increase significantly as dissolved salt contents increase, and 3) as a result, osmotic suctions of soils like sand-bentonite can be expected to change with ground water chemistry or contamination. This section presents results of undrained triaxial compression tests on specimens with varying osmotic suctions.

7.3.1 Effects of Osmotic Suction on Strength

Effects of osmotic suctions on strength were examined by performing undrained triaxial compression tests on specimens at three saturation levels of 65%, 85% and 98%. At each level of saturation, specimens were prepared using NaCl solutions with concentrations of 0.1 M, 0.5 M and 1.0 M instead of the distilled deaired water used in the main program. Total suctions of the specimens were measured by psychrometer before and after the triaxial tests. The osmotic solutions introduced into the specimens elevated their total suctions. Initial conditions of these specimens and the strengths measured from the tests are tabulated in Table 7.3.

Data plotted in Figure 7.5 show undrained shear strength (maximum deviator stress) decreasing with increasing saturation for concentrations of 0.5 M and 1.0 M NaCl. Since testing procedures were the same, the figure also shows the results from the first series of tests as reported in Figure 7.2 for water-prepared specimens (0.0 M). It is important to remember that the specimens were made with the same dry densities. This involved different compaction energies for different pore fluid concentrations. According to Table 7.3 and Figure 7.5, at the same saturation (water content) and dry density, specimens with elevated total suction have consistently lower strength than specimens with distilled water. As mentioned earlier, saturation is not a state variable dictating soil behavior. The strength data are therefore examined in terms of total suctions in Figure 7.6 at saturation levels of 85% and 98%. (Total suctions of specimens at $S_r = 65\%$ with 1.0 M NaCl solutions were beyond the range of the psychrometer.) Figure 7.6 indicates that 1.0 M NaCl solution can elevate the total suction of specimens with saturation of 98% from about 2 MPa to 8 MPa. However, the strength decreases slightly from 634 kPa to 524 kPa. It is suggested that the strength of the tested specimens decreases with increases in total suction arising from increased osmotic suction. Although osmotic suctions or total suctions can be elevated considerably, the elevated total suctions do not produce proportional changes in shear strength and stiffness. The reason for this lies in the changes in interparticle potentials produced by increases in pore fluid concentration (Mitchell 1976). The reasons for this observation will be discussed in Section 7.4.2.1.

**Table 7.3: Summary of quick undrained triaxial tests on specimens
with osmotic agents (confining pressure = 200 kPa)**

Saturation Level (%)	Molality of NaCl (M)	Dry density (Mg/m ³)	Water content (%)	Degree of saturation (%)	Suctions (MPa) (test before /test after)	Maximum strength q _r kPa
65	1	1.657	14.78	64	NA / NA*	1344
	1	1.657	14.47	61	NA / NA	1323
85	1	1.661	19.41	84	NA / NA	890
	1	1.661	19.07	82	NA / NA	867
	0.5	1.653	19.45	83	6.6 / 6.6	921
	0.1	1.648	19.49	83	4.6 / 4.8	1101
	1	1.665	21.97	96	8.1 / NA	524
98	0.5	1.652	22.75	97	5.3 / 5.3	603

N/A* - Data are not available due to suctions beyond measurable range of psychrometers

7.3.2 Effects of Osmotic Suction on Stiffness

In a similar way, changes in osmotic suction affect the stiffness of specimens, here expressed as E_{50} , the secant modulus between the beginning of shearing and 50% of the maximum deviator stress. Figure 7.7 shows that the E_{50} -modulus for unsaturated specimens increases with decreasing saturation. Introducing 1.0 M NaCl increases the osmotic suction but decreases the stiffness. The elastic modulus decreases with increase of total suction. This is again due to the influence of pore fluid chemistry on electrochemical potentials and will be explained later.

7.3.3 Osmotic Suction as a Dominant State Variable

The conclusion that strength and stiffness of buffer decrease when total suctions are increased by osmotic component is drawn from test data on specimens which all had the same dry density and therefore the same average particle separation. This raises the question of whether osmotic suction is an inherent factor (that is, a dominant stress state variable) for strength properties. Alternatively the controlled dry density used in specimen preparation may be responsible for the strength properties.

A complementary series of tests was conducted to clarify this question by using two-stage procedures in the triaxial tests. The first stage involved consolidation of sand-bentonite mixture at a confining pressure of 3 MPa. The second stage involved shearing the specimens at 3 MPa after completion of consolidation. More details of testing procedures were given in Chapter 6. Two specimens were tested. Both had a water content of 19.42% (corresponding to 85% saturation for specimens with dry density 1.67 Mg/m^3). One was prepared with deionized water and the other with 1 M NaCl solution. Stress-strain curves of the two specimens during shearing are shown in Figure 7.8. The curves demonstrate that the specimen with 1 M NaCl solution (and hence higher osmotic suction) had lower strength than the specimen with deionized water. For comparison, Figure 7.8 also shows the stress-strain curves of two specimens compacted at a dry density of 1.67 Mg/m^3 and water content of 19.40%. Thus at two different confining pressures, specimens made with 1 M NaCl pore fluid (and hence, elevated osmotic

suctions) have consistently lower strength than those with no introduced osmotic agents. Osmotic suctions induced by introducing solutions into specimens affect the soil microstructure and must be considered a dominant state variable.

7.3.4 Suction Changes after Specimens Experienced Stressing

Total suctions measured before and after tests as listed in Table 7.3 show that suctions were essentially unchanged. (One specimen had a suction of 8.1 MPa which is at the edge of measurable limit of psychrometers and this resulted in failure of the measurement after shearing.) The specimens were under confining pressure of 0.2 MPa and were sheared to failure at axial strains of about 8%. This suggests that total suctions in buffer are largely reversible even after large non-reversible deformations (Tang *et al.* 1999). Similar results were noted by Wan *et al.* (1995).

7.4 Summary and Discussion

7.4.1 Summary

7.4.1.1 Influences of water content, matric suction and osmotic suction on strength and stiffness

Results obtained from two series of tests indicate that strength and stiffness of specimens with constant dry density and particle spacing increase with decreasing water contents

and decrease with increasing total suctions induced by osmotic agents. It is inferred that strength and stiffness increase with increasing total suction achieved by increasing matric component, but decrease with increasing total suction achieved by increasing the osmotic component. The latter effect is due to the influence of pore fluid concentration on diffuse double layer potentials. Two series of tests were performed in which total initial suctions were measured using psychrometers. Specimens in the first series had different water contents and saturations but were prepared to the same dry density using deionized distilled water. As a result, they had different matric suctions. Those used in the second series were prepared to the same dry density using different concentrations of NaCl as pore fluid at each water content or saturation level. They had different osmotic suctions.

Results of strength *versus* total suction from the two series of tests were presented in Figures 7.4 and 7.6 respectively. All specimens had the same dry density (1.67 Mg/m^3) but differed in the way total suctions were achieved. A comparison can therefore be made of the effects of matric suction and osmotic suction on the strength and stiffness.

Figure 7.9 combines strength data in Figures 7.4 and 7.6 from the two series of tests. Curve AB represents the increase of strength resulting from increases in total suctions caused by decreasing water contents, and resulting changes in saturation. Curve AC shows strengths decreasing as total suctions were increased using osmotic solutions. The specimens had saturation of 98% (therefore water content of 22.70%) and were prepared using NaCl solution concentrations of 0 M, 0.5 M and 1 M. In all cases the initial dry

density was 1.67 Mg/m^3 . Figure 7.9 indicates the relative importance of matric suction compared with osmotic suction. The effect of matric suction on strength is opposite to that of osmotic suction under the test conditions, and is clearly larger than the effect of osmotic suction.

7.4.1.2 Importance of osmotic suction

In most geotechnical problems, effects of osmotic suctions can be neglected as they remain unchanged (Fredlund and Rahardjo 1993). Evidence from the second series of tests indicates that even if there are significant changes in osmotic suctions the influence on strength is still limited. It follows that effects of osmotic suctions seem to be insignificant whether they change or not. Dixon (1995) noted that the bentonite used in the tests has an excess of exchangeable sodium, independent of the pore fluid used during preparation, water in the pores will be salt-rich. Specimens prepared using distilled water have osmotic suction of 1-2 MPa (Tang *et al.* 1997a).

The existence of osmotic suctions cannot be ignored. Because of the relative importance of matric suction and osmotic suction, total suction can only be well understood if the contributions from the two components are clarified. According to test data shown earlier in Figure 4.15 in Chapter 4, total suctions can be elevated pronouncedly by the osmotic component.

In general, changes in total suctions can arise from increases in either matric suction, osmotic suction, or their combination. This negates the possibility proposed by Chattopadhyay (1972) to consider total suction as a stress state variable through algebraically combining the matric and osmotic components. Matric suctions and osmotic suctions may contribute separately as state variables, particularly when dealing with the entire range of soil suction. The mechanism of osmotic suctions at microscopic level is discussed in the following section.

7.4.2 Discussion

7.4.2.1 Mechanism of influence of osmotic suctions

The reason shear strength decreases with osmotic suction (at constant dry density) is clarified by considering the thickness of diffuse double layers round clay particles with saline pore fluid. In clays, long range attractive and repulsive forces develop between particles (Mitchell 1976) over distances of the order of 3 Å to perhaps 100 Å or more from particle surfaces. The attractive forces are primarily due to London van der Waals forces and decrease rapidly with distance from the particle surface. Adsorption of cations by clays and the formation of double layers are responsible for long range repulsive forces between particles. These develop by electrostatic repulsion between adjacent clay particles and associated overlapping diffuse double layers. For densities that are encountered in most soils engineering, electrostatic repulsion is the dominant long range

force. This concept was incorporated by Graham *et al.* (1992) into an understanding of the stress state controlling the behaviour of dense saturated buffer.

The water surrounding bentonite particles in buffer at its reference dry density is only about 2 to 3 molecules thick (Graham *et al.* 1992). Nevertheless, for the following discussion, it will be assumed that diffuse double layer theory is applicable. Clay particle systems are frequently conceptualized as a series of parallel clay particles. The Poisson-Boltzmann equation (Mitchell 1976) for a single particle can be integrated to obtain the mid-plane electrolyte concentration and potential between two clay particles. An approximate indication of the influences of particle spacing and pore fluid chemistry can be seen in terms of the 'thickness' of the double layer as given by:

$$\frac{1}{K} = \left(\frac{D\kappa T}{8\pi n_0 e^2 v^2} \right)^{0.5} \quad [7.1]$$

where $1/K$ = thickness of the double layer, D = dielectric constant, κ = Boltzmann constant, T = temperature (Kelvin), n_0 = bulk solution electrolyte concentration, e = unit electronic charge, v = cation valence. The equation shows that the thickness of the double layer is inversely proportional to the square root of the concentration, other factors remaining constant. Long range interparticle repulsive forces depend on the interaction between adjacent double layers. In general, the thinner the double layer at a given particle separation, the smaller will be the repulsive force, the smaller its contribution to effective stress (Section 2.2.3), and the lower the strength. The thickness of double layers in the bentonite component of buffer decreases when concentrated solutions are

introduced as pore fluid. Strengths therefore decrease when the density is held constant. If the material is allowed to consolidate under drained compression, then the density of the salt-rich material should increase. Under these conditions, strengths would also be expected to increase.

7.4.2.2 Additional research program

The first series of tests which examined the effects of water content on strength and stiffness has been extended to a more extensive program by a fellow student B. Wiebe. Specimens were prepared at dry density of 1.67 Mg/m^3 at various water contents - saturations. Confining pressures were extended to 3 MPa and temperatures to 26°C, 65°C and 100°C. The influence of saturation, temperature, and pressure was examined intensively. Results were reported by Wiebe *et al.* (1998).

It should be remembered that the water content - strength relationship examined by the author, and the influence of saturation, temperature, and pressure on strength examined by Wiebe were interpreted in terms of initial suctions of 'bench' specimens at ambient pressure and temperature. As we know, suction and saturation are both changed under triaxial loading. Further research was therefore undertaken with suctions being monitored during triaxial tests to provide more direct evidence of relationships among the test parameters. Results of this work will be presented in the following chapter - Chapter 8: Results from stress-controlled triaxial tests.

7.5 Results of Tensile Tests

7.5.1 Tensile Strength of Unsaturated Buffer

The data resulting from the tensile tests are shown in Figure 7.10 in the form of load N versus deflection D from seven of these tests. In the early parts of all the tests the stiffness appears to be low, indicating self-adjustment of the system as a whole. Thereafter, the responses are largely linear until tensile fracture occurs. The test data in Figure 7.10 show that comparable tests at each suction level have similar slopes, indicating good consistency of specimen preparation. With increasing suction, the strength and stiffness both increase. Although appreciable displacements develop before failure occurs, the curves indicate the brittle nature of the failure. This is in contrast with the ductile behavior seen in all saturated specimens (Graham *et al.* 1988), and in most unsaturated tests except at low saturation (and hence high suction) and low confining pressure (Wiebe *et al.* 1998). It should be remembered that the measured displacements include specimen deformation, system deformation and non-uniform stresses in the specimen.

The tensile force acting on the mid-plane of the specimen is determined from the measured axial load, the weight of the upper part of the mould with the upper half of the specimen (Figure 7.11).

$$T = N - W \quad [7.2]$$

where N is axial load, W is the weight of upper part of the mould with the upper half of the specimen, T is net tensile load exerting on the failure plane of the specimen. N is measured by load cell and W measured after test. The influence of the wax coating is assumed to be negligible.

The tensile stress at the mid-plane is therefore maximum average:

$$\sigma_1 = \frac{T_{\max}}{A} \quad [7.3]$$

where T_{\max} is the maximum tensile force, and A is the area of the mid-plane, equal to diameter \times length.

Initial conditions and tensile strengths are shown in Table 7.4.

Table 7.4: Specimens and test results

Suction level (MPa)	Test number	Saturation (%)	Dry density (Mg/m ³)	Water content (%)	Tensile strength (kPa)
4.0	1	85	1.66	19.80	228
	2	85	1.66	19.65	248
	3	86	1.67	19.79	230
	4	85	1.68	19.19	225
6.5	1	82	1.68	18.41	257
	2	84	1.67	19.04	267
10.0	1	80	1.69	17.58	311
	2	78	1.68	17.35	318

The data in Table 7.4 show good consistency between comparable results. In all eight tests, the failure surfaces of the specimens were largely horizontal with some roughnesses being observed (see Figures 7.12 and 7.13). There was no indication in the tests that tearing started locally and worked its way across either the diameter or length of the specimens. This permits tensile strength to be calculated at the mid-plane by the expressions [7.2] and [7.3].

Figure 7.14 shows the relationship between tensile strength and total suction. Tensile strength increases with increasing total suction. Note that the strength data in the figure are average values of tensile strength at each suction level, and the data of total suctions are initial suctions of the specimens. The actual suctions at failure were not measured but they can be measured in future tests by incorporating psychrometers into the testing device (Tang *et al.* 1997b).

7.5.2 Discussion of the Testing Methodology

7.5.2.1 Analysis of stress distribution using finite element method

In computing the tensile strengths in Table 7.4 and Figure 7.14 the stress distribution on the failure surface was assumed uniform. This assumption has been examined using finite element method.

Two-dimensional plane strain analysis was conducted using finite element method software SIGMA-W version 4.0. Figure 7.15a shows the finite element mesh for configuring the problem using symmetry. An example of the results is given in Figure 7.15b for a suction of 4 MPa. A maximum tensile force of 1250 N (corresponding to 6250 N/m unit length) was applied to the specimen. Results from FEM are plotted in terms of tensile stress *versus* distance from the specimen center across the failure plane. In the analysis, the mould behaved elastically and the soil behavior was chosen to be either linearly elastic or elastic-perfectly plastic. Elastic parameters for the steel mould are: elastic modulus $E = 200$ GPa, Poisson ratio $\mu = 0.33$. Elastic parameters for unsaturated buffer material at 85% saturation are not available but its secant compression modulus E_{s0} measured at low confining pressure of 200 kPa is approximately $E = 90$ MPa (Figure 7.3). Since values of parameters should not significantly affect the results of stress distribution in this analysis, parameters are therefore assumed: $E = 90$ MPa and $\mu = 0.30$. Results from the linearly elastic model are shown in Figure 7.15b as dotted lines and open circles. Using this soil model, the stresses are not uniformly distributed but show a considerable stress concentration at the edge. The stress concentration ratio is about 2.5.

The discontinuity at the edge of the mould may affect the concentration. The assumption for elasticity of the sand-bentonite material contributed strongly to the concentration value. Since unsaturated sand-bentonite exhibits elastic-plastic behavior instead of linear elasticity (Tang *et al.* 1998b), specimens are not able to withstand concentrated stresses at

their perimeters. Plastic behavior can be expected locally and highly concentrated stresses will be redistributed. This can be expected to produce more uniform stress distribution.

The stress distribution obtained from analysis using an elastic perfectly plastic model ($E = 90 \text{ MPa}$ and $\mu = 0.30$, $c = 200 \text{ kPa}$, $\phi = 20^\circ$) is presented in Figure 7.15b by solid lines and circles. The distribution is now more uniform than in the linearly elastic modeling.

Influence of Poisson ratio on stress distribution is also examined. Unsaturated sand-bentonite mixture at saturation of 85% is expected to have a possible Poisson ratio varying from about 0.3 to 0.4. Figure 7.16 compares the results of stress distribution computed from two Poisson ratios, $\mu = 0.30$ and 0.40 . Curves in Figures 7.16a and 7.16b indicate that higher Poisson ratio ($\mu = 0.40$) seems to give better results, that is, the stress distribution is relatively more uniform in the specimen of either linear elastic model or elastic perfectly plastic model. For the elastic perfectly plastic model in Figure 7.16a, the stress distribution curves are essentially the same for two Poisson ratios. In both cases, values of stresses along the failure surface are close to those by simple calculation, averaging 230 kPa . This appears to justify the simplifying assumptions made in equations [7.2] and [7.3].

7.5.2.2 Optimization of the shapes of tensile moulds

The stress distribution along the failure surface depends on the shape of the forms of a tensile mould. In order to achieve the best stress distribution, analyses on variety of the shapes of the forms have been conducted. A possible alternative is such that square cross-section box of a split mould accommodates a specimen with square cross-section, for example, with dimensions of 50 mm × 50 mm × 100 mm. Figure 7.17 shows part of the cross-section of such a specimen and the box. In finite element analysis, elastic parameters are again assumed: for the steel mould, elastic modulus $E = 200$ GPa, Poisson ratio $\mu = 0.33$; for unsaturated buffer material, $E = 90$ MPa and $\mu = 0.30$. Figure 7.18 compares stress distributions along the failure surface for two types of tensile moulds (referred to as 'semi-circle forms' and 'square box'). The data in Figure 7.18a and 7.18b show the stresses along the failure surface have higher concentrations produced by the 'square box' type of mould than that produced by the 'semi-circle forms' type of mould, although the difference is not remarkable in the case of the soil specimen with elastic perfectly plastic model. It follows that the tensile mould with the semi-circle forms described herein is optimal in shapes among other possible regular shapes.

7.5.2.3 Conclusions

Little has been published in the geotechnical literature about the tensile strength of soils. The tensile mould introduced in this section offers a simple means of performing tensile tests on unsaturated soils. Traditional cylindrical triaxial specimens can be used. The

method produces well-defined tensile failure and consistent, repeatable results. Comparison between the shapes of tensile moulds indicates that the proposed semi-circle forms perform best. Tensile strength increases with increasing suctions.

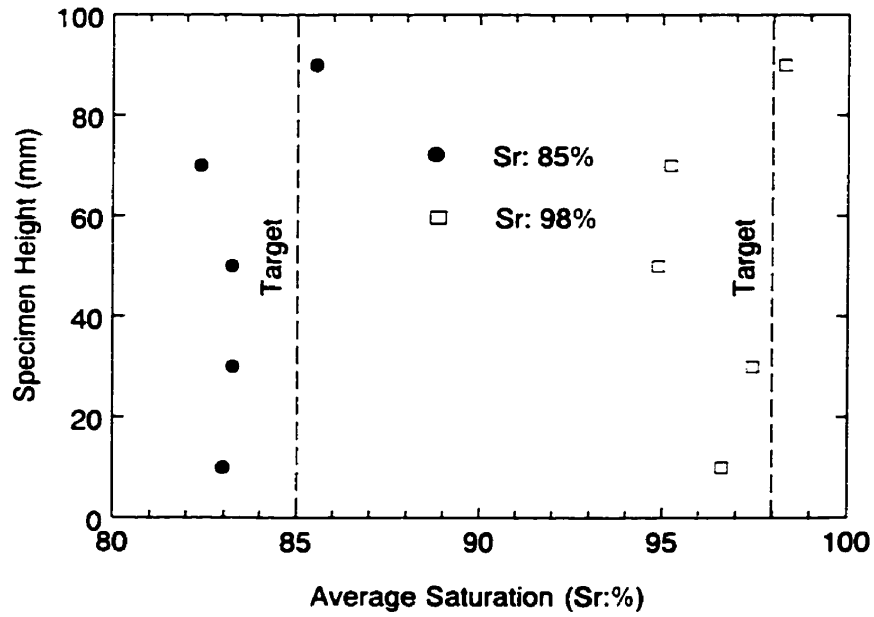
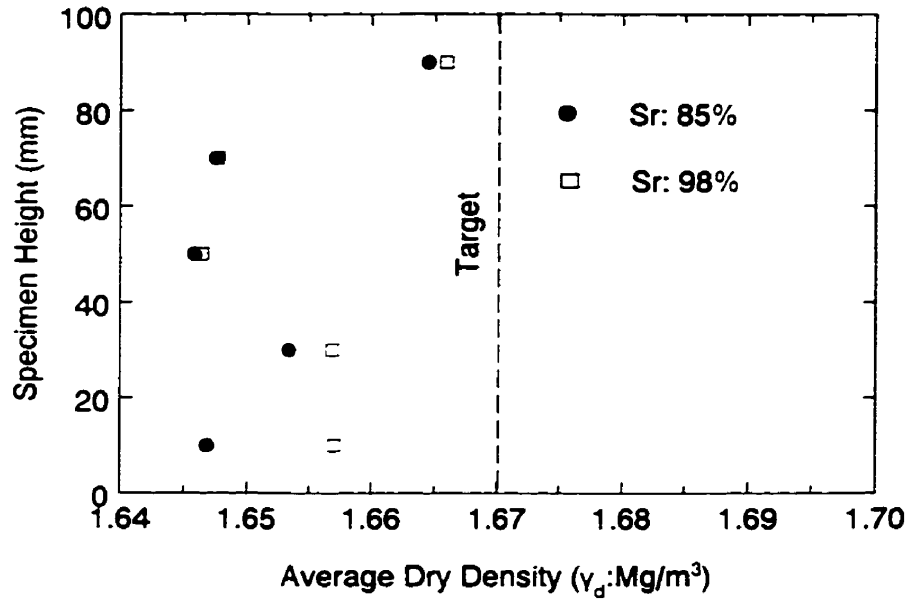


Figure 7.1 Results from quality control tests (Sr=85%, 98%)

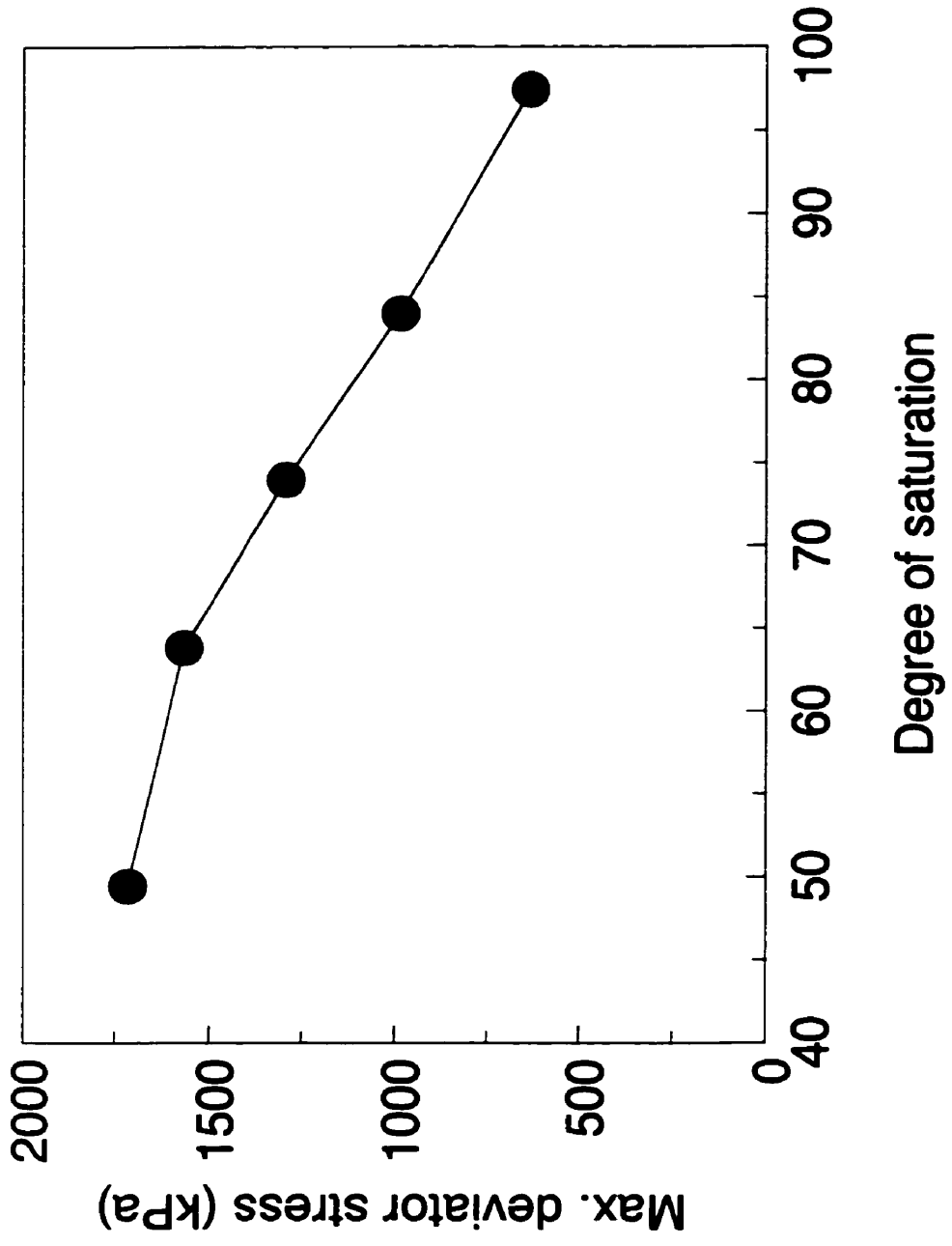


Figure 7.2 Max. deviator stress versus saturation

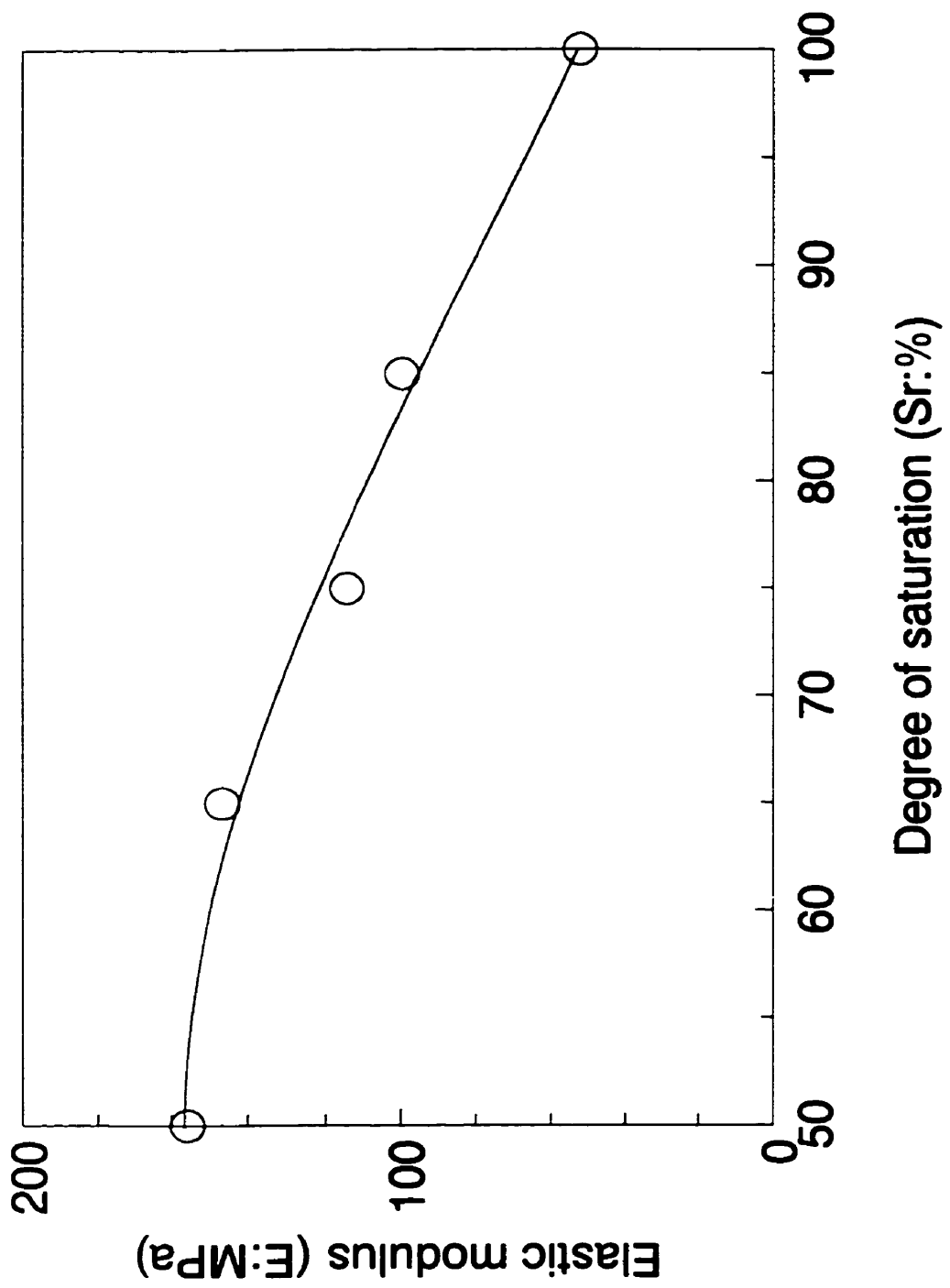


Figure 7.3 Elastic modulus versus saturation

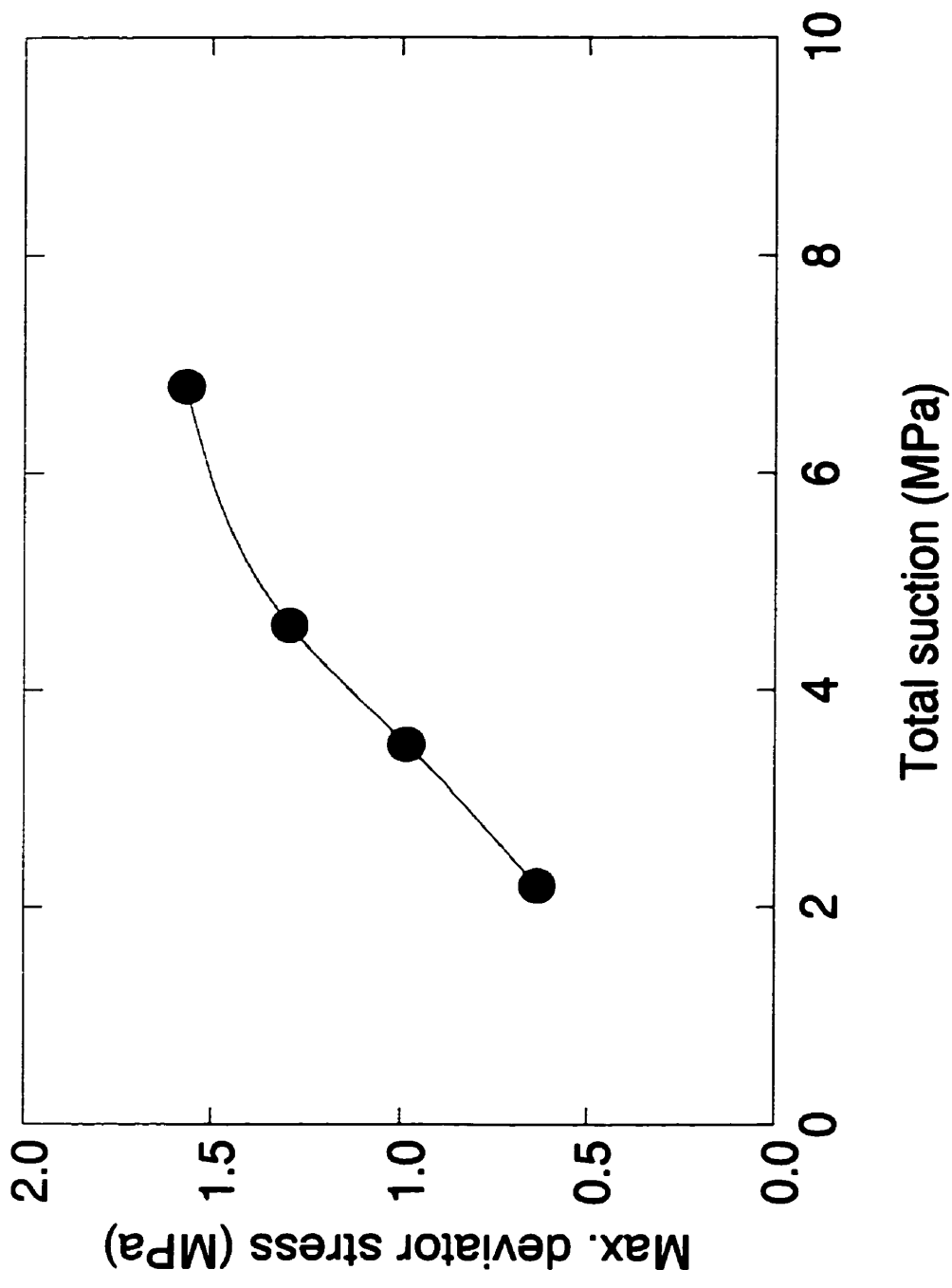


Figure 7.4 Effects of total suctions contributed from matric suction

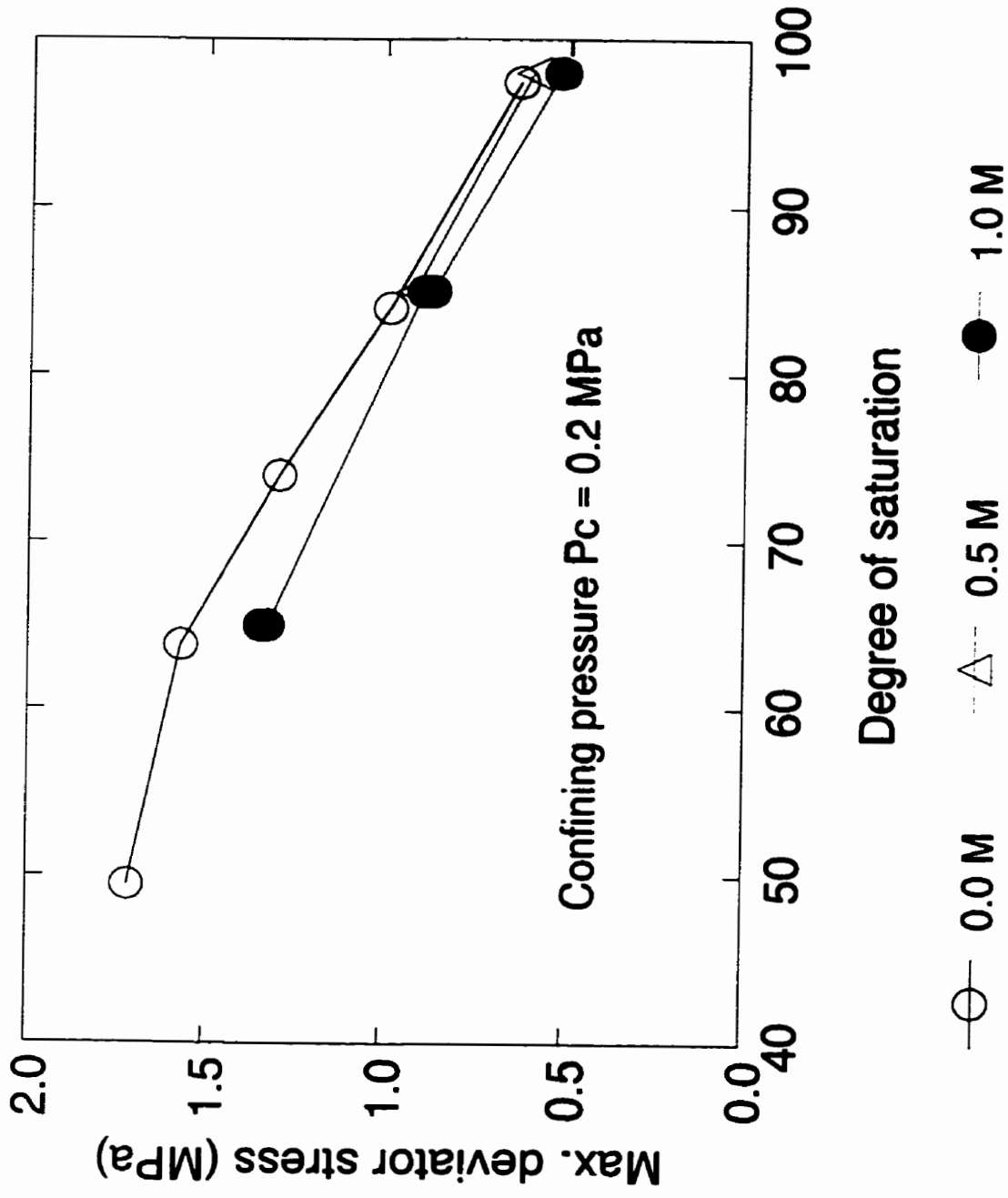


Figure 7.5 Max. deviator stress versus saturation

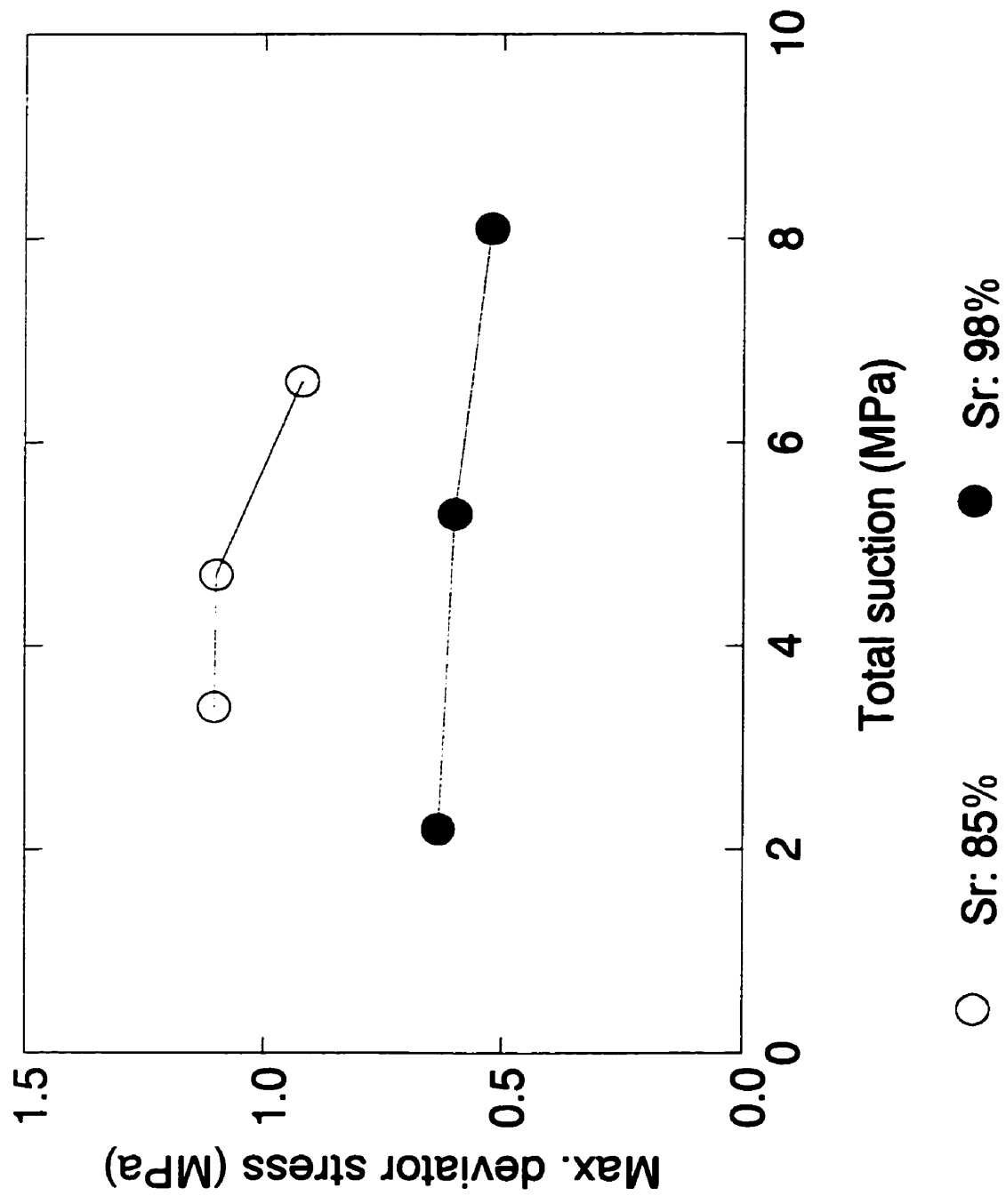


Figure 7.6 Max. deviator stress versus total suction

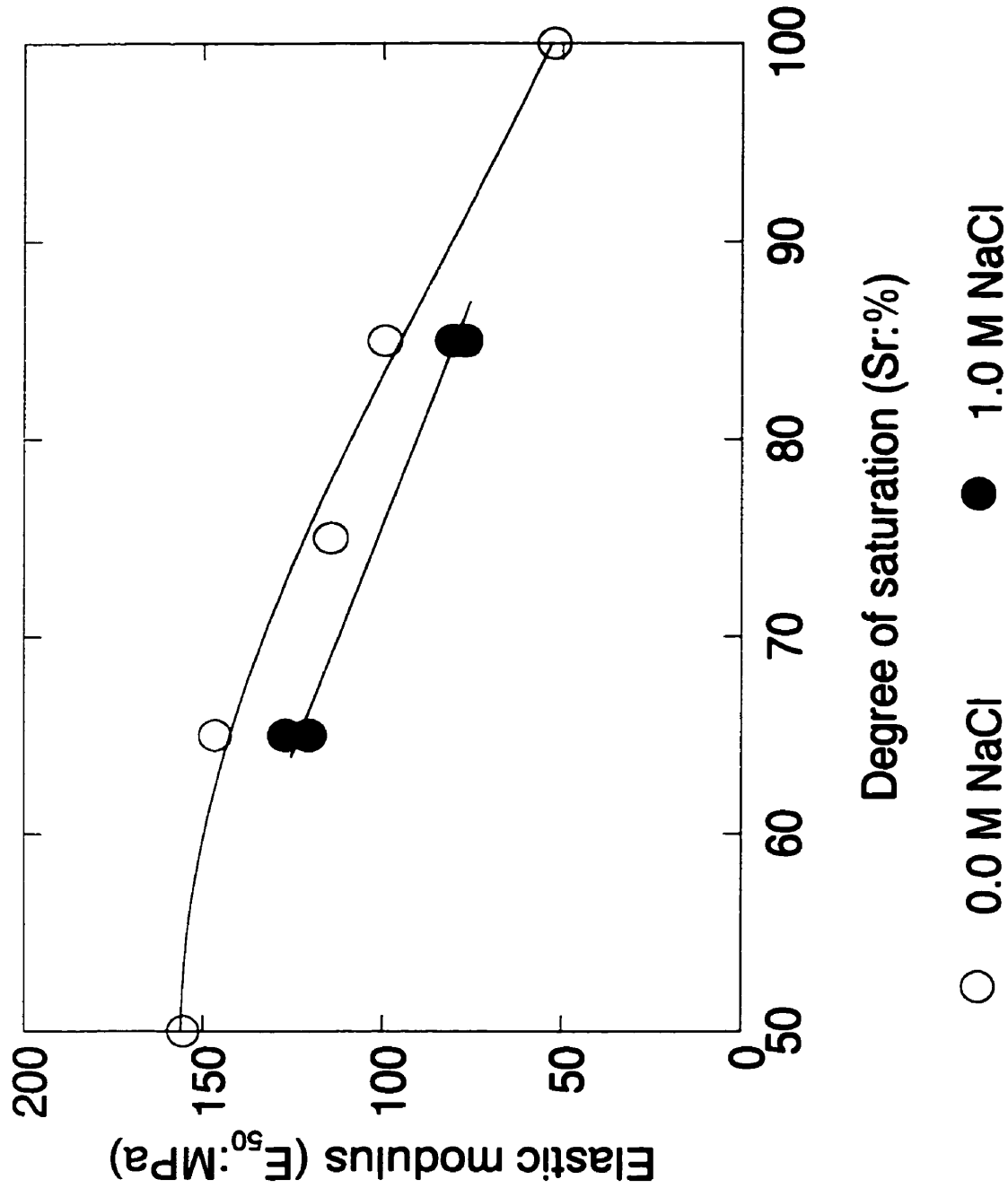


Figure 7.7 Elastic modulus versus saturation

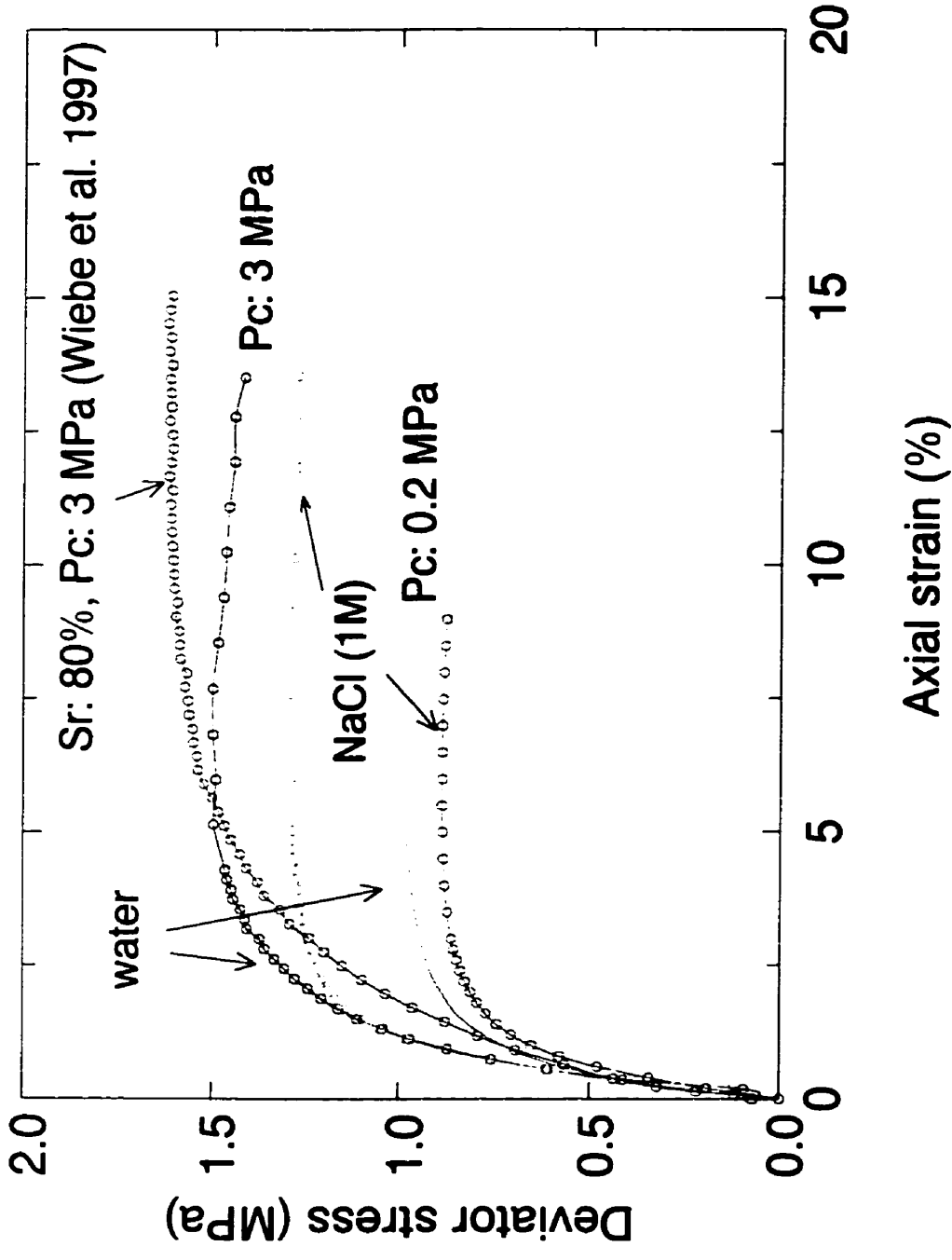


Figure 7.8 Deviator stress vs. axial strain

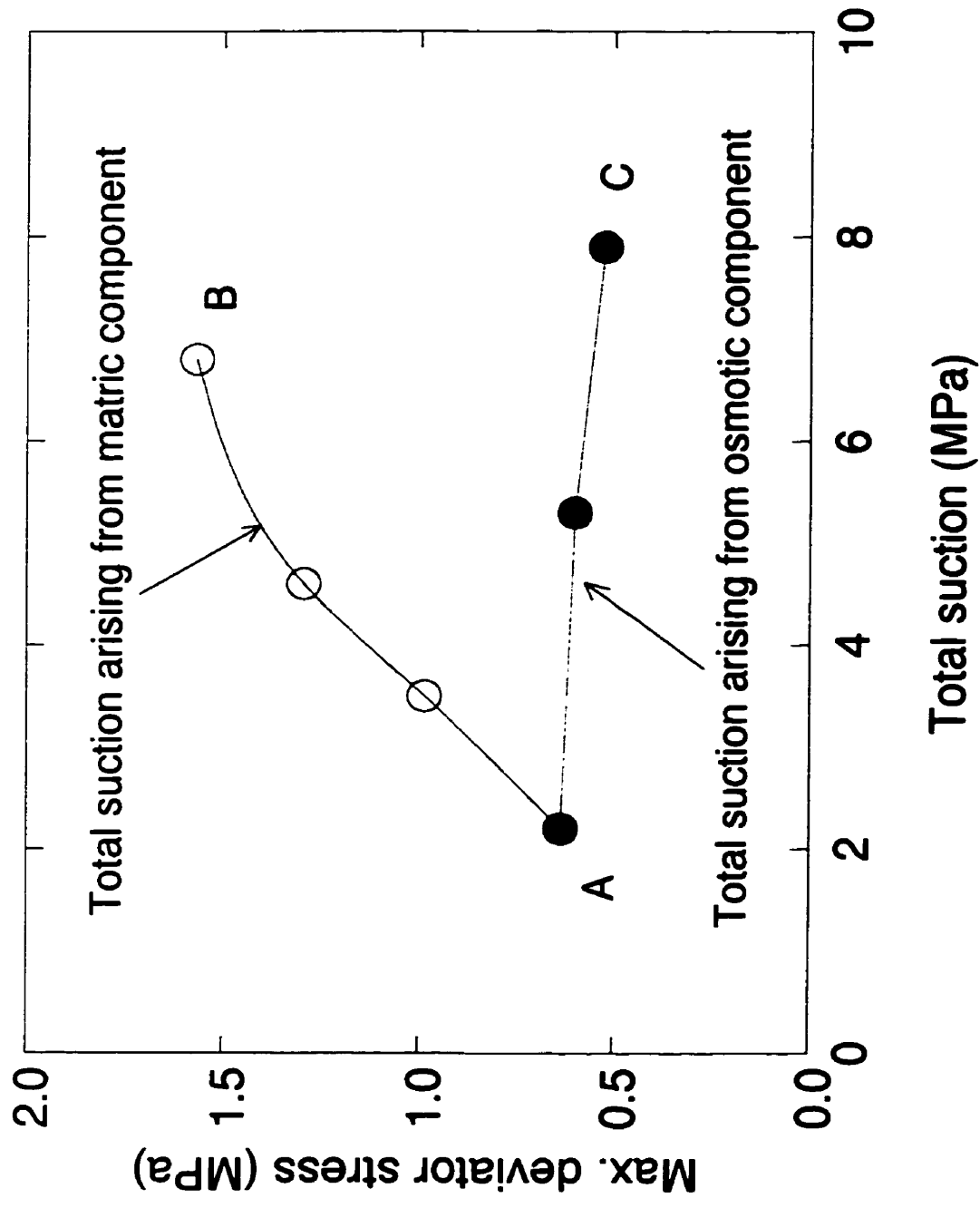


Figure 7.9 Effects of matric suction and osmotic suction on strength

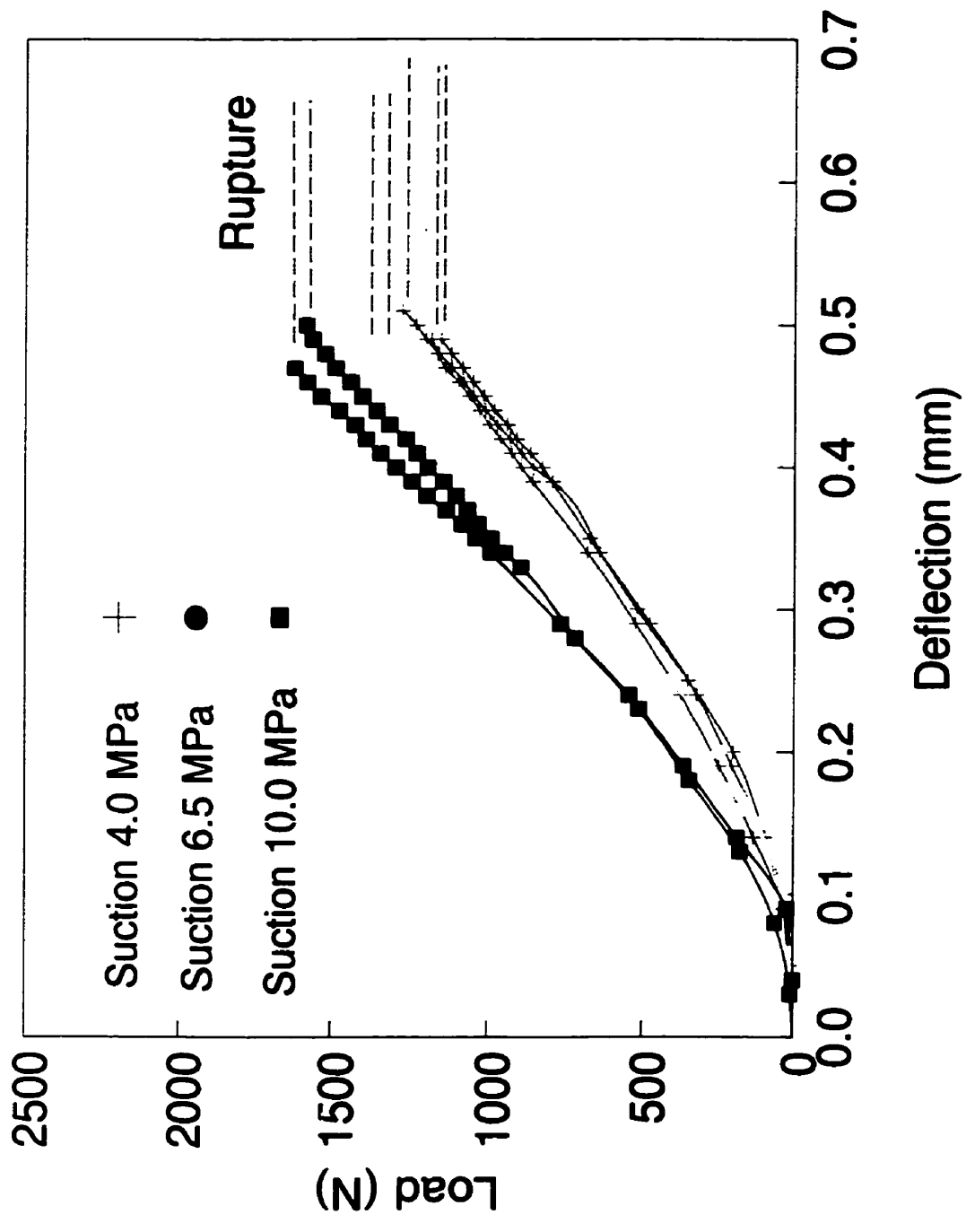


Figure 7.10 Axial load versus axial deflection in tension

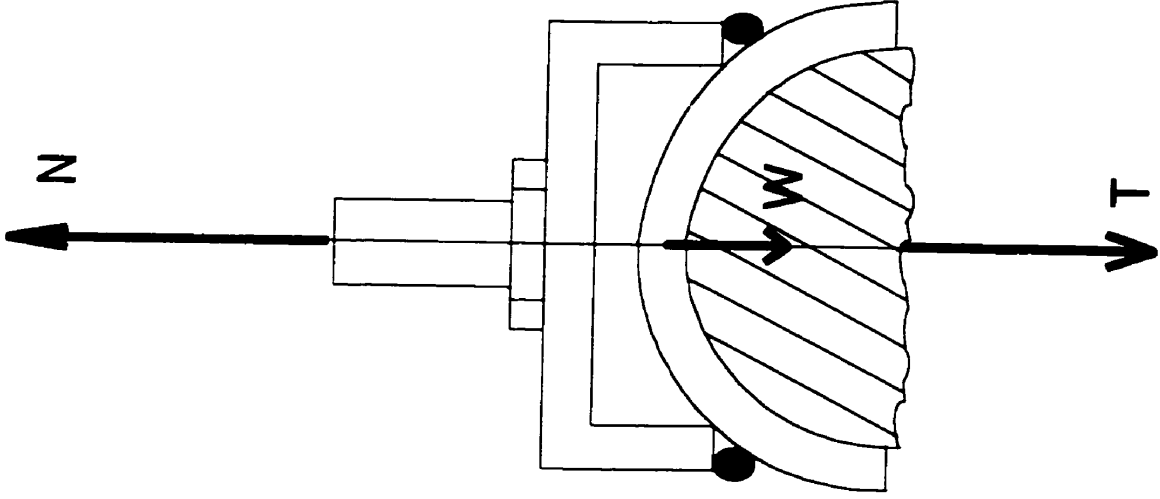


Figure 7.11 Force equilibrium

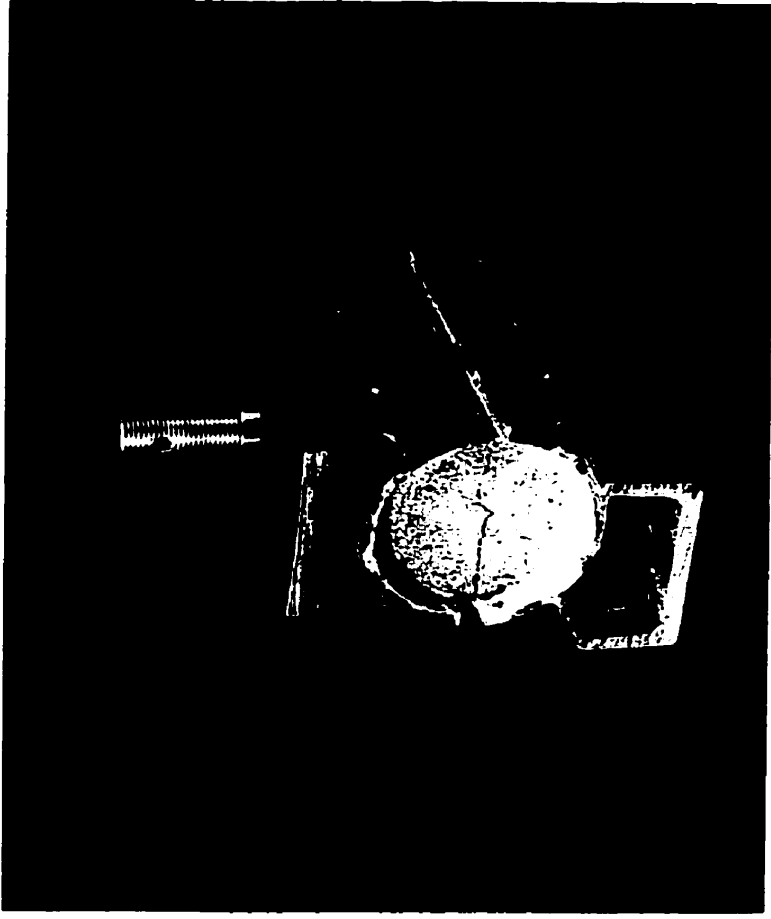


Figure 7.12 Failure of the specimen in tensile mould

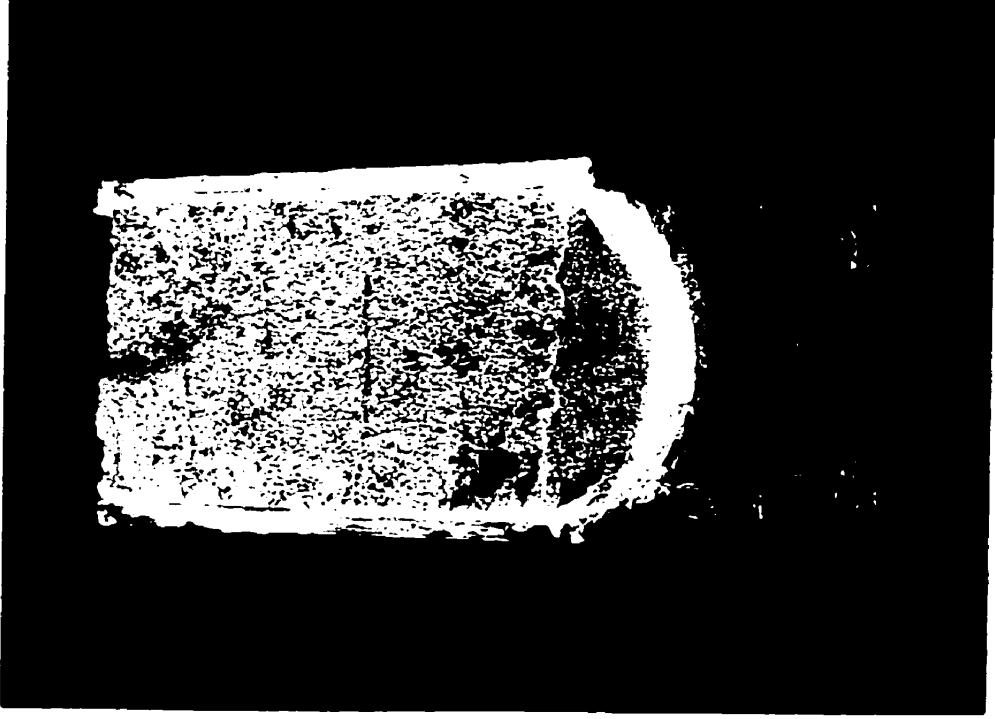


Figure 7.13 Typical failure surface of the specimen

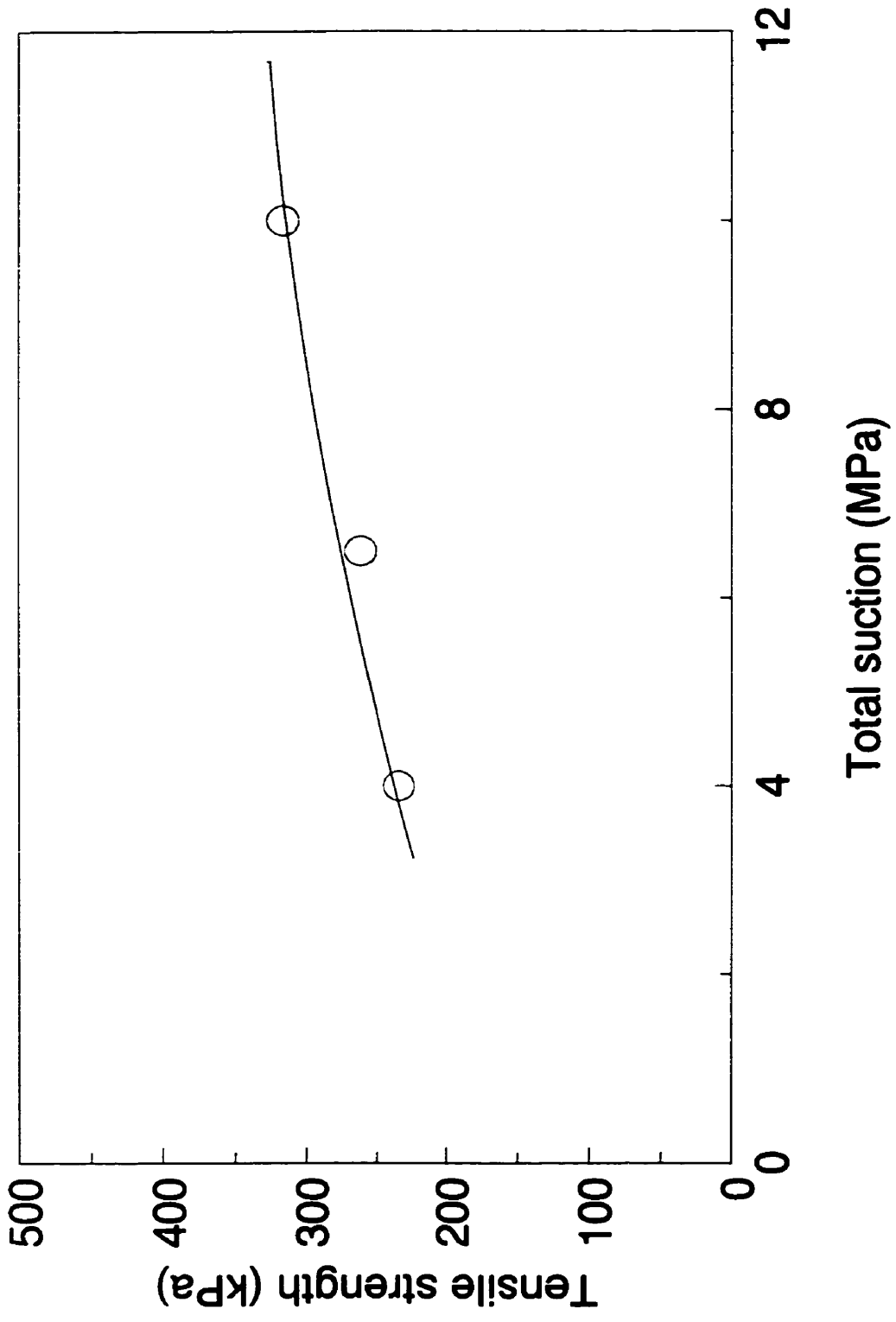


Figure 7.14 Tensile strength versus total suction

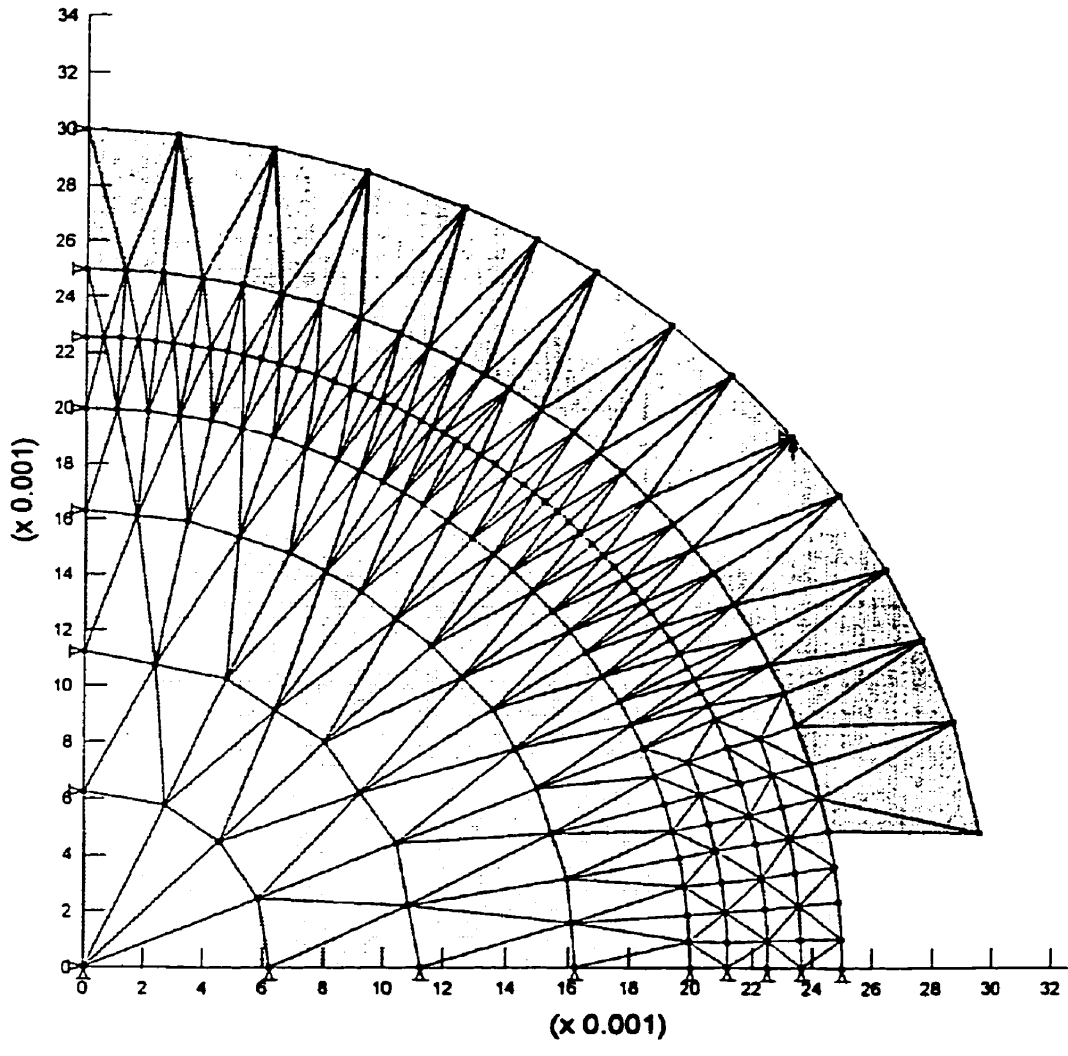


Figure 7.15a Finite element mesh

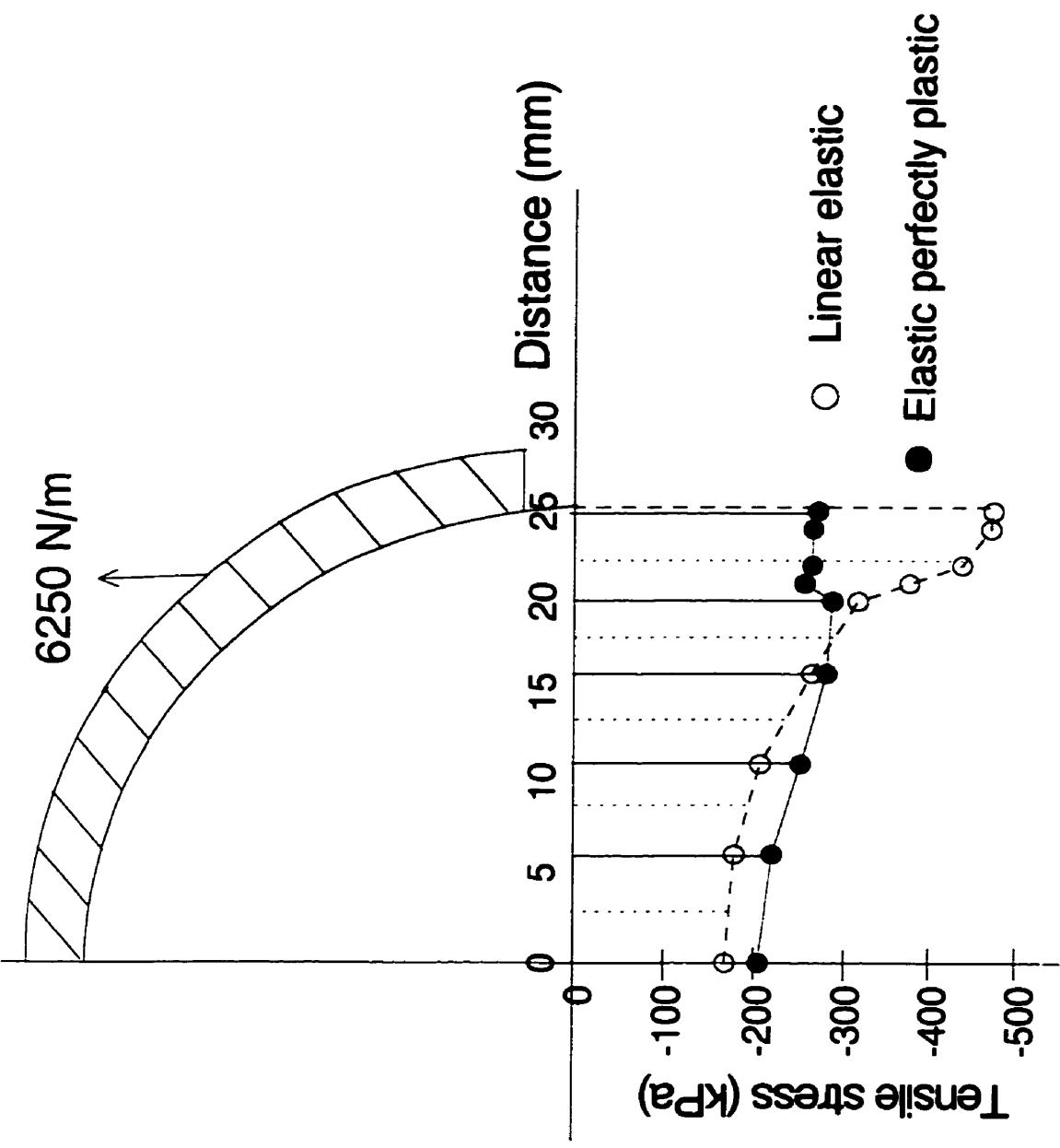


Figure 7.15b Stress distribution along failure plane

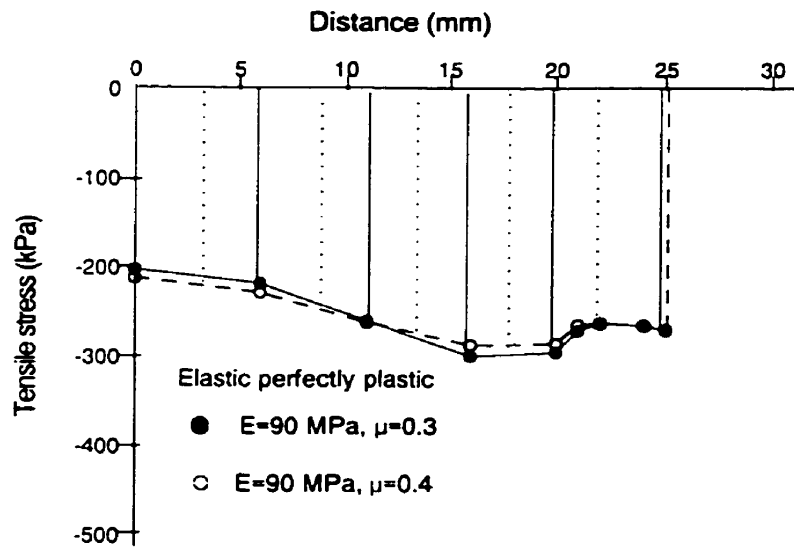
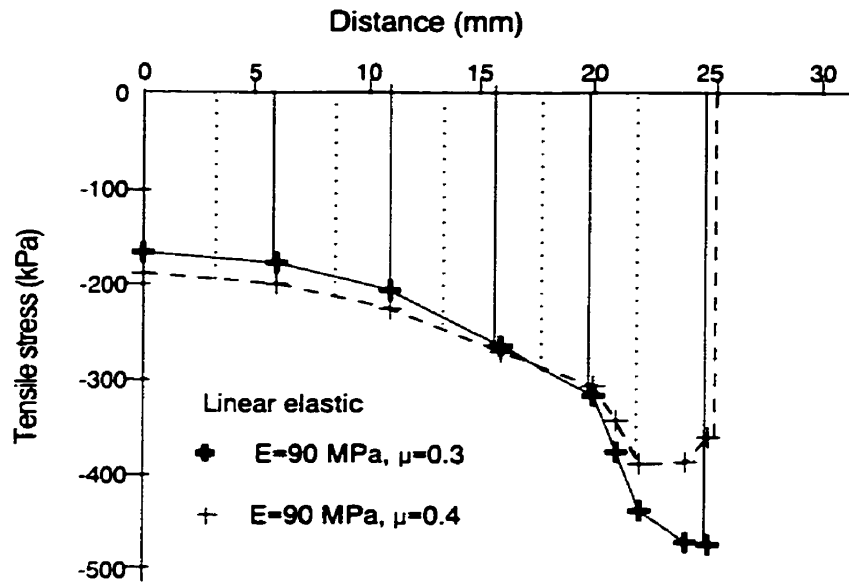


Figure 7.16 Influence of Poisson ratio on stress distribution

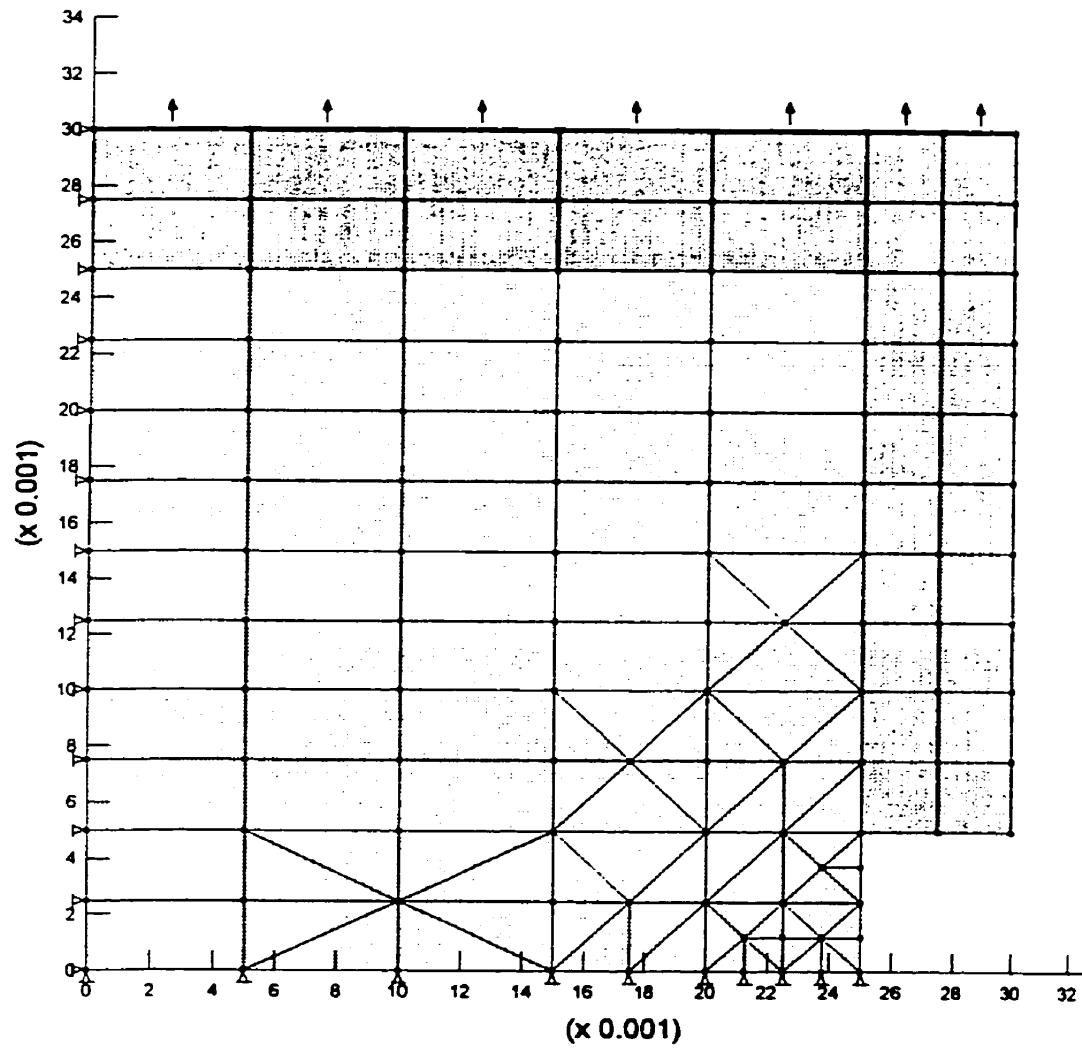


Figure 7.17 Finite element mesh for square specimen

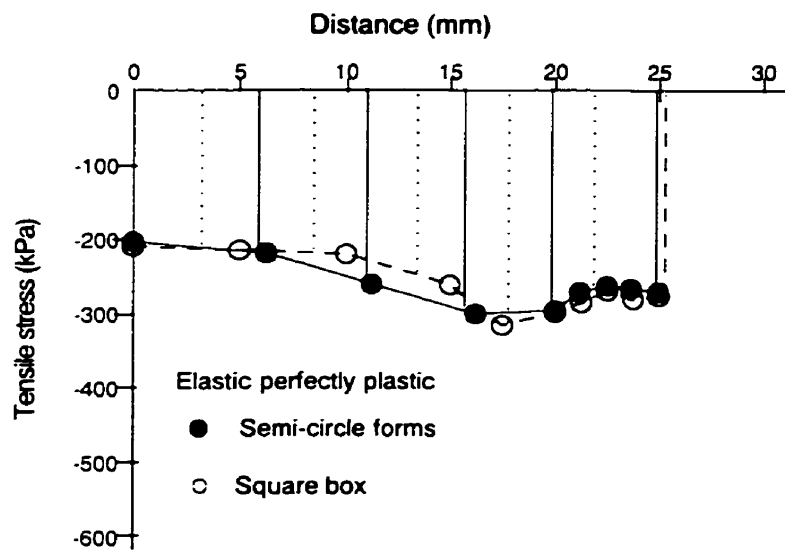
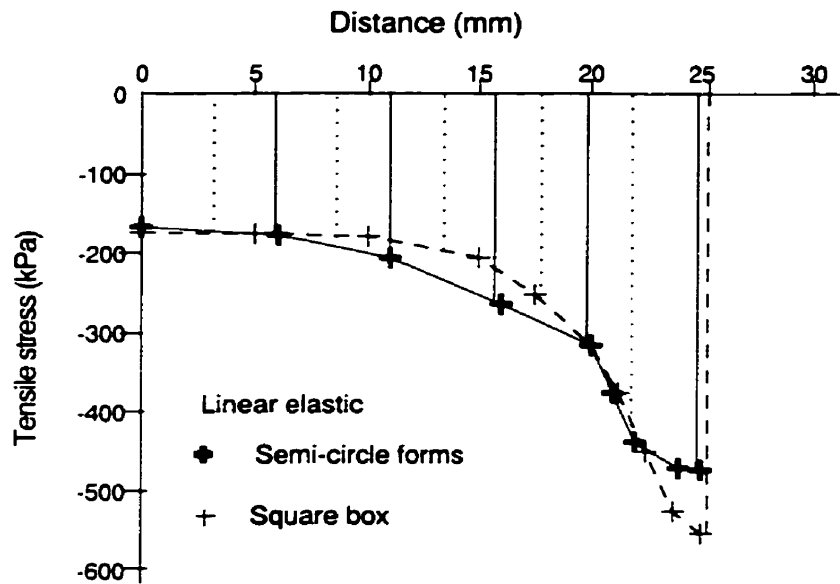


Figure 7.18 Stress distribution at two forms of mould

CHAPTER 8

RESULTS OF STRESS-CONTROLLED TRIAXIAL TESTS

8.1 Introduction

Stress-controlled triaxial tests were carried out to examine suction-dependent stress-strain behavior of unsaturated buffer. The triaxial tests involved compression and shearing using incremental loading along controlled stress paths in p - q space, where total mean stress $p = (\sigma_1 + \sigma_2 + \sigma_3)/3$ and deviator stress $q = (\sigma_1 - \sigma_3)$. The remaining stress, suction, was measured, not controlled. Loading was applied in three phases (1) isotropic compression with confining pressures up to 3 MPa, (2) unloading to 1.5 MPa or 1.0 MPa to achieve an apparent overconsolidation ratio (apparent OCR) of 2 or 3 respectively. (The OCR defined in a conventional way as $OCR = p/p_c$ for unsaturated soils is adjectively termed 'apparent OCR' since suction is disregarded in this definition.) (3) shearing along selected stress paths $\Delta p/\Delta q = -1/3, 0, 1/3, \text{ or } 1$. Isotropic compression was conducted by successively increasing the cell pressure, thus allowing identification of yielding in the tested specimens. Shearing began at a designated apparent OCR. It consisted of applying six (or more) increments of axial load (with corresponding adjustment of cell pressure) until the specimen began to strain rapidly, yield, and

accelerate towards failure. Stress paths were selected so as to permit identification of major elastic-plastic features, namely, yielding, hardening, flow rule and failure. The general procedures used to perform the tests were described in detail in Chapter 6. No drainage was permitted in either the air or water phases so all tests can be characterized as 'constant mass tests'. Vertical strain and lateral strain were measured using non-contacting displacement transducers. Suction changes were monitored by thermocouple psychrometers.

Specimens used in the tests were all formed at saturation of 85%, water content of 19.4%, and dry density of 1.67 Mg/m^3 . As pointed out in Chapter 4, microstructure and starting suctions are dominated by hydration water contents (Wan *et al.* 1995, Tang *et al.* 1997b). Specimens formed with the same initial conditions ensured uniformity of the material being tested. Quality control and consistency data were described in Chapter 7.

This chapter presents representative experimental data of the suction characteristics, stress-strain behavior and strength properties obtained from the testing program. The volume of the data collected from the tests is too large to be presented here in its entirety but is archived in the geotechnical laboratories at the University of Manitoba. The chapter also describes an attempt to interpret the observed behavior using an existing conceptual model for unsaturated soils. It concludes that a new conceptual model is required in order to frame all observed mechanical behavior of unsaturated buffer in this thesis. The new conceptual model will be described later in Chapter 9.

8.2 Initial Conditions of Specimens

Designated suctions of unsaturated specimens used in this thesis have been achieved by three approaches: 1) specimens were compacted from mixtures of sand, bentonite and deionized water to the same dry density but different water contents, saturations, and therefore different matric suctions; 2) specimens were compacted from mixtures of sand, bentonite and concentrated solutions to the same dry density, different water contents and saturations, and hence different total suctions as a combination of matric suctions and osmotic suctions; and 3) specimens were compacted to the same dry density, water content and saturation, and were subsequently dried at controlled suctions using the vapour equilibrium technique. The specimens formed using approaches 1, 2 and 3 were examined in quick undrained triaxial compression tests and in tensile tests. The results were presented in Chapter 7. Approach 3 has been used to prepare the specimens used for the stress-controlled triaxial tests which will be presented in this chapter.

Two series of specimens were used. All specimens were statically compacted at an initial water content w of 19.4%, saturation S_r of 85%, and dry density γ_d of 1.67 Mg/m^3 . The specimens had 50 mm diameter and 100 mm height. The specimens were then either tested immediately (the first series of specimens) or were dried before testing (the second series of specimens).

Five specimens were produced in the first series and tested immediately after compaction. They are therefore referred to as ‘as compacted’ specimens. In each specimen, a small 6 mm diameter hole was drilled in the top surface for accommodating the psychrometer tip to measure suctions. After the specimen was installed in the triaxial cell, total suction was measured before any loading was applied. This was called ‘start (total) suction’. For the specimens in this series, total suctions were expected to be slightly higher than the initial suctions measured when the specimens were formed. This is because some moisture was lost from the specimen in the process of installing it into the cell and evaporation caused by heat generated by drilling the hole for the psychrometer. Decreases in water content produced higher suctions. Initial total suctions of these specimens were about 3.5 MPa as reported earlier in Chapter 4. Start suctions were about 4.2 MPa (see Table 8.1).

Table 8.1: Initial conditions of the ‘as compacted’ specimens

	T16530	T16531	T16533	T16534	T16535
Water content(%)	19.60	19.35	19.54	19.65	19.76
Saturation (%)	84	83	84	81	84
Dry density (Mg/m ³)	1.657	1.657	1.658	1.661	1.661
Specific volume	1.629	1.629	1.628	1.626	1.625
Start suction (MPa)	4.2	4.6	4.2	4.4	3.9

Three specimens were made in the second series which were dried (with corresponding suction increases) after each specimen was compacted and a hole was drilled. These are referred to as ‘after drying’ specimens. A further three identical specimens were also made and dried for quality control assessment. Drying was done by placing each

specimen in a dish inside a desiccator at a controlled suction. Detailed procedures were given earlier in Section 3.4.1. After drying was completed, the specimens had decreased in size and had higher suctions. The suctions measured in the specimens after drying and curing were about 6 MPa. This value was less than the controlled suctions of 6.5 MPa in the desiccators probably because 1) the specimens were only allowed 30 days for equalization which may not have been sufficient to fully reach the equilibrium between suctions in the specimens and the osmotic solutions, and 2) evaporation of water from the specimens and condensation into the solutions in the desiccators decreased the original suctions of the osmotic solutions.

Table 8.2: Initial conditions of the ‘after drying’ specimens

	Prior to drying			After drying		
	T16540	T16541	T16542	T16540	T16541	T16542
Water content(%)	19.55	19.49	19.60	18.34	18.35	18.41
Saturation (%)	84	84	85	80	80	82
Dry density (Mg/m ³)	1.655	1.659	1.662	1.671	1.667	1.681
Specific volume	1.631	1.628	1.625	1.616	1.619	1.607
Diameter (mm)	50.84	50.73	50.85	50.61	50.64	50.57
Length (mm)	100.63	100.59	100.48	100.34	100.43	100.20
Start suction (MPa)				6.0	5.7	5.7

Since the ‘as compacted’ and ‘after drying’ specimens all initially had consistent microstructures, they were regarded as the same ‘soil’ but with different start suction levels (Tang *et al.* 1998b). The ‘after drying’ specimens were expected to produce higher stiffness and probably more dilatation during shear than ‘as compacted’ specimens.

8.3 Stress-strain Behavior under Selected Stress Paths

8.3.1 Stress Paths

Stress paths in the stress-controlled triaxial tests are shown schematically in Figures 8.1 and 8.2. Figure 8.1 shows a suction, mean stress plane for isotropic loading. All specimens were initially compacted and had initial suctions at point a in Figure 8.1. The stress path 1 (aa_1a_2) was followed by the 'as compacted' specimens. The 'after drying' specimens also started at point a, but then, drying was imposed so that the stress state moved to point c. Then isotropic compression was applied along the stress path 2, (cc_1c_2). Subsequent unloading along stress paths a_2a_3 or c_2c_3 allowed specimens to become overconsolidated. This is technically necessary to permit identification of elastic-plastic behavior. The 'as compacted' and the 'after drying' specimens followed similar stress paths but had different start suctions. Testing specimens at two start suction levels allows the effects of suction on soil behavior to be examined.

During isotropic compression, the cell pressures were applied and suction changes were measured. No air or water fluxes were permitted into or out of the specimens. Suctions could not be held constant while applying isotropic compression. As indicated in literature review, no effective techniques for controlling suctions as high as those in unsaturated sand-bentonite (commonly about 2 to 10 MPa) had been identified during

this project. The author understands that this has now been accomplished by James Blatz, the next doctoral student on the project.

Figure 8.2 shows a schematic three-dimensional view of the stress paths selected for shearing in p-q-S space. The specimens at each suction level experienced the same compression procedure but different shearing conditions as expressed by $\Delta p/\Delta q$. Except for one specimen at a_s in Figure 8.2 with apparent OCR = 3, all other specimens had apparent OCR = 2. They were sheared following the stress paths $\Delta p/\Delta q = 1, 1/3, 0,$ or $-1/3$ which are plotted later in Figure 8.10. These are common stress paths used in testing saturated soils to examine elastic-plastic features such as yielding, hardening, strain softening, and failure.

8.3.2 Isotropic Compression

All of the eight 'as compacted' and 'after drying' specimens were consolidated using similar schedules. Isotropic loading was applied by increasing the cell pressure, that is, the confining pressure in the cell. Although drainage was closed to both the air and water phases, the volume of the air phase in unsaturated specimens decreased and the specimens compressed. The effect is similar in some ways to consolidation in saturated specimens except that the deformation rate is much faster as the air phase is compressed. Isotropic compression in this testing program can therefore be called 'constant mass' compression. During isotropic compression, the mean stress $p = \sigma_1 = \sigma_2 = \sigma_3$, and has the

magnitude of the applied cell pressure. Detailed procedures of loading and unloading of isotropic pressure have been described earlier in Section 6.3.4.

8.3.2.1 Yielding under isotropic compression

Figure 8.3 shows typical compression curves for each series of specimen in term of mean stress p ($p = (\sigma_1 + \sigma_2 + \sigma_3)/3 = \sigma_3$) versus volume strain ϵ_v ($\epsilon_v = (\epsilon_1 + 2\epsilon_3)$). The 'as compacted' specimen (T16533) had initial values $w = 19.5\%$, $S_r = 84\%$, $\gamma_d = 1.66 \text{ Mg/m}^3$, and $S = 4.2 \text{ MPa}$; and while the 'after drying' specimen (T16540) had initial values $w = 18.3\%$, $S_r = 80\%$, $\gamma_d = 1.67 \text{ Mg/m}^3$, and $S = 6.0 \text{ MPa}$. As mentioned earlier, the two series of specimens were initially prepared to the same conditions. The 'after drying' specimens which were subsequently dried had lower water content, lower saturation, and therefore higher dry density and suction. The data in the figure show that in the early stages of compression, each of the stress-strain curves appears to be linear. With increasing mean stress, the stiffness decreases considerably. That is, yielding was observed. Yield stresses were then identified from the changes in stiffness in the curves, approximately at 860 kPa and 1200 kPa for the 'as compacted' specimen (T16533) and for the 'after drying' specimen (T16540) respectively. As expected, the 'after drying' specimen had higher stiffness because of its higher dry density, and a higher yield stress because of its higher start total suction. At unloading, fairly good linear behavior was observed. Compared with the linear section during initial compression, the specimens were now stiffer in unloading following plastic hardening. The change of stiffness may

be due to release of anisotropy towards more isotropic behavior. This will be discussed later.

During compression, the volume changes were mainly in the air phase and suction changed correspondingly. Figure 8.4 shows the results of total suction *versus* mean stress for the two specimens T16533 and T16540. At the beginning of loading, the start suctions of the two specimens were 4.2 MPa and 6.0 MPa respectively. Addition of confining pressures up to 3 MPa caused significant reductions of suctions to approximately 1.5 MPa and 2.5 MPa, as a result of compression of the air phase and increasing saturation. More discussion of relationships between suction and stress will be given later in this chapter. It should be noted that the total suction of saturated specimens of sand-bentonite is about 1.5 MPa (Wan 1996, Tang *et al.* 1999), corresponding to the osmotic suction. This is approximately the total suction of the ‘as compacted’ specimen at a confining pressure of 3000 kPa, indicating that the initially unsaturated specimen had compressed sufficiently to become saturated.

Figures 8.3 and 8.4 show typical patterns of compression behavior and suction changes for initially unsaturated buffer specimens under ‘constant mass’ isotropic compression. Yield stresses identified from the data such as those in Figure 8.3 depend on the start suctions and current suctions at the time yield occurred. Yield stresses of all eight specimens were identified from mean stress *versus* volume strain relationships for each of the specimens. Data are summarized in Table 8.3 and are plotted in Figure 8.5. In the

figure. results are shown at points O'_1 and O'_2 for 'as compacted' specimens and 'after drying' specimens respectively. The line II' through O'_1 and O'_2 therefore represents an approximate yield locus under isotropic compression in p-S space. Increasing pressures after O'_1 and O'_2 produce volumetric plastic hardening and cause the yield stresses to increase to g_1 and g_2 respectively. These points were chosen during testing to have the same confining pressure, 3000 kPa. By and large, changes in total suction caused by mean stress followed the lines A_1g_1 and A_2g_2 for 'as compacted' and 'after drying' specimens respectively.

8.3.2.2 Volume change behavior

Volume change behavior for unsaturated soils is commonly examined through two separate (though related) relationships, (1) the relationship between specific volume, mean stress and suction; and (2) the relationship between water content, mean stress and suction relationship. Under the constant mass condition used in this program, water contents were unchanged. The volume change behavior examined is therefore how specific volume is related to suction and mean stress.

Specific volumes have been evaluated from measurements of height and diameter changes using the non-contacting transducers.

Figure 8.6 shows specific volume V versus mean stress p of two unsaturated specimens from each series. Once again, the specimens used were T16533 and T16540. It is believed that this is the first time such relationships have been presented for a densely compacted clay-rich mixture. The data for each specimen in Figure 8.6 can be fitted using two straight lines. At a pressure of 3000 kPa, the specific volume of the specimen T16533 deviates from the fitting line. This is probably because the specimen was close to being fully saturated as discussed in Section 8.3.2.1. As a result, the deduced specific volume resulting from small deformations did not follow the line. The figure shows that the 'after drying' specimen (T16540) had higher yield stress. The slopes of the lines for the two specimens are different, with the 'after drying' specimen being stiffer. The regression lines fitted to the post-yield data for each specimen are as follows:

$$V = 1.660 - 0.0000516 p \quad \text{for the 'as compacted' specimen T16533} \quad [8.1]$$

$$V = 1.645 - 0.0000382 p \quad \text{for the 'after drying' specimen T16540} \quad [8.2]$$

where V is specific volume and p is mean stress in kPa.

A similar observation was made by Matyas and Radhakrishna (1968) who showed that lower start suctions decreased the stiffnesses in compression curves under controlled constant suctions. It should be remembered however that suctions are not constant in the plots shown in Figure 8.6 but decrease with increasing mean stress (Figure 8.4). This is plotted in Figure 8.7 showing volume change in relation to mean stress and suction. The effects of suction on volume change should be taken into account. This will be discussed later in Chapter 9.

8.3.2.3 Anisotropy of the specimens

As mentioned earlier, axial and horizontal displacements were directly measured using non-contacting transducers. Figure 8.8 shows a typical graph from the axial strain ϵ_1 and lateral strain ϵ_3 versus time of the 'as compacted' specimen T16533 under isotropic loading. In the figure, data in the segments 01 and 01' represent strains under isotropic compression during compression up to 3000 kPa, and 12 and 1'2' for strains during unloading to 1500 kPa. Data obtained from subsequent shearing are omitted in this figure. Strains in the figure change in a stepwise manner for each successive constant isotropic pressure. At any given time, stresses in all directions were equal to the cell pressure, that is, $\sigma_1 = \sigma_2 = \sigma_3 = p_c$. However, axial strains ϵ_1 and lateral strains ϵ_3 in the segments 01 and 01' along the curves are obviously not equal. This suggests that the specimen exhibits different compressibility properties in different directions, that is, anisotropy. The specimen is stiffer in the axial direction than in the radial direction. The ratio of vertical strain to lateral strain ϵ_1/ϵ_3 is about 0.5. Observations of similar unequal deformations with approximate ϵ_1/ϵ_3 ratio of 0.75 were obtained by Tang (1996) and Blatz (1998) (Tang *et al.* 1998c) from specimens with the same initial conditions that were dried under controlled suctions in desiccators. Anisotropy led to production of shear strain ϵ_s ($\epsilon_s = 2 \times (\epsilon_1 - \epsilon_3) / 3$) under isotropic compression. The results are illustrated in Figure 8.9 which shows mean stress p versus shear strain ϵ_s . The mean stress of 3000 kPa in isotropic compression produced 0.8% of shear strain (see point 1 in the figure). This is due to the anisotropy of macrostructure that was built into the specimens during compaction.

Anisotropy was also observed by Saadat *et al.* (1989) in saturated buffer specimens. In contrast with the unsaturated specimens, the saturated specimens are stiffer horizontally than vertically. The observed difference of anisotropy in buffer materials between saturated and unsaturated specimens formed by one-dimensional static compression in a rigid mold suggests that the degree and nature of anisotropy depends on saturation levels. This is a somewhat unexpected result that deserves further attention.

It is interesting to note that changes in axial strain ϵ_1 and lateral strain ϵ_3 during isotropic unloading are approximately the same amount as shown by the segments 12 and 1'2' along the curves in Figure 8.8. Changes in shear strain during unloading as shown by the segment 12 in Figure 8.9 are almost negligible, indicating a release of anisotropy in overconsolidated specimens. This suggests that the degree of anisotropy in overconsolidated specimens is likely to be small and the material will behave in an almost isotropic fashion. Lingnau (1993) and Tanaka (1995) formed similar results in saturated specimens.

8.3.3 Shearing

Shearing was carried out by applying axial loads and adjusting cell pressures incrementally to achieve the desired stress paths. Depending on the expected maximum deviator stress, the size of the load increments should be such that there will be a

sufficient number of increments (3-5) to identify yield and establish trends in stress-strain behavior. However, since this is the first doctoral project at the University of Manitoba in which such stress-controlled triaxial tests were performed on unsaturated specimens, there were no data available to provide estimates of the yield stresses. To be conservative, the size of the deviator stress increments was chosen to be 250 kPa in earlier stages of the tests, and 200 kPa or 100 kPa in later stages. As in the compression phase, load increments were again held constant until deformations and suctions remained essentially constant. Typically the increment durations were 24 hours for low stress levels, and 48 hours or longer for high stress levels. Figure 8.10 shows the measured actual stress paths in p-q space. Implicit in the figure is the axis of suction S orthogonal to p-q space. The last applied increment for q might not have been the minimum value required to produce failure. That is, the applied load might have exceeded q_f . In this case, the measured stress-strain behavior was approximated by a fitting curve. This curve was extrapolated between the last value of q that was stable and the final value that produced (or exceeded) failure. The value of q_f plotted in all following figures is this extrapolated value.

8.3.3.1 Stress-strain behavior along selected stress paths

Figure 8.11 shows the stress-strain curves for the 'as compacted' specimens as expressed as deviator stress q *versus* shear strain ϵ_s . The data were obtained from three 'as compacted' specimens T16531, T16533 and T16534. They were all overconsolidated

with apparent OCR = 2 and had start suctions averaging 4.2 MPa. They followed stress paths $\Delta p/\Delta q = 0, -1/3$ and 1 respectively. For clarity the results from the similar specimen - T16530 following the stress path $\Delta p/\Delta q = 1/3$ are excluded from the figure.

As can be seen in Figure 8.11, all three specimens show approximately linear behavior up to about $q = 700 \text{ kPa} - 900 \text{ kPa}$ depending upon stress paths, after which the stress-strain curves became non-linear showing ductile behavior with large strains. Specimen T16534 exhibits clearly strain hardening comparing with specimens T16531 and T16533. The process continued until the specimens reached failure. The data show that specimen T16531 was stiffer and stronger than that specimen T16534. It should be remembered from Figure 8.10 that the specimens were tested along different stress paths. At failure, their mean stresses ranged from about 1000 kPa to 3000 kPa. The behavior is obviously different from that of saturated soils in which shear strength increases with increasing values of $\Delta p/\Delta q$ along a sloped critical state line in p - q space. The difference clearly indicates that the effect of suctions on strength properties is remarkable. The question then arises why the maximum deviator stresses (at failure) were so close for all three specimens despite the different stress paths and mean stresses at failure. Such behavior will be further discussed later in an attempt to find an explanation using an existing conceptual model for unsaturated soils.

The results discussed in the previous paragraphs were obtained from four 'as compacted' specimens with an average start suction of 4.2 MPa. They were all overconsolidated.

That is, each specimen was initially compressed to 3000 kPa and unloaded to mean stress $p = 1500$ kPa before shearing. These test conditions were also used for 'after drying' specimens which had start suctions of about 6 MPa. Three specimens with apparent OCR = 2 were sheared starting at mean stress $p = 1500$ kPa following stress paths $\Delta p/\Delta q = -1/3, 0,$ or 1 . The observed stress-strain behavior of this series of specimens was similar in principle to that of 'as compacted' specimens. Comparison and interpretation of the data from these two series of specimens will be made in the following section and in the next chapter.

One further specimen - T16535 in the 'as compacted' first series with start suction 4.2 MPa had an apparent OCR = 3. Figure 8.12 presents the stress-strain curves of two 'as compacted' specimens with different apparent overconsolidation ratios (apparent OCRs). The specimen T16531 with apparent OCR = 2 was sheared at constant mean stress p of 1500 kPa while specimen T16535 with apparent OCR = 3 sheared at constant mean stress p of 1000 kPa. Both specimens followed similar stress paths during shearing ($\Delta p = 0$) in p - q planes (Figure 8.10). Although they were both the 'as compacted' specimens, they were sheared at different mean stresses therefore different current suctions. At the beginning of shearing, specimen T16531 had current suction of 2.7 MPa and was under mean stress of 1500 kPa. Specimen T16535 was under a lower mean stress of 1000 kPa but had a higher current suction of 3.1 MPa. The data in Figure 8.12 show that the two specimens had largely the same stiffness, indicating both specimens were overconsolidated. As far as their strengths are concerned, specimen T16531 was

stronger. This should be understood as a result of the combined effect of mean stress and suction. Generally, strengths increase with increasing mean stress and with increasing suction. Under the condition of constant mass compression in this program, however, mean stress and suction were not independently controlled. Changes in mean stress causes inverse changes in suction, and strength was controlled by the interrelationship between mean stress p and suction S . This also needs to be examined later using the concepts of conceptual models for unsaturated soils.

Figure 8.13 compares the results from specimen T16533 (with apparent OCR = 2, stress path $\Delta p/\Delta q = -1/3$) and specimen T16535 (with apparent OCR = 3, stress path $\Delta p = 0$). The data in the figure show similarities in the stress-strain behavior and maximum deviator stress at failure. As shown in Figure 8.10, the two specimens followed different stress paths but failed at largely same mean stress p and deviator stress q . Good correlation between the two specimens which followed different stress paths suggests elastic behavior of the two specimens at stress states within the state boundary surface. It will be shown later in the next section that the same stresses p and q also produced the same current suction S . Consequently, the two specimens failed at largely the same stress state of p , q , S , indicating that the position of the state boundary surface is largely independent of the stress path used to reach it.

8.3.3.2 Stress-strain behavior of specimens at different suction levels

The 'as compacted' specimens and the 'after drying' specimens were at different start suction levels. They were tested following similar procedures for both compression and shearing. For a particular stress path, data obtained from specimens at two suction levels are therefore comparable and allow examination of the effect of start suction. Due to the similarity of the results, only one example will be reviewed in detail. It compares data from specimens sheared along stress path $\Delta p/\Delta q = 0$. Data obtained from other tests will be synthesized into a constitutive model in the next chapter.

Figure 8.14 shows results from these two specimens with two different start suction levels. Both specimens had apparent OCR = 2 and were sheared at constant mean stress $p = 1500$ kPa, that is, along the stress paths $\Delta p/\Delta q = 0$ and $p = 1500$ kPa. The 'as compacted' specimen T16531 had initial conditions: $w = 19.4\%$; $S_r = 83\%$; $\gamma_d = 1.66$ Mg/m³; and start suction $S = 4.6$ MPa. At the beginning of shearing, the total suction had decreased due to compression to a value $S = 2.7$ MPa. The 'after drying' specimen T16541 had the following values after drying: $w = 18.35\%$; $S_r = 80\%$; $\gamma_d = 1.67$ Mg/m³; start suction $S = 6.0$ MPa. The suction at the beginning of shearing was $S = 3.8$ MPa. It will be shown later that suctions remained unchanged in these specimens sheared with stress path $\Delta p/\Delta q = 0$. Figure 8.20 shows that the stress-strain behavior of the two specimens was similar, though T16541 with the higher start suction level was stronger than T16531. In detail, T16541 failed at $p = 1500$ kPa, $q = 1601$ kPa and $S = 3.8$ MPa. Specimen T16531 failed at $p = 1500$ kPa, $q = 1390$ kPa and $S = 2.7$ MPa.

Different start suctions in the two specimens resulted in different current suctions and strengths at the same mean stress condition. The results indicate, as expected, that strength is quite strongly but not proportionately influenced by suctions.

8.3.3.3 Yielding and shear strength

The stress-strain curves of deviator stress q versus shear strain ϵ_s , presented earlier (Figures 8.11-13) demonstrate a limited range in which the response to stressing was broadly recoverable and relatively stiff. Responses were non-recoverable and less stiff in later stages of the tests. The stress-strain behavior of unsaturated sand-bentonite therefore can be characterized as being of an elastic-plastic nature. Yielding can be identified from changes in stiffness in plots of deviator stress q vs. shear strain ϵ_s .

Yielding was relatively well defined in relationships of mean stress p and volume strain ϵ_v during compression and yield stresses were easily identified. This was described earlier in Section 8.3.2.1. For stress-strain curves of deviator stress q vs. shear strain ϵ_s , there was usually a transition between pre-yield and post-yield behavior. Identifying yielding in such nonlinear relationships was less clear. Despite the transitions, data can be interpreted as bilinear behavior. Yield stresses were identified from deviator stress and shear strain relationships following procedures used by Graham *et al.* (1983). Other relationships such as σ_1 versus ϵ_1 , σ_3 versus ϵ_3 and Work versus LSSV (the length of the stress vector) as suggested by Graham *et al.* (1983) can be used together to clarify

uncertainties. Figure 8.15 illustrates how yield stresses in q versus ϵ_s relationships have been determined using simple empirical procedures. Two straight lines are used to fit the data, and the yield stress is taken as the intersection of the two lines. Table 8.3 lists the yield stresses selected using these procedures and the current suctions when yield occurred.

Table 8.3: Yield and strength of the specimens at two suction levels

Specimens	Yielding at compression		Yielding at shearing		Strength	
	Yield stress p_v (kPa)	Suction (MPa)	Yield stress q_v (kPa)	Suction (MPa)	q_{max} (kPa)	
‘Compacted’	T16530	900	3.4	1200	-	1374
	T16531	950	3.7	1200	2.5	1390
	T16533	860	3.4	1150	2.9	1291
	T16534	870	3.5	1000	2.0	1250
	T16535	950	3.1	1180	3.0	1250
‘After drying’	T16540	1200	4.3	1480	4.2	1518
	T16541	1250	4.3	1400	3.8	1601
	T16542	1230	4.2	1400	2.3	1634

As mentioned earlier, axial loads and cell pressures were applied incrementally until the specimens failed. In these cases, the stresses applied in the final increment did not necessarily produce the condition for Critical State failure. As a result, determination of the shear strength should be made not only in terms of the final load increment of load, but also the whole trends of the stress-strain curves using a degree of judgement.

Failures occurred in all specimens in the two series. Most tests failed when the axial strains were less than 5%. Figure 8.16 shows data for volume strain ϵ_v and shear strain ϵ_s versus time for the ‘after drying’ specimen T16541. The specimen was compressed,

partially unloaded, and then sheared at constant mean stress p (that is, with $\Delta p/\Delta q = 0$, see Figure 8.10). These three stages of the tests are represented in Figure 8.16 by 01 for isotropic compression, 12 for unloading, 23 for shearing and 34 just after failure. In isotropic compression, the volume strains increased steadily. Anisotropy of the specimen resulted in unequal deformation vertically and horizontally, thereby producing shear strain. There were only limited and largely isotropic changes in volume strain and shear strain during the unloading phase. During shearing, the vertical strain increased steadily whereas horizontal strains decreased. As a result, the shear strain increased markedly. Changes in volume strain during shearing to point 3 were very small. At the last stage after point 3, shear strains increased sharply and volume strain decreased (representing volume increases) significantly, indicating the specimen had failed.

Figure 8.17 presents data for yielding and failure for the two series of specimens with different start suction levels in p - q space. Current suctions at yielding and failure are not marked but can be found in Table 8.3. Two comments can be made about the data in Figure 8.17 and in Table 8.3:

1. Since the current suctions at yielding are different in each test, a simple yield envelope should not be drawn in this figure through the yield points for each series of specimens. From a conceptual and modelling viewpoint, the yield loci should be developed to embrace the effect of suctions.

2. There is no trend in Figure 8.17 to develop a single strength envelope for each series of specimens. Once again, the reason is because each of the shear strengths is associated with its own current suction. Strength envelopes for unsaturated soils which account for the effect of suction can only be developed in p-q-S space. This will be presented in the next chapter - A new elastic-plastic conceptual model for unsaturated soils.

8.3.3.4 Anisotropy during shearing

Anisotropy was observed in specimens during normal compression as discussed in Section 8.3.2.3. The question can then be raised whether the overconsolidated specimens also behaved anisotropically during shearing. In anisotropic specimens, volume strain ϵ_v can be expected to change as a result of changes in deviator stress q during shearing even though mean stress p remains constant.

Figure 8.18 shows volume strain ϵ_v versus deviator stress q in a shearing process at constant mean stress. Data were obtained from two specimens. The 'as compacted' specimen T16535 was overconsolidated with apparent OCR = 3, and was sheared at constant mean stress $p = 1000$ kPa. The 'after drying' specimen T16541 was overconsolidated with apparent OCR = 2, and was sheared at constant mean stress $p = 1500$ kPa. The results show that for both specimens during a large portion of the shearing, increasing deviator stress q made only small changes in volume strain ϵ_v . Only

when the specimens failed, did the volume strains begin to change remarkably. (Volume strains decreasing mean increases in volume.) This does not necessarily reflect dilations in the specimens. Instead, it is probably because the measured data were from bulk or rigid-body deformation at failure which took place with the development at well-developed failure planes. Since shear stress produces only small volume strains. The results indicate that overconsolidated specimens are isotropic during shearing.

8.4 Suction Change Under applied Stresses

Changes in total suctions of unsaturated specimens were monitored using psychrometers during the entire process of the triaxial tests. In this way, psychrometers measured the values of start suctions before any load was applied, suctions at each applied stress state during isotropic loading, during shearing, and suctions after the specimens failed. The tests were conducted at room temperatures from 23°C to 26°C. Temperatures in the specimens were tracked by psychrometer when taking each suction reading. All suction readings produced by psychrometers were corrected to 25°C (Tang *et al.* 1997b). Correction of psychrometer readings taken at temperatures other than 25°C was justified by Wan (1996).

8.4.1 Suction Equilibrium under Loading

When an unsaturated specimen compresses under constant mass conditions, the air phase of the pore voids decreases and saturation increases. Both microstructures and macrostructures are compressed. Suctions are therefore decreased. Figure 8.19 shows changes of total suction with time obtained from the test on the 'as compacted' specimen T16533 (w : 19.5%, S_r : 84%, γ_d : 1.66 Mg/m³). Data in the figure illustrate suction changes in five stages. 1) Approaching a steady value with small fluctuations in ab reflects suction equilibrium in the new environment after installation of the specimen. The selected start suction is given at point b . 2) Significant deductions of suctions occur in the stage of bc where the specimen was loaded in isotropic compression with a succession of load increments. 3) Recovery of the suctions from point c to point d is attributable to partial unloading to an apparent OCR of 2.0. 4) Following changes in suctions during de are not remarkable and they are caused at shearing with $\Delta p/\Delta q = -1/3$. 5) Suctions at point f and beyond are values after the specimen failed and all loadings were released. It is interesting to note that the final suction was close to the start suction. During the test, total suctions changed in response to the external loads (or unloadings) which were implemented by applying axial load and confining pressure incrementally. Each increment was held constant until deformation was complete. Suction changes were associated with deformation of the specimens which were compressed or sheared under constant mass conditions. Figure 8.20 shows equilibration of suctions changing under two mean stress increments. Curve 123 in the figure represents suctions changing in

response to an increase in mean stress p of 250 kPa from 250 kPa to 500 kPa. For the increase of 250 kPa, it took less than 5 hours to reach equilibrium. Curve 1'2'3' is for an increase in mean stress p of 750 kPa from 2250 kPa to 3000 kPa. This took about 40 hours for equilibration. Some of this equilibration is due to sample compression and the remainder to instrumentation effects which are known to be small (Tang 1996).

8.4.2 Suction Response to Stresses and Suction Reversibility

8.4.2.1 Suction changes under isotropic compression

Data for the suctions shown in Figure 8.19 are replotted in Figure 8.21 which relates suctions to applied stresses. Once again, the segment bc illustrates how suctions respond to isotropic compression stresses. At the beginning of loading at point b, the start suction was 4.2 MPa. Addition of confining pressures up to 3000 kPa caused significant reductions of suction to approximately 1.5 MPa, as a result of compression of the air phase and increasing saturation. The segment cd indicates the recovery of suctions during unloading. (Complete unloading would return the suction almost to its initial value (Tang *et al.* 1998a). As reported earlier, similar observation was also made on the specimens of elevated osmotic suctions. Total suctions of these specimens were measured before and after quick undrained triaxial tests and results showed that suctions remained unchanged after specimens experienced large plastic deformations.) The data in Figure 8.21 show largely recoverable behavior of suction during shearing with $\Delta p/\Delta q = -1/3$, suggesting the applicability of the elastic-plastic model for unsaturated soils.

Decreases in mean stress p and increases in deviator stress q during shearing along de allowed further recovery of suctions. However, it needs to be determined whether these changes are caused by decreases in mean stress or through the combination of mean stress and deviator stress in the applied stress tensor.

8.4.2.2 Suction changes at shearing with constant mean stress

The question arises whether shear stress alone can affect suction. It is easy to envision ΔS changing with Δp , but less easy to understand it changing with Δq . Figure 8.22 presents data in p - S space from the 'after drying' specimen T16541 ($w = 18.35\%$, $S_r = 80\%$, $\gamma_d = 1.67 \text{ Mg/m}^3$) that was sheared incrementally using $\Delta\sigma_1 = -0.5\Delta\sigma_3$, so that $\Delta p = 0$. The specimen was sheared starting at point C as shown in the figure. The deviator stress q was increased while the mean stress p was held constant at point C. According to the figure, shearing produced essentially no change in suction which remained at point C. Data from two strain-controlled triaxial compression tests performed by the author on unsaturated specimens with different initial conditions ($w = 18.3\%$, $S_r = 75\%$, $\gamma_d = 1.67 \text{ Mg/m}^3$) also show that suctions remain unchanged during shearing under the condition of constant mean stress. These important results were reported by the author and Graham (Graham *et al.* 1995) and are therefore not presented here.

8.4.2.3 Suction changes at general stress paths in p - q - S space

In this testing program, various stress paths were selected at desired values of $\Delta p/\Delta q$ as

shown in Figure 8.10. Together with the measured values of suctions for each stress state of p and q , this allows stress paths to be drawn in p - q - S space. The stress paths in p - q - S space therefore illustrate how suction relates to mean stress p and deviator stress q in these 'constant-mass' tests. Figure 8.23 shows how total suction S responds to applied stresses p and q during (1) isotropic compression ($q = 0$ and $p = \sigma_1 = \sigma_2 = \sigma_3$) and (2) shearing ($\Delta p/\Delta q = 1$) for the 'as compacted' specimen T16534. The stress path $AO'gO'a$ comes from applied values of p and q , and measured values of S . The three phases of the test are compression along $AO'g$, unloading along gO' , and shearing along $O'a$. During compression, suction S decreases with increasing confining pressure (and hence mean stress p). The resulting paths in the p - S plane appear to be approximately straight (see for example, Figure 8.4). When data along the shearing path $O'a$ are projected on to the p - S plane, the projection falls on the compression line $O'g$. The ends of the vertical lines in Figure 8.23 represent the p , S coordinates of the p , q , S states during shearing. This implies that for the same change of mean stress, suction changes induced by isotropic compression are equal to those induced by changes in mean stress p in the shearing phase. A similar result was obtained from all the different stress paths in Figure 8.10, shown as dotted lines in Figure 8.23. It can therefore be concluded that suction varies only with the isotropic component of the stress tensor (the mean stress p) and is independent of the shear component (the deviator stress q). This is believed to be the first occasion where this relationship has been shown explicitly.

8.4.2.4 Relations between suction, mean stress and deviator stress

A suction - mean stress relationship can therefore be established regardless of deviator stress, at least for a given start suction. In the range shown earlier in Figure 8.5, decreases in suction are largely proportional to the increase in mean stress. This can be expressed as:

$$\Delta p = -v\Delta S \quad [8.3]$$

where v is the slope of suction *versus* mean stress in $p - S$ space.

According to the data of mean stress p and corresponding suction S in Figure 8.5, values of $v = -\Delta p/\Delta S$ for the first series of specimens at low start suction $S = 4.2$ MPa averaged 1.2. From the specimens of second series at high suction level starting from $S = 6$ MPa the average v was also 1.2, indicating that two series of specimen had the same microstructure. The value of $v = 1.2$ can therefore be used to predict suction changes of these specimens at given stress states (p, q) under constant mass compression and shearing.

8.5 Final Evaluation of the Specimens after Tests

After the tests were completed, the specimens were carefully removed from the triaxial cell for final evaluation of their mass and deformation. Table 8.4 shows the data of water contents before the specimens were installed and after the tests were finished. According

to the table. limited water contents were lost during the entire process of tests, averaging 0.67% and 0.36% for the ‘as compacted’ specimens and ‘after drying’ specimens respectively. The slight loss of water content indicates that some drying occurred and explains why the suctions of the specimens measured after triaxial tests were a little higher than the start suctions before testing. (For example, slight increase in total suction was observed in the specimen T16533 as shown in Figure 8.19) The mechanism by which the moisture was lost is not clear but is likely to have occurred during installation or removal of the specimens from the test cell. Similar differences have been found in research with saturated buffer, for example Yarechewski (1993) and Lingnau (1993).

Table 8.4: Comparison of water content change before and after triaxial tests

Specimens		Water content (%)		
		Before test	After test	Change(Δ)
‘Compacted’	T16530	19.60	-	-
	T16531	19.35	18.88	-0.47
	T16533	19.54	18.71	-0.83
	T16534	19.65	19.11	-0.54
	T16535	19.76	18.94	-0.82
‘After drying’	T16540	18.34	18.84	-0.50
	T16541	18.35	18.00	-0.35
	T16542	18.41	18.20	-0.21

8.6 Interpretation of Tests Results Using the Existing Conceptual Model for Unsaturated Soils

As introduced in Chapter 2 – Literature Review, it is now generally accepted that total stress σ , pore air pressure u_a and pore water pressure u_w must be combined into two

independent stress variables in order to describe the mechanical behavior of unsaturated soils (Fredlund and Morgenstern 1977). The commonly used two stress variables are net mean stress and matric suction. Many previous researchers have related the volume change behavior or the shear strength of unsaturated soils to these two stress variables. Volume change and shear strength were treated separately for unsaturated soils in this way. In the past decade, a critical state conceptual model has been developed in more general terms for unsaturated soils based on the philosophy of the Modified Cam Clay model. The developed conceptual model has been used to account for the effects of suction on stress-strain behavior of unsaturated soils (Alonso *et al.* 1990, Delage and Graham 1995).

In this thesis, a broad range of the stress-strain behavior and strength properties of unsaturated buffer material has been examined under drying and wetting, tension, isotropic compression, and shearing. Results have been presented in this chapter and previous chapters. It would be significant if the different aspects of the interrelated behavior of unsaturated sand-bentonite observed under different testing conditions can be synthesized in a generalized model instead of simply a description of a series of isolated and independent relationships. For this reason, the existing critical state conceptual model for unsaturated soils was adopted to interpret the behavior observed and presented in this chapter. Following sections describe an attempt to apply the concepts of the model to the test data.

8.6.1 The Existing Critical State Model for Unsaturated Soils

The existing critical state model has been introduced earlier in Chapter 2 – Literature review, it is outlined below again to help understand its application to testing results.

Yielding locus in p-S space Figure 8.24 shows an initial yield curve $a_1b_1c_1O_1$ in p-S stress space for initial unsaturated specimens subject to isotropic compression or to increases in suctions (Alonso *et al.* 1990, Delage and Graham 1995). Specimens behave elastically within the curve. When plastic straining occurs, the paths at different constant suction levels (such as S_1 and S_2 in the figure) will take the coupled load suction yield curve (LSY) to another position $a_2c_2O_2$ and enlarge the elastic zone. The line O_1O_2 in the figure represents yield under tensile loading.

State boundary surface in p-q-S space and yield envelopes at constant suctions Figure 8.25 shows a graphical, three-dimensional representation of the model for any stress path in p-q-S space. For states that lie inside the state boundary surface the soil behavior is elastic, with movement over the state boundary surface corresponding to expansion of a yield surface in stress space. For soil initially at a stress state O' . With constant suction, yield can be produced by an increase of p (isotropic loading path $O'bc$), an increase of q (shearing path $O'de$), or by any combination of p, q (path $O'fg$). The yield envelope $AO'bfd$ is at a constant suction plane. This could happen at any constant suction plane and the size of such an envelope increases with increasing suction. For simplicity and modelling purposes,

therefore, the state boundary surface is usually viewed as a family of yield envelopes at constant suction planes. This can be seen in Figure 8.26b. In order to differentiate yielding induced by isotropic loading and by shearing, yield curves in p-S space and in q-p space will be termed 'yield locus' and 'yield envelope' respectively in this thesis.

Failure and critical state line With the state boundary surface and critical state lines identified, the failure states can be specified. In Figure 8.26b, a Critical State Line (CSL) with slope M_0 for the saturated specimen with $S = 0$ is directly related to the c, ϕ failure envelope of the materials. With increases in suctions, strength increases. The elliptical yield envelope for unsaturated specimens defined by $CSL(S_1)$ and $CSL(S_2)$ have CSLs associated with suctions S_1 and S_2 ; tensile strengths O_1 and O_2 ; and preconsolidation pressures b_1 and c_1 as shown in the figure. The new CSL lines represent the increased resistance of the material due to suction. As a hypothesis, the effect of suction will be represented by an increase in cohesion, maintaining the slope M of the CSL for saturated conditions (Alonso *et al.* 1990, Wheeler and Sivakumar 1993). The CSLs of unsaturated specimens at any constant suctions are therefore parallel.

8.6.2 Interpretation of Stress-strain Behavior and Strength Properties of Unsaturated Buffer Material

Since the state boundary surface in p-q-S space can be viewed as a family of yield envelopes in p-q space at a series of constant suction planes, the model provides a

convenient presentation of experimental results of tests which are conducted at a series of constant suctions. This is because test data with any constant suction lie in a constant-suction plane in p - q space. In this study however, stress paths in each of the test series were not in such a constant-suction plane (Figures 8.4, 8.21, 8.23). Stress paths in each of the test series are actually in a plane such $AO'gabcd$ as illustrated in Figure 8.27 in which the suctions are changing with the addition of the applied stress increments of p and q .

Schematically, for each series a specimen starts at an initial state A on the axis of suction S in the figure. Under isotropic compression, the mean stress p increases and suction S decreases until the stress state reaches point I on its current yield curve YIL . There, initial yielding occurs. (YIL is the initial yield locus in p - S space for isotropic loading.) With further increases of mean stress p to point g in the figure, the yield locus expands to $Y'gI'L'$. Following decreases in mean stress p to point O' , the specimen becomes overconsolidated. The selected stress paths $\Delta p/\Delta q = 1, 1/3, 0,$ and $-1/3$ correspond to stress paths $O'a, O'b, O'c,$ and $O'd$ respectively in p - q - S space. If the specimen experiences stress changes at constant suction, its range of elastic-plastic behavior can be described by a constant-suction trace on the boundary surface, that is, the section $DO'I'c$.

8.6.2.1 Yield stress in p - S space

Yield stresses under isotropic compression are shown in Figures 8.5 and 8.17. Figure 8.5 shows data of the yield stresses and current suctions at points O_1' and O_2' for series 1 and

series 2 respectively. Two curves $A_1O_1'g_1$ and $A_2O_2'g_2$ in the figure represent suction changes with mean stress. Line II' through O_1' and O_2' represents an approximate initial yield locus LSY in p - S space. Increasing pressures after O_1' and O_2' produce volumetric plastic hardening and cause the yield stresses to increase to g_1 and g_2 respectively, giving different LSY curves $g_1g'_1$ or $g_2g'_2$ respectively.

8.6.2.2 Elastic-plastic behavior under shearing

Elastic-plastic features and failures in saturated soils along various stress paths can be well interpreted using critical state models. Recollection of such a model would help understand better the following discussion on unsaturated soil behavior. This can be typically illustrated in Figure 8.28 which shows an elliptical yield envelope and a straight critical state failure envelope as well as a group of three typical stress paths. Stress path #1 is such that yielding will be observed at stress 1Y, but the specimen will not fail since the stress path does not intersect the failure envelope. A specimen following a stress path such as #2 will yield at 2Y and then, with further stressing, move to failure at 2F. For both of these stress paths, post-yield stressing will involve plastic straining. A specimen that follows a stress path such as #3 will yield and simultaneously fail at stress 3Y, 3F. Then, because the yield surface lies above the failure envelope, it will strain soften to reach critical state failure at 3CS.

Strain hardening In order to understand the influence of suction on the observed strain hardening from T16534 in Figure 8.11, Figure 8.29 illustrates how a state boundary surface evolves for an unsaturated specimen experiencing shearing along the stress path $\Delta p/\Delta q = 1$, namely the stress path O'a shown in Figure 8.27. As mentioned earlier, a specimen is consolidated from point A to point g, its elastic-plastic behavior can be described by a yield curve BgB' in p-S space and by a state boundary surface which can be schematically represented by a series of constant suction planes such as S1, S2, S3 and S4 as shown in Figure 8.29. After hardening to point g, the stress decreases to point O' to achieve an apparent OCR = 2 (with suction surface S3), at which stage shearing is begun following stress path O'aa₁a₂. For any stresses p and q on the line O'a, the specimen behaves elastically since the stresses lie within the state boundary surface. During this stage from O' to a, volume changes will be small but finite and will produce some changes in suction. The p-q-S states therefore move off the initial suction plane S3. At point a, the stress path reaches the already formed surface S2 (S2 is smaller than S3). Further stresses cause plastic straining to begin. From point a to a₁, increasing mean stress p will make S2 expand due to strain hardening, but meanwhile decreasing suction will make S2 shrink. This coupled effect will form a new surface S5 going through point a₁. This process continues through successive yield envelope until finally the stress path reaches failure at a₂ on the critical state failure state for surface S6. This discussion follows ideas proposed by Delage and Graham (1995) and Wan (1996).

Strain softening For a specimen such as the specimen T16533 sheared along the stress path O'd as illustrated in Figure 8.27, the elastic-plastic behavior can be interpreted in terms of stress states relevant to the state boundary surface in Figure 8.30. When the specimen is compressed to point g, the boundary surface with constant planes S1, S3 and S4 is formed and the yield curve in p-S space is BgB'. Then the confining stress decreases to point O' to achieve an apparent OCR = 2 (with its corresponding boundary surface S3), and shearing is begun along O'd. In order to follow the stress path, increasing deviator stresses requires decreasing mean stresses, and therefore increasing suctions (from S3 to S7). As shown in the figure, at point d on the stress path, the current suction corresponds to the already formed surface S7, but deviator stress at d is still within the state boundary surface due to surfaces such as S3, S7, S8, and S4 becoming larger with increasing suctions. Therefore the specimen still behaves elastically. Further shearing from point d to point d_f will lead to rupture since point d_f is a failure state which is above the critical state line CSL for surface S8. If the test was run under strain-controlled conditions, dilation would occur and some plastic hardening would have to be included in the model with corresponding increases in S.

8.6.2.3 Shear strength

The qualitative illustration described above appears to indicate the existing model is able to describe strain hardening, strain softening and failure for unsaturated soils. Questions, however, arise immediately when experimental data are examined quantitatively.

A two dimensional view in q-p space of evolution of the stress state surface in p-q-S space provides a better picture of shear strength relevant to stress-strain behavior. Figure 8.31 shows in a p-q diagram the stress path $O'aa_1a_2$ from the three dimensional view presented in Figure 8.29 for a strain hardening specimen such as T16534 in Figure 8.11. The solid curves S1, S2, S3 and S4 are yield envelopes of constant suction traces in a common stress state boundary surface. The sizes of yield envelopes are governed by the tensile yield curve, preconsolidation pressure and the slope of critical state lines. Critical state lines CSL_2 and CSL_3 are shown in the figure for yield envelopes S2 and S3 respectively. The critical state lines are parallel but increase in q with suction since suction gives rise to higher cohesion. It is assumed that the friction angle remains constant. During shear, strain hardening enlarges the yield envelopes to S5 and S6 and lowers the critical state lines to CSL_5 and CSL_6 due to decrease in suction. Shear strength at critical state at a_2 can be therefore identified as $q_{max} = q_1$ for the specimen following stress path $\Delta p/\Delta q = 1$.

For comparison, the yield envelopes in Figure 8.31 are again shown in Figure 8.32, this time with additional yield envelopes and stress paths related to specimen T16533 ($\Delta p/\Delta q = -1/3$) in Figure 8.11. As demonstrated earlier for strain softening behavior, specimen T16533 behaves elastically until it fails at point d_1 on yield envelope S8. Maximum deviator stress is identified as $q_{max} = q_2$. During shearing, mean stress decreased and suction increased. The specimen gained strength from increase in suction and this is reflected by the enlargement of the yield envelope S3 to S7 and to S8. However, the

increase of envelope size is predominantly governed by the slope of CSL. Although tensile yield stresses increase with increasing suction, it contributes limited magnitude on enlargement of yield envelopes (Tang and Graham 1998, see also Figure 7.14). As such, the model suggests specimen T16533 has much lower strength q_2 than specimen T16541 (maximum deviator stress q_1). The observation that specimens had very close strengths is not explained using the existing model.

Strength properties can be represented by a parameter M which is the slope of the critical line for a saturated soil. Assuming critical state lines of unsaturated soils at any constant suctions are parallel to this line, the M value at any suctions is given:

$$M = \frac{q}{p} \text{ at critical state} \quad [8.4]$$

Table 8.5 shows values of M for the tested unsaturated specimens. Data are plotted in Figure 8.33 showing that M increases significantly with increasing suction. It can be as high as 1.53 at $S = 4.3$ MPa. The M -values of specimens which failed at different suctions are all higher than that of saturated specimens which was 0.53 as reported by Graham *et al.* (1989). The highest M value of 1.53 corresponds to a friction angle of 38° . This friction angle is obviously much too high for a highly plastic clay. This observation indicates that the existing conceptual model which interprets data at series of constant suction planes cannot be used to explain the observed mechanical behavior of unsaturated soils.

Table 8.5: Stress at failure and M values

Test ($\Delta p/\Delta q$)	T16530 (1/3)	T16531 (0)	T16533 (-1/3)	T16534 (1)	T16535 (0)	T16540 (-1/3)	T16541 (0)	T16542 (1)
q_f (kPa)	1374	1390	1291	1250	1250	1519	1601	1634
p_f (kPa)	1959	1500	1070	2750	1000	994	1500	3134
S_f (MPa)	2.40*	2.76	3.00	1.79	3.10	4.30	4.00	2.10
ϕ' (°)	18.3	23.7	30.2	12.1	31.1	37.6	27.0	13.8
M	0.70	0.93	1.21	0.45	1.25	1.53	1.07	0.52

where: $\sin(\phi') = 3M/(6+M)$

$$M = q_f/p_f$$

* Due to failed measurement at this point, suction value is inferred using expression [8.3].

8.7 Summary

Eight stress-controlled triaxial compression tests were conducted on unsaturated sand-bentonite specimens at two start suction levels. Suctions, vertical and lateral displacements of the specimens were measured during compression and the following shearing phase. The stress-strain behavior and suction change characteristics of unsaturated sand-bentonite can be summarized as follows:

- 1) Suctions measured using psychrometers incorporated into the triaxial cell are repeatable during compression and comparable during shearing for all eight tested specimens. This indicates that the proposed technique for installing psychrometers works well.

- 2) Under constant mass conditions, total suction in an initially unsaturated specimen tends to decrease with increasing total stress. Decreases in suction are largely proportional to the increases in mean stress. Total suction recovers after release of loading, that is, total suctions remain largely unchanged after specimens experience deformation, even large plastic deformation.
- 3) Suctions vary only in response to changes in the mean stress component of the stress tensor and not to changes in the deviator stress component.
- 4) Unsaturated sand-bentonite exhibits yielding behavior that can be characterized by elastic-plastic modeling. Yielding is observed in both isotropic compression and shearing.
- 5) Based on the test results of the specimens at two start suction levels, stress-strain behavior and shear strength are strongly affected by start suctions and current suctions.

The summarized soil behavior provides experimental evidence to support only some aspects of the existing conceptual model. Yield data of isotropic compression tests prove the existence of yield locus in p - S space (Alonso *et al.* 1990). The data for volume change appear to support the general form of volumetric constitutive behavior in V - p - S space proposed by Delage and Graham (1995). An improved model is needed if all the observations are to be included.

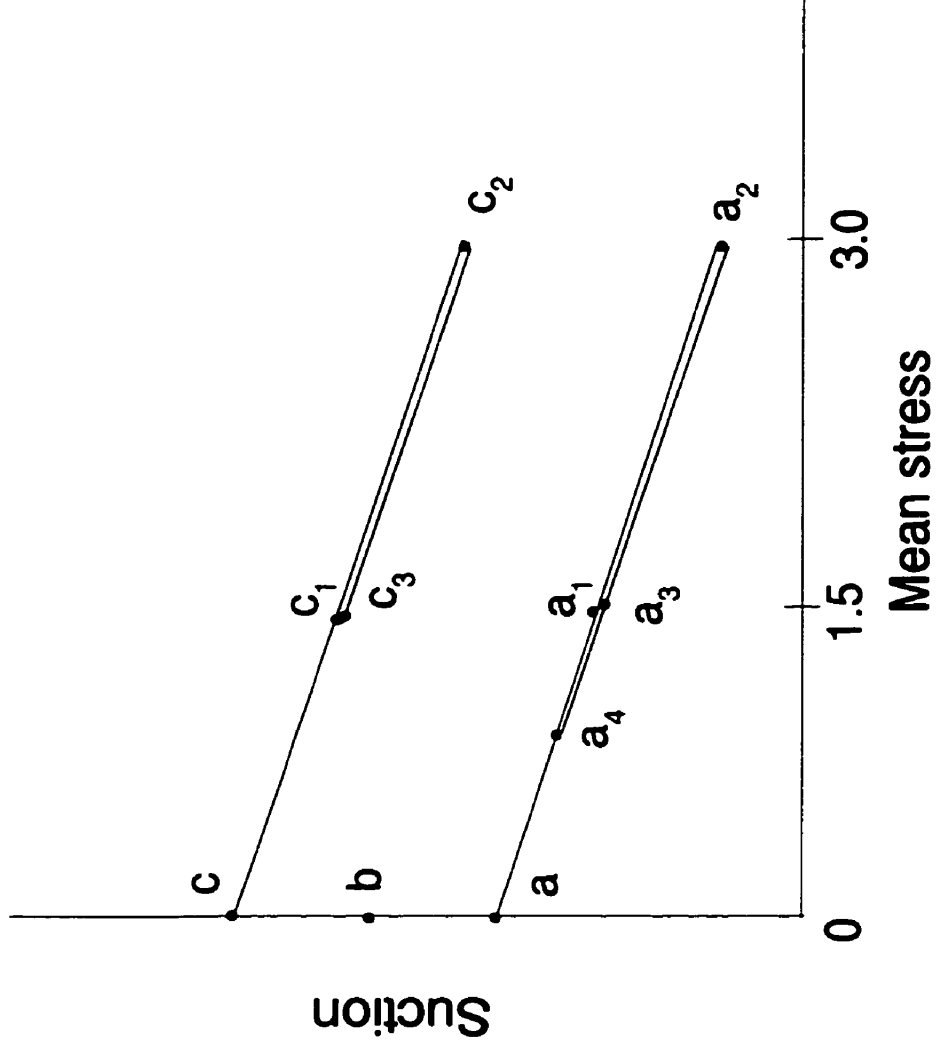


Figure 8.1 Stress paths for isotropic loading in p-S space

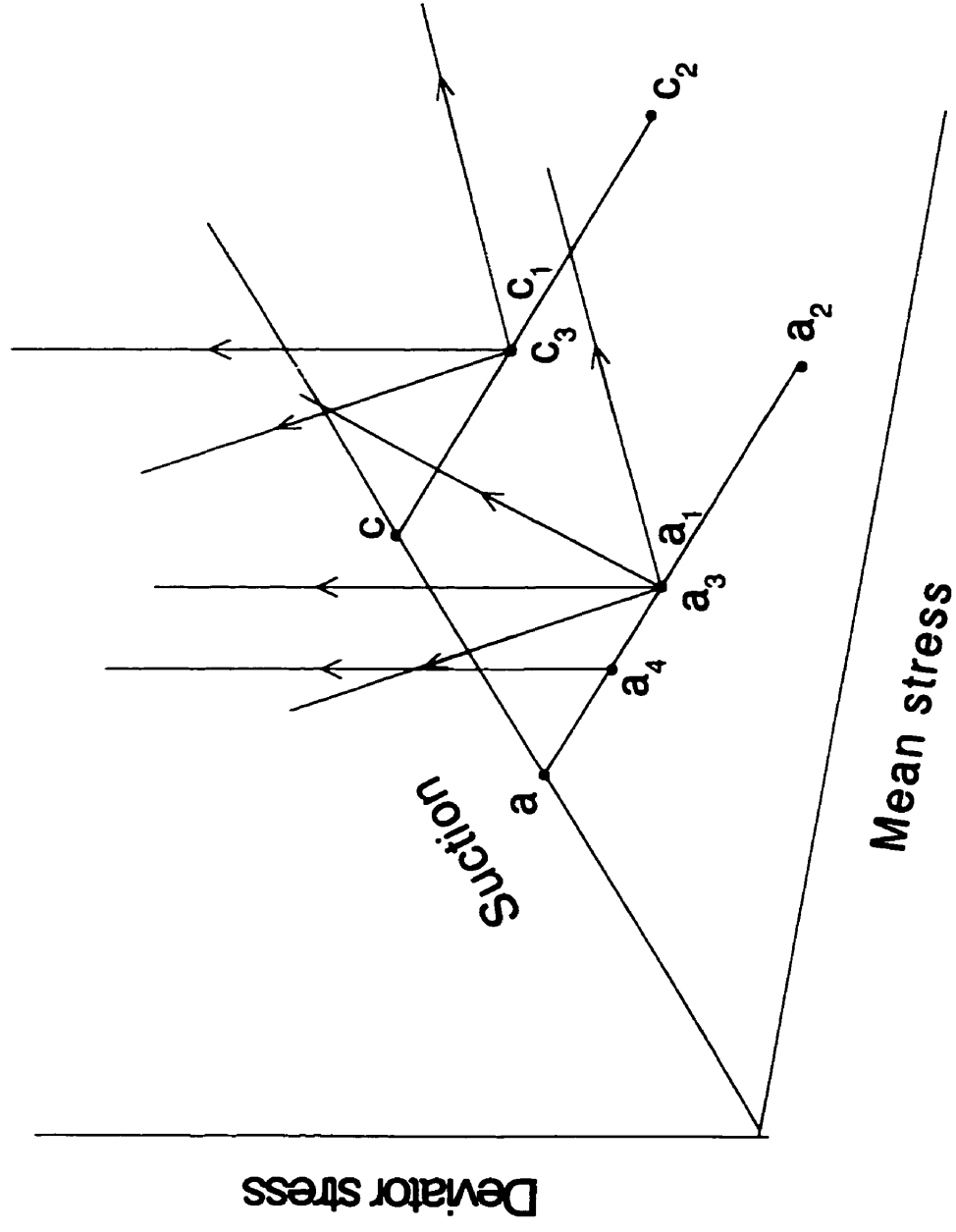


Figure 8.2 Selected stress paths for shearing
at apparent OCR = 2 or 3

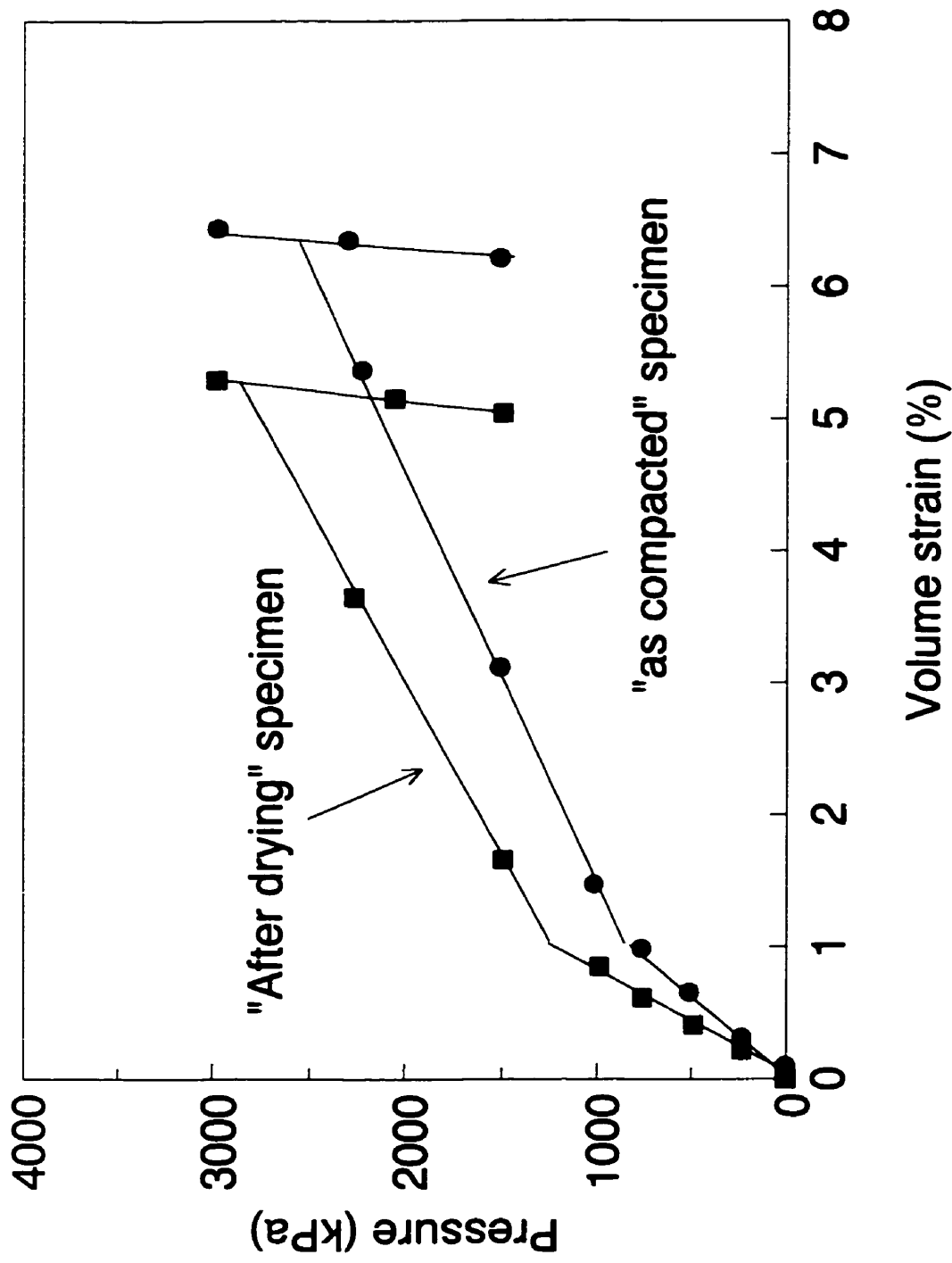


Figure 8.3 Typical consolidation curves (T16533/T16540)

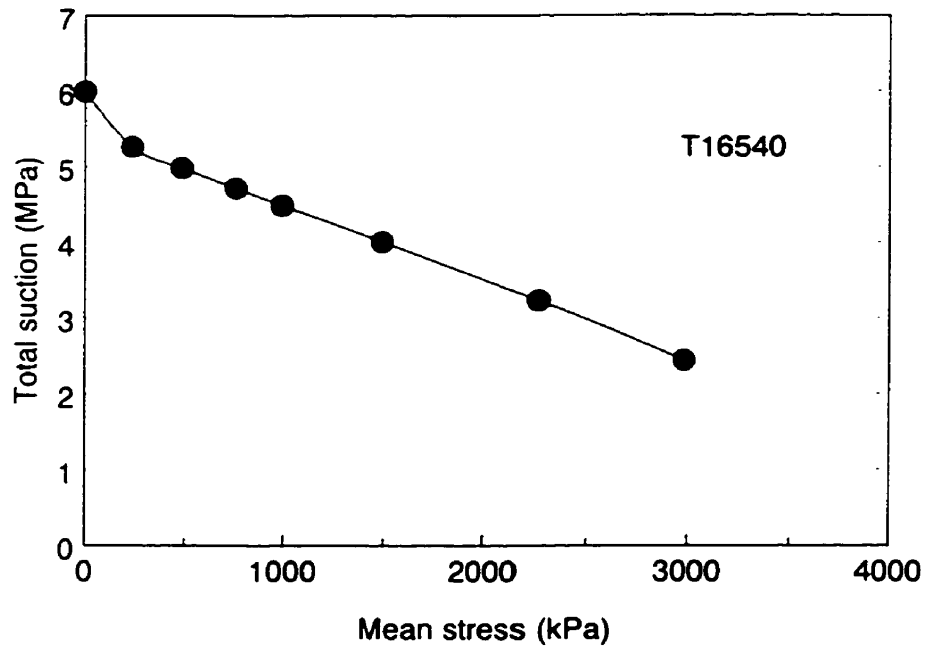
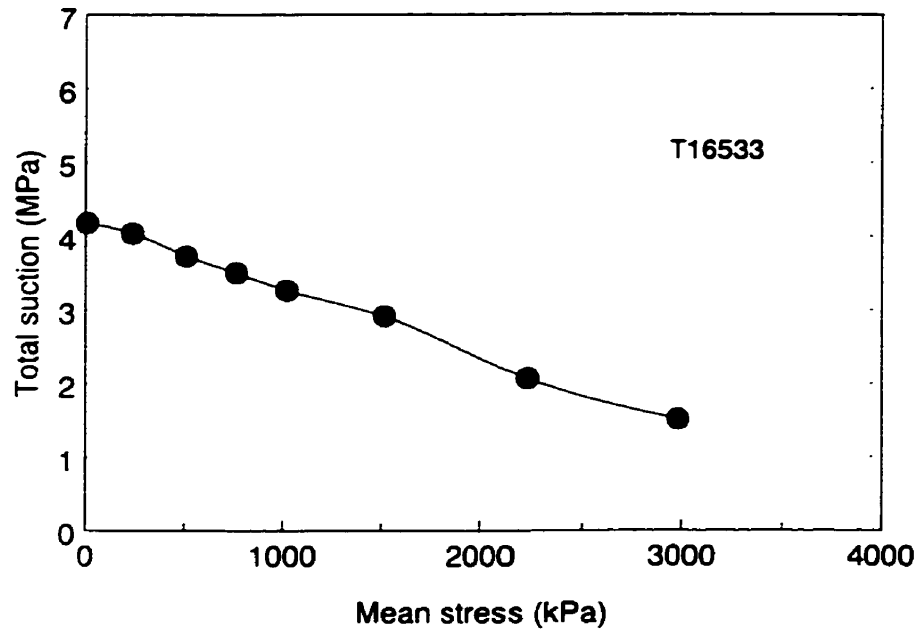


Figure 8.4 Suction changes under isotropic compression

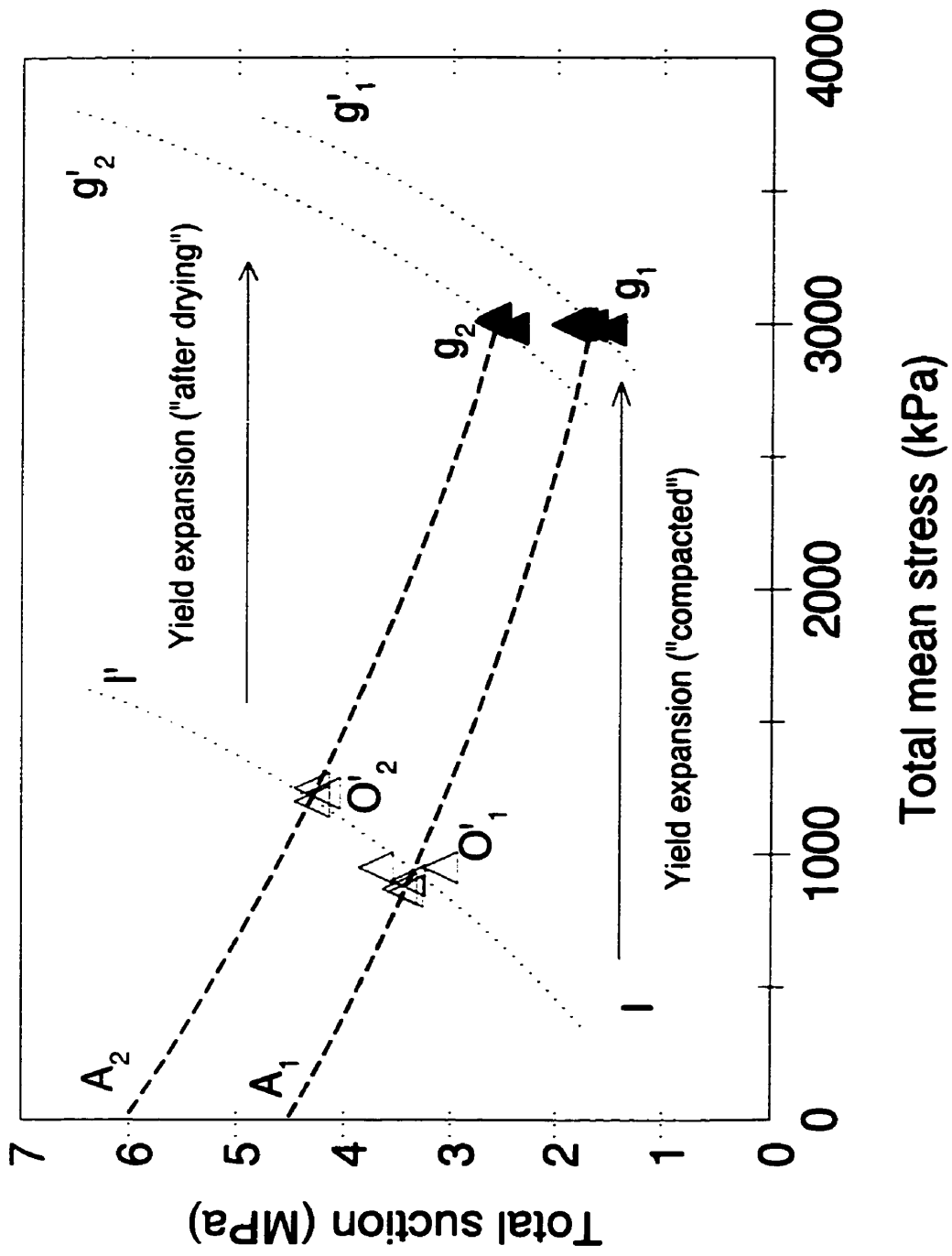


Figure 8.5 Expansion of yield locus in p-S space

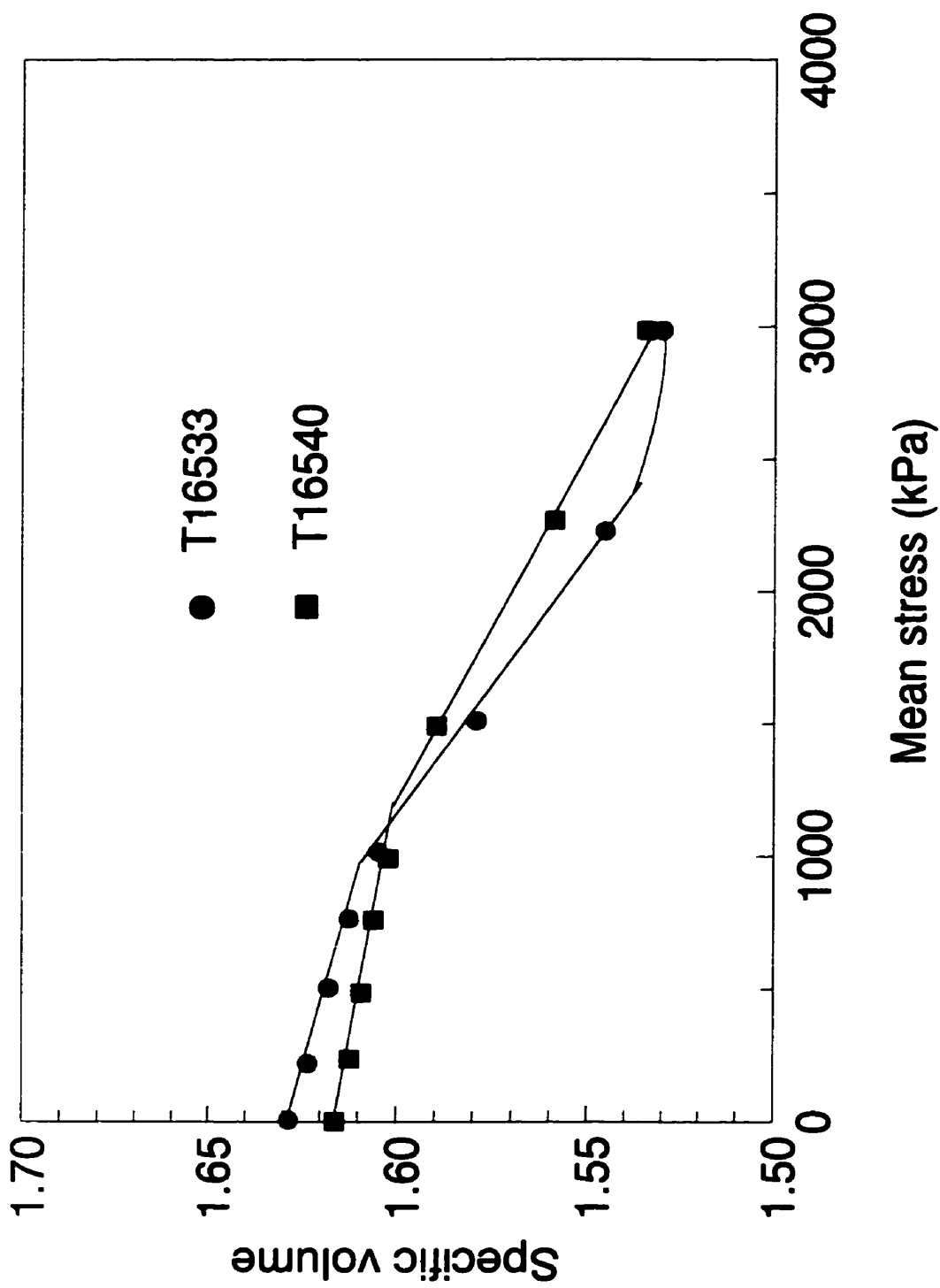


Figure 8.6 Specific volume versus mean stress

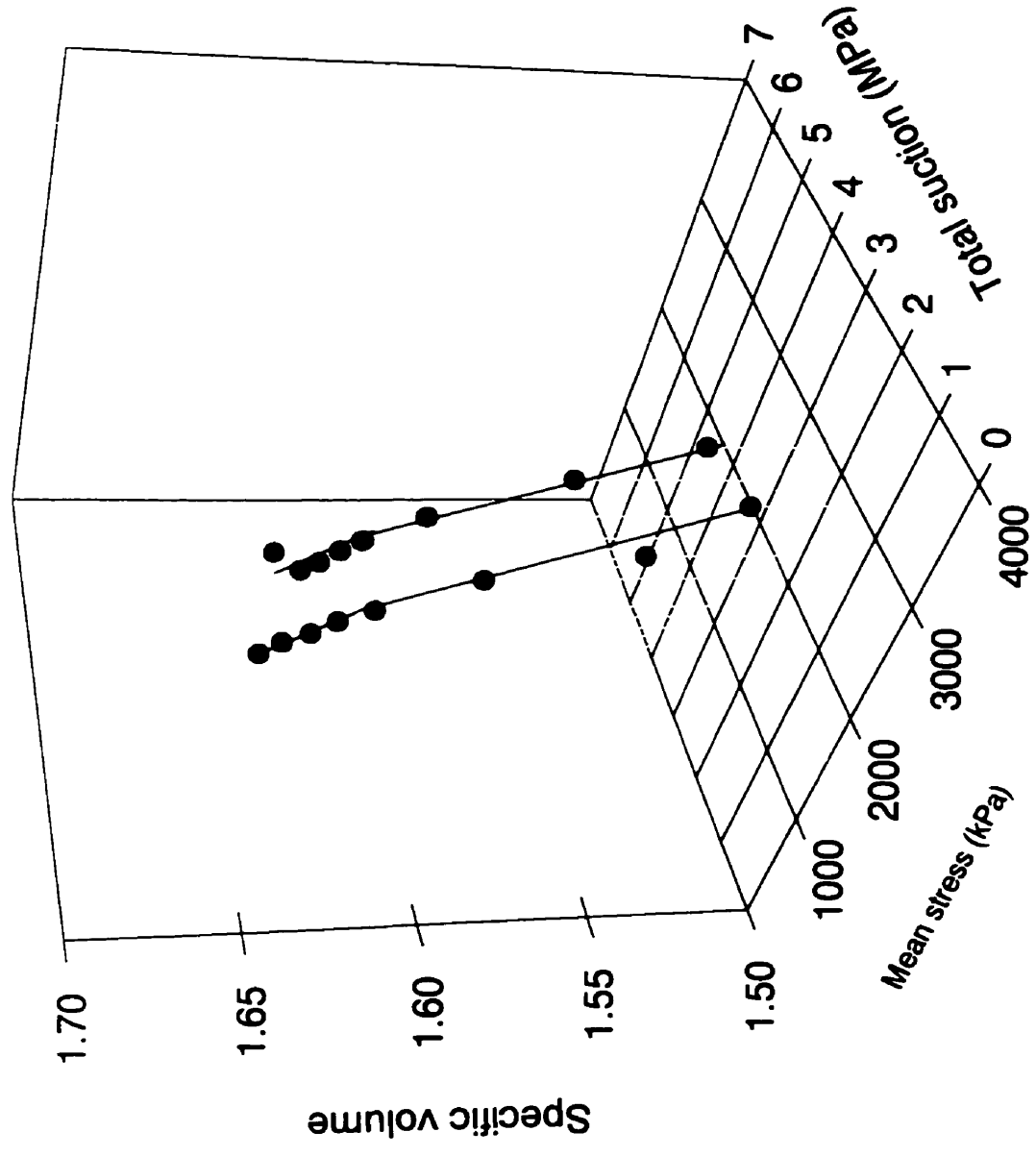


Figure 8.7 Volume change with mean stress and total suction

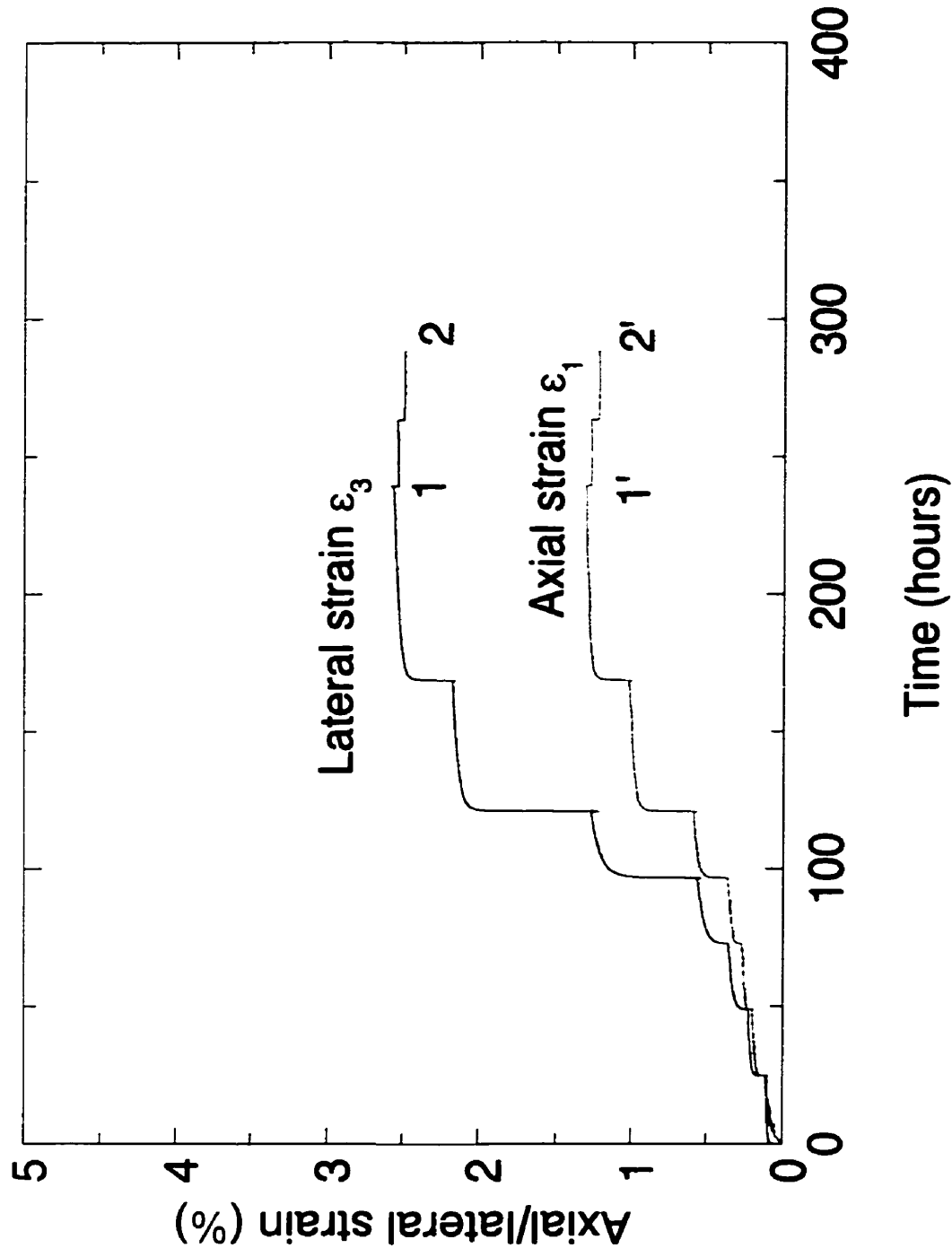


Figure 8.8 Axial strain ϵ_1 and lateral strain ϵ_3 with time (T16533)

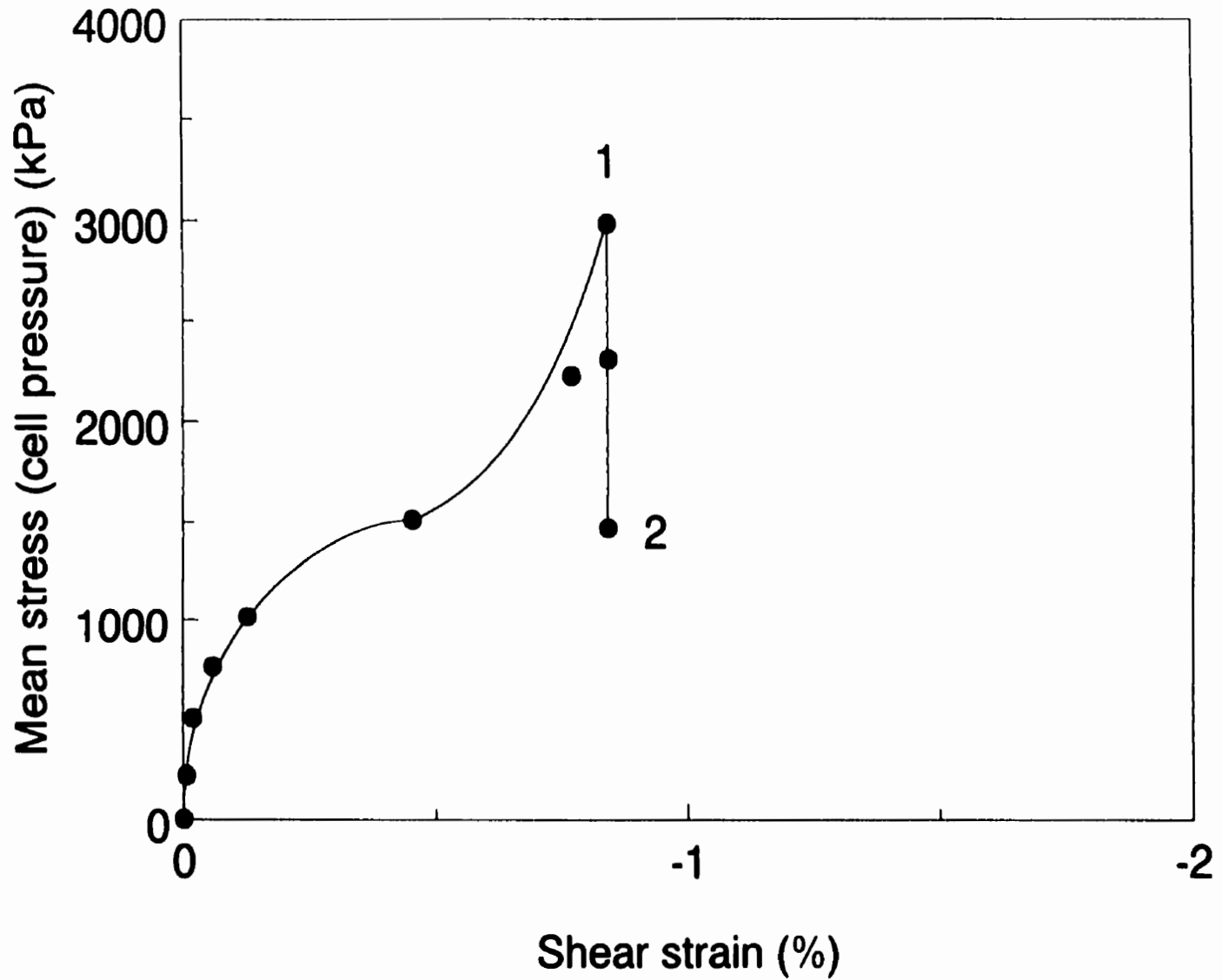


Figure 8.9 Shear strain under isotropic compression (T16533)

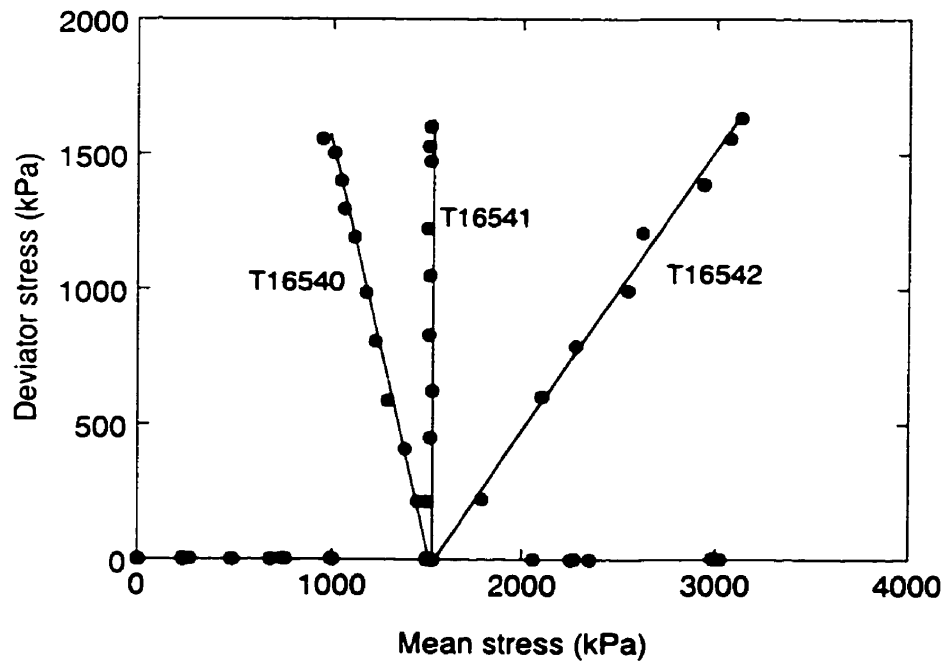
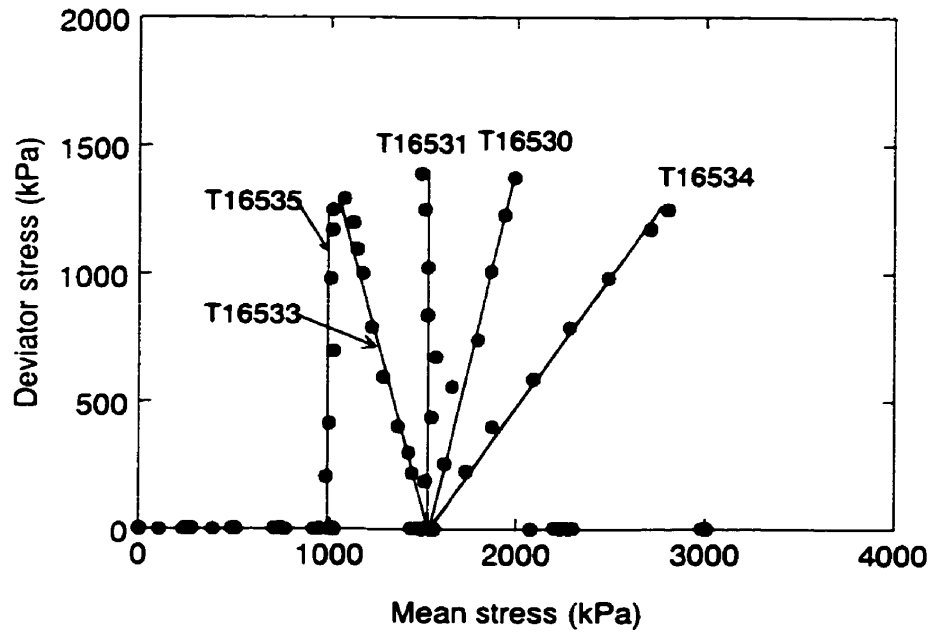


Figure 8.10 Stress paths at shearing for specimens at two start suction levels.

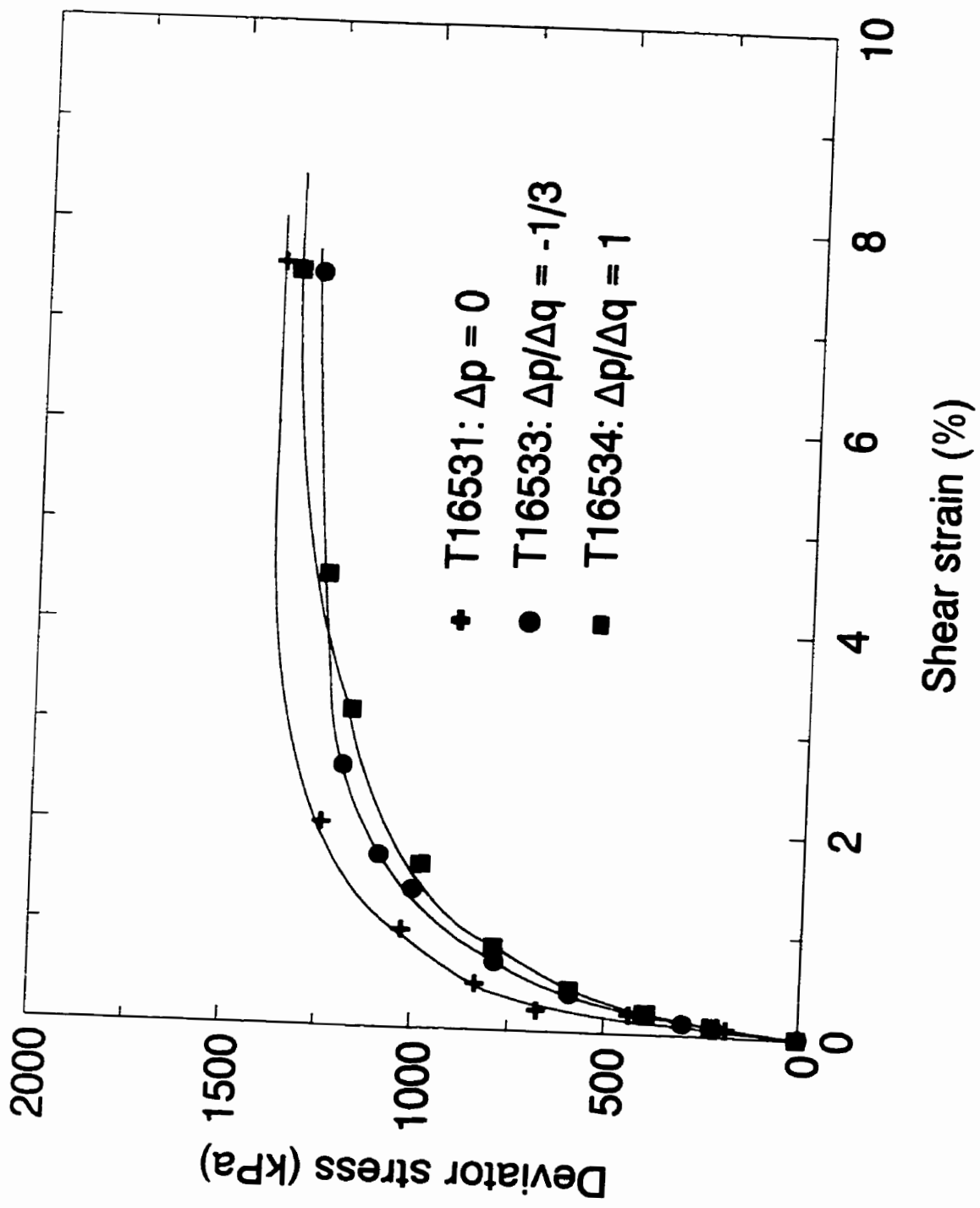


Figure 8.11 Deviator stress versus shear strain

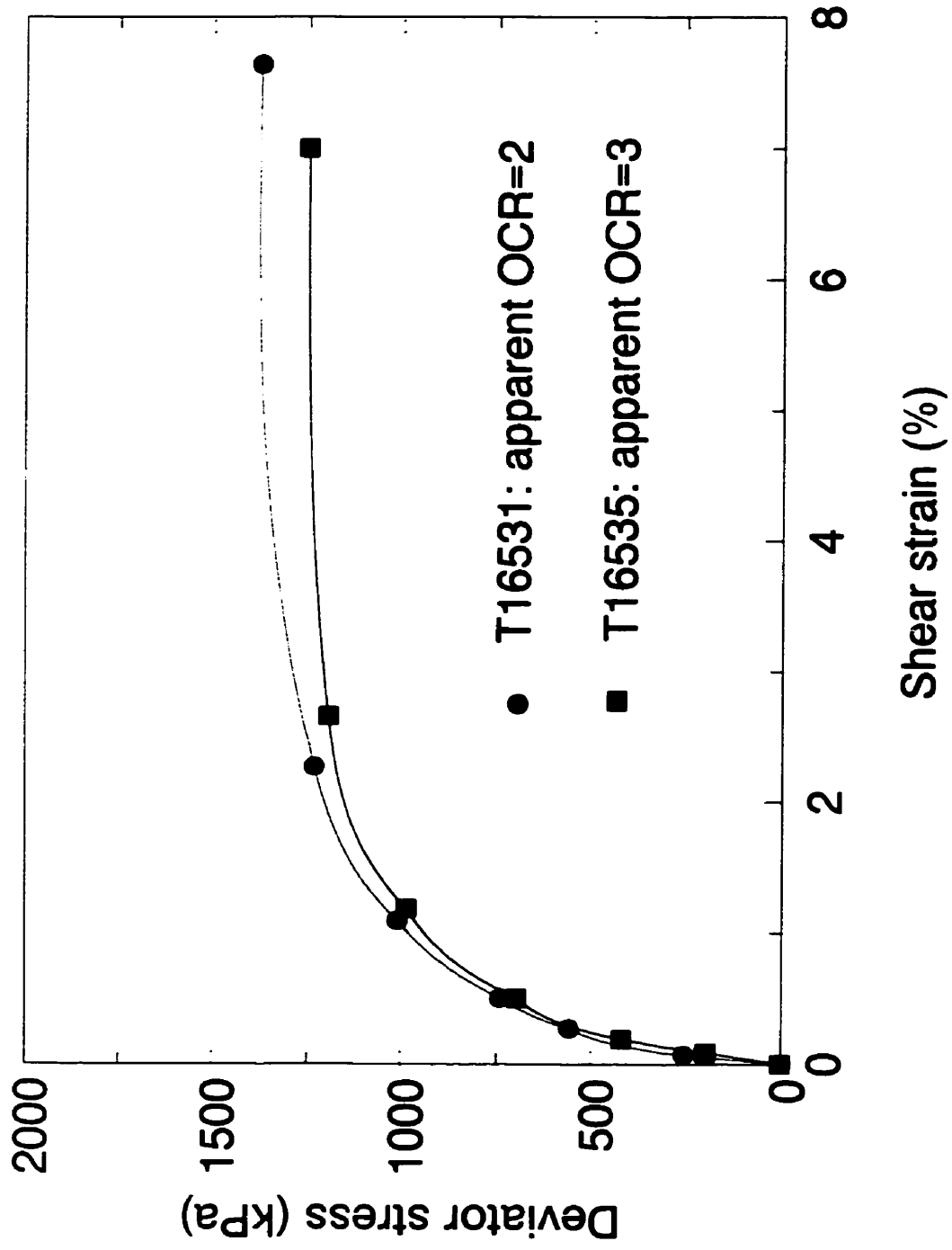


Figure 8.12 Stress-strain behavior for specimens sheared at apparent OCR=2 and 3

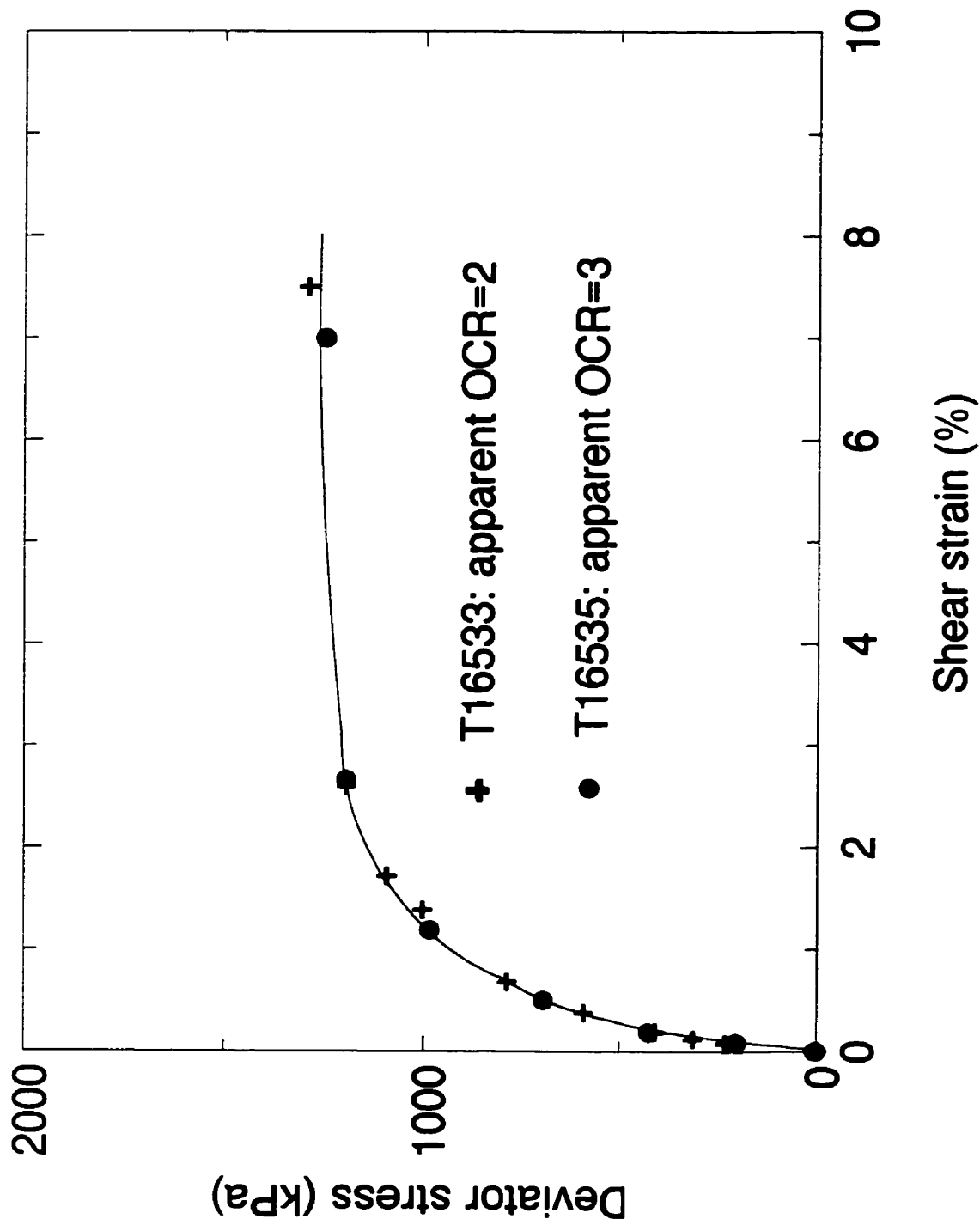


Figure 8.13 Deviator stress versus shear strain

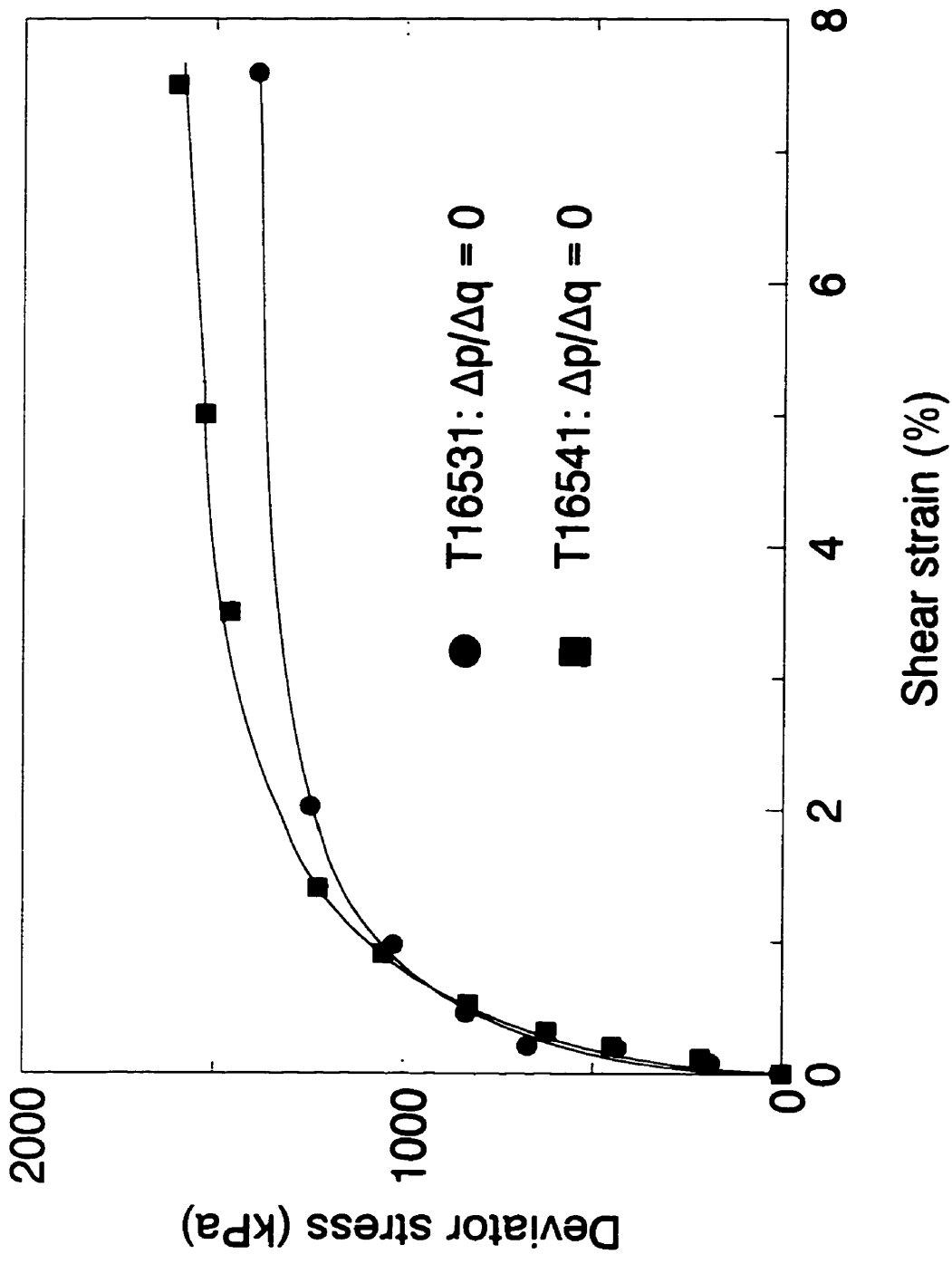


Figure 8.14 Deviator stress vs. shear strain

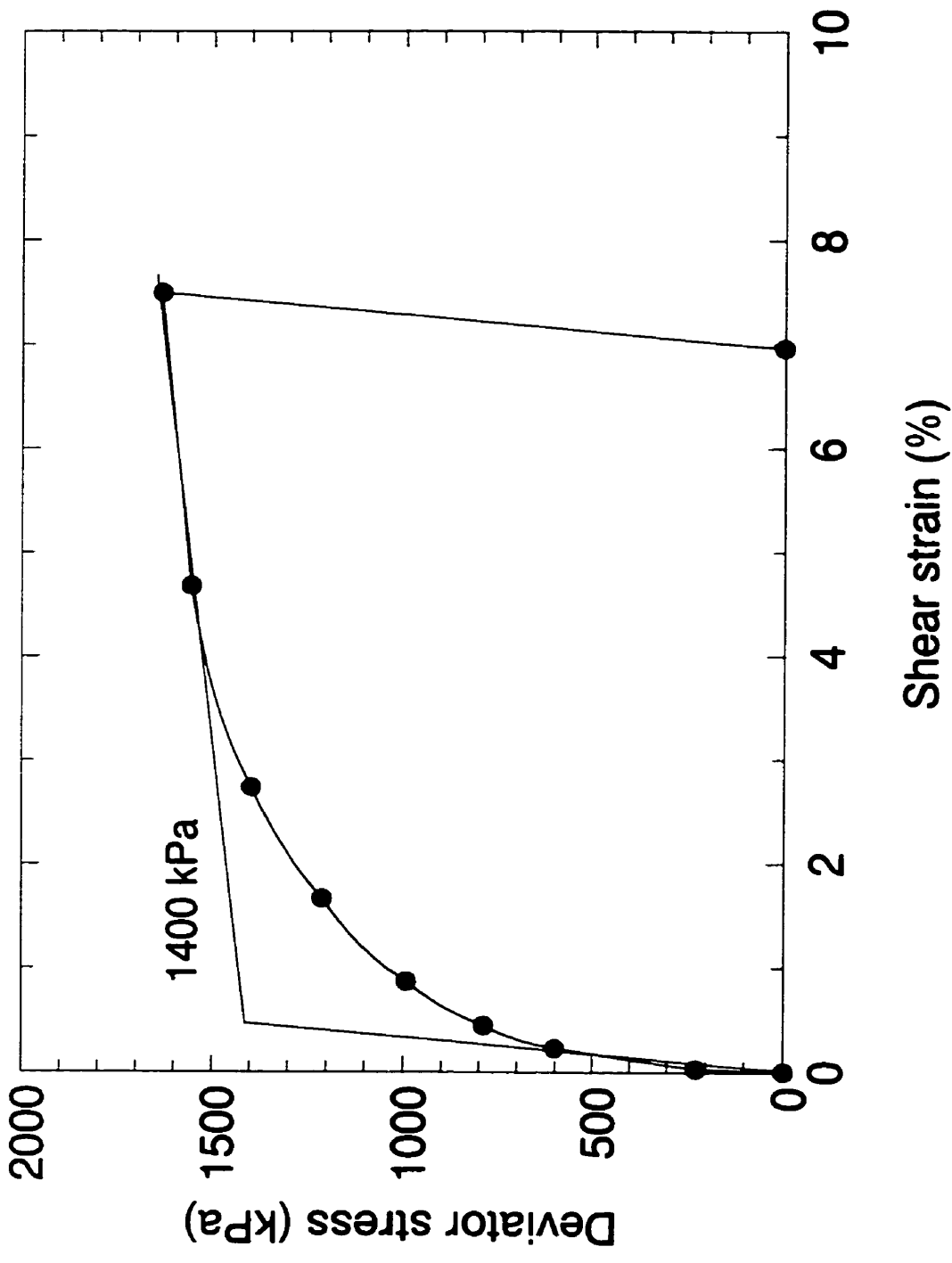


Figure 8.15 Identification of yield stress using bi-linear model

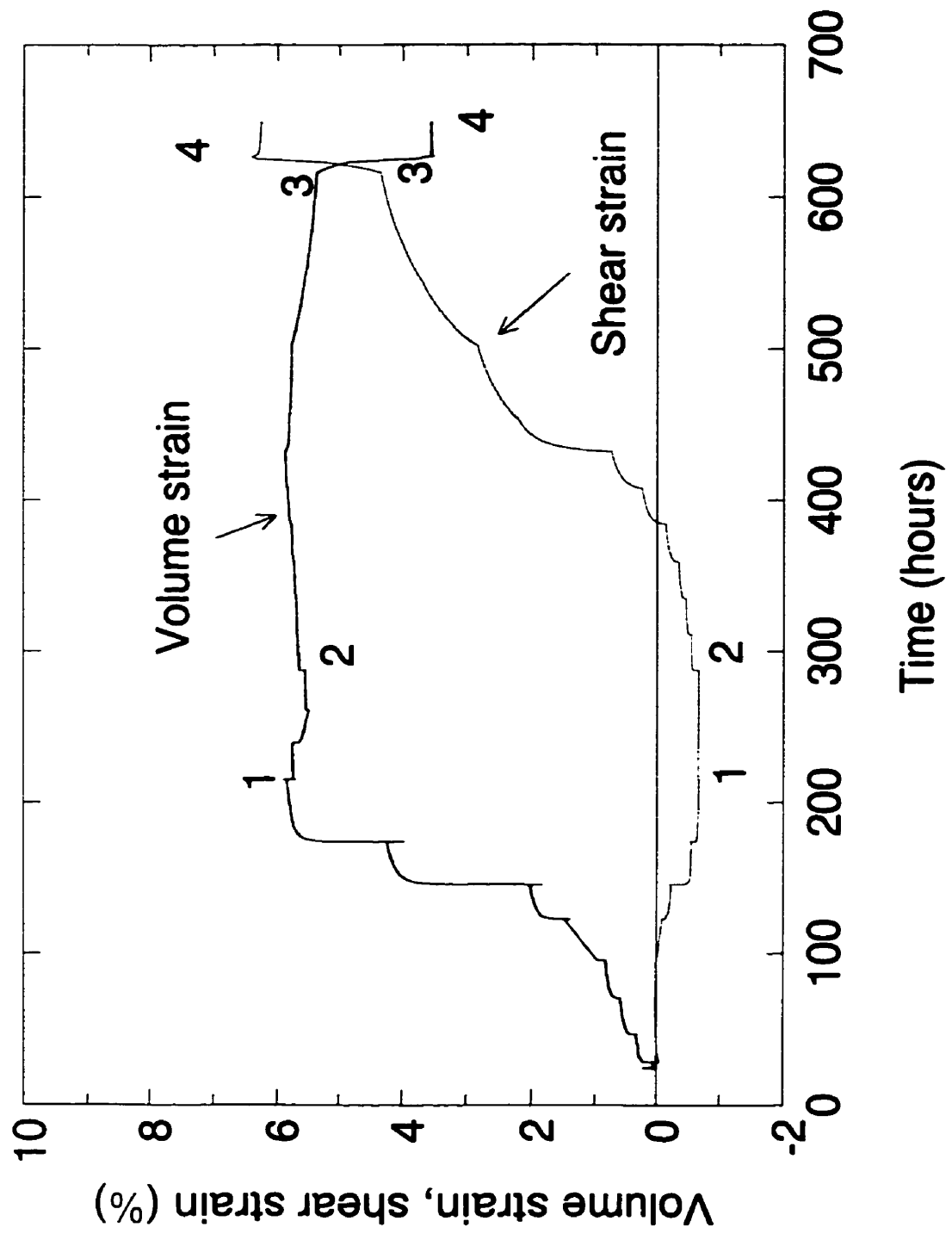


Figure 8.16 Volume strain and shear strain with time (T16541)

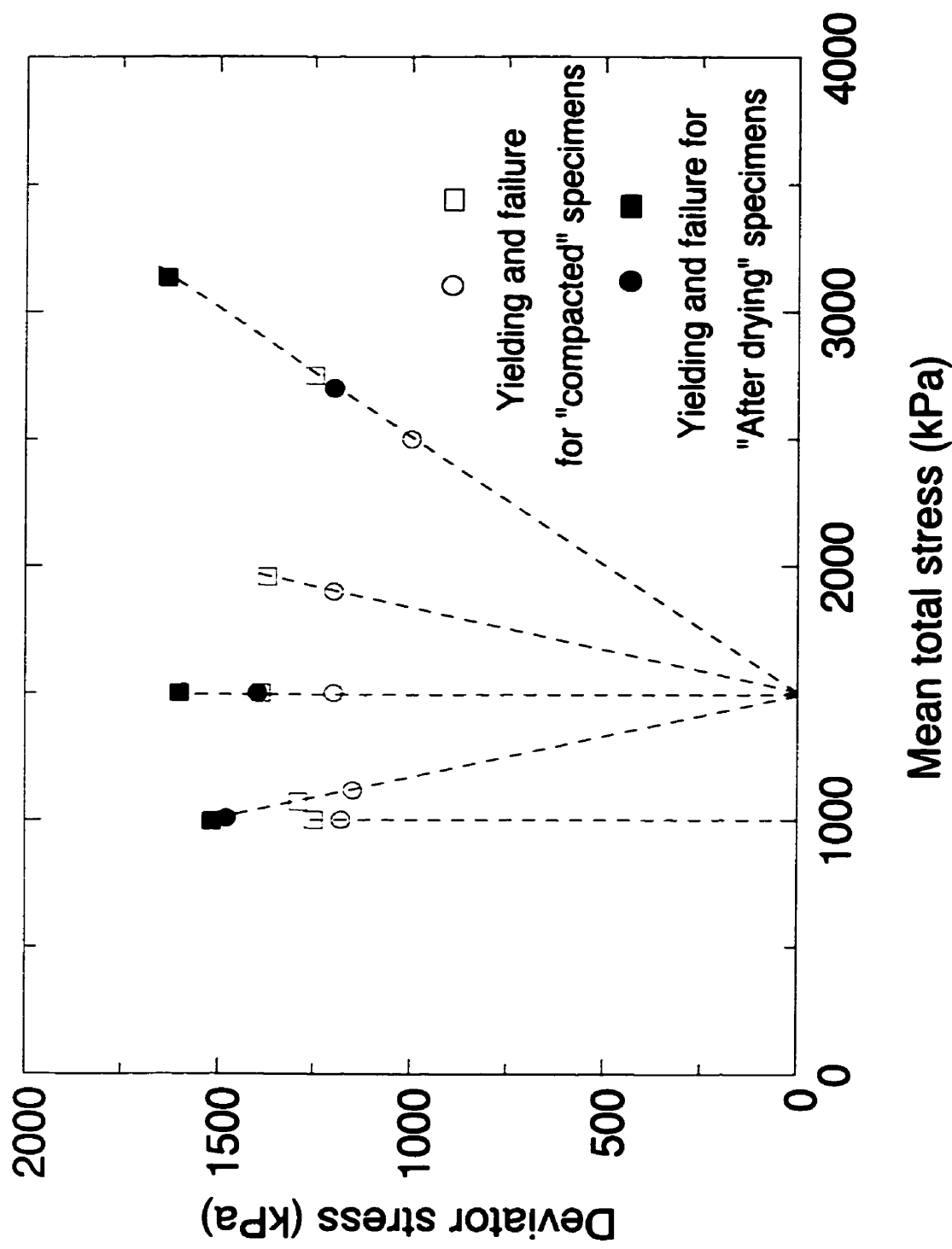


Figure 8.17 Yield stress and shear strength in p-q space

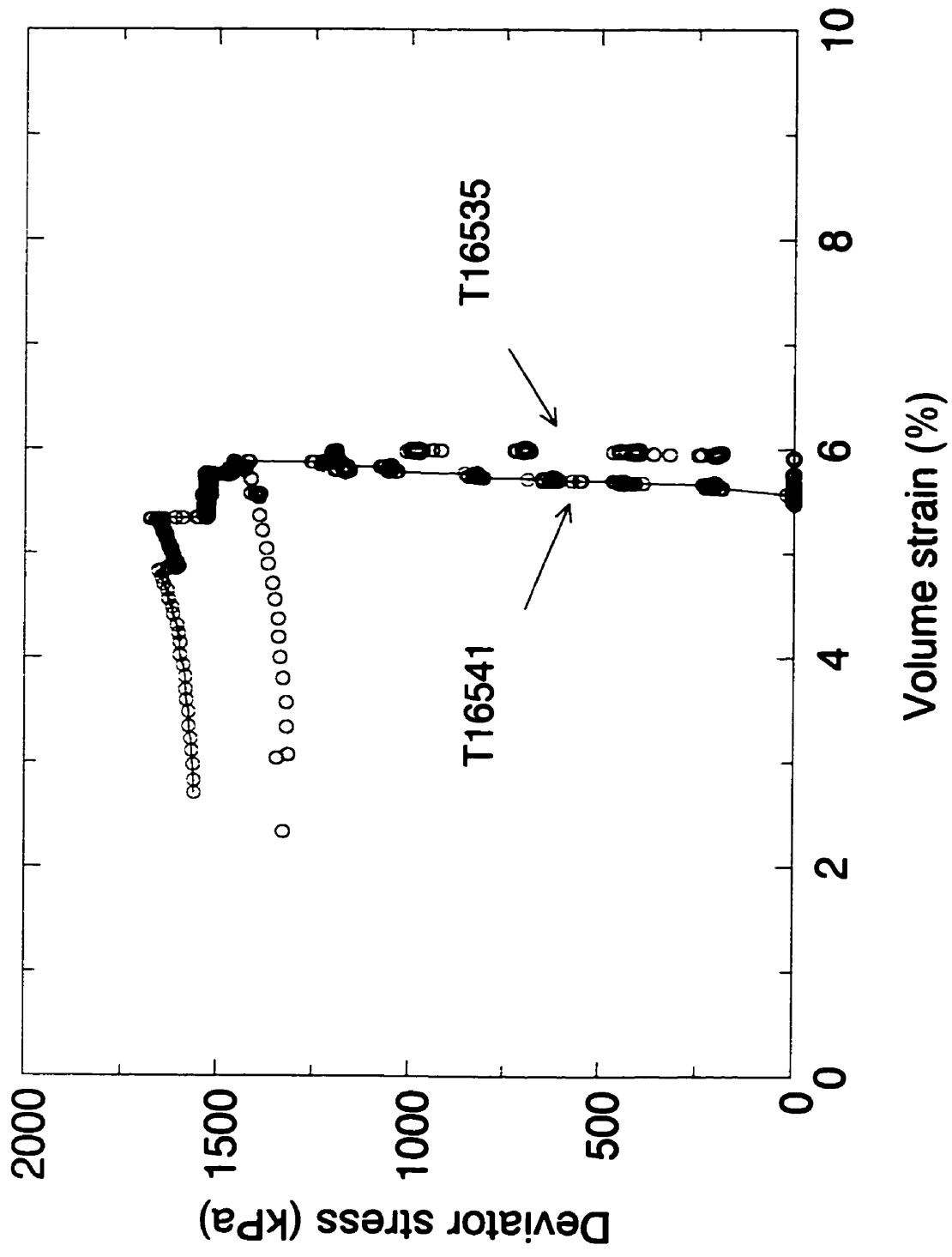


Figure 8.18 Deviator stress versus volume strain

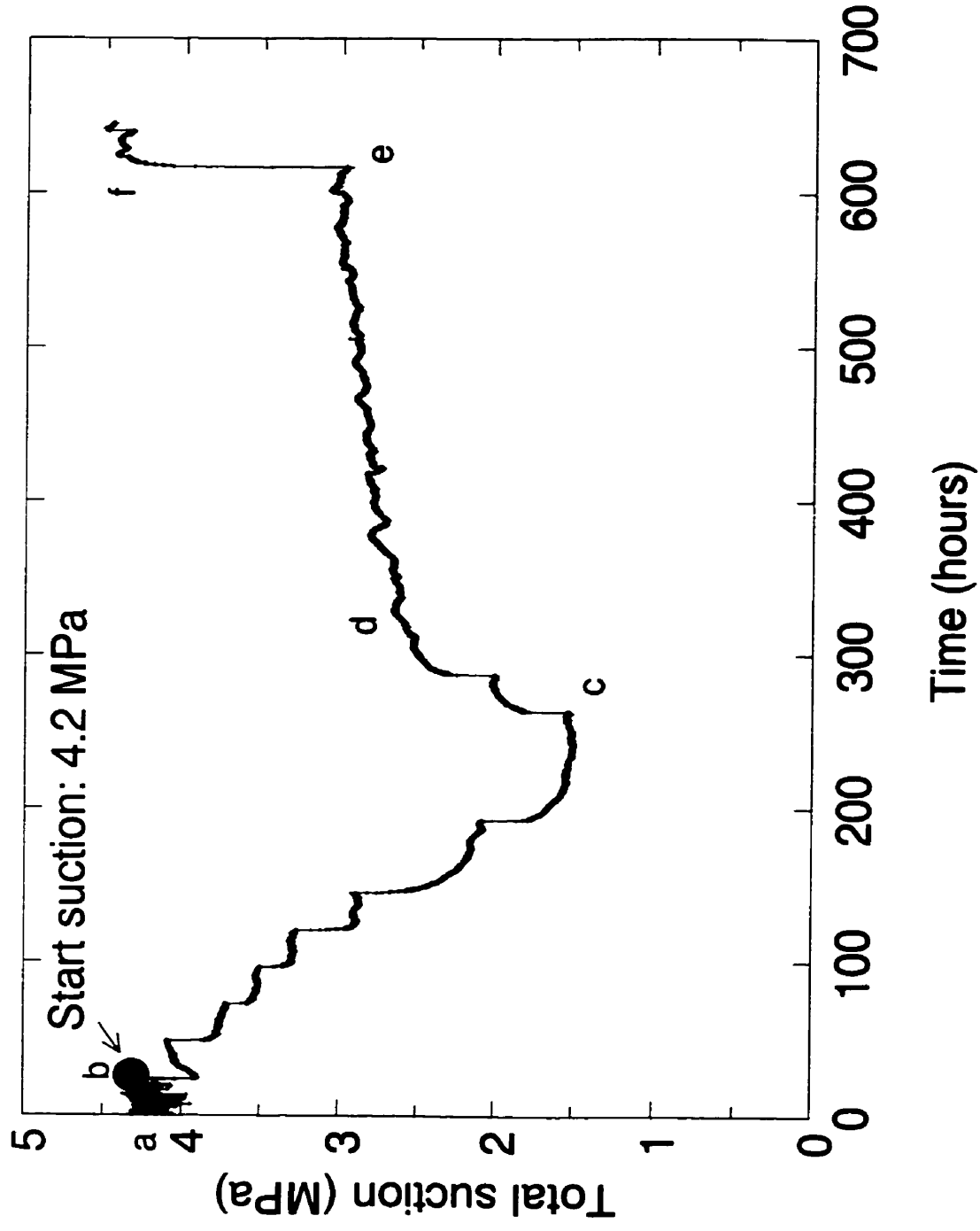


Figure 8.19 Suction change with time in triaxial testing (T16533)

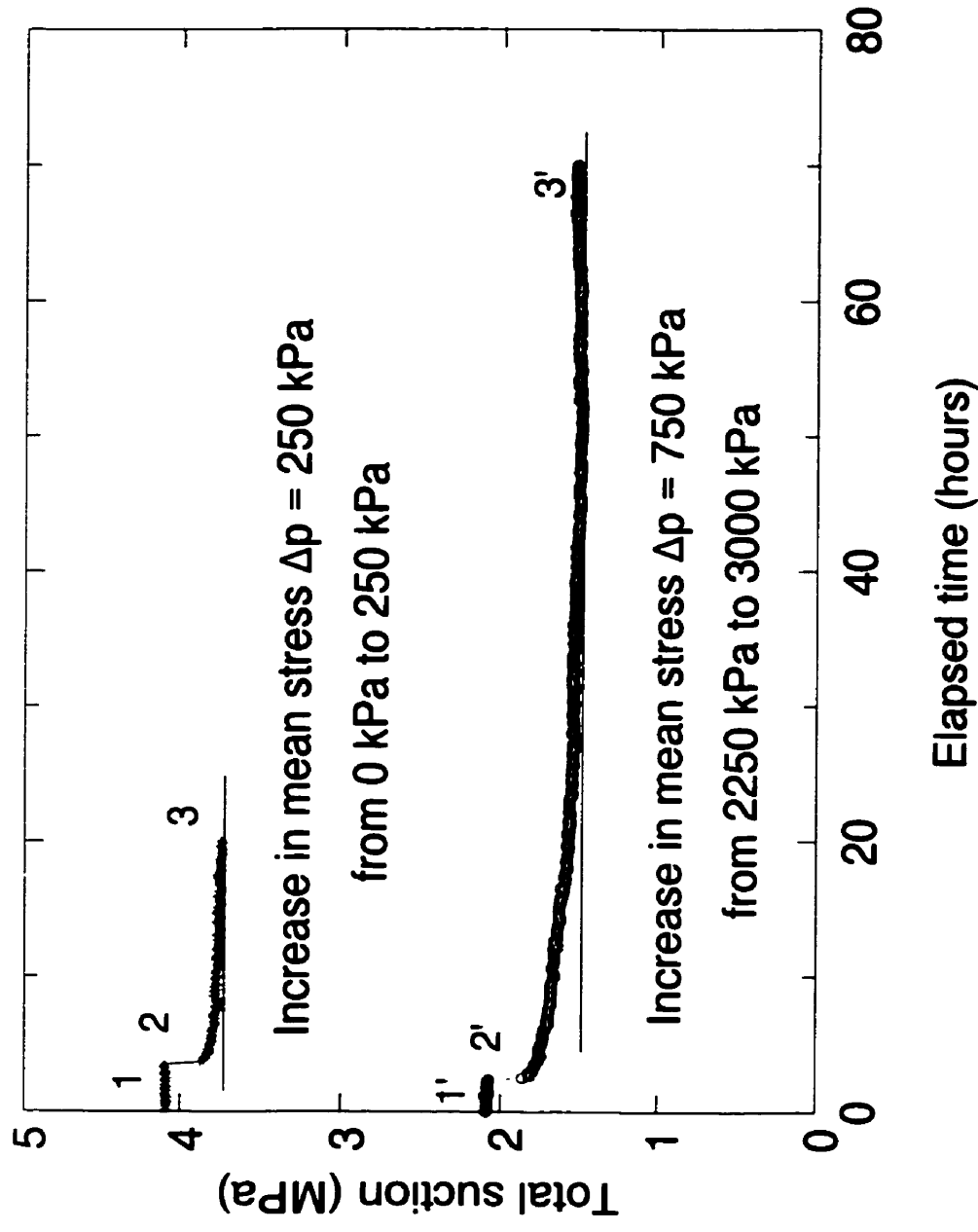


Figure 8.20 Equilibrium of suctions at mean stress increments (T16533)

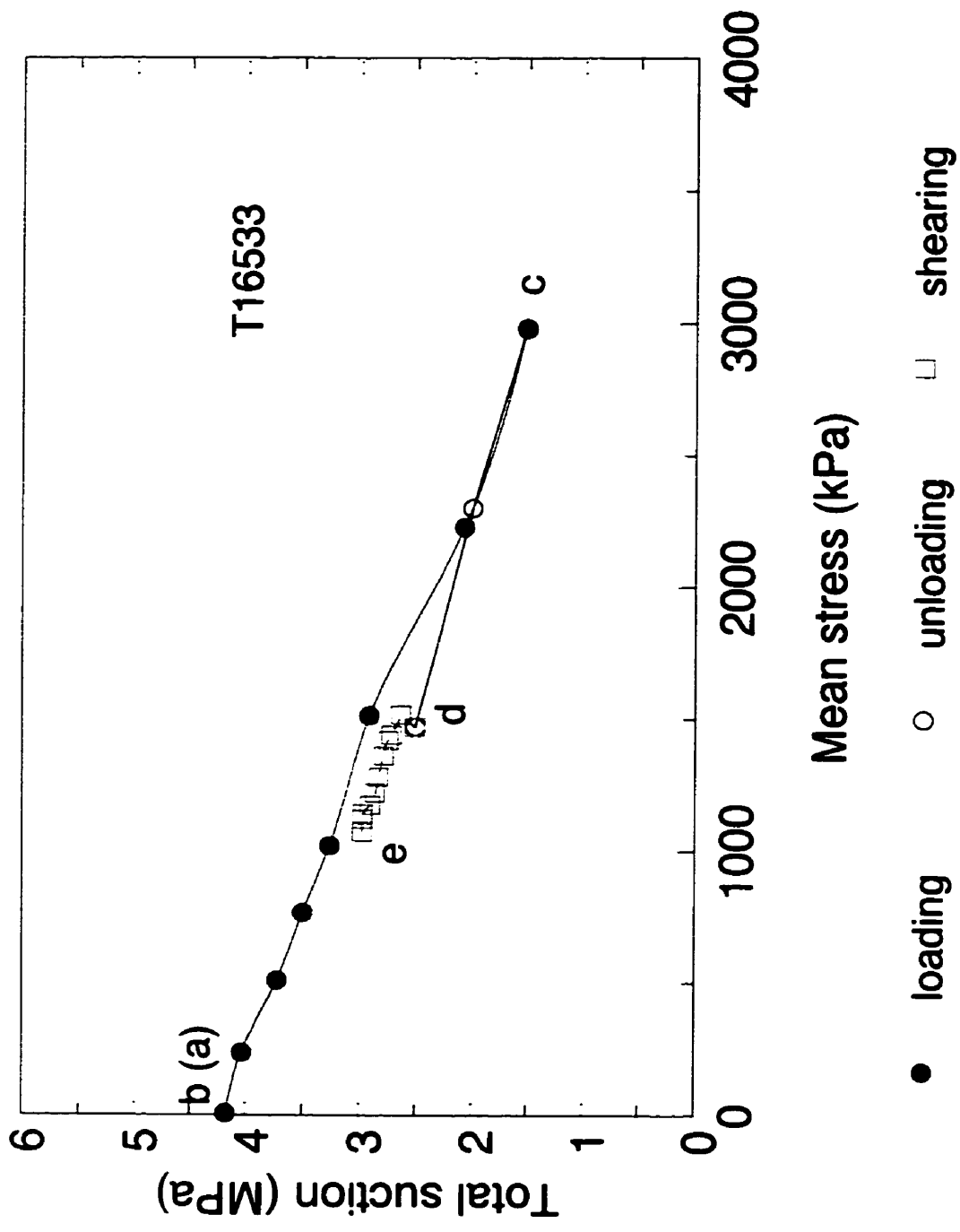


Figure 8.21 Suction changes during triaxial test (T16533)

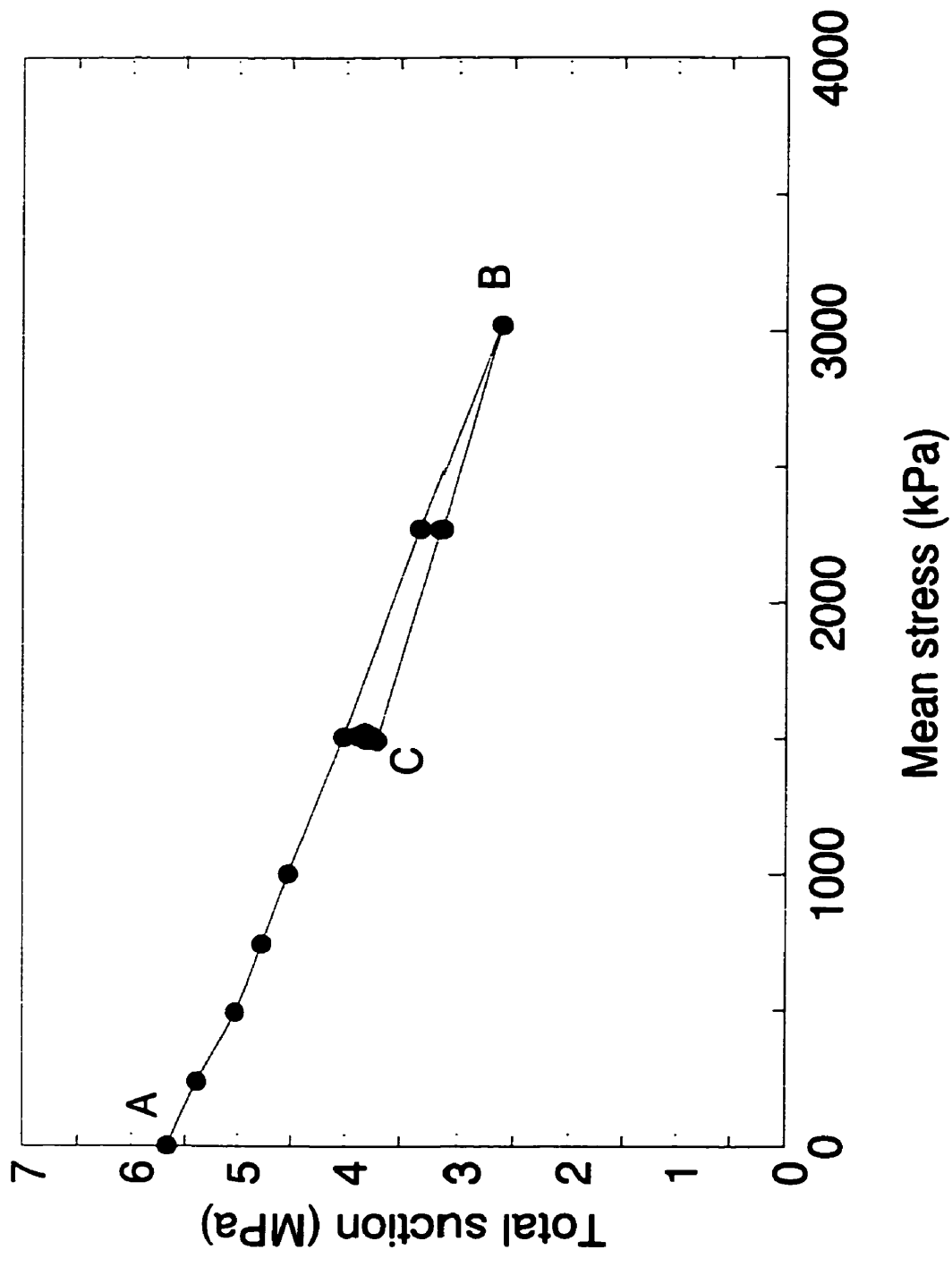


Figure 8.22 Suction changes at shearing
with constant mean stress (T16541)

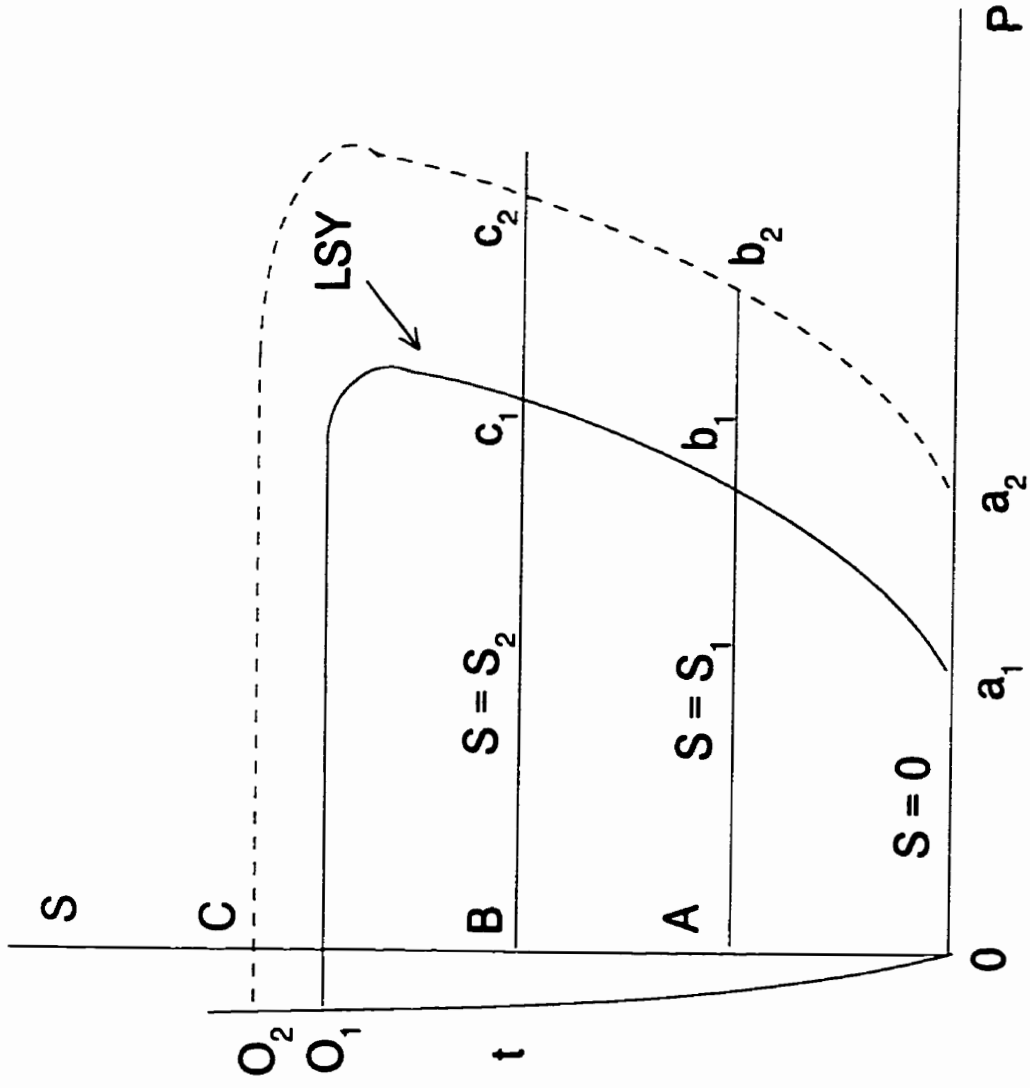


Figure 8.24 Yield loci at isotropic loading in p - S space

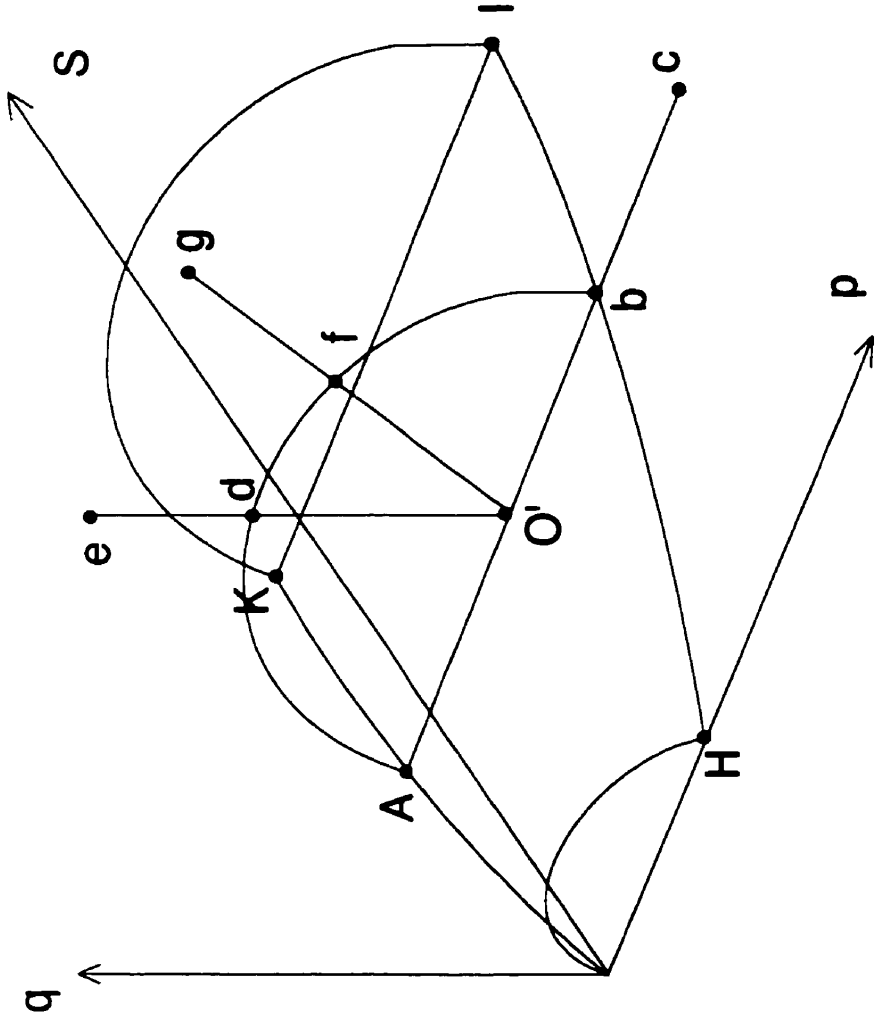


Figure 8.25 A conceptual model for unsaturated soils

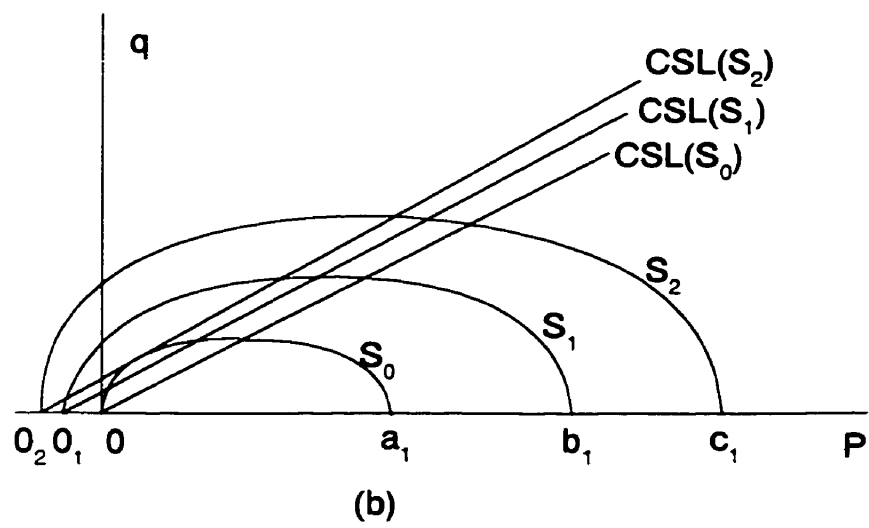
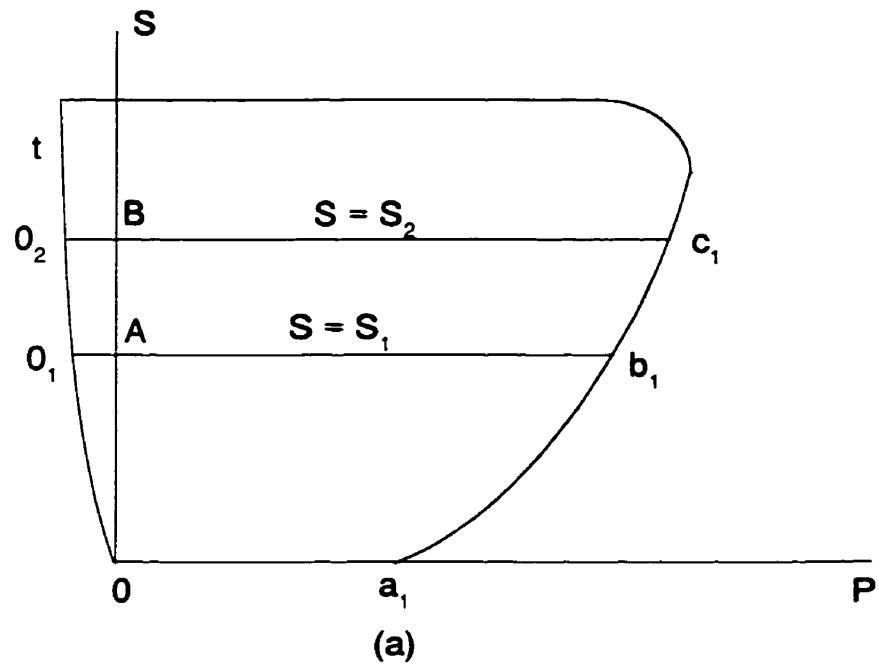


Figure 8.26 Yield loci at different suction levels

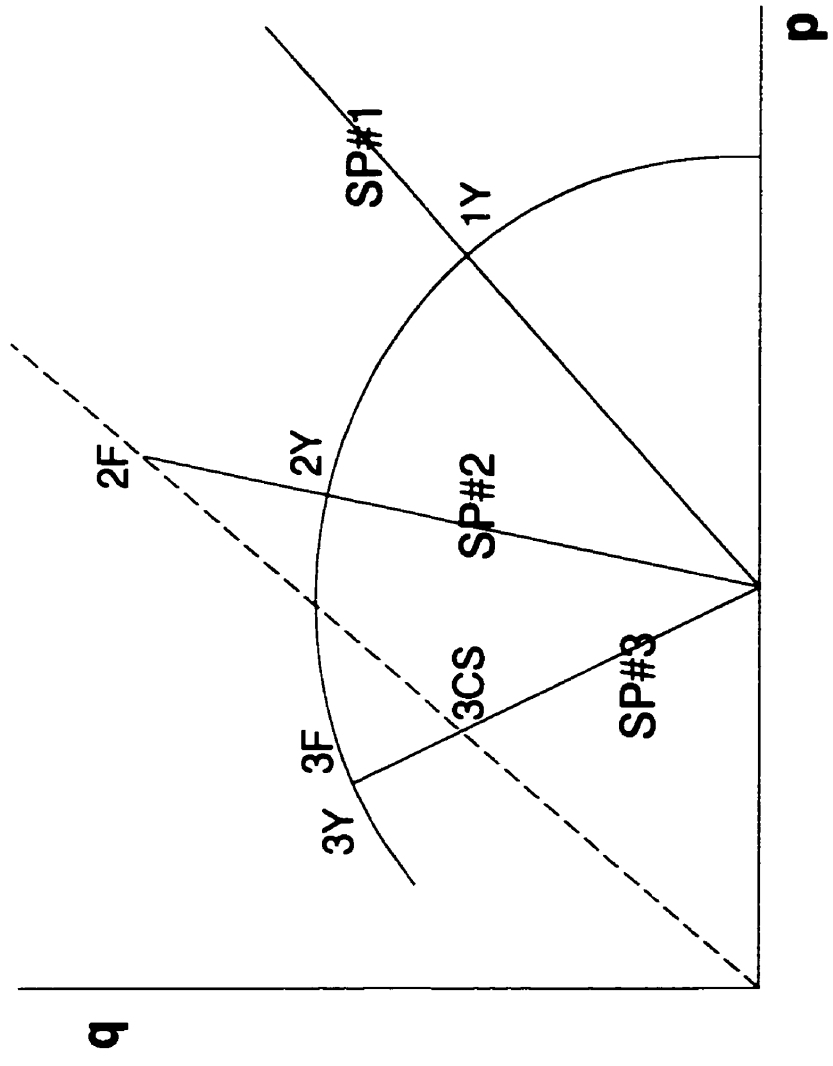


Figure 8.28 Traditional model to show yield and failure along stress paths

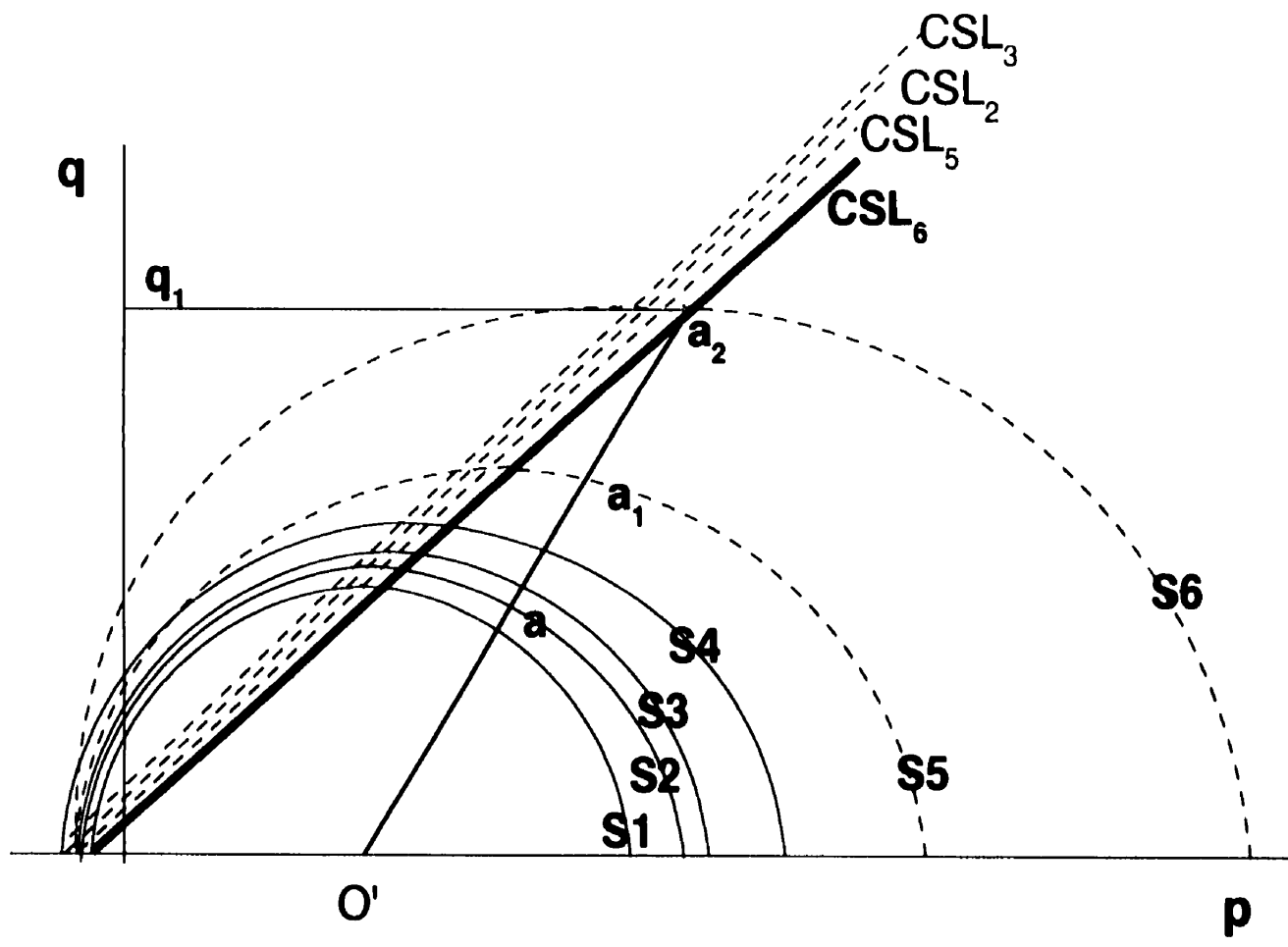


Figure 8.31 Failures after strain hardening for unsaturated soils

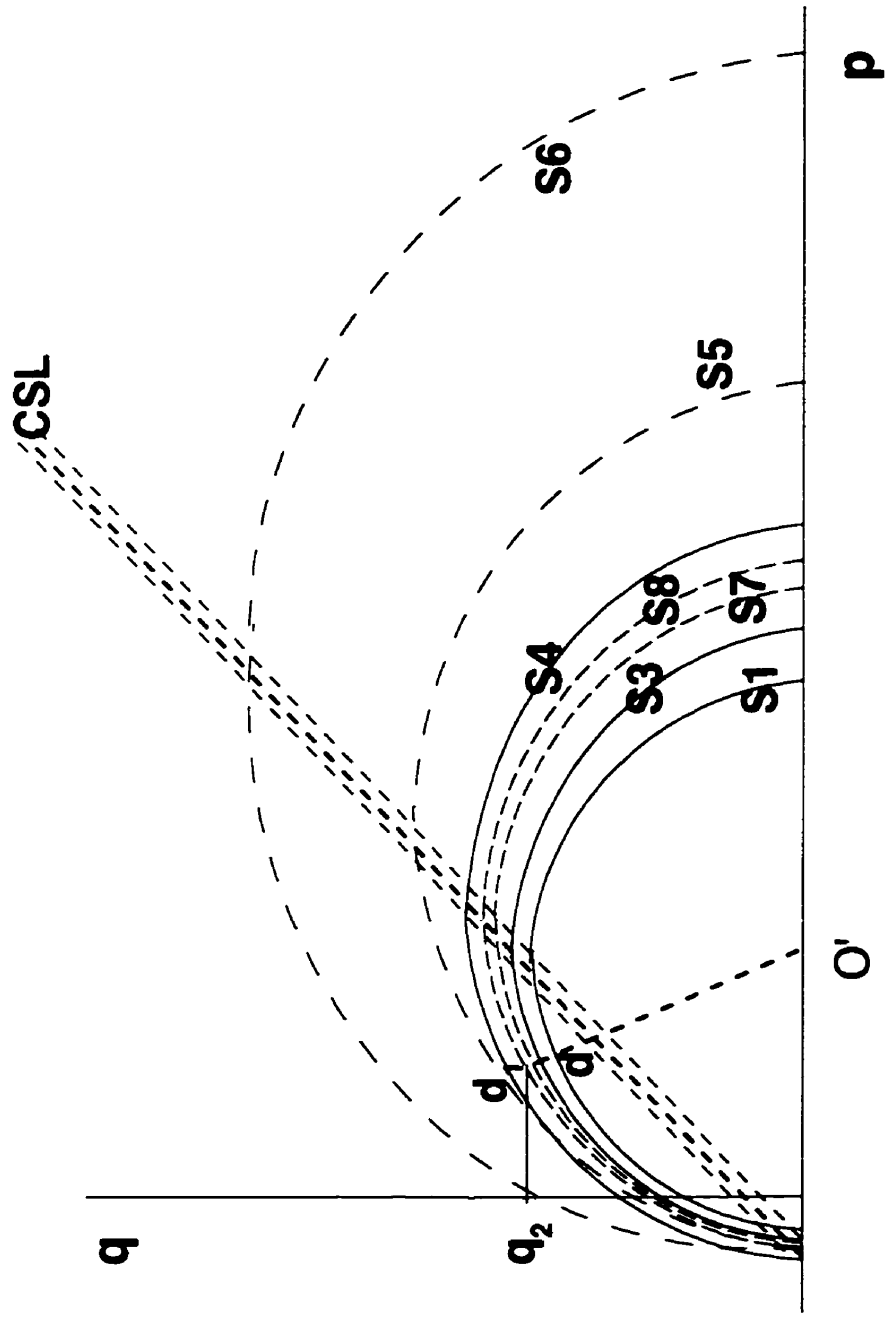


Figure 8.32 Failure of a specimen along a stress path
with decreasing mean stress

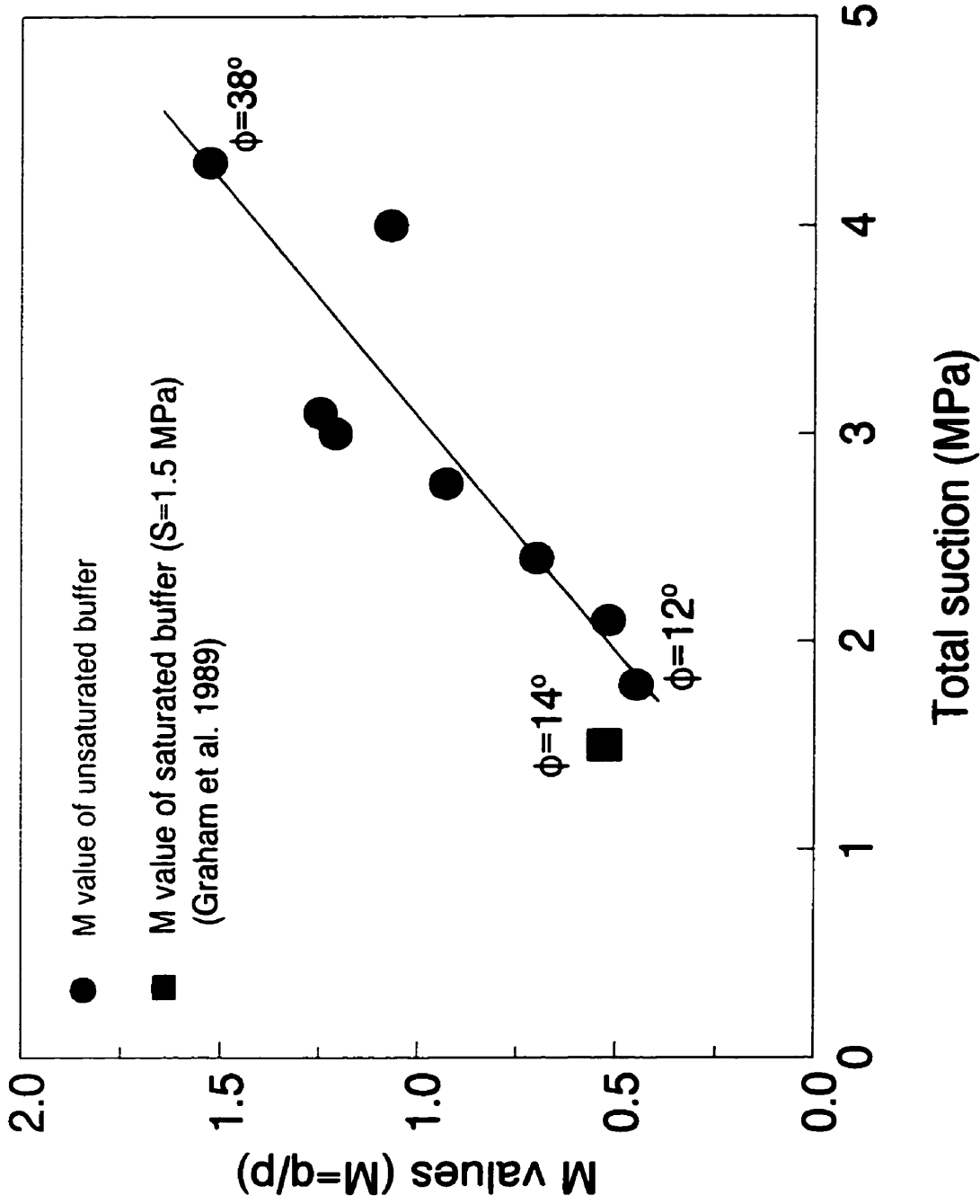


Figure 8.33 Conventional M values versus total suction

CHAPTER 9

A NEW ELASTIC-PLASTIC CONCEPTUAL MODEL FOR UNSATURATED SOILS

9.1 Introduction

The existing elastic-plastic conceptual model for unsaturated soils has been used as a framework for describing elastic-plastic features for many soils (Alonso *et al.* 1990, Wheeler and Sivakumar 1992, Cui and Delage 1996, Wan 1996). The model features elliptical yield loci in p-q space at any constant suction, with the yield loci increasing in size as suctions increase. As illustrated in Chapter 8, however, the model cannot successfully describe all behavior of the unsaturated buffer material that forms the basis of this thesis.

A new elastic-plastic conceptual model is developed in this chapter. Differences between the proposed model and the existing model are highlighted. The chapter then demonstrates how the model encompasses the features of stress-strain behavior of unsaturated sand-bentonite which were presented earlier in Chapter 8. Finally, the model is calibrated using data obtained from the stress-controlled triaxial tests.

The new conceptual model includes for the first time a yield envelope in q - S space. Two parameters – equivalent pressure and stress ratio are introduced as alternatives for two commonly used stress variables, namely net mean stress ($p-u_j$) and matric suction (u_j-u_w). This leads to establishment of a stress state boundary surface in the three-dimensional stress space p - q - S . Concepts of yielding, hardening law, flow rule and failure criteria used for saturated soils are incorporated into the stress state boundary surface to form an integrated model. Together with volume change characteristics in V - p - S space as illustrated schematically by Delage and Graham (1995), the proposed model can describe well the elastic-plastic behavior of unsaturated buffer observed in the experimental program.

9.2 A New Elastic-plastic Conceptual Model for Unsaturated Soils

Elastic-plastic soil mechanics assumes that soils have initially an elastic response to loading. This is eventually followed by yielding and the onset of non-recoverable straining. Ideally, a generalized framework includes the following features: 1) elasticity, 2) a yield criterion used to separate recoverable and non-recoverable behavior, 3) a volumetric hardening law, 4) a flow rule, and 5) a failure criterion.

9.2.1 Yield Curve in p-S Space for Isotropic Loadings

Numerous experiments have shown initially stiff and linear behavior of unsaturated soils during small increases in pressure or matric suction (for example, Matyas and Radhakrishna 1968, Ho *et al.* 1992, Maatouk *et al.* 1995). In elastic-plastic modelling, this is interpreted to mean that yielding can be induced by changes in either mean stress (and externally applied pressure), or suction (an internal stress variable), or by combinations of pressure and suction (Delage and Graham 1995). It will be helpful to review some of the discussion on loading- and suction-induced yielding that was introduced in Chapter 2.

As illustrated by Alonso *et al.* (1987), Figure 9.1a shows a saturated specimen (Suction $S = 0$) being loaded from A, yielding at B, compressing plastically with volumetric hardening to C, and then being unloaded to D. The corresponding V-lnp' behavior is shown in Figure 9.1b. A second unsaturated specimen ($S > 0$) starts from L, is loaded through its yield stress M down its stress hardening line to N, and then unloaded to O. The compression behavior is again shown in Figure 9.1b. The compression line MN is less steep than BC. The line LY1 joining B and M represents the loading yield line corresponding to the outer limit of states of stress and suction lower than had been previously experienced. The locus LY2 joining C and N represents a subsequent loading yield line produced by plastic hardening from B to C, or from M to N. Strain hardening

from B to C and from M to N is usually assumed to produce same amount of plastic volumetric strain.

Experimental data confirm that unsaturated soils also yield when suctions are increased (Alonso *et al.* 1990). In schematic terms, Figure 9.2 shows a specimen starting at P, being loaded with increasing suction until it yields at Q, and then suction hardening from Q to R. Unloading returns the specimen to the same stress as before at S, but the specific volume has decreased. Point Q is typical of a series of suctions that define the suction yield line SY1. Point R reached by plastic suction hardening is on a subsequent suction yield line SY2. Experimental evidence for the shapes of SY1 and SY2 is limited.

Alonso *et al.* (1987) used two separate yield curves (the dotted lines in Figure 9.3) to describe the observed yielding behavior in p - S space. Here p is net mean stress and S is matric suction. (Strictly they should be denoted as $(p-u_v)$ and S_m respectively.) Yield curves such as LY1 or LY2 in Figure 9.1 are represented in Figure 9.3 by a 'loading collapse' line LC. Similarly, SY1 and SY2 are represented in Figure 9.3 by a 'suction increase' line SI. The lines LC and SI correspond respectively to the outer limit of states of stress and suction higher than have been previously experienced through pressure increase or suction increase due to drying. Note that the LC line can also be reached by suction decreases that accompany wetting. Delage and Graham (1995) argued that similar mechanisms of plastic hardening in the soil microstructure produced the lines LC and SI and the two lines should perhaps be coupled. On the basis of the understanding of soil microstructure outlined in

Section 2.2 in Chapter 2, Delage and Graham (1995) envisaged a single yield envelope LSY (the dash line in Figure 9.3). This line provides a common yield curve for loading, suction increase, and suction decrease that depends on the initial microstructure of the clay. As before, plastic hardening will produce a series of LSY lines at successively lower specific volumes. Within the boundaries of each LSY line, soil is expected to behave elastically. It should be noted however that an LSY yield line does not lie on a plane of constant volume.

Experimental evidence obtained from tensile tests on unsaturated buffer indicates that soils also gain tensile strength from increased suctions (Tang and Graham 1998). Figure 9.3 also shows a yield curve O_t based on the understanding of tensile tests performed by the author. With the explanation provided in the previous paragraph, a sharp discontinuity will develop at the intersection between O_t and the SI line or LSY in p - S space. This appears to be unreasonable - the coupled yield curve LSY should probably extend smoothly into the tension region. Therefore, a yield curve in p - S space will probably take the form of a smooth curve such as the solid line LSY' in Figure 9.3. As yet, this remains to be confirmed by experimental data.

9.2.2 Yield Envelopes in p-q Space and in q-S Space

Yield envelopes also need to be determined in p-q space and q-S space in order to describe elastic-plastic behavior when unsaturated soils are under shearing. Here q is deviator stress. Less experimental work has been done in this area.

Figure 9.4 shows two LSYs in p-S stress space - an initial yield curve $a_1b_1c_1O_1$ and a yield curve $a_2b_2c_2O_2$ which is developed from the initial yield curve following plastic volumetric hardening. Initial yielding of the specimen is expected at point a_1 when the soil experiences increase in only pressure p along Oa_1a_2 with suction is held as zero. A sample made in the same way with the same water content, density and degree of saturation, will yield at point c_1 when it experiences increase in suction along Oc_1c_2 with external stress p held at zero. Further loading of stress p or suction S produces plastic strain hardening. As a result, the paths will take the yield curve to the position $a_2b_2c_2O_2$ and enlarge the elastic zone.

When a specimen is sheared starting at a stress state ($p, S, q = 0$) within the yield curve $a_1b_1c_1O_1$, yielding is also expected when the stress state (p, S, q) reaches a yield surface in p-q-S space. Under saturated conditions ($S = 0$) along the stress path Oa_1a_2 in Figure 9.4, the shape of the yield envelope in p-q space is well known for isotropic specimens (Figure 9.5). Elliptical yield envelopes y_1 and y_2 in Figure 9.5 represent respectively initial yielding and a yield envelope developed by further plastic straining. Failure states

are shown in the figure by a critical state line with a slope M_p . The slope M_p is singularly related to internal friction angle ϕ' of the saturated soil. In the particular case shown in the figure for zero suction, failure is only related to the deviator stress q and mean stress p . Therefore M_p can be defined as:

$$M_p = \frac{q}{p} \text{ at critical state} \quad [9.1]$$

This expression indicates that strength q_{cs} at critical state (CS) increases linearly with applied mean stress. For unsaturated soils, strength is considered to be contributed by both pressure and suction separately (Fredlund 1979, Toll 1990, Graham *et al.* 1995). The form of strength changes with increasing suction at $p = 0$ is shown in Figure 9.6a in $p = 0$, q - S space. The failure curve is not straight but exhibits a linear portion at the beginning and then gradually levels off, representing strengths that remain largely unchanged at high suctions (Fredlund *et al.* 1995). (In sands and silts, the strength can actually decrease at high suctions when the degree of saturation becomes low.)

Experimental evidence indicates that suction, as an independent stress variable, acts similarly to mean stress in many ways (Tang *et al.* 1999). It is easy to understand that a specimen at S_0 in Figure 9.6b initially behaves elastically when it is sheared because its suction is less than the initial yielding suction at c_1 (Figure 9.6b). Following a stress path such as $S_0S_1S_f$, the specimen will fail at point S_f when the failure curve OAB is reached. In this hypothetical test, suction was increasing continuously during shear. In the same way as was observed in Figure 9.2, increasing suctions along the stress path $Oc_1c_2c_3$,

causes yielding and plastic hardening behavior. Similarly, shearing along $S_oS_1S_r$ will also produce yielding and plastic behavior. Yielding during shear is also associated with yielding under isotropic loading conditions. This tends to suggest that there is probably a yield envelope in q-S space that represents yielding stresses q_y varying with suctions. By generalization, the separate yield envelopes in p-q and q-S spaces will produce a yield surface in p-q-S space.

While yielding induced by increasing suction (Figure 9.3) and the strength envelope in q-S space (Figure 9.6a) have been examined experimentally (Alonso *et al.* 1990, Delage and Graham 1995), no experimental evidence has yet been presented for yield envelopes in q-S space. To begin, it appears reasonable to assume that yield envelopes in q-S space will be elliptical in the same way as has been shown for saturated isotropic clays and for temperature effects. Other shapes could also have been chosen. To the author's knowledge, this is the first time that a closed yield envelope has been proposed in q-S space. The proposed yield envelope induced by suction is called a suction yield (SY) envelope. The existence and shape of such an envelope need to be confirmed with experimental data.

Figure 9.6b shows yield envelopes (y_1 , y_2 and y_3) and critical state conditions in q-S space at $p = 0$. When suction increases along the isotropic stress path Oc_1c_2 (Figure 9.4), the corresponding yield envelopes are y_1 and y_2 in q-S space in Figure 9.6b. By analogy with Figure 9.5, a strength parameter M_s can be defined:

$$M_s = \frac{q}{S} \text{ at critical state} \quad [9.2]$$

The subscript 's' indicates the strength parameter is associated with suction. It should be noted that critical state in q-S space does not follow a straight line as in p-q space, and therefore M_s is not a constant but changes with increasing suction. M_s is related to ϕ^b as defined by Fredlund (1979). Testing results indicate that M_s (also called M^b by Maatouk *et al.* 1995, Wiebe *et al.* 1998) is equal to the constant value of M_p (in q-p space) until suctions are sufficient to cause air to enter the pore spaces (Escario and Saez 1986, Fredlund *et al.* 1987). This probably suggests that a change from two phases (soil particles and water) to three phases (soil particles, water and air) causes changes in friction angle and hence the values of M_s . As suctions further increase with decreasing water contents, strength remains largely unchanged. There is no clear explanation for this observation. High suctions are associated with lower water content and smaller line contacts between the air-water interface and particle surfaces. A shrinkage limit can be reached where water content (and hence suction) decreases without further volume change being made (Williams and Sibley 1992, Tang *et al.* 1998c). The observation that there is no further change in strength at high suction is probably related to this volume change limit.

Specimens experiencing applied pressures with zero suction (that is, saturated soils) and specimens under suctions with zero applied external stress are two extreme cases. A general case usually involves a combined application of both suction S and external stress

p. The stress path Ob_1b_2 in Figure 9.4 shows a soil experiencing both pressure and suction increases at a constant stress ratio ($\eta_s = S/p$). A specimen will yield at b_1 when it hits the initial yield locus $a_1b_1c_1O_1$. Further straining (and plastic hardening) makes the yield locus $a_1b_1c_1O_1$ move to $a_2b_2c_2O_2$. As discussed earlier, it is postulated that expansion of the yield locus can be achieved by increasing mean stress p from a_1 to a_2 , or by increasing suction from c_1 to c_2 . Yield envelopes in p - q space for loading of mean stress ($S = 0$) and in q - S space for suction loading ($p = 0$) are similarly assumed to be elliptical in shape. If this assumption is made (and it appears reasonable to the author to do so), then yield envelopes corresponding to shearing in a plane vertical to the stress path line Ob_1b_2 could also be expected to be elliptical. Figure 9.7 shows such a yield envelope and a critical state line with a slope M_{ps} .

$$M_{ps} = \frac{q}{\sqrt{S^2 + p^2}} \quad \text{at critical state} \quad [9.3]$$

It should also be noted that M_{ps} is defined along a stress path vector in p - S space. The length of the vector p_e defines the magnitude of stress state (p , S) and its direction η_s defines the ratio of suction S over pressure p .

$$p_e = \sqrt{S^2 + p^2} \quad [9.4]$$

$$\eta_s = S/p \quad [9.5]$$

Because of the fundamental similarity between mean pressure and internal suction, p_e is a pressure variable that represents a combination of both internal stress suction and external stress p . It has been called here an 'equivalent pressure'. The two parameters p_e and η_s are an alternative way of defining a stress state in the two stress variables p and S .

The equivalent pressure p_e is equal to p for saturated soils in which suction $S = 0$. In unsaturated soils experiencing only suction changes without external stress being applied ($\dot{p} = 0$), $p_e = S$. Therefore, M_p and M_s defined in expressions [9.1] and [9.2] can be rewritten as:

$$M = \frac{q}{p_e} \text{ at critical state} \quad [9.6]$$

The parameter M describes Critical State strengths at any stress ratio $\eta_s = S/p$. Since M_s is not constant, M in [9.4] will not be constant, so $M = M(p_e, \eta_s)$.

9.2.3 State Boundary Surface and Yield Envelopes

On the basis of the preceding section regarding yield loci in p - S space and yield envelopes in q - p and q - S spaces, a three-dimensional view of the state boundary surface in p - q - S space for unsaturated soils can be presented in Figure 9.8. The state boundary surface can be viewed as a family of yield envelopes in a series of vertical planes along constant stress ratios η_1 , η_2 , and η_3 as shown in the figure. The yield envelopes are all elliptical but differ in size depending on the stress ratio η_s . Critical State lines in Figure 9.8 are OF_1 , OF_2 , and OF_3 with slopes of M_1 , M_2 and M_3 respectively. As discussed earlier, the value of M_i ($i = 1, 2, 3$) may change when suctions are higher than the air entry value. At low suctions, M_i is approximately constant and is equal to M_p (or M as usually defined for saturated soils) for saturated soils. Figure 9.8 is strictly applicable in the form shown for cases where $M_s = M$, that is before air entry. At lower saturations

(and higher suctions) the curvature of the strength envelope shown in Figure 9.6 will lead to an evolution of the yield surface into a more asymmetric shape. For now, this restriction will be neglected.

In the usual way, the state boundary surface defines the limit of elastic (recoverable, small strain) behavior. All stress states lying within this state boundary surface can by definition be attained with fully recoverable deformations. It can of course be enlarged through plastic volumetric hardening or diminished through plastic volumetric softening. With the exception of the saturated condition ($S = 0$), Figure 9.8 leaves undefined the question of what happens when q/p_c is larger than M . The model in Figure 9.8 grows out of an understanding of the important concept of stress ratio $\eta_s = S/p$, and can be termed a 'stress-ratio based model'.

The state boundary surface of the 'stress-ratio based model' (Figure 9.8) is obviously different from the state boundary surface proposed by Alonso *et al.* (1990) and shown in Figure 2.6. The latter can be viewed as a family of elliptical yield envelopes in constant suction planes, and can therefore be termed a 'constant-suction based model'. In this model, all yield envelopes have the same shape but are different in size. That is, like in saturated soils, all critical state lines are parallel with a constant slope of M (and hence a constant friction angle). Using the 'constant-suction based model', there is a similarity of elastic-plastic behavior of unsaturated soils at different constant suctions. Some parameters of soil behavior have been therefore assumed to be functions of suction. For

example, the stiffness parameter λ is defined as $\lambda = \lambda(S)$ (Wheeler and Sivakumar 1995, Maatouk *et al.* 1995). This suggests that suction is an intrinsic physical property of unsaturated soils. In contrast, the new 'stress-ratio based model' regards suction as an independent stress variable, which together with mean stress, affects mechanical behavior of unsaturated soils.

The yield envelopes associated with the state boundary surface in Figure 9.8 also clarify the uncertainties stated in Section 1.1.1.3 that introduction of a coupled load suction yield line in p - S space results in higher suction producing a smaller yield envelope at the transition from the load yield line to the suction yield line. In the newly developed model in Figure 9.8, a coupled load suction yield line produces smooth changes in yield envelope in q - p_c plane at transition. Yielding in p - S space is related to two factors namely suction or mean stress. The new model represents a continuous change from yield behavior dominated by p -changes to another dominated by S -changes. The maximum size of yield envelope is formed when both factors contribute most.

Volume change characteristics of unsaturated soils are usually described using two separate constitutive equations which relate specific volume V and water content w to mean stress p and suction S (Fredlund and Morgenstern 1976). Under the condition of constant mass in triaxial testing such as that used in this program, water contents are unchanged, the volume change behavior that needs to be examined is therefore how specific volume relates to suction and mean stress. Figure 9.9 illustrates schematically

the relationship between specific volume V , mean stress p and suction S which is developed and described in detail by Delage and Graham (1995).

9.2.4 Hardening Law

Plastic hardening or plastic softening can both be observed during shear loading depending on stress paths in p - q - S space. During plastic strain hardening, volumes decrease and the yield envelope expands, with the current stress state lying on a series of successively changing state boundary surfaces. During strain softening the yield envelope contracts, with the current stress state lying on a series of diminishing envelopes. The hardening law controls how the yield envelope changes in position and magnitude with plastic straining.

Figure 9.10a shows increases in the extent of the elastic region as a yield locus experiences plastic hardening under isotropic loading and moves from $LSY1$ to $LSY2$. Corresponding volumetric strains are shown in Figure 9.10b. Hardening can be caused by increasing pressure along Oa_1a_2 , increasing suction along Oc_1c_2 , or increasing both pressure and suction along Ob_1b_2 . For saturated soils (along stress path Oa_1a_2), it is common to use the isotropic consolidation line $Oa'_1a'_2$, plotted in V - $\ln p'$ space to represent the hardening line. The line, of slope λ in the post-yield range $a'_1a'_2$, represents total volume strain. The unload/reload line, of slope κ represents purely elastic volume strain.

For unsaturated soils, volumetric changes induced by increasing suctions differ quantitatively from those induced by increasing pressure. This is reflected as different slopes of $a'_1a'_2$ (volume change due to pressure) and $c'_1c'_2$ (volume change due to suction). For any intermediate stress path such as Ob_1b_2 , volume change is affected by both suction and pressure. Based on the understanding of the concepts of 'stress-ratio based model', volumetric hardening can be represented by following expression:

$$V = V_0(p, S) - \lambda(p, S) \ln p_e \quad [9.7]$$

where $V_0(p, S)$ is specific volume at $p_e = 1$, and $\lambda(p, S)$ is the slope of $V - \ln p_e$ relationship representing the stiffness with respect to equivalent pressure p_e .

Experimental data obtained from saturated soils and soil-water characteristic curves for unsaturated soils indicate that V versus $\ln p'$ and V versus $\ln S$ relationships in Figure 9.10 can usually be assumed as straight lines $a'_1a'_2$ and $c'_1c'_2$. The two relationships correspond to stress paths of $\eta_s = 0$ and $\eta_s = \infty$ respectively. For a stress path with a constant intermediate stress ratio η_s such as Ob_1b_2 , it is also probably reasonable to assume a linear relationship, and thereby a straight line $b'_1b'_2$. That is if the slope of $b'_1b'_2$ in $V - \ln p_e$ space is linear, then the hardening law presented in expression [9.7] can be defined as:

$$V = V_0(\eta_s) - \lambda(\eta_s) \ln p_e \quad [9.8]$$

9.2.5 Failure and Flow Rule

Conceptual models have been successfully used to explain elastic-plastic features and failures in saturated soils along various stress paths. Figure 9.11 shows an elliptical yield envelope and a straight critical state line based on the proposed 'stress-ratio based model' for unsaturated soils. Elastic-plastic behavior depends on stress paths in this constant stress ratio plane. Stress path #1 is such that yielding will be observed at stress 1Y, but the specimen will not fail since the stress path does not intersect the critical state line. A specimen following a stress path such as #2 will yield at 2Y and then, with further stressing, move to failure at 2F. For both of these stress paths, post-yield stressing will involve plastic compression straining. A specimen that follows a stress path such as #3 will yield and simultaneously fail at stress 3Y, 3F. Then, because the yield surface lies above the critical state line, it will expand plastically and strain soften to reach critical state failure at 3CS.

In elastic-plastic modelling, volume strain ϵ_v and shear strain ϵ_s are divided into elastic and plastic parts. That is, $\epsilon_v = \epsilon_v^e + \epsilon_v^p$, and $\epsilon_s = \epsilon_s^e + \epsilon_s^p$. The flow rule describes the relationship between plastic shear strains and plastic volume strains. The flow rule also relates the shape of the yield envelope to the plastic potential. The plastic potential is a function, such that plastic strain increment vector directions $\arctan \dot{\epsilon}_s^p / \dot{\epsilon}_v^p$ are perpendicular to it. When this function is the same shape as the yield envelope, the flow rule is termed associated. In this case, the directions of the incremental plastic volumetric

strain and shear strain are parallel to the η_s line and deviator stress q respectively. When the plastic potential is a different shape from the yield envelope, the flow rule is termed non-associated. By plotting the plastic strain vectors at the yield stress of each test on the shape of the plastic potential, and association or non-association of the flow rule can be determined.

9.3 Interpretation of the Stress-strain Behavior of Unsaturated Buffer

Stress-strain behavior and strength properties of unsaturated buffer were examined in two series of stress-controlled triaxial tests in this program. Figure 9.12 shows schematically the stress paths of the triaxial tests for one series. The tests were carried out under undrained, constant-mass conditions.

A typical specimen started at an initial state A on the axis of suction S in the figure. Under isotropic compression, mean stress p increased and suction S decreased until the stress state reached point I on its current yield curve YIL (shown dotted) in p -S space. There, initial yielding occurred. (YIL is the initial yield locus in p -S space for isotropic loading.) With further increases of mean stress p to point g in the figure, the yield locus expanded to $ega'b'c'$ and formed a 3-D state boundary surface in p - q -S space. Following subsequent decreases in mean stress p to point O', the specimen became over-consolidated. It was then sheared starting from point O' and followed one of the selected

stress paths $\Delta p/\Delta q = 1, 1/3, 0,$ and $-1/3$ corresponding to stress paths O'a, O'b, O'c, and O'd respectively in p-q-S space. The curve gabcd is a trace yield envelope in the 3-D state boundary surface. It lies in a vertical plane above AO'g since suctions are independent of the q-component of the stress tensor (Tang *et al.* 1997b). As discussed in Section 9.2.3, the state boundary surface can be enlarged through plastic volumetric hardening or diminished through plastic volumetric softening. Finally, the specimens were sheared to large strains when they failed and reached critical state.

As demonstrated in the previous chapter, the existing 'constant-suction based model' is not able to explain the stress-strain behavior of unsaturated buffer that was observed in the triaxial tests. The following section describes how the 'stress-ratio based model' can be applied to the triaxial test results. Figure 9.12 shows a state boundary surface of the proposed model which is composed of a series of elliptical yield envelopes in q-p_c planes. The yield locus ega'b'c' in p-S space for isotropic loading has not been shown closed on the S axis since yielding induced by increasing suction was not identified in the range of suctions tested in this study (see Section 4.7).

9.3.1 Strain Hardening

Strain hardening is expected for a specimen (whether it is saturated or unsaturated) experiencing shearing beyond the elastic region along the stress path $\Delta p/\Delta q = 1$, the stress path O'a shown in Figure 9.12. Figure 9.13 illustrates how a state boundary surface of the 'stress-ratio based model' evolves for an unsaturated specimen sheared along such a

stress path. Elastic-plastic behavior of a specimen which is isotropically compressed from point A to point g can be described by a yield curve YC_1 in p - S space. After the mean stress decreases to point O' or a_1 , the specimen is over-consolidated and its elastic-plastic behavior is now governed by a state boundary surface which is already formed and associated with the yield curve YC_1 . Yield envelopes in q - p_e planes depend on current stress state (p, S) or stress ratio η_s . The state boundary surface evolves when further yielding occurs due to shearing. For any stresses p, q and S on the line a_1a_2 , the specimen behaves elastically since the stresses lie within the state boundary surface. During this stage from a_1 to a_2 , volume changes will be small but finite and will produce some changes in equivalent pressure p_e and stress ratio η_s . The p - q - S states therefore move to the yield envelope y_2 . Note that stressing along a_1a_2 is done within the state boundary surface defined by YC_1 . Further stressing causes plastic straining to begin the evolution (expansion or compression) of the state boundary surface. From point a_2 to a_3 , increasing mean stress p will make the state boundary surface expand, and YC_1 expand to YC_2 . The yield envelope (and the η_s plane) through a_3 is now through y_3 on YC_2 . This process continues through successive yield envelopes until finally the stress path reaches failure at a_4 on the critical failure state line L_4 for envelope y_4 . Experimental evidence of strain hardening and loading to eventual failure is shown in Figure 9.14. Specimen T16542 following stress path $\Delta p/\Delta q = 1$ exhibits a typical stress-strain behavior (the dotted curve $OA'B'$ in the figure) which shows initially stiff elastic behavior followed by strain hardening and finally failure at critical state. As demonstrated in Chapter 8, failure of a specimen following stress path $\Delta p/\Delta q = 1$ can be not explained using the earlier

'constant-suction model' whose critical state lines of unsaturated specimens are parallel to those of saturated specimens. As observed in numerous experimental results from saturated soils, specimens do not fail until very high shear strength for stress path $\Delta p/\Delta q = 1$ (Wood 1990).

9.3.2 Strain Softening

For a specimen sheared along the stress path $O'd$ as illustrated in Figure 9.12, the elastic-plastic behavior can be interpreted in terms of stress states relevant to the state boundary surface in Figure 9.15. When the specimen is compressed to point g , the boundary surface with envelopes y_1 , y_2 and y_3 is formed and the yield curve in p - S space is YC_1 . Then the mean stress is decreased to point d_1 or point O' , and shearing is begun along $d_1d_2d_3$ ($O'd$ in Figure 9.12). In order to follow the stress path, increasing deviator stresses require decreasing mean stresses, and therefore increasing suctions, producing successively higher stress ratios η_s . The corresponding yield envelopes are y_1 , y_2 and y_3 as shown in the figure. At point d_2 on the stress path, the current deviator stress is still on the initial state boundary surface, and therefore the specimen still behaves elastically. Further shearing from point d_2 to point d_3 will lead to rupture since point d_3 is a failure state which is above the critical state line L_3 for yield envelope y_3 . Stress-strain behavior of a specimen following stress path $\Delta p/\Delta q = -1/3$ is shown in Figure 9.14 (the solid curve OAB in the figure for specimen T16540). The stress-strain behavior of the specimen T16540 can be viewed in two stages. Stage OA is largely elastic and the following stage

AB indicates a transition from elastic behavior to failure. In these stress-controlled triaxial tests, strain softening cannot be monitored and therefore cannot be seen in the observed stress-strain curves. In comparison with the strain hardening behavior of the curve OA'B', it is reasonable to suggest that the specimen following stress path $\Delta p/\Delta q = -1/3$ in Figure 9.14 behaves by-and-large elastically but not linearly before failure.

Behavior of other specimens following different stress paths can be interpreted in similar ways using the proposed 'stress-ratio based model'.

9.4 Development of an Elastic-plastic Model for Unsaturated Sand-bentonite

9.4.1 Yielding

Yielding was observed under isotropic compression in both series of tests. Yield stresses are shown in Figure 9.16. In the testing program, all specimens were consolidated to points g_1 and g_2 following the lines of $A_1O_1'g_1$ or $A_2O_2'g_2$. They were then subsequently unloaded to $p = p_c/2$ or $p_c/3$. Initial yield stresses were identified at points O_1' and O_2' for specimens from series 1 and series 2 respectively. As expected, measured suctions during isotropic compression decreased with increasing pressure. The relationships appear to be only lightly curved and can be approximated by two straight lines. The specimens at the beginning of loading had average suction values located at A_1 and A_2 . They can be therefore expressed as follows:

$$S_t = S_0 - \Delta p/v \quad [9.9]$$

where S_t is current total suction, p is mean stress, S_0 is the starting total suction, and v is slope of the p - S lines. Expression [9.9] can be written as:

$$\Delta p = v \Delta S_t \quad [9.10]$$

The measured slope v for both series of specimens is 1.2.

$$\Delta p = 1.2 \Delta S_t \quad [9.11]$$

The curved line II' through O_1' and O_2' represents an approximate initial yield locus LSY under isotropic compression in p - S space for the specimens after initial compaction. Before data at more yield stresses are available, a linear relationship may be assumed for small changes in p and S (Bolzon *et al.* 1996). Experimentally from this program, the slope α of the straight line II' in the range of p from about 0.8 – 1.3 MPa is:

$$\alpha = \frac{p_o' - p_o}{S_o' - S_o} = 0.33 \quad [9.12]$$

where p_o' , S_o' , p_o , S_o are mean stress and total suction at yielding for series 1 and series 2 of specimens respectively.

Increasing pressures after O_1' and O_2' produce volumetric plastic hardening and cause the yield stresses to increase to g_1 and g_2 respectively. These points were chosen during testing to have the same confining pressure, $p = 3$ MPa. However they lie on different LSY curves $g_1g'_1$ or $g_2g'_2$ respectively as shown in Figure 9.16.

As a first approximation, the curves $g_1g'_1$ and $g_2g'_2$ can be assumed to be parallel to the initial yield locus II' . The LSY curves $g_1g'_1$ and $g_2g'_2$ for specimens of series 1 and series 2 can therefore be approximated over small changes in p (or S) as follows:

$$p - 0.33 \times (S_t - S_c) - 3000 = 0 \quad [9.13]$$

where S_t is current total suction in MPa, S_c is total suction at isotropic pressure at 3000 kPa. That is, $S_c = S_{g1}$ and $S_c = S_{g2}$ for specimens of series 1 and series 2 respectively.

Results from the drying-wetting tests presented in Chapter 4 indicate that unsaturated buffer specimens (S_t : 85%, w : 19.4%, and γ_d : 1.67 Mg/m³) behave elastically with increasing total suction even up to 10 MPa of total suction used in the tests. Suction yielding stresses have therefore not been identified. For this reason, the test results of the present study do not allow the determination of a full, closed yield locus in p - S space such as the one schematically shown earlier in Figure 9.3.

In modelling terms, the yield locus for unsaturated buffer can be drawn schematically in p - S space in Figure 9.17 in a form of open funnel even though earlier discussion introduced the idea that it will be closed. The open funnel is applicable to the stress paths examined in this thesis. The figure also shows two stress paths Ab_1b_2 and Bc_1c_2 which correspond to stress paths $A_1O'_1g_1$ or $A_2O'_2g_2$ in Figure 9.16 for tests under constant mass condition. The effects of suctions on the motion of yield loci and on preconsolidation pressures for over-consolidated specimens are noted as follows. Yield loci a_2c_2 and a_3b_2 were formed after specimens starting from different initial suctions at A and B were compressed to the same mean stress p_o . Following unloading from b_2 or c_2 , the specimens

become over-consolidated. The idea of 'preconsolidation pressure' is a concept which arises from the behaviour of saturated soils. It is the past highest effective pressure that a specimen has encountered. However, more care needs to be taken to define preconsolidation pressures for unsaturated soils. They are not simply the mean stress p at c_2 and b_2 where unloading starts, but rather, pressures lying at the extreme end of their yield envelopes in constant η_c or $q-p_c$ planes. For example, a specimen is unloaded from point b_2 along the line Ab_1b_2 to point i , giving a current suction S_i and mean stress p_i . The associated yield envelope in the $q-p_c$ plane for this stress state (p_i, S_i) lies on a radial stress path Oi which extends to intersect with common yield locus a_3b_2 . The corresponding equivalent pressure p'_c on the yield locus a_3b_2 becomes the pre-consolidation pressure denoted here as p'_{cc} . That is, pressures of over-consolidated specimens are associated with current suction, mean stress and the yield locus in p - S space. By definition,

$$p'_{cc} = \sqrt{p_c^2 + S_c^2} \quad [9.14]$$

$$\frac{S_c}{p_c} = \frac{S_i}{p_i} = \eta_c \quad [9.15]$$

Expressions [9.14] and [9.15], together with expression [9.13] for yield locus, can be used to determine preconsolidation equivalent pressure p'_{cc} for the tested unsaturated sand-bentonite buffer material.

9.4.2 State Boundary Surface and Yield Envelopes

According to the 'stress-ratio based model', the state boundary surface in p-q-S space for unsaturated soils should be viewed as a family of yield envelopes in a series of vertical planes along stress paths at constant stress ratios of S/p . Experimental development of such a state boundary surface can therefore be made by determining a series of yield envelopes in q-p_c with constant stress ratios. In this study however, the test series did not follow stress paths of constant stress ratios, but rather paths with $\Delta S/\Delta p = -1.2$. Stress paths of test series 1 and 2 separately were presented earlier. Figure 9.12 shows one of these series schematically. Note that the stress ratio η_s changes with the addition of the applied stress increments of p and q. Specimens yielded at points a, b, c, and d on the state boundary surface depending on stress paths during shearing. The state boundary surface is then defined schematically by the yield envelopes of e, Oaa', Obb', and Occ' shown in Figure 9.12. Points f, a, b, and c are on the stress state boundary surface and points e, a', b', and c' lie on a yield curve in p-S space.

Figure 9.18 shows data for yield stresses during the shearing phase of the two series of tests. Note however that the results must really be considered in p-q-S space, and not just in the p-q space shown in Figure 9.18. Yielding occurs at different suctions and mean stresses, giving different constant stress ratios η_s . In contrast with what is usually done for saturated soils, the data in Figure 9.18 should not simply be connected to produce yield envelopes. More careful treatment of the results is needed. Each yielding data

point corresponds to a different vertical plane with constant stress ratio η_s and yield trace on the state boundary surface. The trace varies in size and depends on the respective preconsolidation equivalent pressure p_{ec} in p - S space. The best way to interpret the yielding data is to normalize in such a way that yield data in planes of constant stress ratios can be mapped to the yield envelope for the corresponding saturated soil ($\eta_s = 0$ due to zero suction with $S_r = 100\%$). This follows the developing trend in unsaturated soil mechanics to make sure that any model reduces to the special case for saturated soil when $S = 0$, $S_r = 100\%$.

Normalization has been conducted here for the first time with respect to preconsolidation equivalent pressure p_{ec} . The pressure p_{ec} for each value of q - p - S at yielding is determined using expressions [9.12] – [9.14]. Results are tabulated in Table 9.1. It should be noted that the yield loci in p - S space for the two series of specimens are different as shown in Figure 9.17, thereby producing different preconsolidation equivalent pressures for the same stress ratio. It should also be remembered that saturated buffer specimens have an osmotic suction of about 1.5 MPa on average (Wan 1996, Tang *et al.* 1997a). Suction data measured in the testing program are total suctions S_t . It is believed that osmotic suction changed very little during triaxial tests (Fredlund and Rahardjo 1993, Tang *et al.* 1997a), and therefore matric suctions can be calculated from measured total suctions minus the constant osmotic suction value, here taken to be about 1.5 MPa. Calculated matric suctions are used for all plots in the proposed model.

Using this approach, any stress state at yielding (q, p_e) can be normalized by:

$$q/p_{ec} \text{ and } p_e/p_{ec}$$

The values before and after normalization are tabulated in Table 9.1.

Table 9.1: Normalization of yield stress

Test	T16530	T16531	T16533	T16534	T16535	T16540	T16541	T16542
($\Delta p/\Delta q$)	(1/3)	(0)	(-1/3)	(1)	(0)	(-1/3)	(0)	(1)
q_y (kPa)	1200	1200	1150	1000	1190	1490	1450	1200
p_y (kPa)	1900	1500	1120	2500	1000	1010	1500	2700
S_y (MPa)	2.40*	2.76	2.90	2.00	3.05	4.10	3.70	2.45
S_m (MPa)	0.90	1.26	1.40	0.50	1.55	2.60	2.20	0.95
η	0.47	0.84	1.25	0.20	1.55	2.57	1.47	0.35
p_c (kPa)	3556	4151	5106	3212	6141	17303	5047	2946
S_{mc} (kPa)	1.68	3.49	6.38	0.64	9.52	44.54	7.40	1.04
p_{ec} (kPa)	3935	5421	8174	3276	11328	47785	8958	3123
p_{ey} (kPa)	2102	1959	1793	2550	1845	2789	2663	2862
q_{ey}/p_{ec}	0.30	0.22	0.14	0.31	0.11	0.03	0.16	0.38
p_{ey}/p_{ec}	0.53	0.36	0.22	0.78	0.16	0.06	0.30	0.92

where: q_y , p_y and S_y are respectively deviator stress, mean stress, and total suction at yielding

$$S_m \text{ is matric suction } S_m = S_y - S_\pi = S_y - 1.5 \text{ (Osmotic suction } S_\pi \approx 1.5 \text{ MPa)}$$

p_c and S_{mc} are mean stress and matric suction at preconsolidation equivalent pressure point

$$p_{ec} = \sqrt{p_c^2 + S_{mc}^2} \text{ is preconsolidation equivalent pressure}$$

$$p_{ey} = \sqrt{p_y^2 + S_{my}^2} \text{ is equivalent pressure}$$

* Due to failed measurement at this point, suction value is inferred

using expression [8.3].

Figure 9.19 plots the normalized yield data represented in Table 9.1 and in Figure 9.18. An additional yield data $p_e/p_{ec} = 1$ at $q/p_{ec} = 0$ is shown in the figure as well. For specimens under isotropic compression immediately before unloading, such as points b_2 and c_2 in Figure 9.17, their equivalent pressure p_e is equal to p_{ec} , and hence $p_e/p_{ec} = 1$.

Also shown in the figure are yield data obtained from triaxial tests conducted on saturated buffer (Oswell 1991). The saturated buffer had the same dry density ($\gamma_d = 1.67 \text{ Mg/m}^3$) but slightly different water content ($w = 22\%$). Both sets of data for saturated specimens and for unsaturated specimens exhibit scatter to some degree, but generally they constitute a unified normalized yield envelope. The scatter is not noticeably worse than values obtained from much simpler tests on saturated specimens of many clays. The single yield envelope obtained in Figure 9.19 indicates good agreement of normalization on data from both unsaturated and saturated specimens. It is interesting to note that normalization of the unsaturated data was conducted using preconsolidation equivalent pressures p_{ec} obtained from the present study while yield data for saturated specimens were normalized using the classic definition of preconsolidation pressure p'_c and results obtained by Oswell (1991). The good agreement between unsaturated and saturated data in Figure 9.19 validates the use of equivalent pressure p_e as a stress variable (in conjunction with the stress ratio η_s) as a way of combining the effects of mean stress and suction. This appears to provide for the first time a way of examining p , q , S -data at different stress states relative to the state boundary surface. The yield envelope of the saturated buffer developed by previous researchers (Oswell 1991, Graham *et al.* 1992) can be used as a reference for the same soil under unsaturated conditions.

The shape of the unified yield envelope is not elliptical but is typical of results obtained for many clayey soils that are inherently anisotropic (Graham *et al.* 1986, Wood 1990, Cui and Delage 1990). Low normalized values of q_y/p_{cc} and p_y/p_{cc} (less than about 0.2) are noted in the figure for the unsaturated tests. This may possibly be due to the assumption that the yield curve LSY in p-S space is straight (Figure 9.16), giving preconsolidation equivalent pressures p_{cc} that are a little too high. As pointed out earlier, LSY yield curves should be curved and closed, producing smaller values of p_{cc} , and hence larger values of q_y/p_{cc} and p_y/p_{cc} .

9.4.3 Flow Rule

As mentioned earlier, in elastic-plastic modelling, strains are divided into elastic and plastic parts, that is, $\Delta\varepsilon_v = \Delta\varepsilon_v^e + \Delta\varepsilon_v^p$, and $\Delta\varepsilon_s = \Delta\varepsilon_s^e + \Delta\varepsilon_s^p$. The 'association' of the flow rule can be examined by comparing the direction of the plastic strain vectors $\Delta\varepsilon_s^p/\Delta\varepsilon_v^p$ to the normals of the yield envelope.

An attempt was made to determine $\Delta\varepsilon_v^p$ and $\Delta\varepsilon_s^p$ at yielding for all the unsaturated buffer specimens that were tested, and in this way to examine the nature of the flow rule for this material. Figures 9.20 and 9.21 illustrate typically how to determine elastic and plastic strain components in plots of q versus ε_s and p versus ε_v respectively. Plastic strains have been separated from elastic strains graphically following the technique used by Oswell (1991). The plastic strains are scaled off the graphs at the separation of the elastic and

plastic segments in the stress-strain plots, for the selected applied stress increment. The increment of plastic shear strain $\Delta\varepsilon_s^p$, is easily and accurately determined. As illustrated in Figure 9.20, $\Delta\varepsilon_s^p = 5\%$ for $\Delta q = 100$ kPa at the yielding point. During shear, the mean stress p increases from approximately 1500 kPa to 2000 kPa. As shown in Figure 9.21, the increase in mean stress p produces a total of 0.2% volumetric strain. The plastic volume strain $\Delta\varepsilon_v^p$, out of the small magnitude of total volume change (0.2%) is difficult to determine accurately. This is because the stress paths during shearing used in the testing program lie in a vertical plane which is broadly vertical to each yield envelope as shown in Figure 9.12. To follow the stress paths, increases in mean stress must be accompanied by decreases in suction, or vice versa, thereby producing small variations of equivalent pressure for all stress paths during shear. Consequently, the stress paths give rise to large shearing strains but to small volume strains under shear. As a result, it has not been possible to determine the plastic strain increment vectors with confidence. Data for $\Delta\varepsilon_s^p$, and $\Delta\varepsilon_v^p$, have therefore not been included in the yield envelope diagram in Figure 9.19.

Non-associated flow rules have been suggested for several unsaturated soils in terms of 'constant-suction based model', for example, as reported by Alonso *et al.* (1990), Wheeler and Sivakumar (1994), and Cui and Delage (1996). It should be noted however, that measurements frequently underestimate plastic volume strains, particularly in load-controlled tests. Some of the materials may be more 'associated' than the data suggest.

The question of whether the flow rule for unsaturated buffer is associated or non-associated cannot be determined until more test data are available.

9.4.4 Hardening Law

Isotropic compression tests on two series of unsaturated specimens provide a data base of volume change measurements to determine parameters for the hardening law. In Figure 9.22, two representative stress paths of specimens T16533 and T16540 from each series show suction change *versus* mean stress. Volume changes are plotted in Figure 9.23 in terms of specific volume V and mean stress p . Each curve exhibits two approximately linear segments representing separate elastic zones and plastic zones of behaviour in the same way as in overconsolidated saturated soils. Since in these constant-mass tests, suction changes accompanied compression, volume change can be understood better in a V - p - S space as shown in Figure 9.24. In this figure, a volumetric state boundary surface (Delage and Graham 1995) has been drawn in schematically to fit the data. The behavior of initial yielding and strain hardening as shown in the figure appears to support the model suggested by Delage and Graham (1995).

As pointed out in Section 9.2.4, the volumetric hardening law is defined as follows:

$$V = V_0(\eta_s) - \lambda(\eta_s) \ln(p_e) \quad [9.16]$$

The expression relates specific volume V to equivalent pressure p_e through two parameters V_0 and λ . V_0 is specific volume at $p_e = 1$ and λ is stiffness parameter. Both V_0 and λ depend on the stress ratio η_s .

Although the volume change data plotted in Figure 9.23 do not directly allow the relationships between V_0 and λ to the stress ratio η_s to be evaluated, a number of imaginary stress paths with constant stress ratios can be selected in the post-yield range in Figure 9.22. Measured volume changes along these imaginary selected stress paths η_1 , η_2 , and η_3 are shown in Figure 9.24 (arithmetic scale) and in Figure 9.25 in a diagram (log scale) of specific volume *versus* equivalent pressure p_e . As seen in the figure, the stiffness parameter $\lambda(\eta_i)$ varies somewhat with stress ratio η_i ($i = 1, 2, 3$). The higher the stress ratio, the greater the stiffness parameter. This reflects the fact that specimens become stiffer at higher suctions (Graham *et al.* 1995). Values of $\lambda(\eta_i)$ are determined by:

$$\lambda(\eta_i) = \Delta V / \Delta \ln p_e \quad [9.17]$$

Table 9.2 presents the calculated parameters V_0 and λ at the selected stress ratio η_i . It should be noted that only limited data are available at this stage for assessment of the parameters of the hardening law. More data can be expected to provide a better understanding of the mechanisms involved within the framework established in preceding paragraphs.

Table 9.2: Parameters of stiffness

	$\eta_1 = 0.3$	$\eta_2 = 0.8$	$\eta_3 = 1.8$
V_0	1.944	1.916	1.920
λ	0.051	0.045	0.041

As expected, the test results in Figure 9.25 show that specific volume decreases under proportional application of suction and pressure, that is, when the stress path follows a line with constant stress ratio η_i . An example is a specimen that is compressed with increasing equivalent pressure from a_2 to b_2 along a stress path η_2 . However, for an arbitrary stress path such as from point a_0 to a_1 in Figure 9.25 or Figure 9.22, the equivalent pressure decreases from 2.7 MPa to 2.1 MPa ($p_e = (S_m^2 + p^2)^{1/2}$), this also leads to a decrease of specific volume from about 1.630 to 1.605. This is because equivalent pressure is a combination of suction and mean stress. Because the effects of pressure and suction on volume change are not equal quantitatively (Tang *et al.* 1998c), mechanical behavior can only be described using both equivalent pressure p_e and stress ratio η_s . The model developed in this thesis reflects the fact that the behavior of unsaturated soils depends on two stress variables, mean stress and suction or their alternatives equivalent pressure p_e and stress ratio η_s .

9.4.5 Critical State and M-values

All specimens in the two test series failed during shearing along the various stress paths shown in Figure 9.18. The figure shows the values of applied stresses q and p when failure occurred and also shows stress data at yielding. Visual inspection of the data indicates that the different stress paths $\Delta p/\Delta q = -1/3, 0, 1/3$ and 1 produce differences between the deviator stresses q at failure and at yielding. This suggests a transition from strain hardening when $\Delta p/\Delta q = 1$ and $1/3$ to strain softening when $\Delta p/\Delta q = 0$ and $-1/3$. This appears to support the concepts of the proposed state boundary surface illustrated in Figure 9.12. This figure shows that lower values of $\Delta p/\Delta q$ produce higher values of stress ratio η_s , and therefore larger yield envelopes. For specimens sheared at the selected stress paths O'a, O'b, O'c, and O'd, a transition from strain hardening to strain softening is therefore expected.

Once again, effect of suction on strength should be taken into account. Table 9.3 lists stress states (q, p, S) at failure. Equivalent pressure p_e and M value of failure envelope are calculated from

$$M = \frac{q}{p_e} \quad [9.18]$$

A value of $M = 0.53$ was reported by Graham *et al.* (1989) for saturated buffer at stresses up to about 3 MPa, giving a friction angle ϕ' of 14° . That is, the material is clay-dominated, with the sand acting simply as a filler. Values of M obtained from the

unsaturated specimens in this program varies from 0.45 to 0.71 depending on the stress ratio η_s . The corresponding friction angles vary from 13.6° to 18.5°.

Figure 9.26 compares M-values for unsaturated buffer and saturated buffer. The average of the M-values for unsaturated specimens is slightly higher than the M value of saturated buffer but generally shows good agreement. That is, Critical State failure in the stress-ratio controlled model may be associated with friction angles that are approximately constant. It is not clear whether the variation of M in Figure 9.26 is systematic or random. It is remembered that some specimens failed with little or no plastic strain hardening, implying that deviator stresses q at failure were above critical state lines. Deviator stresses q at critical states could not be measured in the stress-controlled triaxial tests performed in the program. In this case, values of M obtained from calculation using deviator stress q_f at failure can be expected to be slightly higher than values that correspond properly to q at critical state.

The M-data for unsaturated specimens of Series 1 show relatively more variations compared with the M-data of Series 2. As shown in Figure 9.16, specimens of Series 1 produce a larger yield locus LSY1 in p-S space than specimens of Series 2, but the equivalent pressure p_e are smaller. As a result, at high stress ratio η_s , specimens of Series 1 tend more to be above critical state lines than the specimens of Series 2 because of the way the tests were conducted. This will produce higher M-values. Despite the complex

shape of the SBS in Figure 9.8, the ellipses have the same general shape – M is related to the ratio of minimum to maximum axis.

It is interesting to note that in this material and in the stress range used in the tests, the value of M is largely independent of suction as shown in Figure 9.26. That is, the friction angle ϕ' is about equal at any stress ratio η_s . This is very different from the values produced by the constant-suction model in Table 8-5. The relatively constant value of ϕ' is explained by the fact that the buffer material is highly plastic clay and suction can be very high (for example, suction is 40 MPa at water content of about 10% (see Figure 4.10)). In the tested range of suction ($S < 6.5$ MPa), the fact that M -values of unsaturated specimens are approximately equal to the M -value of saturated buffer confirms that at low suctions ϕ' and ϕ^b are about equal as observed by Escario and Saez (1986) and Fredlund *et al.* (1987). The author notes that this behaviour is different from what is commonly reported for sands, silts, and low-plastic clays. In these materials, ϕ^b tends to decrease with increasing suction. The difference may lie in the surface activity of bentonite in the buffer which is much higher than in other soil types. At very high suctions, some differences may be present. At these suctions, two effects will be competing. In one, high suctions will be working on successively smaller surface areas in the pedal aggregates. In the other, particle separations may approach conditions where van der Waals attractive forces may induce properties approaching those of ceramics.

Table 9.3: Stresses at failure and the related parameters

Test ($\Delta p/\Delta q$)	T16530 (1/3)	T16531 (0)	T16533 (-1/3)	T16534 (1)	T16535 (0)	T16540 (-1/3)	T16541 (0)	T16542 (1)
q_f (kPa)	1374	1390	1291	1250	1250	1519	1601	1634
p_f (kPa)	1959	1500	1070	2750	1000	994	1500	3134
S_f (MPa)	2.40*	2.76	3.00	1.79	3.10	4.30	4.00	2.10
S_m (MPa)	0.90	1.26	1.50	0.29	1.60	2.80	2.50	0.60
p_c (kPa)	2156	1959	1843	2765	1887	2971	2915	3191
η	0.46	0.84	1.40	0.11	1.60	2.82	1.67	0.19
M	0.64	0.71	0.70	0.45	0.66	0.51	0.55	0.51
ϕ' (°)	16.7	18.5	18.3	12.1	17.4	13.6	14.6	13.6
M_p	0.70	0.93	1.21	0.45	1.25	1.53	1.07	0.52

where: S_m is matric suction at failure $S_m = S_f - S_z = S_f - 1.5$ (osmotic suction $S_z \approx 1.5$ MPa)

$$\text{Equivalent pressure } p_c = \sqrt{p^2 + S_m^2}$$

$$M = q_f/p_c$$

$$\sin(\phi') = 3M/(6+M)$$

$$M_p = q_f/p_f$$

* Due to failed measurement at this point, suction value is inferred

using expression [8.3].

For comparison, Table 9.3 also shows conventional values of M_p for p-changes only. Here $M_p = q/p$ at critical state, where p is net mean stress or mean stress in this case. (u_s is negligible in this testing program, Wiebe 1996). The value of M_p defines the slope of the critical state line for an unsaturated specimen whose yield envelope and critical state line lie in a constant suction plane. According to the 'constant-suction based model', M_p at

any suction is equal to the M value of the soil at saturated states. Figure 9.27 shows values of the conventional M_p versus total suction. Data in the figure show that with this interpretation, M increases significantly with increasing suction. It can be as high as 1.53 at $S = 4.3$ MPa, giving a friction angle of 38° . This friction angle is obviously much too high for a saturated highly plastic clay. This observation supports the idea expressed previously that the mechanical behavior of unsaturated soils should not simply be examined at a series of constant suction values. The author considers that the contrasting interpretations arising from Figures 9.26 and 9.27 involve an innovative and very helpful way of understanding the shear behaviour of unsaturated plastic clays.

9.5 Discussion and Conclusion

This chapter has presented a new conceptual model for the elastic-plastic behaviour of unsaturated soils, specifically a high-plastic sand-bentonite mixture. A new yield envelope in q - S space has been proposed and a stress state boundary surface in p - q - S space has been elaborated based on the concept of constant stress ratio $\eta_s = S/p$. The model provides a good explanation for the elastic-plastic behavior of unsaturated buffer material as observed in stress-controlled triaxial tests conducted in this program. Yield envelopes were examined and normalization was performed to synthesize all data to a unified yield envelope. Determination of parameters used in the model has been demonstrated by fitting the model to data obtained in the tests.

The proposed model examines the behavior of unsaturated soils in terms of two variables: equivalent pressure p_e and stress ratio η_s . This is consistent with the generally accepted idea that two stress variables, usually taken to be the net mean stress ($p-u_d$) and matric suction (u_s-u_w), are required to describe unsaturated soil properties. (More generally, modeling requires also definition of the deviator stress q , the total volume change ϵ_v and changes in water content.) The proposed model differs from the existing model (Alonso *et al.* 1990) which describes soil behavior under external stress at any constant suction.

Although the data that have been measured for stress-strain behavior and strength properties can be interpreted well using the proposed model, some of the assumptions of the model need further examination and confirmation with additional data. For example, 'closure' of the yield locus in p - S space at high suctions needs to be confirmed experimentally in tests, which identify yielding through increasing suctions under various constant pressures. Tests of this nature on unsaturated buffer material are currently being conducted by fellow graduate student James Blatz at the University of Manitoba.

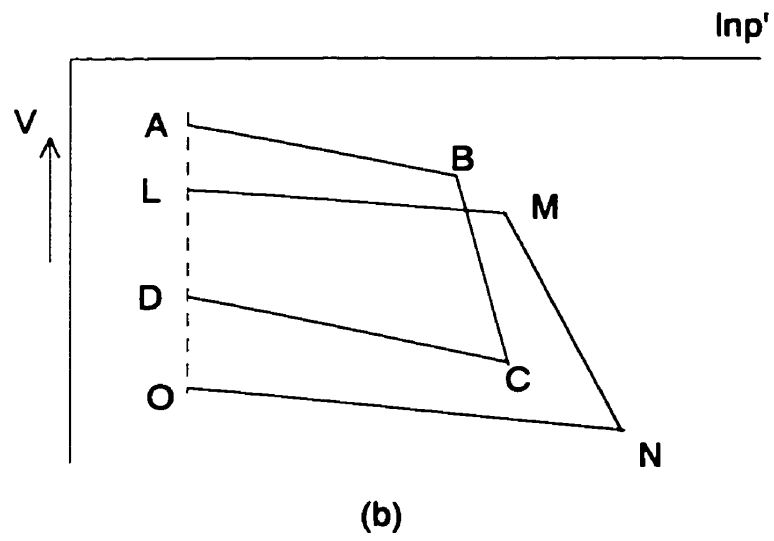
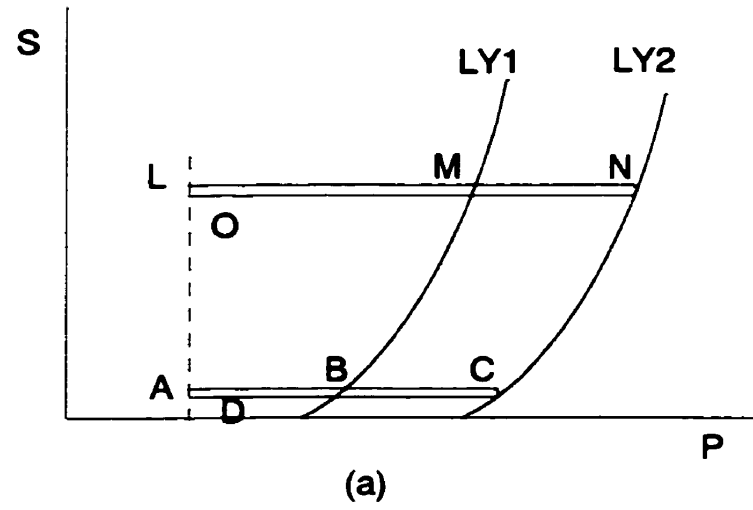


Figure 9.1 Schematic of load-induced yielding and development of a hardening surface (Alonso et al. 1987)

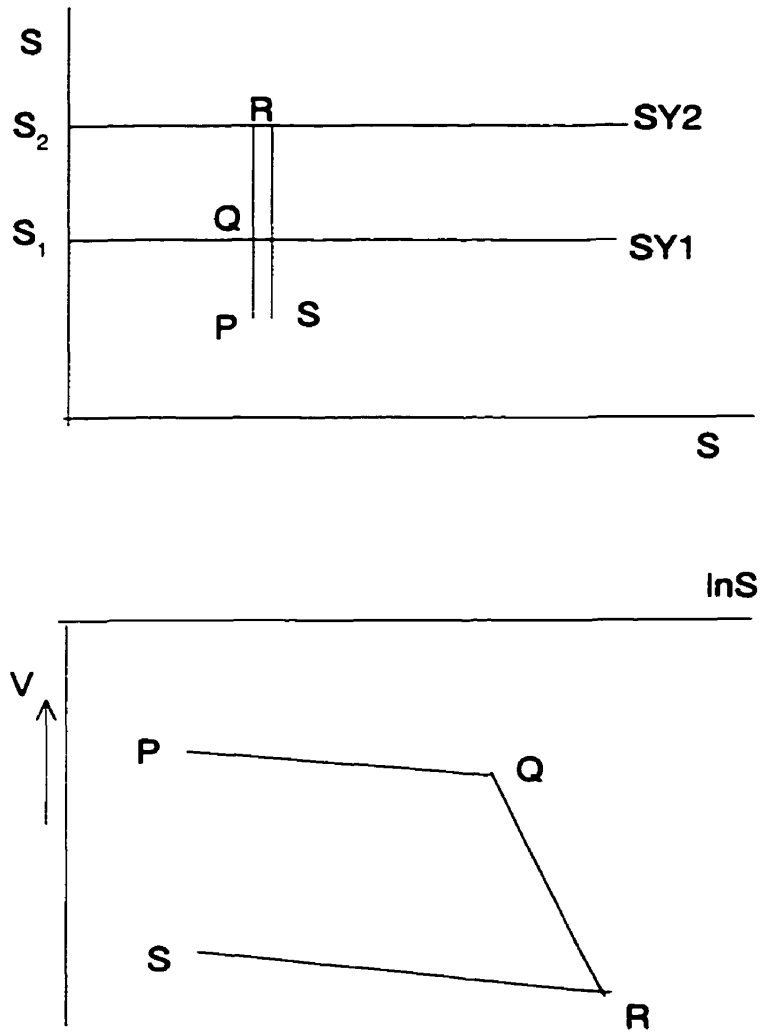


Figure 9.2 Schematic of suction-induced yielding and development of a hardening surface (Alonso et al. 1987)

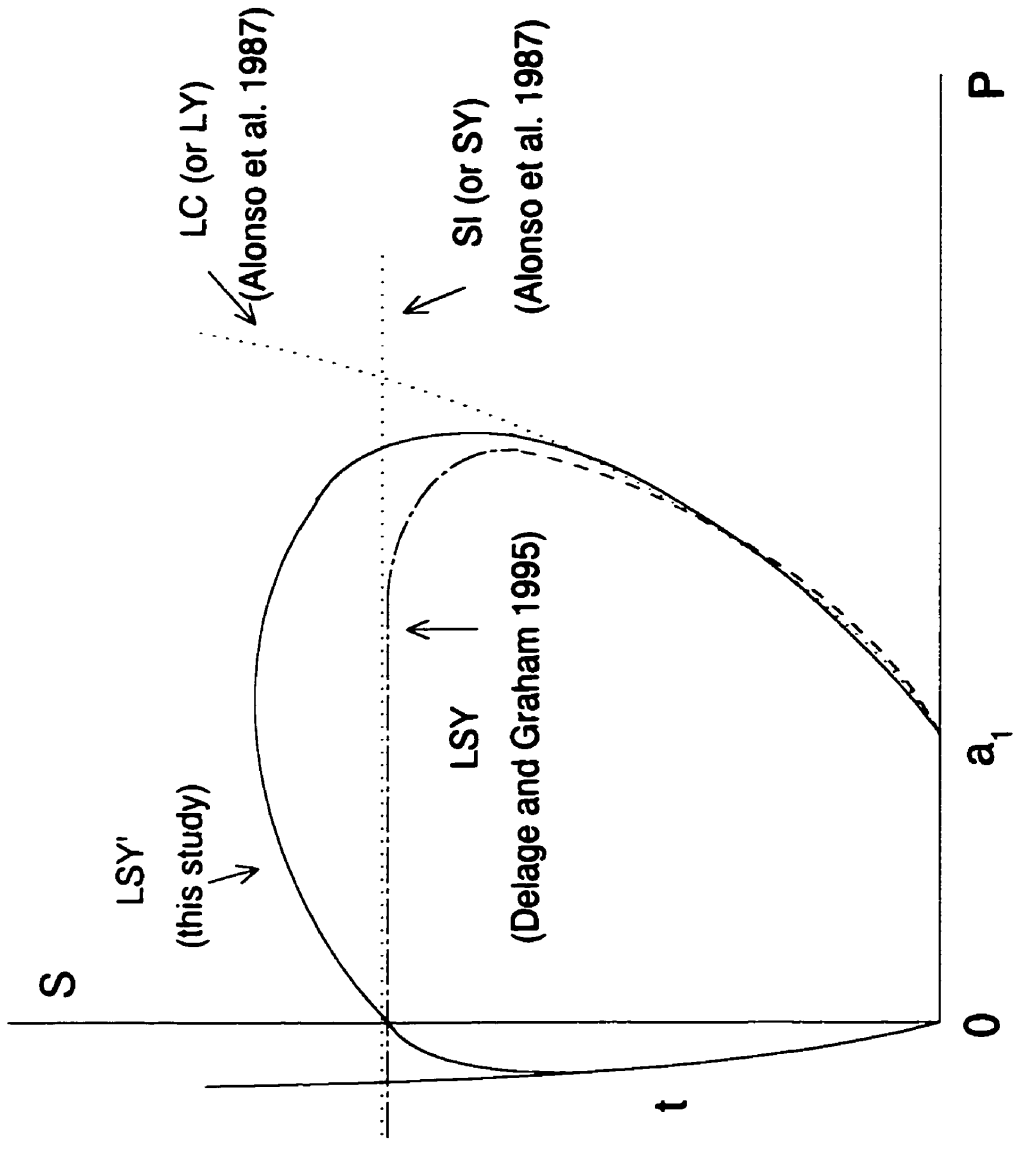


Figure 9.3 Yield curves under isotropic loading in p-S space

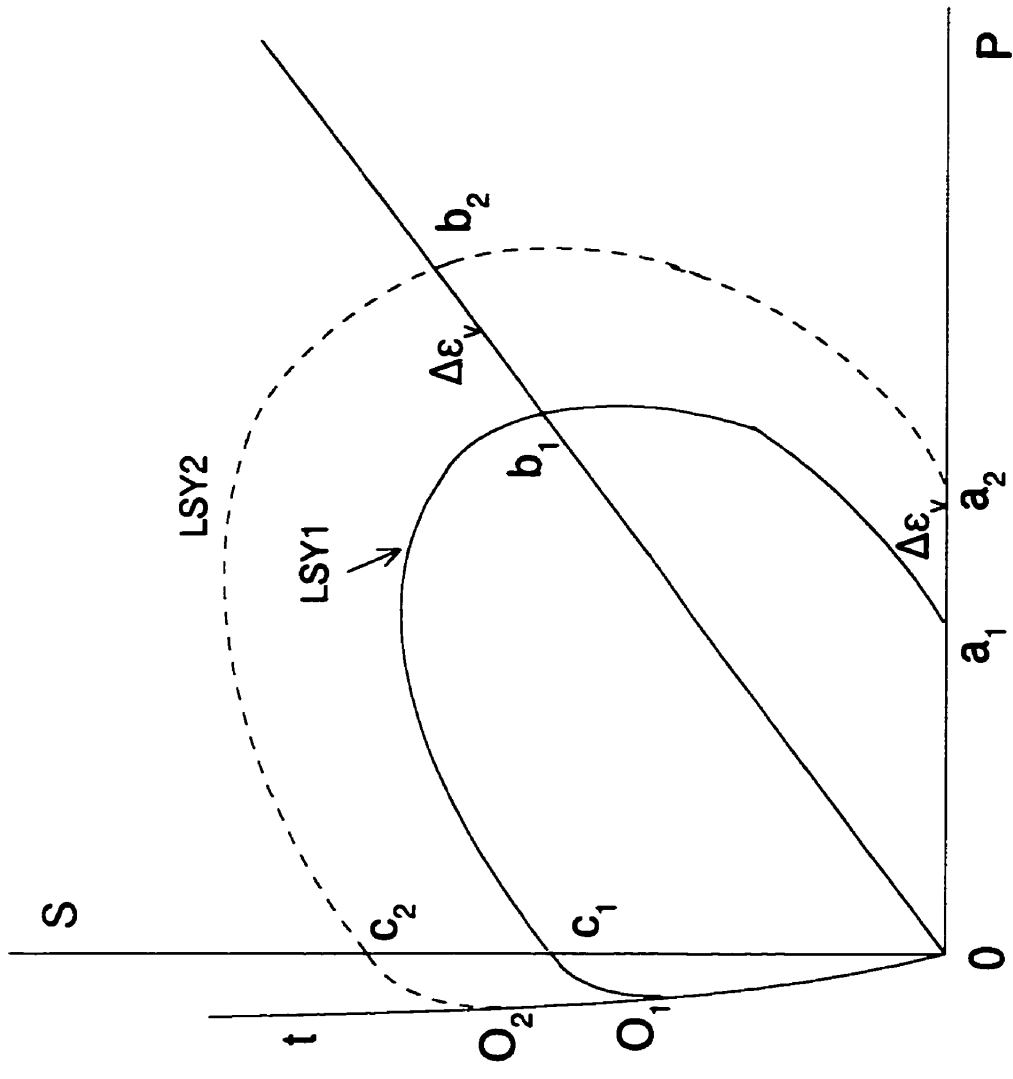


Figure 9.4 Yield envelopes at isotropic loading in p-S space

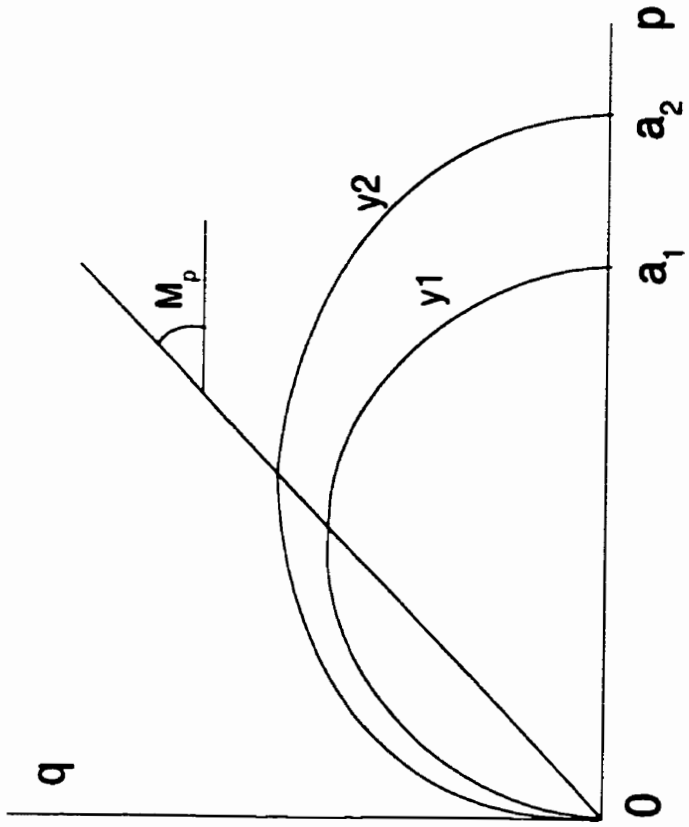
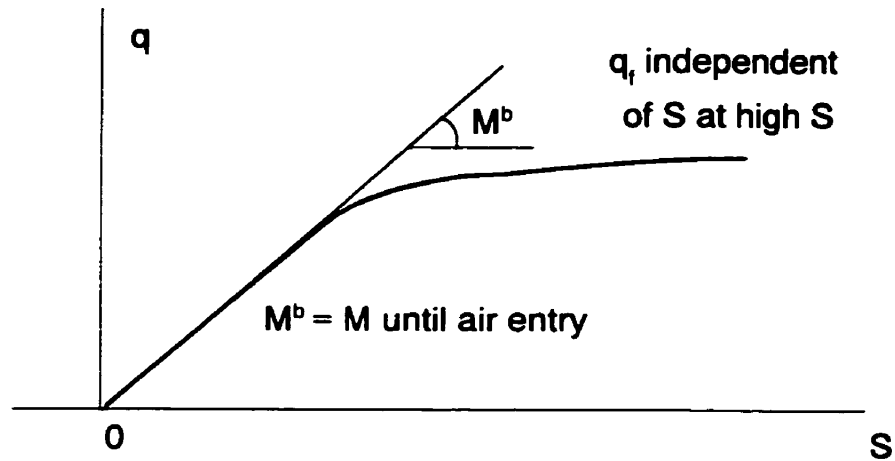
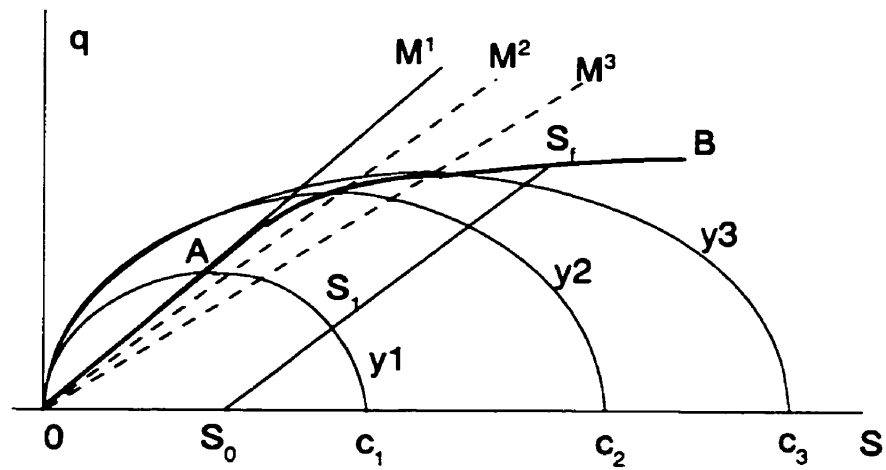


Figure 9.5 Yield envelopes for zero suction



a) Shear strength surface in $q - S$ space
(after Delage and Graham 1995)



b) Yield envelopes with increasing suction at $p = 0$

Figure 9.6 Yield envelopes in $q - S$ space

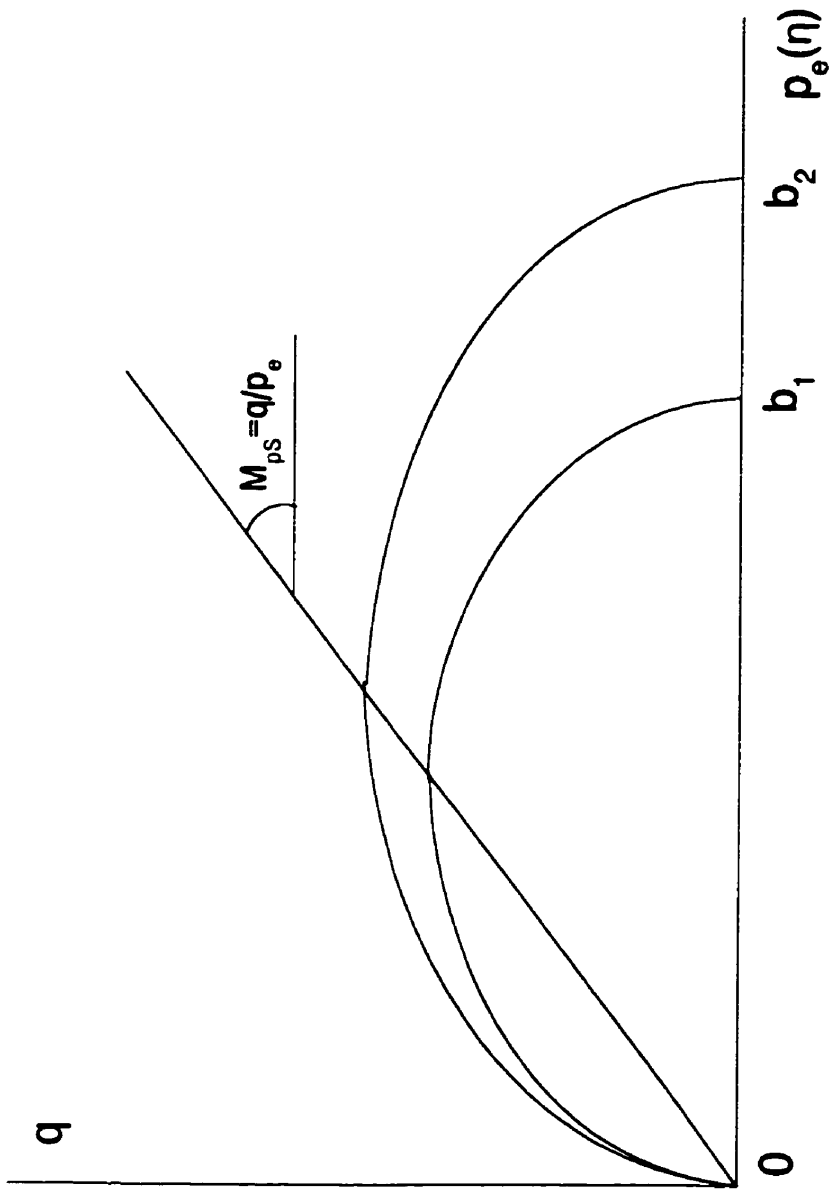


Figure 9.7 Yield envelopes in p - S space at stress ratio η

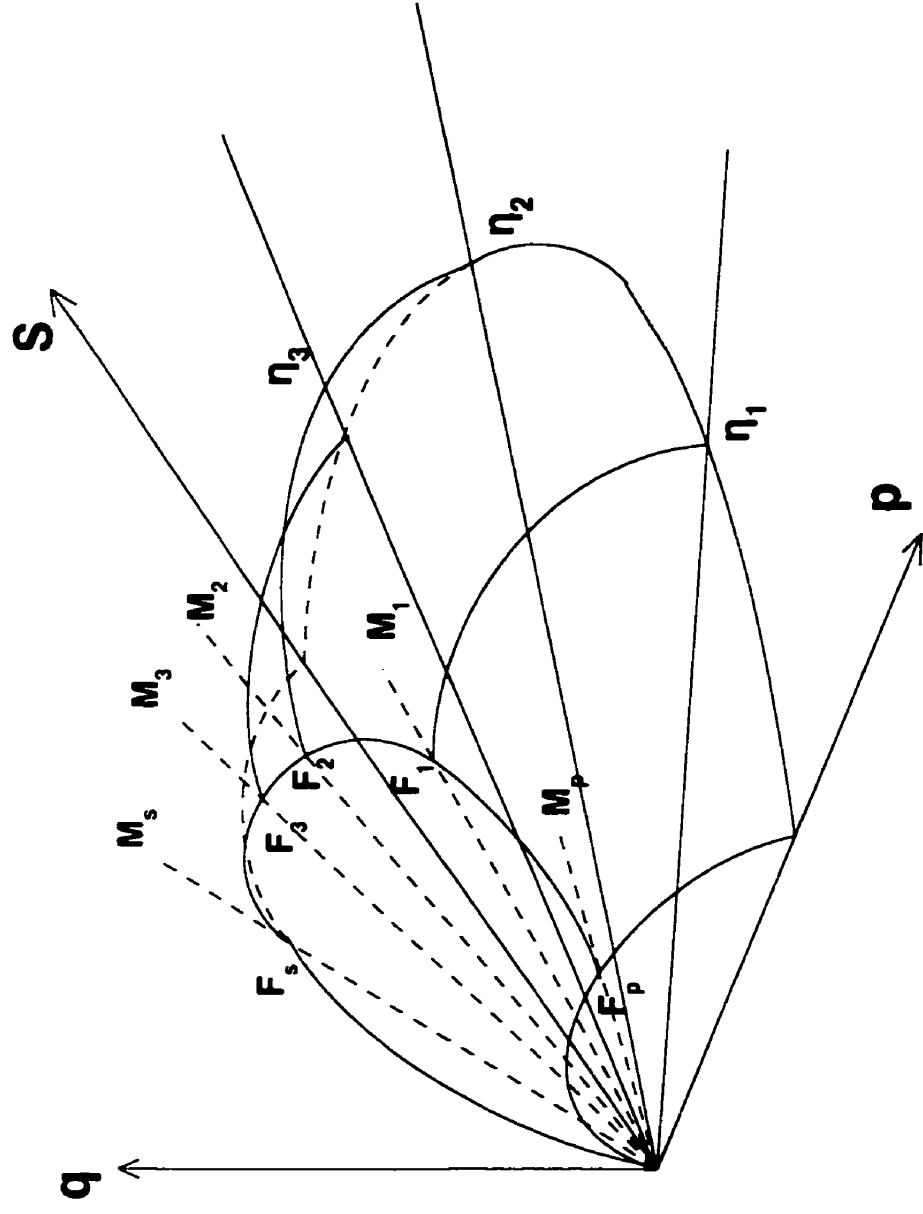


Figure 9.8 State boundary surface of the proposed conceptual model for unsaturated soils

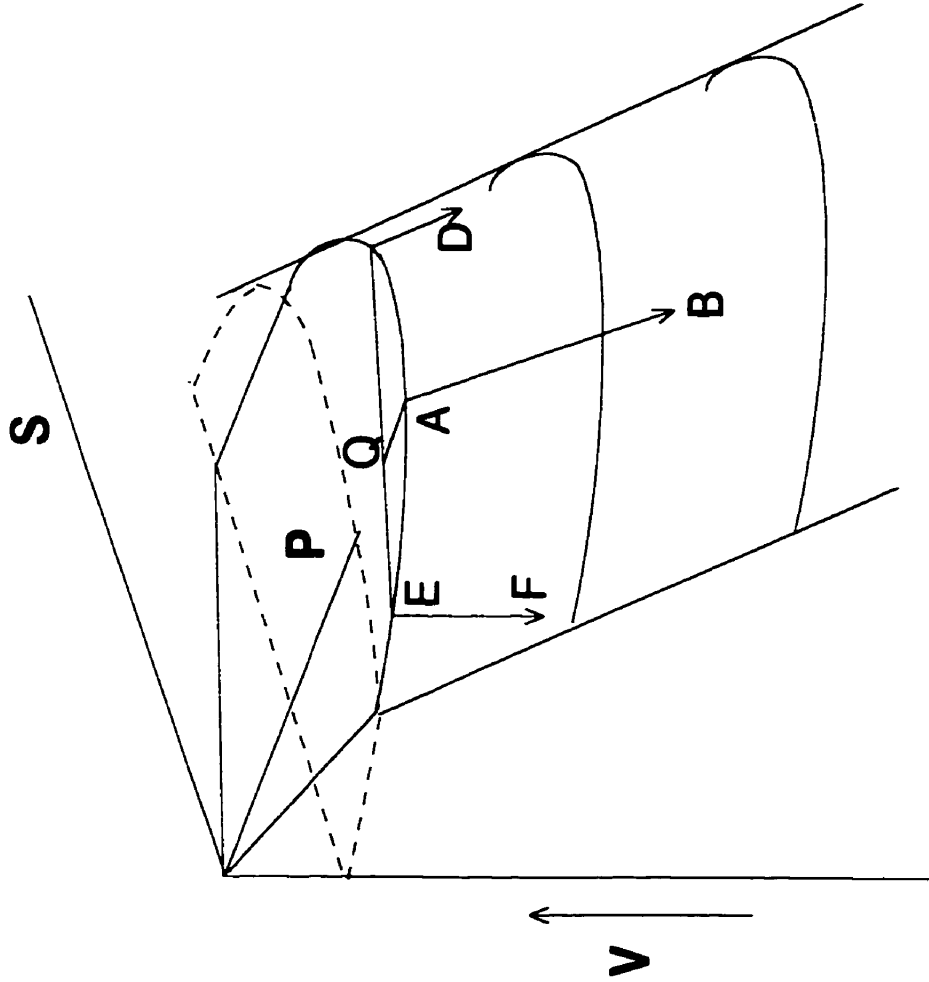
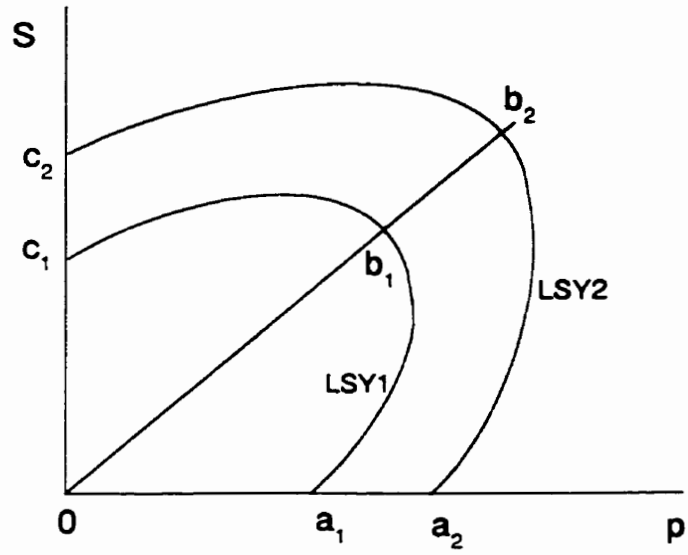
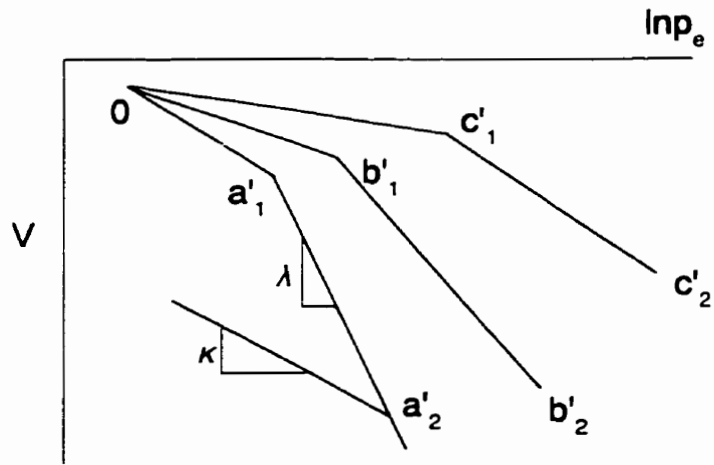


Figure 9.9 Compressibility for unsaturated soils
 (Delage and Graham 1995)



(a)



(b)

Figure 9.10 Volumetric hardening

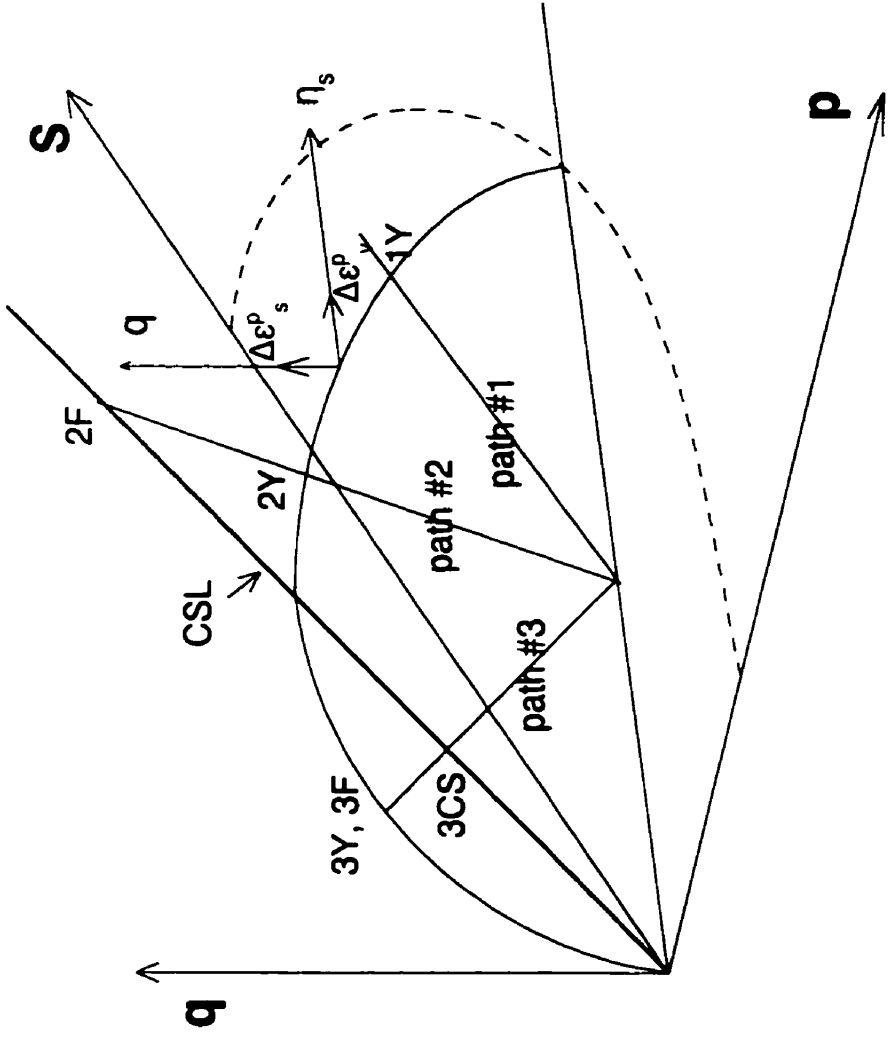


Figure 9.11 Elastic plastic behavior along various stress paths

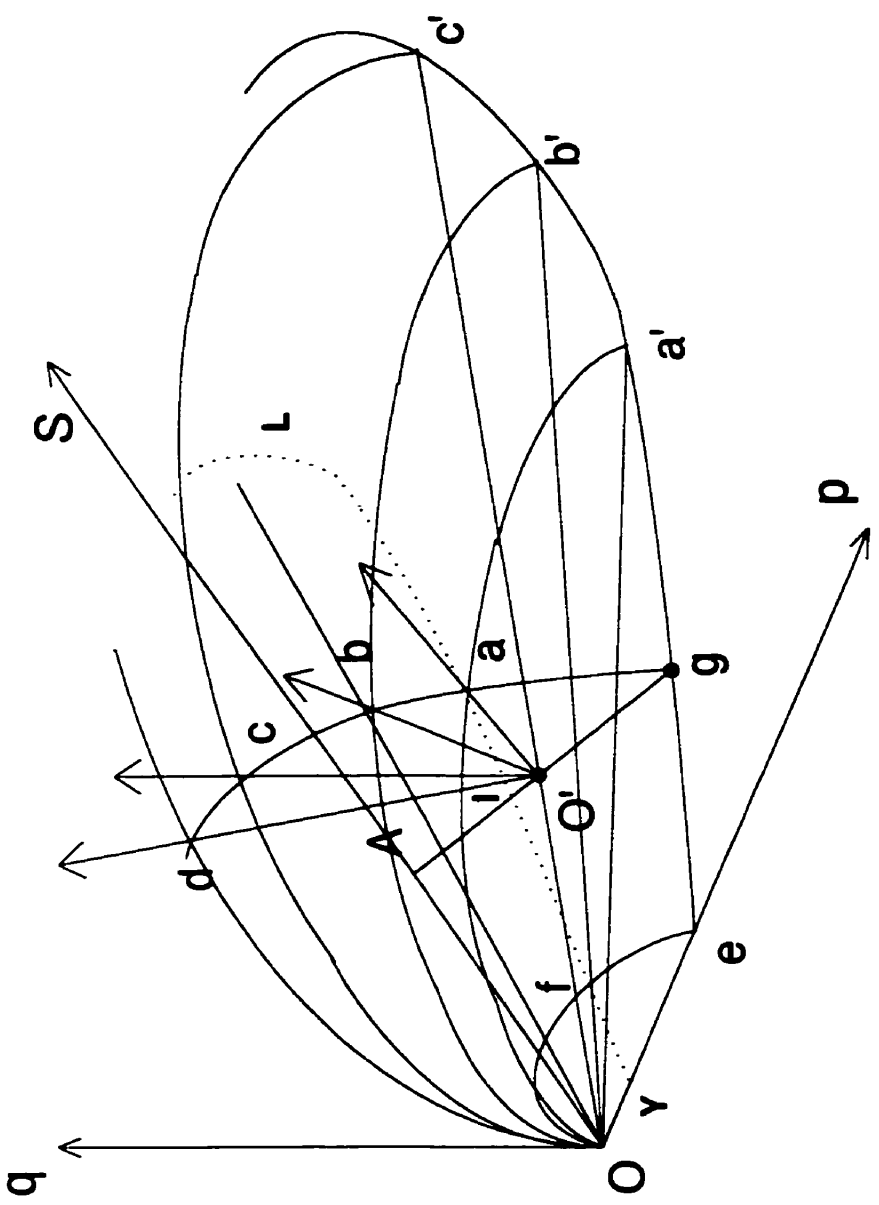


Figure 9.12 State boundary surface and yield envelopes

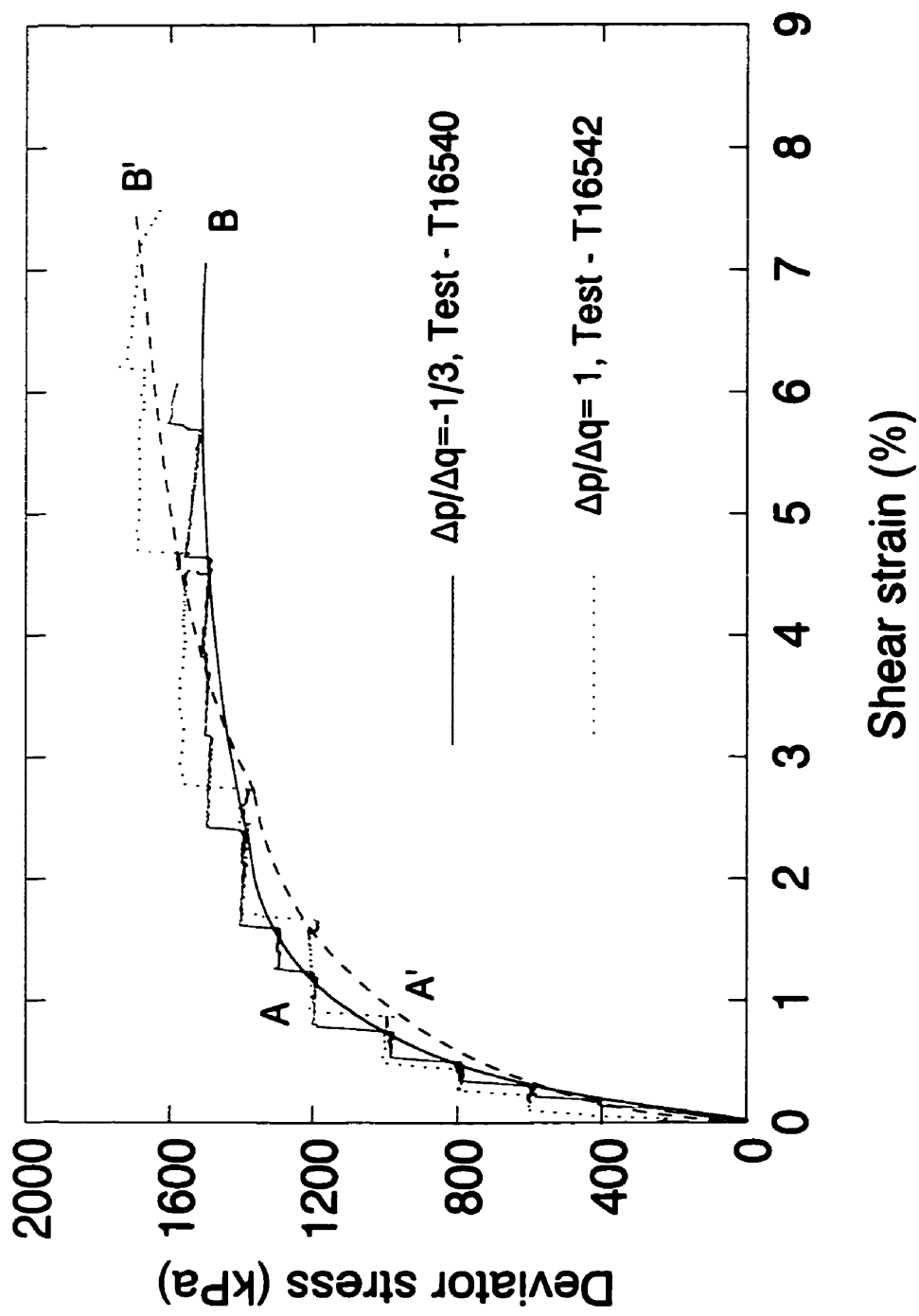


Figure 9.14 Stress-strain behavior at two stress paths

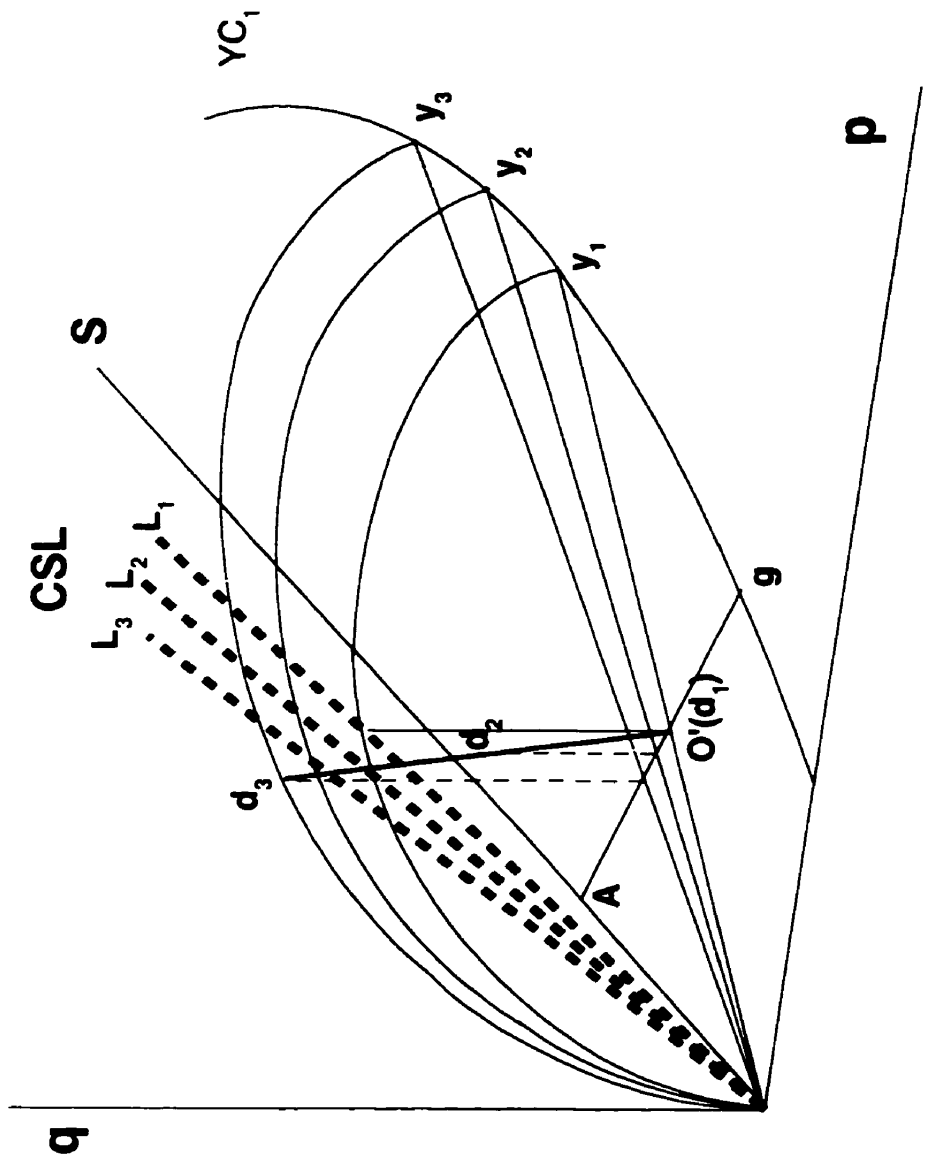


Figure 9.15 Strain softening

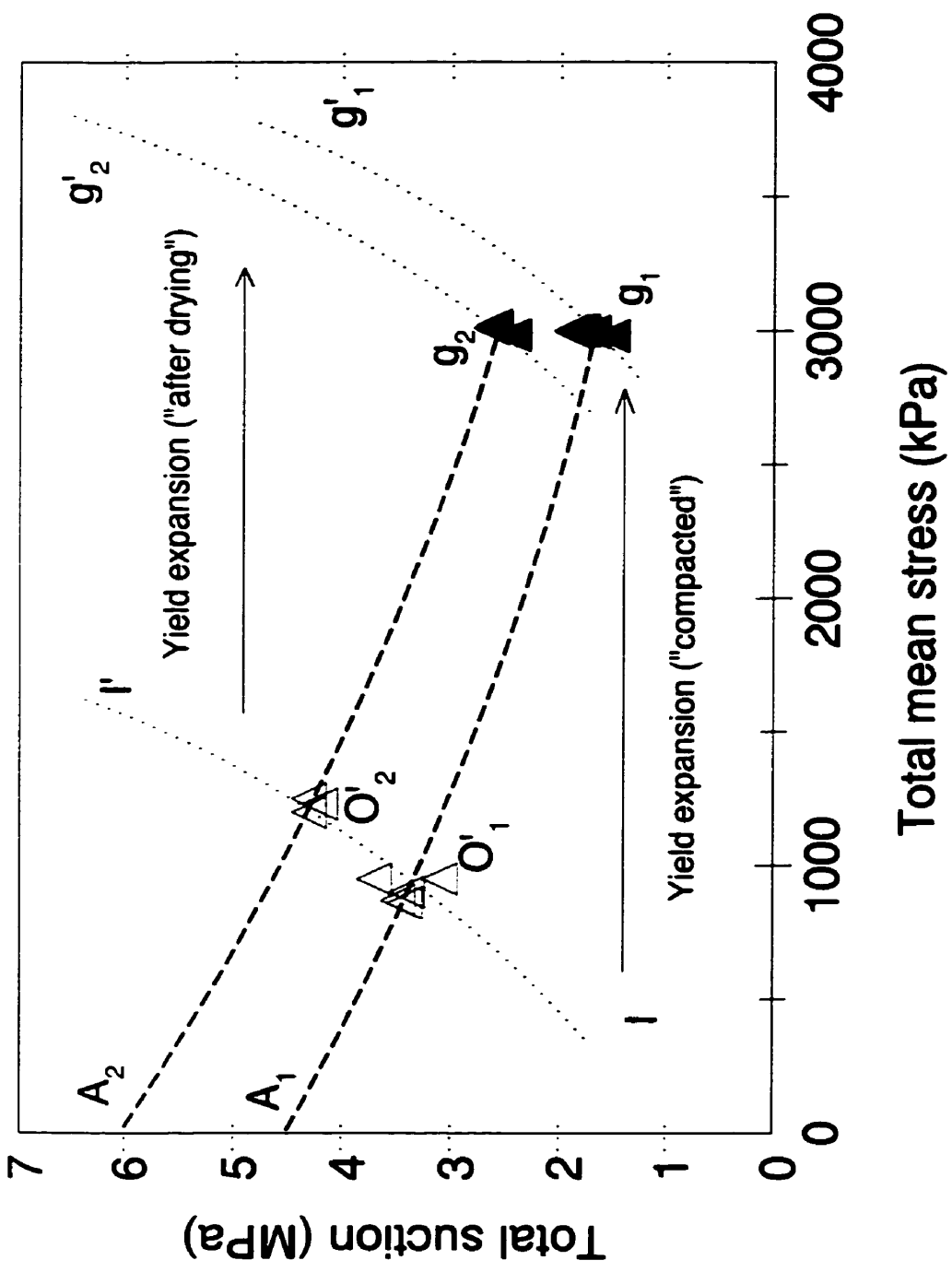


Figure 9.16 Expansion of yield locus in p-S space

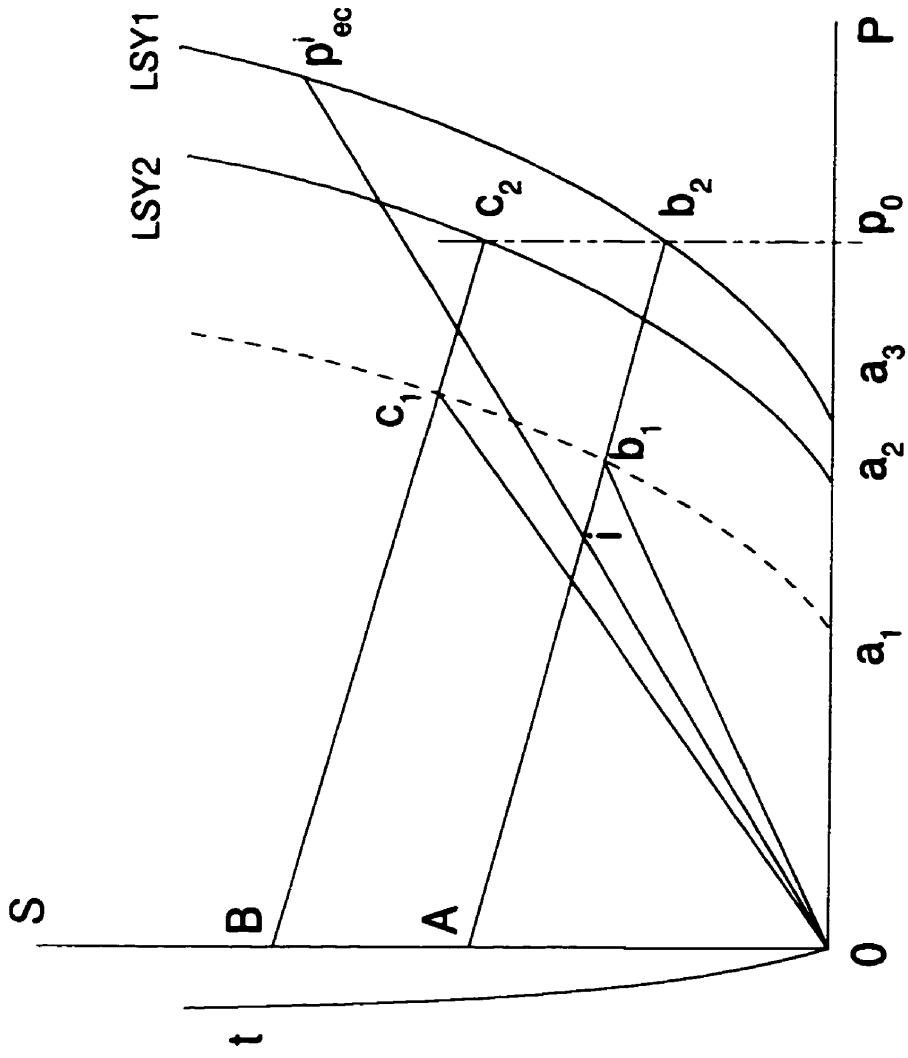


Figure 9.17 Yield loci and motion under isotropic compression in p-S space

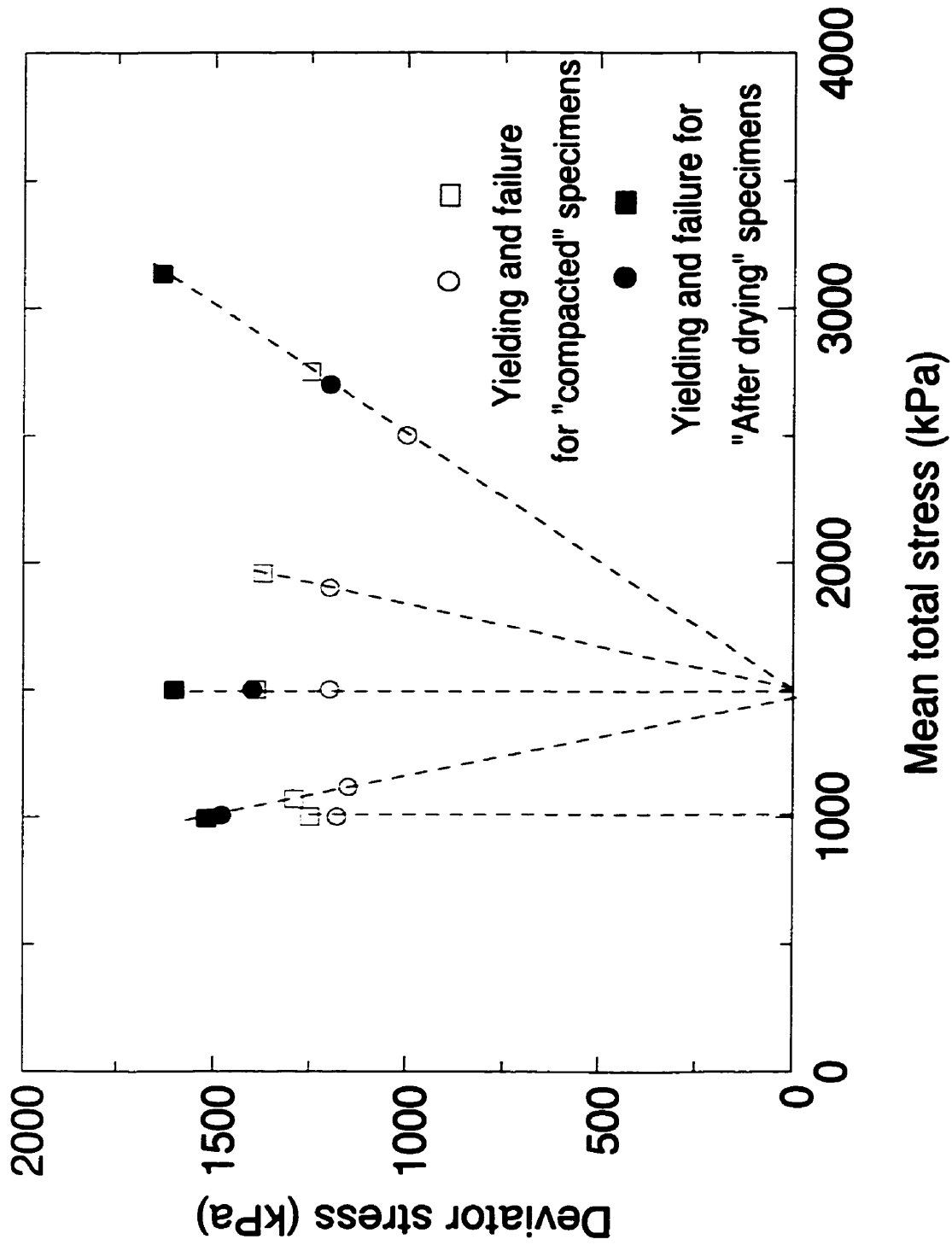


Figure 9.18 Yield stress and shear strength in p-q space

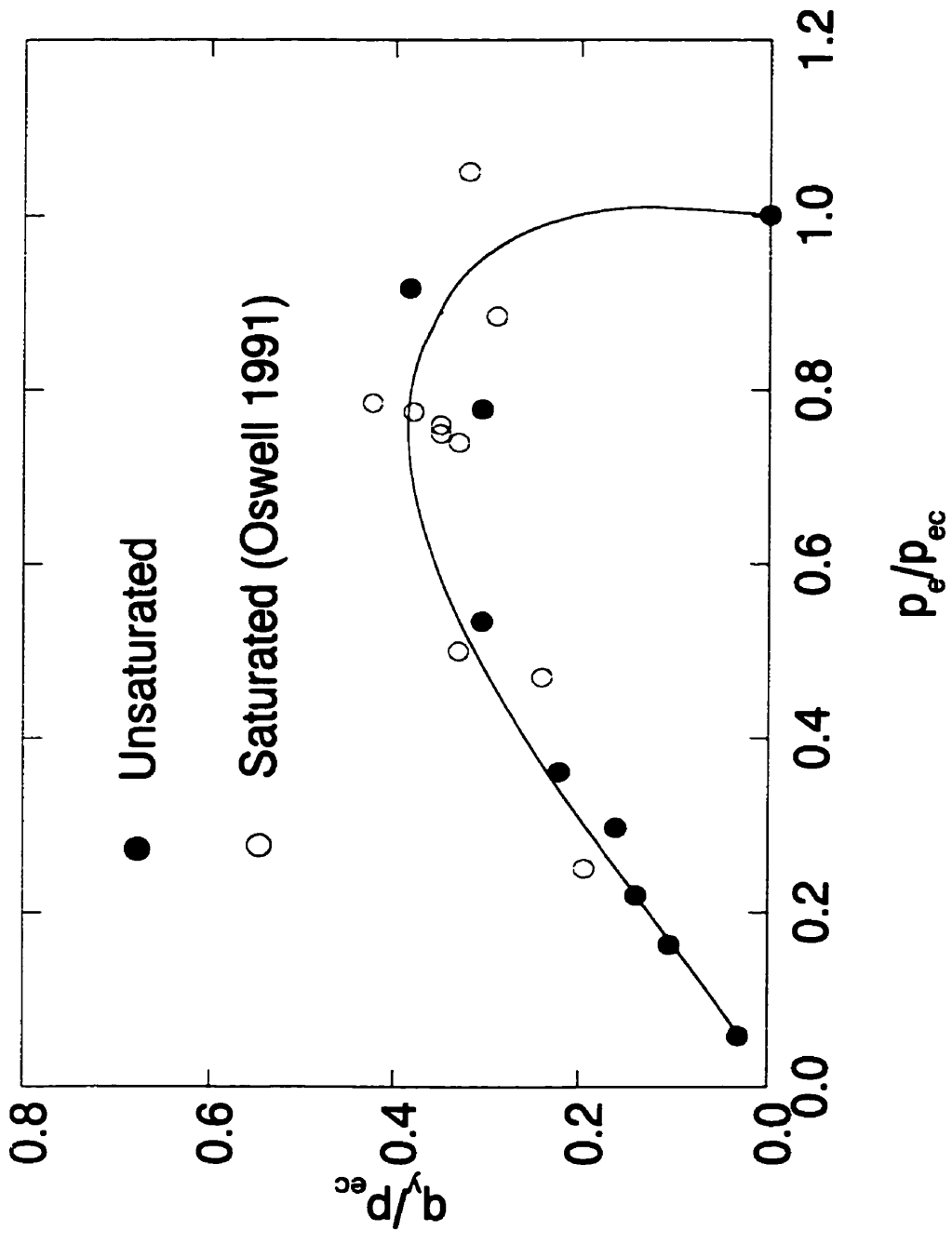


Figure 9.19 Normalized yield data and yield envelope

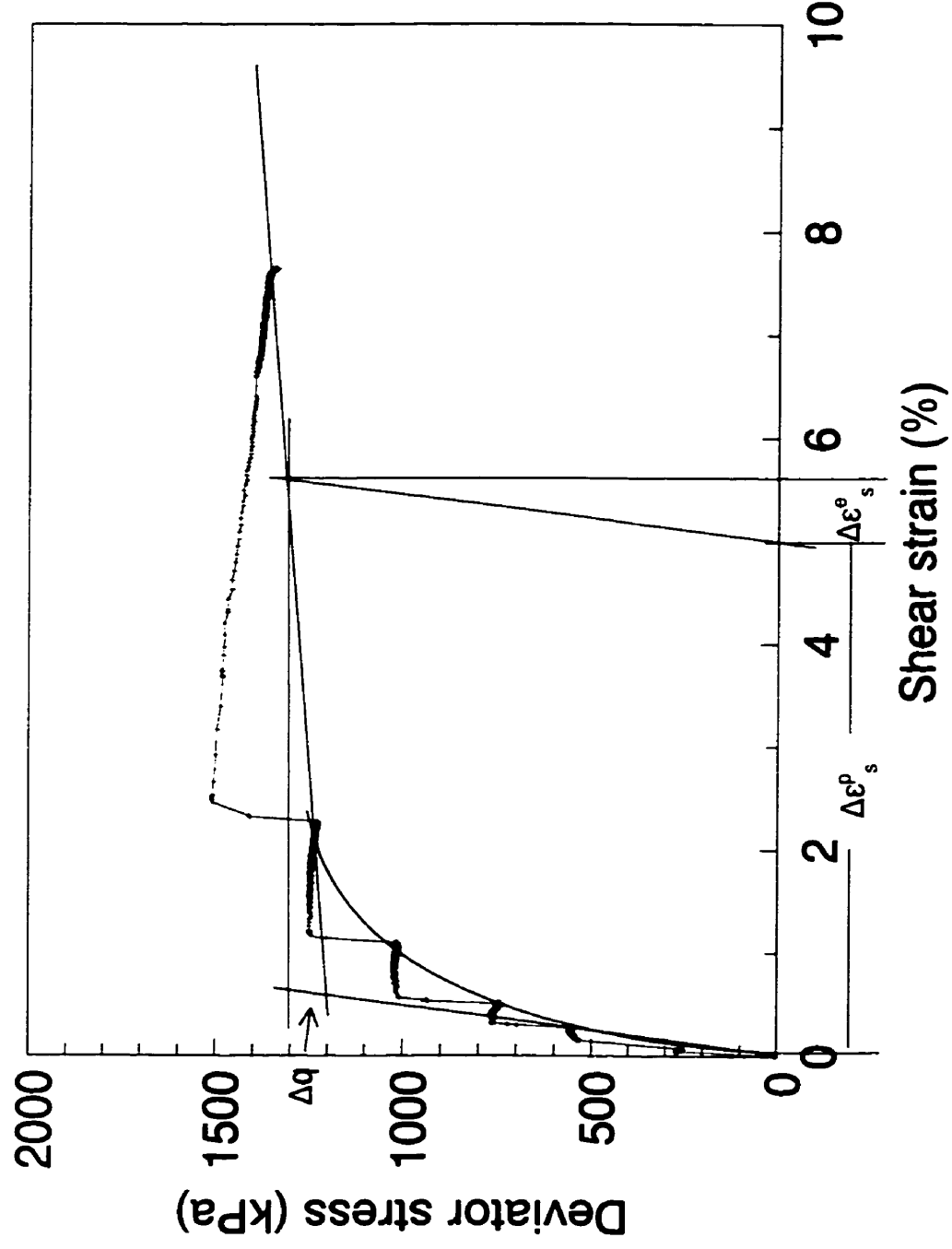


Figure 9.20 Strain increments for a given Δq (T16530)

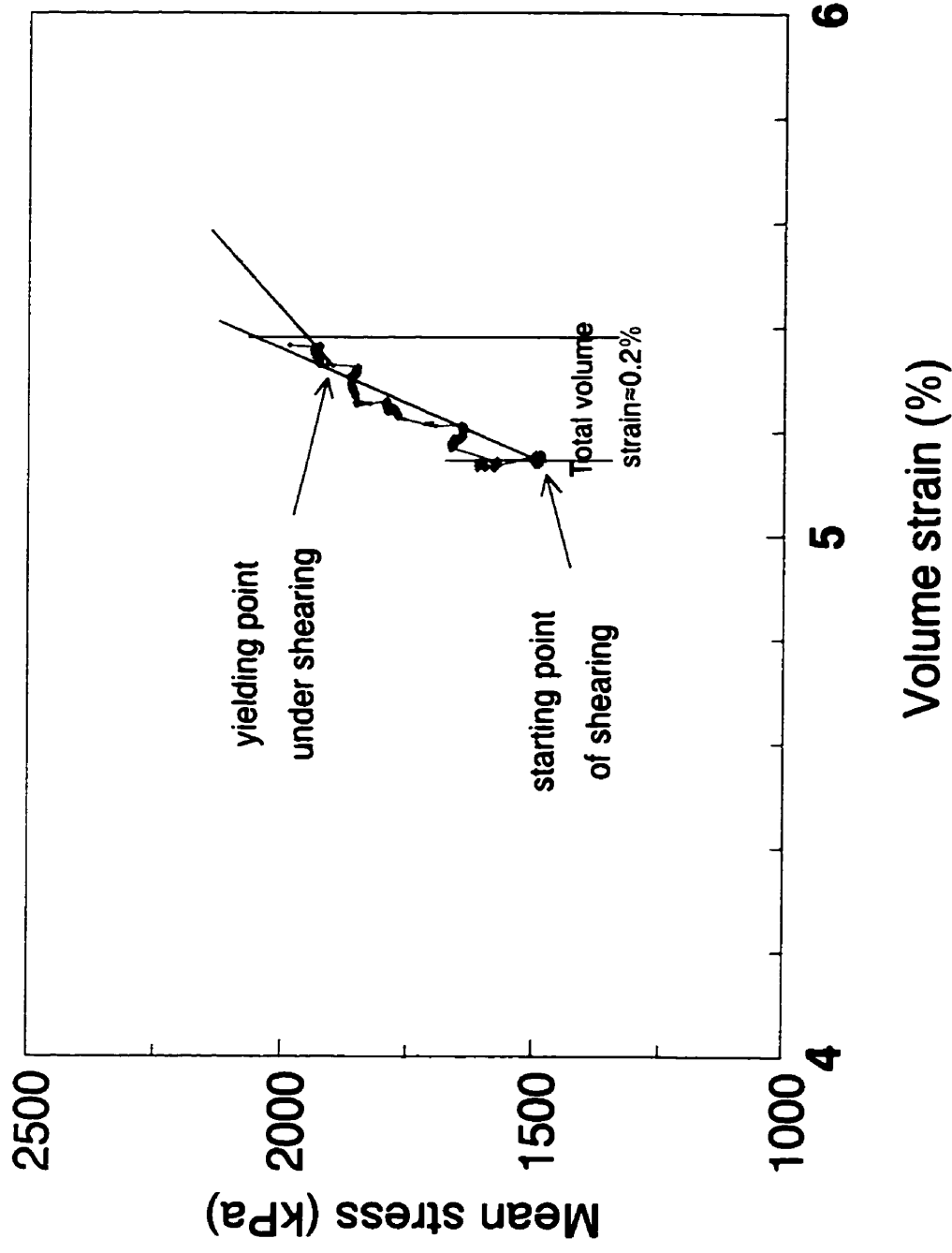


Figure 9.21 Mean stress vs. volume strain at shearing (T16530)

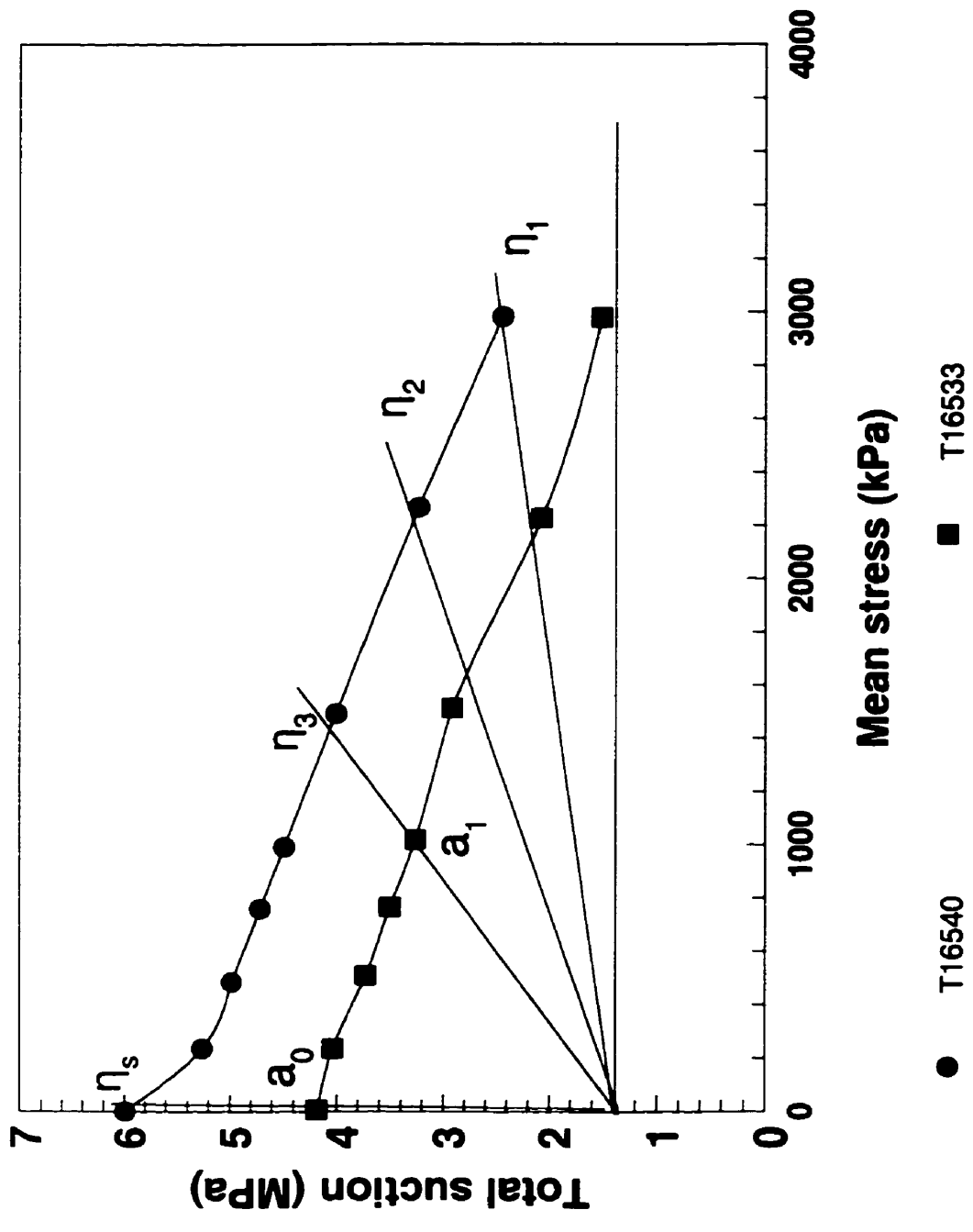


Figure 9.22 Suction change under isotropic compression

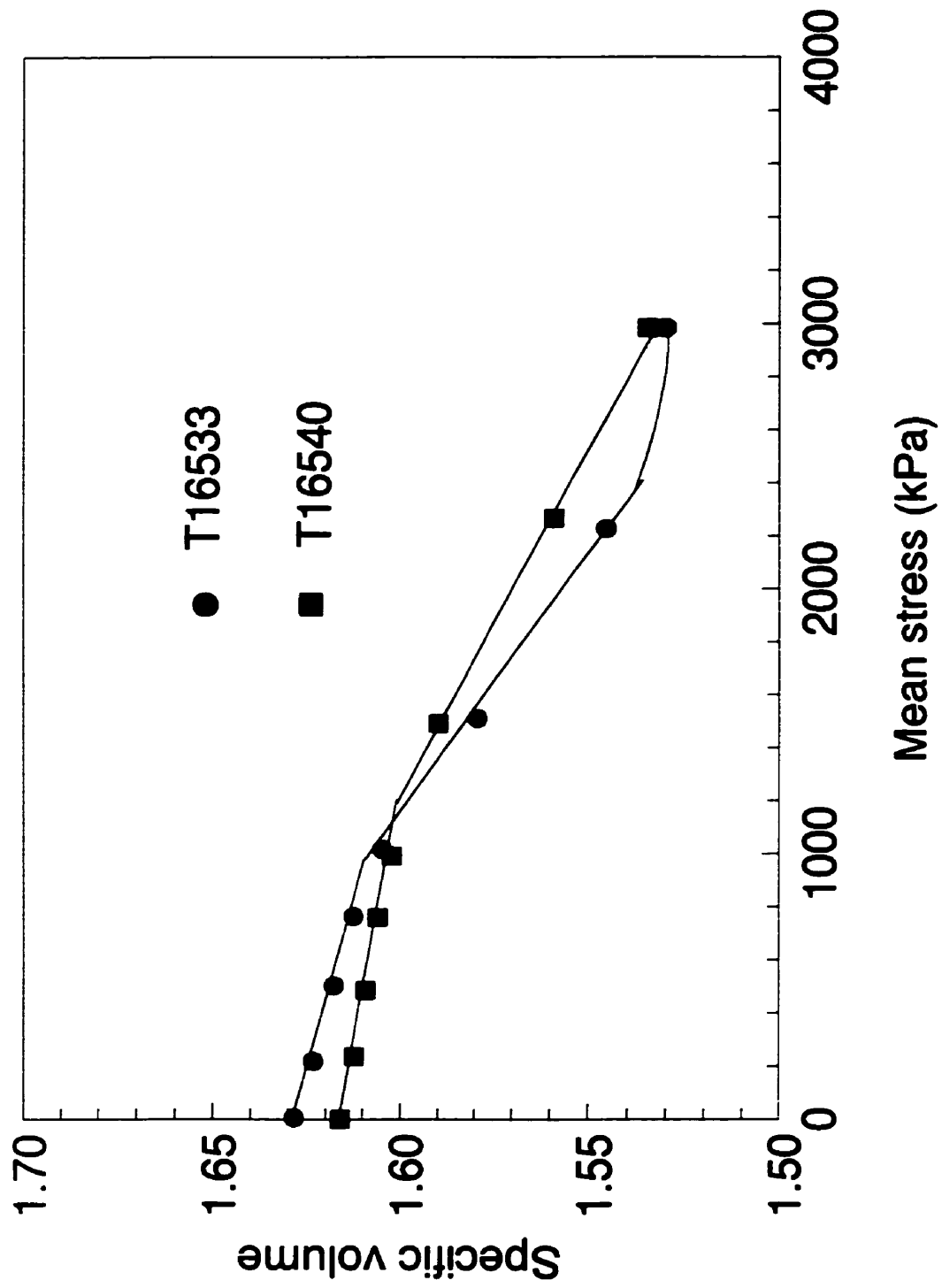


Figure 9.23 Specific volume versus mean stress

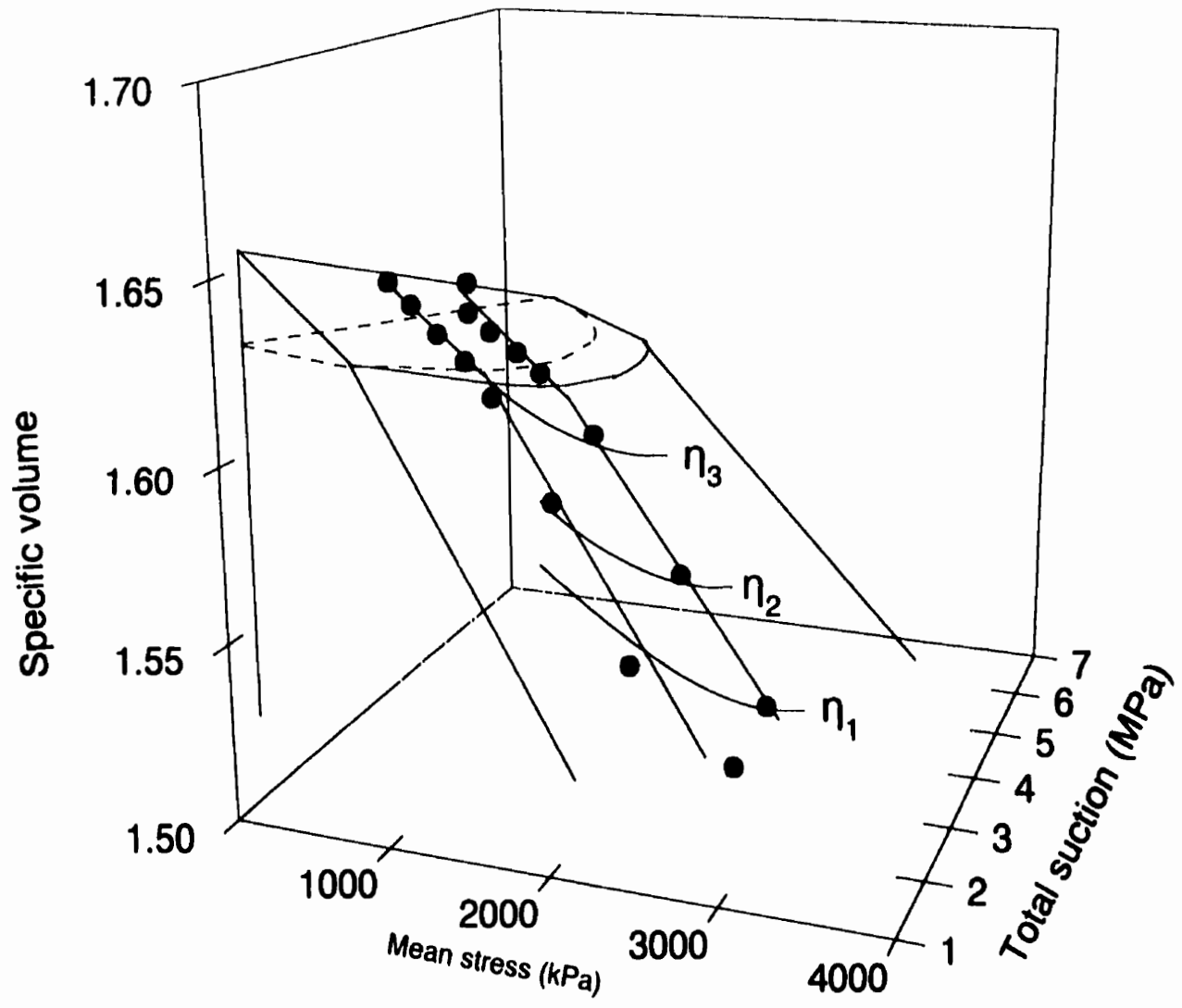


Figure 9.24 Volume change with mean stress and total suction

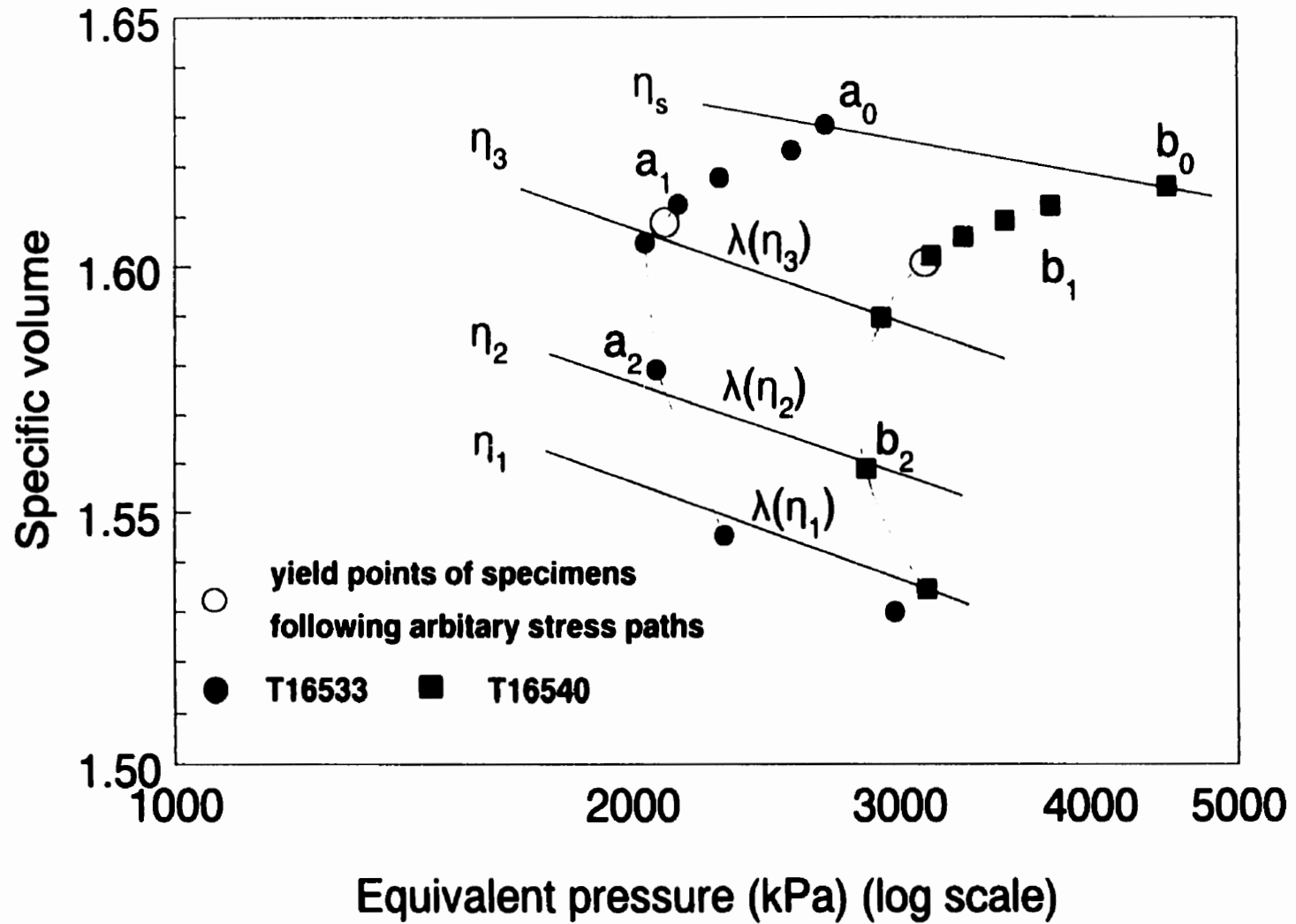


Figure 9.25 Specific volume versus equivalent pressure

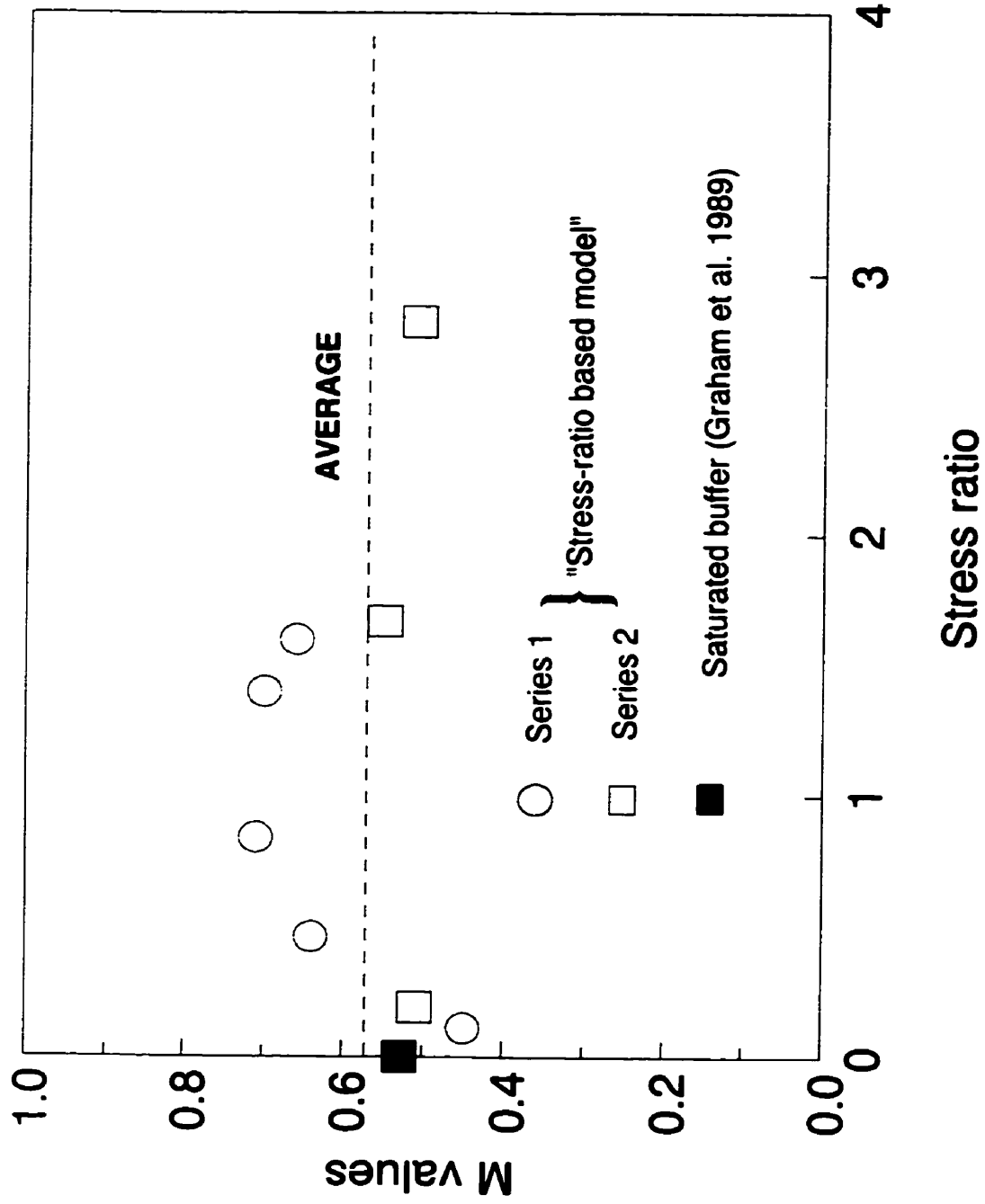


Figure 9.26 M values versus stress ratio

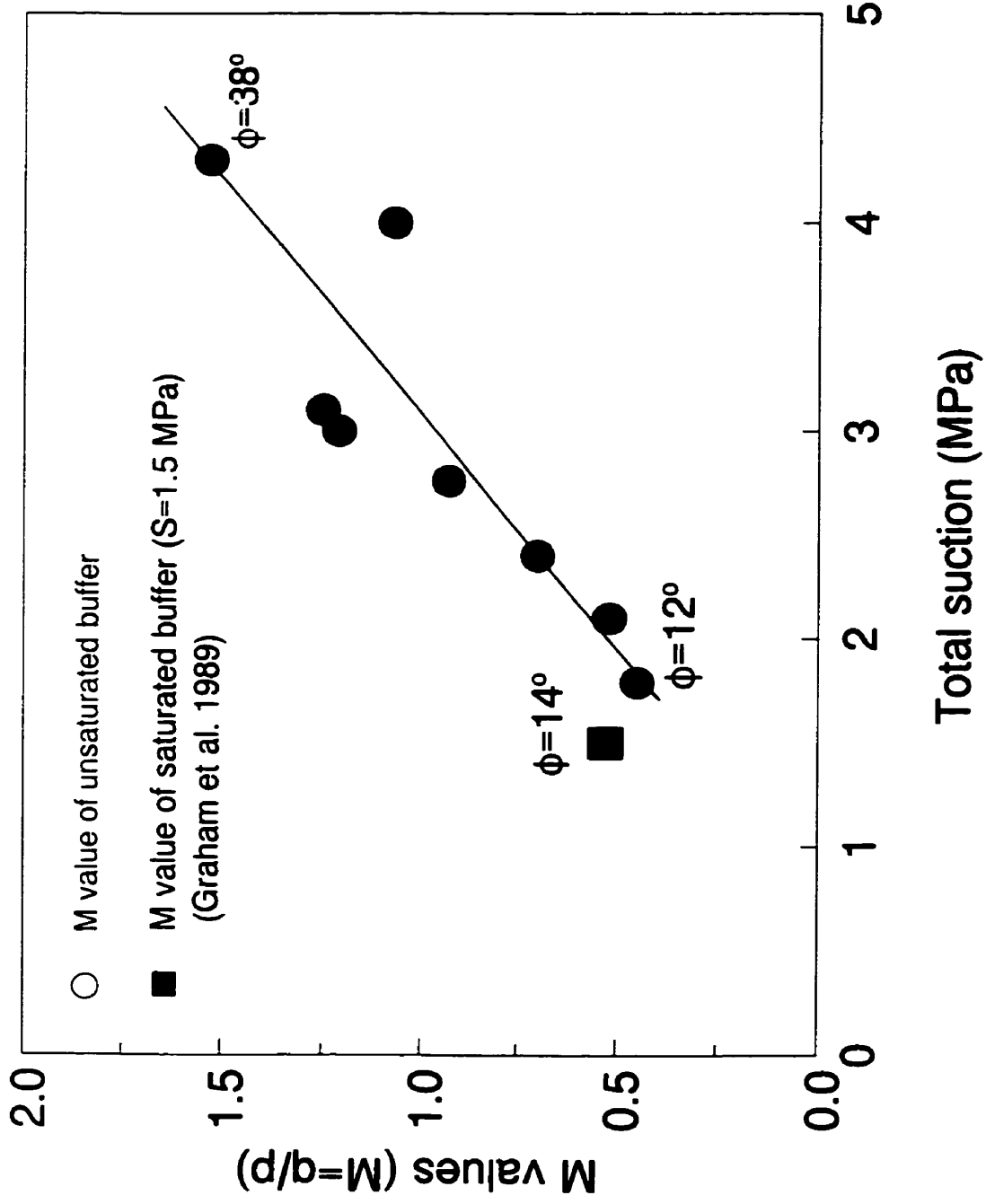


Figure 9.27 Conventional M values versus total suction

CHAPTER 10

REVIEW, CONCLUSIONS AND SUGGESTIONS FOR FURTHER WORK

10.1 Review and Summary

This doctoral program was intended to achieve following objectives: 1) establishing and developing experimental techniques for testing unsaturated soils, especially soils with high suctions in the geotechnical laboratories at the University of Manitoba; 2) investigating suction characteristics, stress-strain and strength behavior of unsaturated sand-bentonite; and 3) developing an elastic-plastic model. The preceding chapters have described a series of experiment techniques, an extensive laboratory testing program and a new elastic-plastic model in detail. They are reviewed and summarized as follows:

- 1) Suction measurement techniques have been used and established in the geotechnical laboratories at the University of Manitoba. They include filter paper, vapour equilibrium methods, and the psychrometer technique with a multi-channel Campbell Scientific CR-7 system. These techniques are common but usually used for measuring suctions on unsaturated soil specimens alone. In this thesis, a unique

technique for incorporating psychrometers into triaxial tests is proposed. Results of measured suctions of unsaturated specimens at complicated triaxial test conditions provide a valuable database for examining suction-dependent mechanical properties of unsaturated sand-bentonite. Tensile testing methodology and equipment for testing unsaturated soil specimens have also been developed. This allows for the first time tensile strength be experimentally evaluated.

2) Following four broad types of tests have been carried out:

(a) Measurement of suctions was undertaken on saturated and unsaturated sand-bentonite specimens. Use of specimens formed at different water contents led to establishment of suction - water content relationships. A soil-water characteristic curve was determined by measuring the suctions of specimens prepared at the same initial water content and subsequently dried. Differences between the suction - water content relationship and the soil-water characteristic curve have been clarified.

(b) Quick-undrained triaxial compression tests were carried out on specimens of saturations ranging from 50% to 98%. The resulting data from the separate series of triaxial tests and suction measurement tests provide a preliminary understanding of how saturations and initial suctions affect strength and compressibility. The effects of osmotic suctions on strength were also examined in a separate series of specimens whose suctions were elevated by additional osmotic agents.

- (c) A series of tensile tests was performed on traditional cylindrical triaxial specimens. A unique tensile mould has been designed and simple testing procedures have been developed. Specimens at three suction levels were tested. Tensile strengths arising from increased suctions in these specimens were determined. The testing produces well-defined tensile failure and consistent, repeatable results, which further define the relationship of total suction and tensile strength of unsaturated sand-bentonite.
- (d) Stress-controlled triaxial tests have been conducted on unsaturated specimens at two start suction levels. During triaxial tests, suction changes were monitored by psychrometer and deformations measured by non-contacting displacement sensors. The specimens were sheared following selected stress paths. Results obtained from this type of test allow the examination of major features of elastic-plastic behavior and strength properties of unsaturated buffer. The tests are therefore the pivotal of this doctoral project.
- 3) A new elastic-plastic conceptual model has been developed. The new conceptual model includes for the first time a yield envelope in q - S space. Two parameters – equivalent pressure and stress ratio are introduced as alternatives of two commonly used stress variables, namely net mean stress ($p-u_a$) and matric suction (u_a-u_w). This leads to establishment of a stress state boundary surface in the three-dimensional stress space p - q - S . Concepts of yielding, hardening law, flow rule and failure criterion used for saturated soils are incorporated into the stress state boundary

surface to form an integrated model. Together with volume change characteristics in V-p-S space as illustrated schematically by Delage and Graham (1995), the proposed model can describe well the elastic-plastic behavior of unsaturated buffer observed in the experimental program. The model is calibrated using data obtained from the stress-controlled triaxial tests.

10.2 Conclusions

Chapter 1 presented three hypotheses that formed the basis of the work described in succeeding chapters. Conclusions relating to these hypotheses can be drawn as follows:

Hypothesis 1: Matric suction and osmotic suction are separate stress state variables, with disparate effects in controlling strength and compressibility. Total suction can be reliably used as a state variable in describing mechanical properties only when contributions from both components are clarified.

Conclusions for hypothesis 1 can be drawn from Sections 7.2 and 7.3 which describe the test results of strength and compressibility of specimens prepared at various initial matric suctions and osmotic suctions. The data show that the strength and stiffness of buffer whose density is kept constant increase significantly with increases in matric suction, but decrease slightly when total suctions are increased by additional osmotic agents. Roles played by osmotic suction and matric suction in controlling strength and stiffness are not

quantitatively equivalent. While matric and osmotic suctions combine algebraically, it is unlikely that total suction can be used as a single stress state variable.

Hypothesis 2: Laboratory tests in which suctions are carefully measured or controlled can reveal major features of suction-dependent constitutive behavior and strength properties.

Using the technique developed in this program for measuring suction in triaxial tests, stress-controlled triaxial tests following a series of selected stress paths allowed elastic plastic stress-strain behavior to be examined under various stressing conditions. Detailed results presented in Section 8.3 indicated unsaturated specimens exhibited yielding, strain hardening or strain softening, and finally failed. The stress-strain behavior and shear strength are strongly affected by start suctions and suction changes under complicated external loading.

Hypothesis 3: Like saturated sand-bentonite, unsaturated sand-bentonite buffer exhibits stress-strain behavior that can be characterized as elastic-plastic. Well-developed theory for saturated soils can be extended into an elastic-plastic model with suction as an independent variable to embrace the effects of suction. The generalized model can describe elastic-plastic features of both saturated and unsaturated behavior.

Referring to Sections 8.3 and 8.6, yielding was observed in both isotropic compression and shearing. The behavior of unsaturated sand-bentonite can be characterized by elastic-plastic modeling. However, not all aspects of the observed elastic-plastic behavior can be

interpreted using traditional concepts for saturated soils or an existing conceptual model for unsaturated soils. As described in Chapter 9, the modified Cam Clay critical state model can be extended to include the effects of suction. The developed new conceptual model presented in Chapter 9 stems from a newly defined stress state boundary surface. This surface is based on the concepts of stress ratio and equivalent pressure which are combined from contributions from both matric suction and net mean stress. In association with this stress state boundary surface, the yield envelopes for unsaturated state of specimens and the yield envelope for saturated specimens can be synthesized into a unified yield envelope after normalization is performed. The developed conceptual model established in p-q-S space, together with a volume change relationship in V-p-S space (Delage and Graham 1995), allows understanding of the behavior of unsaturated soils such as buffer under a wide variety of stress paths. Further experimental confirmation is required.

Additional conclusions which validate the hypotheses in a more general way are as follows:

- 1) The technique developed in this program for assembling a psychrometer in a triaxial load cap, then incorporating the assembly into a triaxial cell improves existing approaches. Stainless steel screen shield psychrometers are preferred to porous ceramic shield psychrometers because of their quicker responses to suction change, the small size of the tips, and their capability of withstanding distortion. Psychrometers can be installed in triaxial specimens and can read suctions at elevated

pressures over long periods. Suctions measured using psychrometers incorporated into the triaxial cell are repeatable during compression and comparable during shearing for all eight tested specimens. This indicates that the proposed technique for installing psychrometers works successfully. Psychrometers work best for moderately high to high suctions, say from about 0.5 MPa to 8 MPa.

- 2) The methodology of performing tensile tests developed in this thesis offers a simple and reliable means for evaluating tensile strengths of unsaturated soils which arise from increased suctions. The method produces well-defined tensile failure and consistent, repeatable results. The introduced tensile mould allows traditional cylindrical triaxial specimens be used. Theoretical comparison between the shapes of tensile moulds indicates that the proposed semi-circle forms perform best.
- 3) Suctions of initially unsaturated specimens under constant mass conditions decrease with increasing total stress. Total suction recovers after release of loading, even after experiencing large plastic deformation. Under more complicated stress conditions during shear, suctions vary only in response to changes in the mean stress component of the stress tensor and not to changes in the deviator stress component.
- 4) Soil-water characteristic curves of buffer are not unique but depend on water content history. In particular, the microstructure is largely predetermined by the water content at the time of initial hydration, but is largely independent of subsequent changes in dry density. This is consistent with conclusions presented by Wan (1996). Following drying to the same water content, specimens with higher initial water contents have higher suctions. Consequently, specimens for an elastic-plastic model

should be prepared in a way that all of the specimens are compacted at the same initial conditions.

10.3 Recommendations for Future Research

While the major objectives have been achieved, nonetheless, as in all projects, some proposals have arisen for future research.

1) Location of installation of psychrometers into the specimens needs to be verified.

Incorporating psychrometers into triaxial tests has been successfully made and reliable and repeatable results have been obtained. In this program, psychrometer tips sense suctions at the top of specimens. Questions have been raised whether suctions measured at the ends of the specimen are representative of suctions in the centre of specimens during shear loading. Although in a theoretical sense it is understandable that they should be, since suction is a scalar variable like pore water pressure which is always measured at the ends of saturated specimens, experimental confirmation is needed to verify that the same suction readings can be obtained at any point after suction reaches equilibrium throughout a specimen. Comparison should be made of installations of more than one psychrometer in different locations of one specimen to examine their suction readings of the specimen under various stressing conditions.

The author understands that this research is now under way at the University of Manitoba.

2) *SWCCs of unsaturated specimens under constant pressures need to be determined.*

The soil-water characteristic curve is usually defined as the water content – suction relationship of specimens under no external loading. The relationship is also important for specimens at constant pressure levels in both practical and modelling terms and this needs to be examined.

3) *Suction needs to be controlled during triaxial tests.*

The influence of suction on stress-strain behavior and soil strength has been tested using triaxial tests and tensile tests. Suctions were measured using psychrometers during the tests. Application and control of suction in the same way that mean stress p and deviator stress q can be controlled in triaxial tests will allow arbitrary stress paths in p - q - S space be used for exploring the influence on soil behavior in more explicit ways. Therefore, suctions should be controlled instead of simply being measured during triaxial tests.

4) *Triaxial tests should be also performed under drained conditions.*

In this study, triaxial compression tests were carried out under ‘undrained’ constant mass conditions. Drainage of air and water is more realistic in engineering

applications. Controlled water uptake tests carried out in a triaxial apparatus are therefore recommended. Air pressure needs to be measured as well.

5) *Triaxial tests need to be carried out with controlled suctions and constant stress ratio $\eta=S/p$.*

The proposed model rationalizes all aspects of the observed mechanical behavior of unsaturated sand-bentonite. However, experimental data obtained from this testing program have not provided sufficient data to verify all components of the proposed model. The model itself is still conceptual in some elements. Further research to verify the model should be focused on: 1) verifying the closure of yield locus in p-S space by examining the coupled yielding induced by suctions and pressure; 2) verifying the yield envelope in q-S space with mean stress p being held zero; and 3) performing triaxial tests along stress paths of constant stress ratio S/p.

REFERENCES

- Aitchison, G.D. 1965. Ed., Moisture equilibrium and moisture changes in soils beneath covered areas. A symp. in print, G.D. Aitchison, Ed. Australia:Butterworths, 1965, 278pp.
- Blatz, J., Tang, G.X., Graham, J. and Wan, A. 1999. Psychrometer techniques for measuring suction in the triaxial test. Proc. 52nd Canadian Geotechnical Conference, Regina, Saskatchewan. August 1999.
- Bolzon, G., Schrefler, B.A., and Zienkiewicz, O.C. 1996. Elastoplastic soil constitutive laws generalized to partially saturated states. *Geotechnique*, **46**(2): 279-289.
- Ahmed, S., Lovell, C.W., and Diamond, S. 1974. Pore sizes and strength of compacted clay. *ASCE Journal of the Geotech. Eng. Div.*, **100**: 407-425.
- Al-Khafaf, S. and Hanks, R.J. 1974. Evaluation of the filter paper method for estimating soil water potential. *Soil Science*, **117**(4).
- Alonso, E.E., Gens, A., and Josa, A. 1990. A constitutive model for partially saturated soils. *Geotechnique*, **40**: 405-430.
- Alonso, E.E., Gens, A., and Hight, D.W. 1987. Special problem soils, General Report. Proc. 9th European Conf. Soil Mech. Found. Eng., (Dublin, Ireland) **3**: 1087-1146.
- ASTM D 4404 - 84. 1992. Standard test method for determination of pore volume and pore volume distribution of soil and rock by mercury intrusion porosimetry.
- ASTM D 5298 - 92. 1992. Standard test method for measurement of soil potential (suction) using filter paper. *Annual Book of ASTM Standards*, **15**(09):1312-1316.
- ASTM D 698 - 91. Test method for laboratory compaction characteristics of soil using standard effort.
- Bailey, W.A. 1965. The effects of salt on the consolidation behavior of saturated remolded clays. Contract Report No. 3 – 101. Conducted for U.S. Army Engineer Waterways Experiment Station, Vicksburg, Miss.
- Barbour, S.L. 1987. The role of physicochemical effects on the behavior of clay soils. Proc. of 40th Canadian Geotechnical Conference. Regina, Saskatchewan, 323-342.

- Barbour, S.L. and Fredlund, D.G. 1989. Mechanisms of osmotic flow and volume change in clay. *Canadian Geotechnical Journal*, **26**:551-562.
- Barbour, S.L. and Yang, N. 1993. A review of the influence of clay-brine interactions on the geotechnical properties of Ca-montmorillonite clayey soils from western Canada. *Canadian Geotechnical Journal*, **30**:920-934.
- Barbour, S.L. and Fredlund, D.G. 1989. Physico-chemical state variables for clay soils. Proc. of the 12th Int. Conf. on Soil Mech. and Found. Eng. (Rio de Janeiro, Brazil), 1839-1843.
- Barden, L. 1971. Examples of clay structure and its influence on engineering behavior. Roscoe Memorial Symposium, Cambridge.
- Barden, L. and Sides, G.R. 1970. Engineering behavior and structure of compacted clay. *Journal of the Soil Mechanics and Foundations Division, Proceedings of the American Society of Civil Engineers*, **96**: 1171-1200.
- Bishop, A.W. 1961. The measurement of pore pressure in a triaxial test. Proc. Conf. Pore Pressure and Suction in Soils. London. publ. Butterworths, London, England.
- Bishop, A.W. 1959. The principle of effective stress. Lecture delivered in Oslo, Norway, in 1955; published in *Teknisk Ukeblad*, **106** (39): 859-863.
- Bishop, A.W. and Donald, I.B. 1961. The experimental study of partly saturated soil in the triaxial apparatus. Proc. 5th Int. Conf. Soil. Mech. Found. Eng. Paris, **1**:13-21.
- Bishop, A.W. and Garga, V.K. 1969. Drained tension tests on London clay. *Geotechnique*, **19**: 309-313.
- Bishop, A.W. and Wesley, L.D. 1975. A hydraulic triaxial apparatus for controlled stress path testing. *Geotechnique*, **25** (4): 657-670.
- Bishop, A.W., Alpin, I., Blight, G.E., and Donald, I.B. 1960. Factors controlling the shear strength of partly saturated cohesive soils. ASCE Research Conf. on Shear Strength of Cohesive Soils, (Univ. of CO, Boulder CO).
- Bishop, A.W. and Blight, G.E. 1963. Some aspects of effective stress in saturated and unsaturated soils. *Géotechnique*, **13**(3): 177-197.
- Blight, G.E. 1983. Aspects of the capillary model for unsaturated soils. Proc. 7th Asian Conf. SMFE 1: 3-7. Haifa.

- Bolzon, G., Schrefler, B.A. and Zienkiewicz, O.C. 1996. Elastoplastic soil constitutive laws generalized to partially saturated states. *Geotechnique*, **46**(2):279-289.
- Brewer, R. 1964. *Fabric and mineral analysis of soils*. John Wiley & Sons, Inc., New York.
- Briscoe, R. 1986. Thermocouple psychrometers for water potential measurements. NATO ASI Series Advanced Agricultural Instrumentation. 193-209.
- Brown, R.W. 1970. Measurement of water potential with thermocouple psychrometers: construction and application. USDA For. Serv. Res. Pap. INT-80, Intermt. For. and Range Exp. Stn., Ogden, Utah.
- Campbell Scientific Inc. 1984. S3497X Psychrometer software and A3497 TC Psychrometer cooling current interface. Part of the manual for the Campbell Scientific CR-7 measurement and control system. Logan, Utah, USA.
- Campbell, J.D. and Gardner, W.H. 1971. Psychrometric measurement of soil potential: temperature and bulk density effects. *Soil Sci. Soc. Amer.*, **35**: 8-12.
- Chandler, R.J. and Gutierrez, C.I. 1986. The filter-paper method of suction measurement. *Geotechnique*, **36**: 265-268.
- Chattopadhyay, P.K. 1972. Residual shear strength of some pure clay minerals. Ph.D dissertation, University of Alberta, Edmonton, Canada. 340pp.
- Cheung, S.C.H., Gary, M.N., and Dixon, D.A. 1987. Hydraulic and ionic diffusion properties of bentonite-sand buffer materials. *Coupled Processes Associated with Nuclear Waste Repositories*, 393-407.
- Clay Technology Ab, Lund Sweden. 1995. Thermal elastic-plastic modelling of clay soils, including sand-bentonite buffer, May 1995.
- Coleman, J.D. 1962. Stress-strain relations for partly saturated soils. *Geotechnique*, (Correspondence) **12**(4): 348-350.
- Conlon, R.J. 1966. Landslide on the touloustouc river, Quebec. *Canadian Geotechnical Journal*, **3**(3):113-114.
- Corey, A.T. 1957. Measurement of water and air permeability in unsaturated soil. *Proc. Soil Sci. Soc. Amer.*, **21**(1): 7-10.
- Croney, D. and Coleman, J.D. 1948. Soil thermodynamics applied to the movement of moisture in road foundations. *Proc. of the 7th Int. Conf. Appl. Mech.* **3**:163-177.

- Croney, D., Coleman, J.D. and Black, W.P.M. 1958. Studies of the movement and distribution of water in soil in relation to highway design and performance. HRB Special Report 40: 226-252, Washington, D.C.
- Daniel, D.E. 1983. Permeability test for unsaturated soil. *Geotech. Testing Journal*, **6**(2).
- Delage, P., Howat, M.D., and Cui, Y. 1995. Relationship between suction and swelling properties in a heavily compacted unsaturated clay. Int. wkshp on Hydro-thermo-mechanics of eng. clay barriers and geol. barriers. McGill University, Montreal, Canada. July 1995.
- Delage, P. and Graham, J. 1995. Understanding the behavior of unsaturated soils requires reliable conceptual model. State of the Art Report, Proceedings of 1st Int. Conf. on Unsaturated Soils, Paris, France, 1995, 1223-1256.
- Delage, P. and Lefebvre, G. 1984. Study of the structure of a sensitive champlain clay and of its evolution during consolidation. *Canadian Geotechnical Journal*, **21**:21-35.
- Delage, P., Tessier, D., and Marcel-Audiguier, M. 1982. Use of the cryoscan apparatus for observation of freeze-fractured planes of a sensitive Quebec clay in scanning electron microscopy. *Canadian Geotechnical Journal*, **19**:111-114.
- Dixon, D.A., Gray, M.N., and Graham, J. 1996. Swelling and hydraulic properties of bentonites from Japan, Canada and the U.S.A. Second International Congress on Environmental Geotechnics, Osaka, Japan, November 1996.
- Dixon, D.A. and Gray, M.N. 1985. The engineering properties of buffer material. *Technical report TR-350*, Fuel Waste Technology Branch, Whiteshell Laboratories, Pinawa MB, Canada.
- Dixon, D.A. and Woodcock, D.R. 1986. Physical and engineering properties of candidate buffer materials. Technical Record, TR-352, AECL (Pinawa, MB).
- Dixon, D.A., Wan, A.W.L., Graham, J., and Kjartanson, B.H. 1991. Assessing pressure-volume equilibrium in bentonite-based materials. 44th Canadian Geotech. Soc. Conf. (Calgary, Canada), Sept. 1991. **2**(61).
- Donald, I.B. 1956. Shear strength measurements in unsaturated non-cohesive soils with negative pore pressures. Proc. of the Second Australian-New Zealand Conf. on Soil Mech. and Found. Eng., The New Zealand Inst. of Engineers, (Christchurch, N.Z.).
- EIS 1994 Environmental impact statement on the concept for disposal of Canada's nuclear fuel waste. Atomic Energy of Canada Limited, AECL-10711, Sept. 1994.

- Edil, T.B. and Motan, S.E. 1984. Laboratory evaluation of soil suction components. *Geotechnical Testing Journal*, 7(4):173-181.
- Edil, T.B., Motan, S.E., and Toha, F.X. 1981. Mechanical behaviour and testing methods of unsaturated soils. *Laboratory Shear Strength of Soil*, ASTM STP 740, R.N. Yong and F.C. Townsend, Eds., ASTM, 114-129.
- Escario, V. and Saez, J. 1986. The shear strength of partly saturated soils. *Geotechnique*, 36(3):453-456.
- Escario, V. and, Jucá, J.F.T. 1989. Strength and deformation of partly saturated soils, Proc. of the 12th Int. Conf. on Soil Mech. and Found. Eng. (Rio de Janeiro, Brazil). August 1989, 43-46.
- Escario, V. 1980. Suction controlled penetration and shear tests. Proc. 4th Int. Conf. Expansive Soils (Denver, CO), ASCE, 2:787-797.
- Fawcett, R.G. and Collis-George, N. 1967. A filter-paper method for determining the moisture characteristics of soil. *Australian Journal of Experimental Agriculture and Animal Husbandry* 7:162-167.
- Fredlund, D.G. 1995. The scope of unsaturated soil mechanics: an overview. 1st. Int. Conf. on Unsaturated Soils, Paris, Sept. 1995. 3, 1155-1177, eds. E.E.Alonso and P.Delage. Balkema. Rotterdam.
- Fredlund, D.G. 1989. The character of the shear strength envelope for unsaturated soils. The Victor de Mello Volume, the 12th Int. Conf. on Soil Mech. and Found. Eng., (Rio de Janeiro, Brazil). 142-149.
- Fredlund, D.G. 1985. Soil mechanics principles that embrace unsaturated soils. Proc. 11th Int. Conf. Soil Mech. Found. Eng. (San Francisco, CA), 2:465-473.
- Fredlund, D.G. 1979. Appropriate concepts and technology for unsaturated soils. *Canadian Geotechnical Journal*, 16:121-139.
- Fredlund, D.G. and Xing, A. 1994. Equations for the soil-water characteristic curve. *Canadian Geotechnical Journal*. 31:521-532.
- Fredlund, D.G. and Rahardjo, H. 1993. An overview of unsaturated soil behavior. *Unsaturated Soils*, Geotechnical Engi. Division/ASCE. October 24-28, 1993. Dallas, Texas.

- Fredlund, D.G. and Rahardjo, H. 1993. *Soil Mechanics for Unsaturated Soil*. A Wiley-Interscience Publication. John Wiley & Sons, Inc., New York, NY.
- Fredlund, D.G. and Morgenstern, N.R. 1977. Stress strain variables for unsaturated soils. *Proc. American Society of Civil Engineers*. **103**, GT5, 447-466.
- Fredlund, D.G. and Morgenstern, N.R. 1976. Constitutive relations for volume change in unsaturated soils. *Canadian Geotechnical Journal*, **13**:261-276.
- Fredlund, D.G., Vanapalli, S.K., Xing, A., and Pufahl, D.E. 1995. Predicting the shear strength function for unsaturated soils using the soil-water characteristic curve. *Unsaturated Soils*. *Proc. 1st Int. Conf. on Unsaturated Soils, Paris, September 1995*, **1**, 63-69. *eds. E.E.Alonso and P.Delage, publ. Balkema, Rotterdam.*
- Fredlund, D.G., Rahardjo, H., and Gan, J.K.M. 1987. Non-linearity of strength envelope for unsaturated soils. *Proc. 6th Int. Conf. Expansive Soils (New Delhi)*. 49-54.
- Fredlund, D.G., Morgenstern, N.R., and Widger, R.A. 1978. The shear strength of unsaturated soils. *Canadian Geotechnical Journal*, **15**:313-321.
- Gan, L.K.M. and Fredlund, D.G. 1988. Multistage direct shear testing of unsaturated soils. *ASTM Geotechnical Testing Journal*. **11**(2):132-138.
- Gens, A. and Alonso, E.E. 1992. A framework for the behavior of unsaturated expansive clays. *Canadian Geotechnical Journal*, **29**:1013-1032.
- Graham, J., Tang, G.X., Blatz, J., Rajapakse, R.K.N.D, and Chandler, N. 1999. Elastic-plastic behaviour of an unsaturated sand-bentonite mixture. XI Pan-American Conference on Soil Mechanics and Foundation Engineering. August 1999, Foz Do Iguacu, Brazil.
- Graham, J., Tang, X., Wiebe, B., Zhou, Y., and Rajapakse, R.K.N.D. 1996. Modelling of sand-bentonite buffer for use in the Canadian nuclear fuel waste management program. Final Report: Contract No. WS102679. pp.1-158. June 1996.
- Graham, J., with Chandler, N., Dixon, D.A., Roach, P.J., To, T. and Wan, A.W.L. 1996. The buffer/container experiment: Volume 4 - results, synthesis, issues. AECL pp.344 plus approx. 200 figures, photographs, and computer animations.
- Graham, J., Tang, X., Wiebe, B., Rajapakse, R.K.N.D., and Zhou, Y. 1995. Progress report on 2nd year of contract no. WS102679: Modelling of sand-bentonite buffer for use in the Canadian Nuclear Fuel Waste Management Program. AECL-Research, July 1995. 170pp.

- Graham, J., Tanaka, N., Crilly, T., Yuen, K., and Tang, X. 1994. Progress report on 1st year of Contract No. WS102679: Modelling of sand-bentonite buffer for use in the Canadian nuclear fuel waste management program. Unpublished research report to AECL, May 1994. 101pp. plus 103 figures.
- Graham, J., Wiebe, B., Tang, X. and Onofrei, C. 1995. Strength and stiffness of unsaturated sand-bentonite 'buffer'. Proceedings of 1st Int. Conf. on Unsaturated Soils. Paris, France, 1995, pp. 89-94, eds. E.E.Alonso and P.Delage, publ. Balkema, Rotterdam 1995.
- Graham, J., Lingnau, B.E., Yarechewski, D.S., Tanaka, N. and Crilly, T. 1993. Thermo-elastic-plastic modelling of sand-bentonite buffer for use in underground disposal of nuclear fuel waste. Final Report to Atomic Energy of Canada Limited, Contract WS-30J-79981, July 1993, 95pp. plus Figures.
- Graham, J., Oswell, J.M., and Gray, M.N. 1992. The effective stress concept in saturated active clays. Canadian Geotechnical Journal **29**, 1033-1043.
- Graham, J. 1992. The effective stress concept in saturated sand-clay buffer. Canadian Geotechnical Journal. **29**:1033-1043.
- Graham, J. 1989. Expansive and collapsible soils. 12th international conference on soil mechanics and foundations engineering. Rio de Janeiro.
- Graham, J., Saadat, F., Gray, M.N., Dixon, D.A. and Zhang, Q.Y. 1988. Strength and volume change behavior of sand-bentonite mixtures. Can. Geotech. J., **26**:292-305.
- Graham, J., Gray, M.N., Sun, B.C.C., and Dixon, D.A. 1986. Strength and volume change characteristics of a sand-bentonite buffer. Proc. of the 2nd. Int. Conf. on Radioactive Waste Management, (Winnipeg, MB).
- Graham, J., Shields, D.H., and Sun, B.C.C. 1985. Stress-strain relationships in sand-clay buffer materials. Proc. of the 17th Info. Meeting of the Canadian Nuclear Fuel Waste Management Program, Engineered Barriers and Wasteforms, Toronto, May 1985.
- Graham, J., Noonan, M.L. and Lew, K.V. 1983. Yield states and stress-strain relationships in a natural plastic clay. Canadian Geotechnical Journal, **20**(3):502-516.
- Gray, M.N., Cheung, S.C.H., and Dixon, D.A., 1984. Influence of sand content on swelling pressures and structures developed in statically compacted Na-bentonite. AECL Report, AECL-7825.

- Gray, M.N., Cheung, S.C.H., and Dixon, D.A. 1984. Swelling pressures of compacted bentonite/sand mixtures. Proceedings, 44th Materials Research Society Symposium on Scientific Basis for Nuclear Waste Management, (Boston, Mass), 8:523-530.
- Grim, R.E. 1953. Clay Mineralogy. McGraw-Hill, (New York, NY) 384pp.
- Gulhati, S.K. and Satija, B.S. 1981. Shear strength of partially saturated soils. Proc. 10th Int. Conf. Soil Mech. Found. Eng. (Stockholm), 1:609-612.
- Habib, S.A. and Karube, D. 1993. Swelling pressure behavior under controlled suction. Geotechnical Testing Journal, 16(2). 271-275.
- Hamblin, A.P. 1981. Filter-paper method for routine measurement of field water potential. Journal of Hydrology. 53:355-360.
- Ho, D.Y. and Fredlund, D.G. 1982. A multistage triaxial test for unsaturated soils. Geotechnical Testing Journal, 5, No.1/2. 18-25.
- Ho, D.Y., Fredlund, D.G., and Rahardjo, H. 1992. Volume change indices during loading and unloading of an unsaturated soil. Canadian Geotechnical Journal, 29:195-207.
- Ho, D.Y.F. and Fredlund, D.G. 1989. Laboratory measurement of the volumetric deformation moduli for two unsaturated soils. Proc. 42nd Canadian Geotechnical Conference, Winnipeg, Manitoba, Oct. 1989. pp.50-60.
- Ho, Y.A. and Pufahl, D.E. 1987. The effects of brine contamination on the properties of fine grained soils. Geotech. Practice for Waste Disposal. ASCE Spec. Conf. 547-561.
- Jennings, J.E. and Burland, J.B. 1962. Limitations to the use of effective stress in partly saturated soils. Géotechnique, 12(2):125-144.
- Josa, A., Alonso, E.E., Lloret, A., and Gens, A. 1987. Stress-strain behaviour of partially saturated soils. Proc. 9th European Conf. Soil Mech. Found. Eng., (Dublin, Ireland) 2:561-564.
- Kassif, G. and Ben Shalom A. 1971. Experimental relationship between swell pressure and suction. Geotechnique 21(3):245-255.
- Khan, M.H. and Hoag, D.L. 1979. A noncontacting transducer for measurement of lateral strains. Canadian Geotechnical Journal, 16:409-411.
- Kjartanson, B.H. and Gray, M.N. 1987. Buffer/container experiments in the underground research laboratory. 40th Canadian Geotechnical Conference, Regina, Saskatchewan. Oct. 1987.

- Krahn, J. and Fredlund, D.G. 1972. On total matric and osmotic suction. *Journal of Soil Science*, **114**(5):339-348.
- Lambe, T.W. 1958. The structure of compacted clay. *Journal of soil mechanics and foundation engineering*. American Society of Civil Engineers. **84**.
- Lambe, T.W. 1962. Soil stabilization. Chapter 4 of *Foundation Engineering*, G.A. Leonards (ed.), McGraw-Hill, (New York, NY).
- Lambe, T.W. and Whitman, R.V. 1979. *Soil Mechanics*. John Wiley & Sons, Inc., New York, NY, 553pp.
- Lang, A.R.G. 1967. Osmotic coefficients and water potentials of sodium chloride solutions from 0 to 40°C. *Australian Journal of Chemistry*, **20**:2017-2023.
- Lapierre, C., Leroueil, S., and Locat, J. 1990. Mercury intrusion and permeability of louisville clay. *Canadian Geotechnical Journal*, **27**:761-773.
- Lingnau, B.E. and Graham, J. 1994. Synopsis of stress-strain properties of saturated buffer. Unpublished research report to AECL, June 1994. 48pp. plus 29 computer disks.
- Lingnau, B.E. 1993. Consolidated undrained triaxial behaviour of a sand-bentonite mixture at elevated temperature. Ph.D. Thesis, Department of Civil Engineering, University of Manitoba, (Winnipeg, Manitoba).
- Lingnau, B.E., Graham, J., and Tanaka, N. 1995. A behavioural model for sand-bentonite at elevated temperatures. 10th PanAmerican Conference on Soil Mechanics and Foundations Engineering, **1**, 252-263. Guadalajara, Mexico, October 1995.
- Lingnau, B.E., Graham, J., Yarechewski, D., Tanaka, N., and Gray, M.N. 1996. Effects of temperature on strength and compressibility of sand-bentonite buffer. *Engineering Geology*, **41**:103-115.
- Lingnau, B.E., Yarechewski, D., Graham, J., Tanaka, N., and Gray, M.N. 1993. Stress-strain properties of sand-bentonite buffer at elevated temperatures. Proc. International Workshop on Thermo-mechanics of Clays and Clay Barriers, Bergamo, Italy, October 1993.
- Lingnau, B.E., Graham, J., and Tanaka, N. 1995. Isothermal modeling of sand-bentonite mixtures at elevated temperatures. *Canadian Geotechnical Journal*, **32**:78-88.

- Matyas, E.L. and Radhakrishna, H.S. 1968. Volume change characteristics of partially saturated soils. *Geotechnique*, **18**(4):432-448.
- McQueen, I.S. and Miller, R.F. 1968. Calibration and evaluation of a wide-range gravimetric method for measuring moisture stress. *Soil Science* **106**(3).
- Metten, U. 1966. *Desalination by reverse osmosis*. MIT. Press, Cambridge, MA.
- Meyn, R.L. and White, R.S. 1972. Calibration of thermocouple psychrometers: A suggested procedure for development of a reliable predictive model, *Psychrometry in Water Relations Research*. pp. 56-63.
- Mitchell, J.K. 1976. *Fundamentals of soil behaviour*. J.Wiley & Sons Publishers (Toronto, ON).
- Morris, P.H., Graham, J., and Williams, D.J. 1992. Cracking in drying soils. *Canadian Geotechnical Journal*, **29**:263-277.
- Musa, A.M. 1982. On the yield of a compacted clayey soil. M.Sc. Thesis. University of Wales, Cardiff, Wales.
- Olson, R.E. and Lanfelder, L.J. 1965. Pore water pressure in unsaturated soils. *Proc. ASCE Journal, Soil Mech. Found. Div.*, **91**, SM4:127-150.
- Oswell, J.M. 1991. Elastic-plastic behaviour of a sand-bentonite mixture. Ph.D. Thesis, Department of Civil Engineering, University of Manitoba, (Winnipeg, Manitoba).
- Pile, K.C. 1980. The relationship between matrix and solute suction, swelling pressure, and magnitude of swelling in reactive clays. *Proceedings of 3rd Australia-New Zealand conference on geomechanics*, **6**(1):197-201, 1980.
- Prapaharan, S., Altschaeffl, A.G. and Dempsey, B.J. 1985. Moisture curve of compacted clay: Mercury intrusion method. *Journal of Geotech. Engineering*, **111**(9):1139-1143.
- Quigley, R.M. 1984. Quantitative mineralogy and preliminary porewater chemistry of candidate buffer and backfill materials for a nuclear fuel waste disposal vault, AECL report, AECL-7827.
- Rawlins, S.L. and Campbell, G.S. 1986. *Water potential: thermocouple psychrometry methods of soil analysis. Part 1. Physical and Mineralogical Methods - Agronomy Monograph no.9 (2nd Edition)*. 597-618.
- Richards, B.G. 1965. Measurement of the free energy of soil moisture by the psychrometric technique using thermistors, in *moisture equilibria and moisture*

- changes in soils beneath covered areas. A Symp. In Print. Butterworths (Australia), 39-46.
- Richards, B.G. 1974. Behaviour of unsaturated soils, in soil mechanics--new horizons, I.K. Lee ed. New York: American Elsevier, 112-157.
- Richards, B.G. 1978. Application of an experimental based non-linear constitutive model of soils in laboratory and field tests. Aust. Geomech. Journal, G8: 20-30.
- Ridley, A.M. and Burland, J.B. 1993. A new instrument for the measurement of soil moisture suction. Geotechnique **43**(2):321-324.
- Roscoe, K.H. and Burland, J.B. 1968. On the generalized stress-strain behaviour of 'wet' clay. In: Engineering Plasticity, Cambridge University Press, London, UK:535-609.
- Roscoe, K.H., Schofield, A.N., and Worth, C.P. 1958. On the yielding of soils. Geotechnique, **9**(1): 22-53.
- Saadat, F. 1989. Constitutive modeling of the behaviour of a sand-bentonite mixture. Ph.D. Thesis, Department of Civil Engineering, University of Manitoba, Winnipeg, Manitoba, Canada.
- Saadat, F., Graham, J., and Gray, M.N. 1989. High pressure behaviour of sand-bentonite buffer for nuclear fuel waste containment. 42nd Canadian Geotech. Conf. (Winnipeg, MB). Oct. 1989.
- Schofield, A.N. and Wroth, C.P. 1968. Critical state soil mechanics. McGraw Hill, London, U.K. 310pp.
- Sibley, J.W., Smyth, G.K., and Williams, D.J. 1990. Suction-moisture content calibration of filter papers from different boxes. Geotechnical Testing Journal, **13**(3): 257-262.
- Sridharan, A., Altschaeffl, A.G., and Diamond, S. 1971. Pore size distribution studies. ASCE Journal of the Soil Mechanics and Foundations Division, **97**:771-787.
- Stepkowska, E.T. 1980. Study in physical theory of expansiveness in clays. Proceedings of the Fourth Int. Conf. of Expansive Soils, (Denver, CO), **1**:136-157.
- Sun, B.C.-C. 1986. Stress-strain properties in sand-clay buffer materials. M.Sc. Thesis, University of Manitoba, (Winnipeg, MB).
- Tanaka, N. 1995. Thermal elastic plastic behavior and modelling of saturated clays. Ph.D. Thesis. Department of Civil Engineering, University of Manitoba, (Winnipeg, Manitoba).

- Tang, G.X., Graham, J., Blatz, J., Gray M. and Rajapakse, R. 1999. Suctions, stresses and strengths in unsaturated sand-bentonite. In review, *International Journal of Engineering Geology*.
- Tang, G.X. and Graham, J. 1998. A methodology of testing tensile strength of unsaturated soils. In review, *ASTM Geotechnical Testing Journal*.
- Tang, G.X., Graham, J., Blatz, J., Rajapakse, R. and Gray M. 1998a. Suction characteristics of unsaturated sand-bentonite. *Proc. of International Workshop on Key Issue in Waste Isolation Research*. Barcelona, Spain. December 1998.
- Tang, G.X., Graham, J. and Wan, A. 1998b. On yielding behavior of an unsaturated sand bentonite mixture. *Proceedings of 2nd International Conf. on Unsaturated Soils*, Beijing, China. August 1998. 149-154.
- Tang, G.X., Blatz, J. and Graham, J. 1998c. Volume changes in unsaturated sand-bentonite caused by suction-controlled drying and wetting. *Proc. 51st Canadian Geotechnical Conference*, Edmonton, Alberta, 1998. 95-100.
- Tang, G.X., Graham, J. and Fredlund, D.G. 1997a. Effects of osmotic suction on strength and stiffness of compacted sand-bentonite. *Proc. 50th Canadian Geotechnical Conference. Golden Jubilee*. Ottawa, 1997. 641-648.
- Tang, G.X., Graham, J. and Wan, A. 1997b. Measuring total suctions by psychrometers in triaxial tests. *Proc. XIVth International Conference on Soil Mechanics and Foundation Engineering*, Hamburg, Germany, 1997. 1:213-216.
- Tang, G.X., Graham, J. and Wan, A. 1997c. Determination of soil-water characteristic curves of highly plastic clays. *Proc. of 50th Canadian Geotechnical Conference, Golden Jubilee*. Ottawa, 1997, 633-640.
- Tang, X. 1996. Suction characteristics and elastic-plastic Critical State modelling of unsaturated buffer. Ph.D. Candidacy Examination, Department of Civil and Geological Engineering, University of Manitoba, Winnipeg, Manitoba.
- Terzaghi, K. 1936. The shearing resistance of saturated soils and the angle between the planes of shear. *Proc. First Int. Conf. Soil Mech.*, 1:54-56.
- Toll, D.G. 1990. A framework for unsaturated soils behavior (discussion). *Geotechnique*, 41(1):159-161.
- van Olphen, H. 1963. *An introduction to clay colloid chemistry*. Interscience, (New York, NY) 301pp.

- Vanapalli, S.K., Fredlund, D.G., Pufahl, D.E., and Clifton, A.W. 1996. Predicting the shear strength function for unsaturated soils using the soil-water characteristic curve. *Canadian Geotechnical Journal*, **33**:379-392.
- Wan, A.W.-L. 1987. Compaction and strength characteristics of sand-clay buffer material formed at swelling pressure-water content equilibrium. M.Sc. thesis. University of Manitoba.
- Wan, A.W.-L., Gray, M.N., and Graham, J. 1995. On the relations of suction, moisture content, and soil structure in compacted clays. Proc. of 1st. Int. Conf. on Unsaturated Soils. Paris, (1995), 215-222, eds. E.E.Alonso and P.Delage, publ. Balkema, Rotterdam.
- Wan, A.W.L. Graham, J., and Gray, M.N. 1990. Influence of soil structure on the stress-strain behaviour of sand-bentonite mixtures. *Geotechnical Testing Journal*, GTJODJ, **13**(3):179-187.
- Wan, A.W.L. 1996. The use of thermocouple psychrometers to measure in-situ suctions and water contents in compacted clays. Ph.D. Thesis. Department of Civil and Geological Engineering, University of Manitoba, (Winnipeg, Manitoba).
- Wheeler, S.J. and Sivakumar, V. 1995. An elasto-plastic critical state framework for unsaturated soil. *Geotechnique*, **45**(1):35-53.
- Wheeler, S.J. 1988. The undrained shear strength of soils containing large gas bubbles. *Geotechnique*, **38**(3):399-413.
- Wiebe, B., Graham, J., Tang, G.X. and Dixon, D. 1998. Influence of pressure, saturation and temperature on unsaturated buffer materials. *Canadian Geotechnical Journal*, **35**:194-205.
- Wiebe, B., Graham, J., Tang, G.X., and Dixon, D. 1997. Effect of temperature on stress-strain behaviour of unsaturated sand-bentonite. Proc. of 50th Canadian Geotechnical Conference, Golden Jubilee. Ottawa, 1997.
- Wiebe, B.J. 1996. The effect of confining pressure, temperature, and suction on the strength and stiffness of unsaturated buffer. M.Sc. Thesis, Department of Civil and Geological Engineering, University of Manitoba, (Winnipeg, Manitoba).
- Williams, D.J. and Sibley, J.W. 1992. The behaviour at the shrinkage limit of clay undergoing drying. *Geotechnical Testing Journal*, GTJODJ, **15**(3):217-222.

- Wood, D.M. 1990. Soil behavior and critical state soil mechanics. Cambridge University Press, UK. 1990.
- Yarechewski, D.S. 1993. Constant mean effective stress tests on sand-bentonite specimens at elevated temperature. M.Sc. Thesis, University of Manitoba, Department of Civil Engineering, Winnipeg, MB.
- Yong, R.N., Mohamed A.M.O. and Warkentin, B.P. 1992. Principles of Contaminant Transport in Soils. Elsevier Scientific Publishing Co., (New York, NY) 327 pp.
- Yong, R.N. and Warkentin, B.P. 1975. Soil properties and behaviour. Elsevier Scientific Publishing Co., (New York, NY) 449 pp.
- Yong, R.N., Japp, R.D., and How, G. 1971. Shear strength of partially saturated clays. Proc. 4th Asian Reg. Conf. Soil Mech. Found. Eng., (Bangkok) 2:183-187.
- Young, J.F. 1967. Humidity control in the laboratory using salt solutions - a review. Journal of Apply Chemistry. 17.